

INTRODUCTION

This chapter presents background information on predictive mineral discovery, particularly in Australia, and on gold as a global commodity. Why is it important to generate new information on the size and whereabouts of gold deposits, and what are the implications of such work? The chapter further sets the scene for the research carried out during my Ph.D. candidature. The project aims and objectives are defined and an overview is given of the regional geology of the study areas. The chapter concludes with a section on the structure of this dissertation.

1.1 MOTIVATION AND BACKGROUND

1.1.1 Predictive mineral discovery

Mineral exploration is a global business that is continuously changing. Most of the money invested in mineral exploration is spent on finding and testing targets that will never be mines. Mineral exploration is also a very fluid business, where thoughts on mineralising processes change very rapidly. One of the earliest works that addressed research into metallogenic processes was ‘De Re Metallica’ (Agricola 1556). In this work, Agricola touches on the basis of mineral exploration, and notes that “...a miner must have the greatest skills in his work that he may know first off all what mountain or hill, what valley or plain, can be prospected, or what he should leave alone. Moreover, he must understand the veins, stringers and seams in the rocks. Then he must be thoroughly familiar with the many and varied species of earths’ juices, gems, stones, marbles, rocks, metals and compounds.” In the present day, we have a wealth of knowledge on all the

subjects and processes mentioned by Agricola (1556), however, the discovery of a large ore body still seems to be controlled by luck rather than wisdom. Nevertheless, the development of new techniques through intensive research has been proven to be valuable for the discovery of new ore bodies and extended exploration around already discovered ore bodies (Hronsky 2004). The research presented in this dissertation is aimed at using multi-disciplinary methods to broaden the understanding of the tectonic setting in which ore deposits (in particular gold deposits) form. In my opinion, the creation of such knowledge can prove critical in the future discovery of ore systems.

1.1.2 pmd*CRC and the A1-project

The Cooperative Research Centre for predictive mineral discovery (*pmd**CRC) was established in Australia as a partnership between mining corporations and the research community (including government organisations) to focus research on issues that are of critical importance to the discovery of ore deposits. This partnership resulted from a rising awareness that despite high levels of expenditure and access to new mining technologies, the average cost of discovery of an ore deposit had risen to levels that are unattractive to investors and miners. The main focus of the *pmd**CRC is to improve understanding of geological processes to target orebodies more effectively.

My Ph.D. research project forms an integral part of the *pmd**CRC’s Architecture or A1-project. The aim of the A1-project is to determine a set of critical geological, geophysical and geochemical parameters that

can be used to identify favourable loci for the development of ore deposits. As part of this, an understanding of the factors that control mineralising processes along fault structures will be determined by reviewing mineralised and barren fault systems around the world. The A1-project entails a number of studies in key areas that have been selected for more detailed research on metallogenesis and tectonic controls on mineralisation. My Ph.D. research contributes to the A1-project as the low-data density, moderate endowment end-member of the selected key areas. Research outcomes can be compared to similar key area studies in high-data density, high-endowment regions, such as the Yilgarn region of Western Australia. My research in particular may provide insights into where gold deposits occur and the parameters that control their distribution. Results from my research can be applied elsewhere and may aid in the future discovery of gold deposits in gold-hosting terranes.

1.1.3 Focus on gold and use of gold in everyday life

One property of gold that distinguishes it from all other known metals, is its universal status as a monetary standard. Gold has been used as a medium of exchange since ca. 3000 B.C. Today, its main use lies in personal adornment (i.e. jewellery), but gold can be used in a range of other products and fields as a result of its physical and chemical properties. Possibly one of its most important applications is in electronic equipment, because unlike other metals, it does not tarnish or corrode. Gold is the third-most conductive metal after silver and copper, exceptionally transmitting

electricity and heat. Gold is also the most malleable of all metals. It can be drawn into tiny wires or threads without breaking and can be shaped or extended into extremely thin sheets. This characteristic makes it great for coatings of high quality compact discs or electronic wiring (for instance in camcorders). It is also used in computers, microchips, printers and modems. Gold pellets and compounds are used in medicines and are currently being tested for AIDS treatment. Further applications of gold can be found in the space industry, dentistry and the automotive industry. A breakdown of the main consumer markets for gold is given in Figure 1.1.

Gold is being increasingly used in today's society. This means that the discovery of new gold deposits will become progressively more important to balance the demand for gold as a result of changing consumer demands and potentially emerging products. Presently, the discovery rate of new gold deposits is declining, while the average costs per discovery are rising (Fig. 1.2) and may lag behind the consumer's demand. That's one reason why research like that presented in this dissertation becomes more and more important.

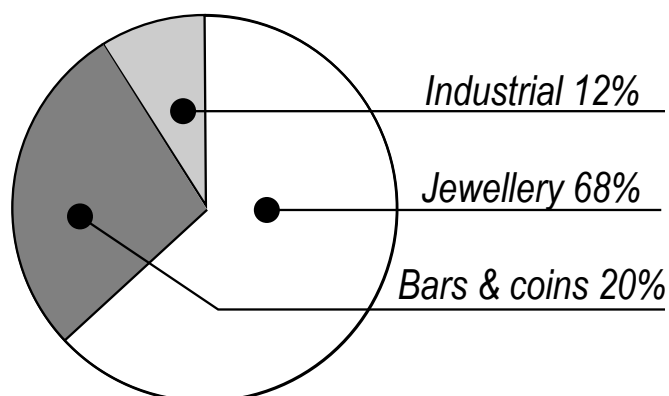


Fig. 1. 1: Pie chart representing the main markets consuming newly-mined gold (adapted from Placer Dome Ltd. website).

Growth in Gold Production (1997-2001)

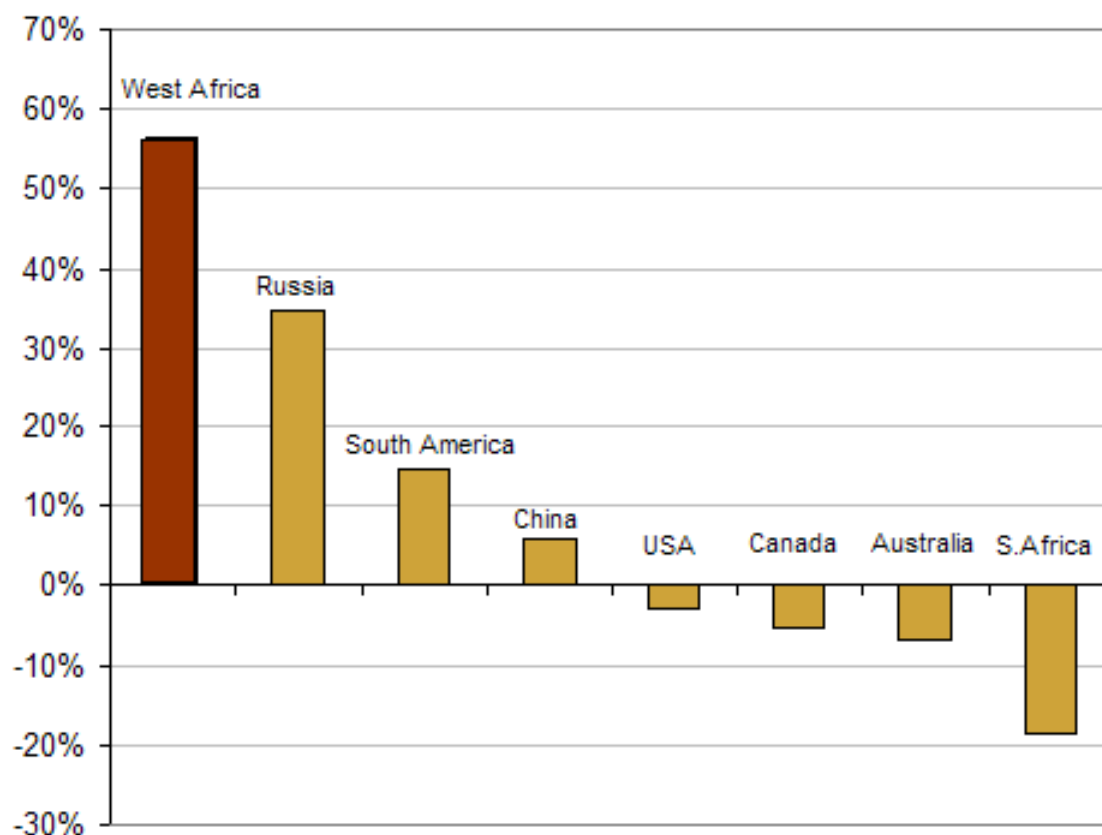


Fig. 1.2: Number of major discoveries per year versus exploration expenditures over the last three decades (after Schodde 2004).

1.2 PROJECT AIMS AND OBJECTIVES

The overall aim of my Ph.D. research is to unravel the Palaeozoic tectono-metallogenic evolution of the northern Tasman Fold Belt System in northeastern Australia (Fig. 1.3). The geological setting of the northern Tasman Fold Belt System will be discussed in the next section. Outcomes of my research provide an architectural framework for predictive mineral discovery in northeastern Queensland that may be valuable for companies exploring in that area, or can be applied to analogous tectonic regions elsewhere. The main objectives of my research are to:

1. Unravel the Early to Middle Palaeozoic

tectonic and metallogenic evolution of the Hodgkinson and Broken River provinces;

2. Create an understanding of the genesis of gold deposits within the Hodgkinson and Broken River provinces by comparing the nature, timing and metallogenic characteristics of selected gold deposits;
3. Assess the nature and role of large-scale fault structures in the evolution of the Hodgkinson and Broken River provinces and the development of gold deposits in these provinces.

A key characteristic of my research is the approach used, where results from a number of methods on all scales and in various disciplines are integrated to generate a better

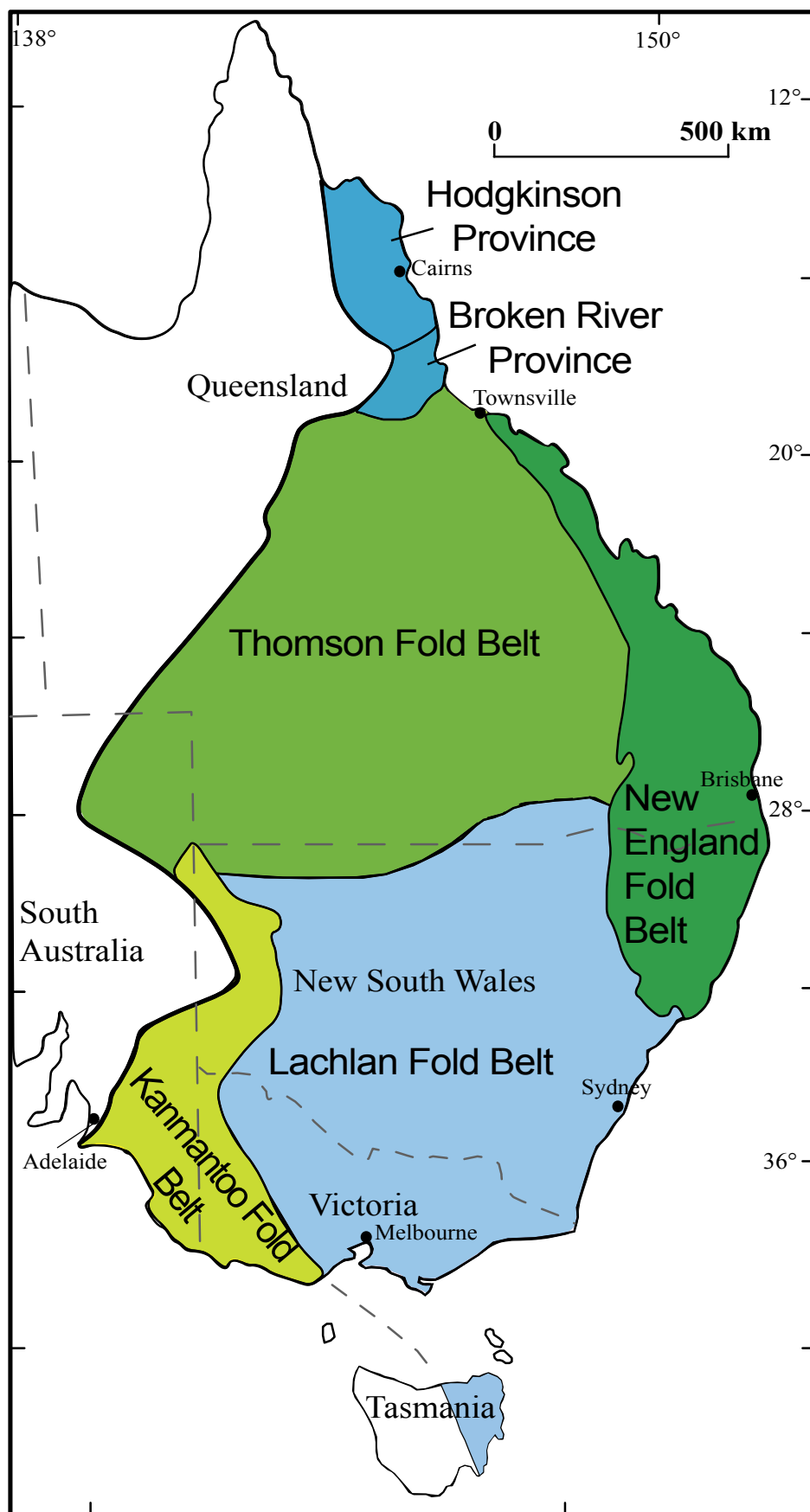


Fig. 1.3: Subdivision of the Tasman Fold Belt System in Eastern Australia (after Wellman 1995).

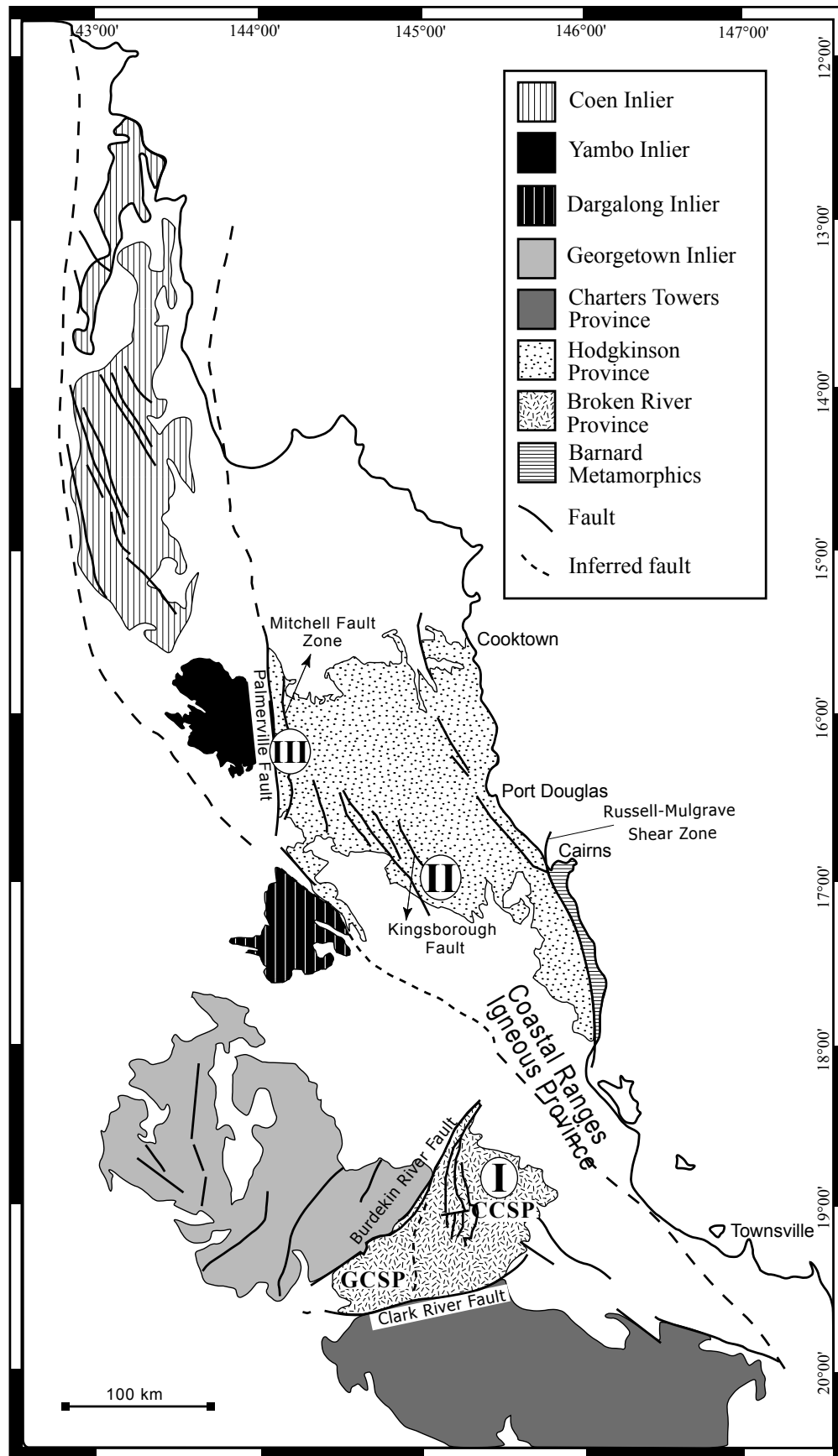


Fig. 1.4: Geological framework of northeastern Queensland with key study areas indicated in Roman capitals. GCSP = Graveyard Creek Subprovince, CCSP = Camel Creek Subprovince.

understanding of tectonic and metallogenic processes during the Palaeozoic evolution of the northern Tasman Fold Belt System. Field research as part of my project was mainly carried out in selected key areas that are indicated in Figure 1.4. These include the Amanda Bel Goldfield (I), the Northcote District in the Hodgkinson Goldfield (II) and the Palmerville Fault region (III).

Research methods are discussed in detail in the chapters of this dissertation and generally include:

- Investigation of gold deposits to understand their genesis, and use their characteristics as a key to tectonic evolution of the Hodgkinson and Broken River provinces;
- Geochronological investigations to constrain the timing of gold mineralisation in the Hodgkinson and Broken River provinces;
- Basalt geochemistry as a key to tectonic and magmatic evolution of the Hodgkinson and Broken River

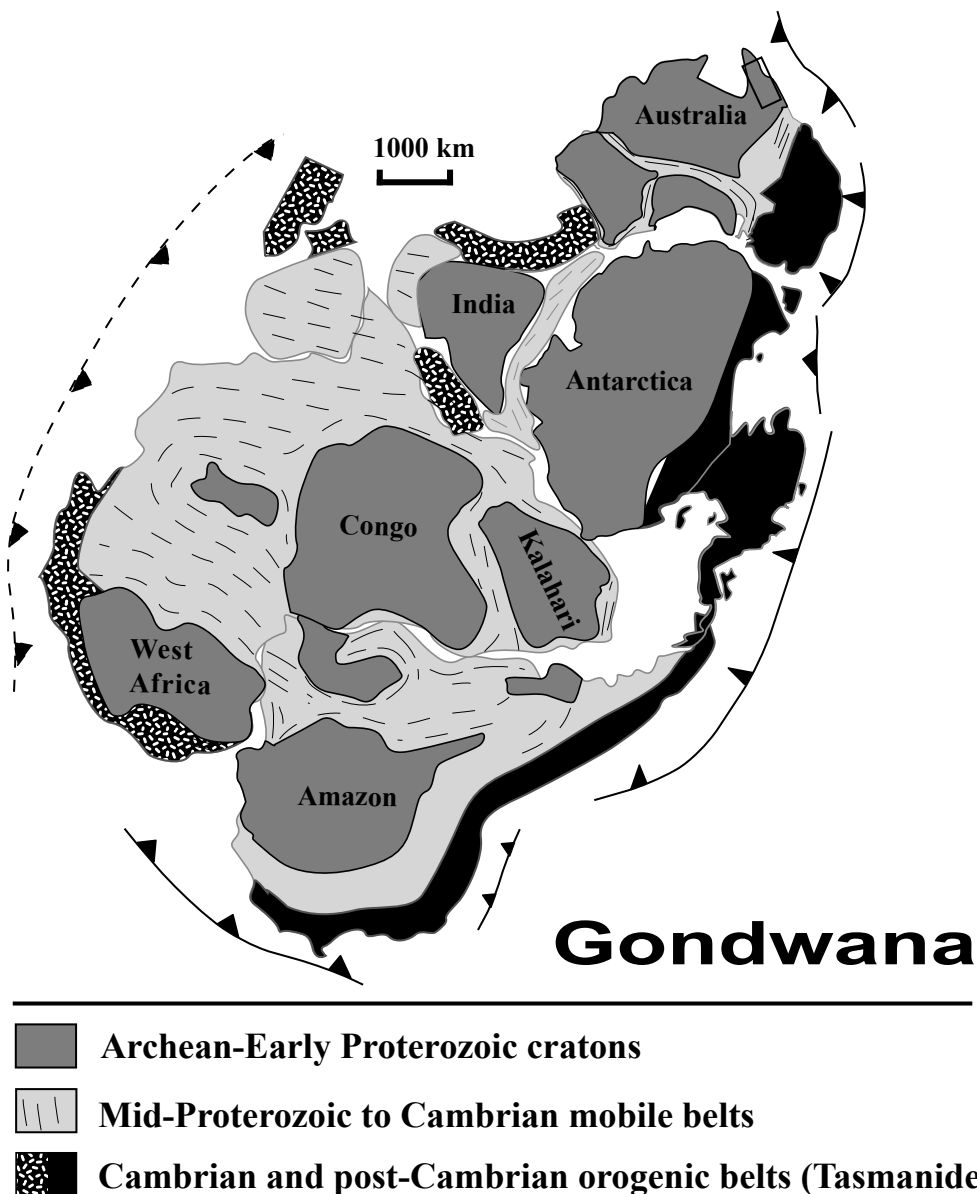


Fig. 1.5: The extent of the Terra Australis Orogen in black (after Cawood 2005) formed as a result of subduction along the margin of Gondwana in the Palaeozoic. Inset in northeastern Australia shows the location of the northern Tasman Fold Belt System.

- provinces;
- Geophysical investigations to understand the nature and role of fault structures in the evolution of the Hodgkinson Province;
 - Numerical modelling to obtain insights in the role of fault structures in deformation and mineralisation processes applicable to the Hodgkinson and Broken River provinces;
 - Investigation of large-scale tectonic processes that could control the development of world-class ore deposits.

1.3 REGIONAL GEOLOGICAL SETTING

1.3.1 The Tasman Fold Belt System in Australia

The Neoproterozoic to Late Palaeozoic Terra Australis Orogen extends across the former margins of Gondwana in Australasia, Antarctica, South Africa and South America (Fig. 1.5; Cawood 2005). The dominantly Palaeozoic Tasman Fold Belt System (Fig. 1.3) forms the Australian section of the Terra Australis Orogen and makes up the eastern third of the Australian continent. The Tasman Fold Belt System includes the Kanmantoo, Lachlan, Thompson, New England and Hodgkinson-Broken River fold belts (e.g. Coney *et al.* 1990; Scheibner & Veevers 2000). Overlying Mesozoic basin sequences of the Sydney, Bowen and Eromanga Basins obscure the boundaries between the various fold belts.

The Tasman Fold Belt System forms a composite of strato-tectonic assemblages and micro-continental ribbons that accreted onto the Australian margin of Gondwana as a result of increased coupling along the continental

margin during ongoing Palaeozoic subduction (e.g. Cawood 2005). The evolution of the Tasman Fold Belt System is controlled by the progressive ocean-ward retreat of the hinge of a subduction zone at the eastern margin of Gondwana (e.g. Cawood 2005). Thick, deep-water turbidite sequences and volcanic arcs that formed as a result of subduction and roll-back of the subduction system, were sequentially accreted onto the continental margin of Gondwana to form a mature continental-margin mountain chain (e.g. Coney *et al.* 1990). In Australia, collision of a series of terranes related to this subduction added ~30% to the size of the ancient Australian cratonic core (Foster *et al.* 1999). The present-day tectono-stratigraphy of Eastern Australia provides insights into the nature of these tectonic processes.

The Hodgkinson and Broken River Provinces (Fig. 1.4) are located in northeast Queensland, Australia and represent the northernmost extremity of the Tasman Fold Belt System. The provinces form a major element in the Tasman Fold Belt System and comprise of largely Ordovician-Devonian strata. The provinces are considered to have once been a continuous fold belt (e.g. Arnold & Fawcner 1980), but are presently separated by Late Palaeozoic granites and felsic volcanics belonging to the Kennedy Igneous Association. The geodynamical evolution of the Hodgkinson and Broken River provinces remains contentious. Creating a better understanding of their evolution is therefore a main research question in this dissertation as mentioned earlier.

1.3.2 Hodgkinson Province

The Hodgkinson Province is located in the northernmost part of the Tasman Fold Belt System and covers an area between 144°00' and

146°00' E and 15°50' and 17°00' S. It forms a belt ~500 km long from south of Innisfail to Cape Melville.

The Province is bounded to the west by the Palmerville Fault, which separates the Palaeozoic rocks in the province from the Precambrian Coen, Dargalong and Yambo inliers to the west (Fig. 1.4). From east to west, the belt that forms the Hodgkinson Province is ~150 km wide, but the province may extend well beyond the present coastline as based on the recognition of basement lithologies similar to those found in the Hodgkinson Province in drillcore collected from the western flank of the offshore Queensland Plateau (Feary *et al.* 1993).

The province is characterised by linear strike ridges and valleys in the west, which may reach lengths of many kilometers in a north-south direction. Ridges reflect the presence of erosion resistant lithologies (chert, quartzose sandstone and limestone) within a structurally deformed sequence. Maximum elevations reach up to 480 m and a slight increase in elevation can be identified from south to north. The remainder of the province forms a monotonously undulating landscape. The transition between the two landscapes is relatively abrupt and is characterised by the Mitchell Fault Zone (Fig. 1.6). The Palmerville Fault separates the province from the almost featureless, gently undulating Precambrian terrain to the west of the province.

The general geology of the Hodgkinson Province is illustrated in Figure 1.6 and a comprehensive summary of geological characteristics is given in Bultitude *et al.* (1993) and Bultitude *et al.* (1997) and summarised in Figure 7. Additional detail is provided in the relevant chapters in this dissertation.

The Hodgkinson Province comprises an eastward-younging sequence of Ordovician to Devonian volcano-sedimentary rocks that have been intruded by numerous Carboniferous to Permian, I- and S-type granites.

A number of deformation phases have been recognized in the Hodgkinson Province. Details on the timing and characteristics associated with these deformation phases are provided in Chapters 3, 4, 5 and 7. During these various deformation phases, rocks in the Hodgkinson Province have predominantly undergone mild, lower greenschist facies (chlorite zone), to upper greenschist facies (biotite zone) metamorphism (Bultitude *et al.* 1993).

In terms of mineralisation, the Hodgkinson Province has a long mining history and a wide range of minerals is present, including gold, tin, tungsten, molybdenum, copper, lead and silver. Much of the mineralisation is closely associated, either genetically or spatially, with Carboniferous-Permian igneous rocks. Regional scale, north to northwest-trending structures that host gold mineralisation reflect the dominant structural grain of the province. Main gold-producing areas include the West Normanby, Palmer River and Hodgkinson goldfields. Background information and details on gold and other mineralisation in the Hodgkinson Province is provided in this dissertation. For a complete description of known mineralisation and resources, the reader is referred to Garrad & Bultitude (1999).

1.3.3 Broken River Province

The Broken River Province is located to the south of the Hodgkinson Province in the northernmost part of the Tasman Fold Belt System and covers an area between 144°15' and 145°45' E and 18°30' and 19°45' S (Fig.

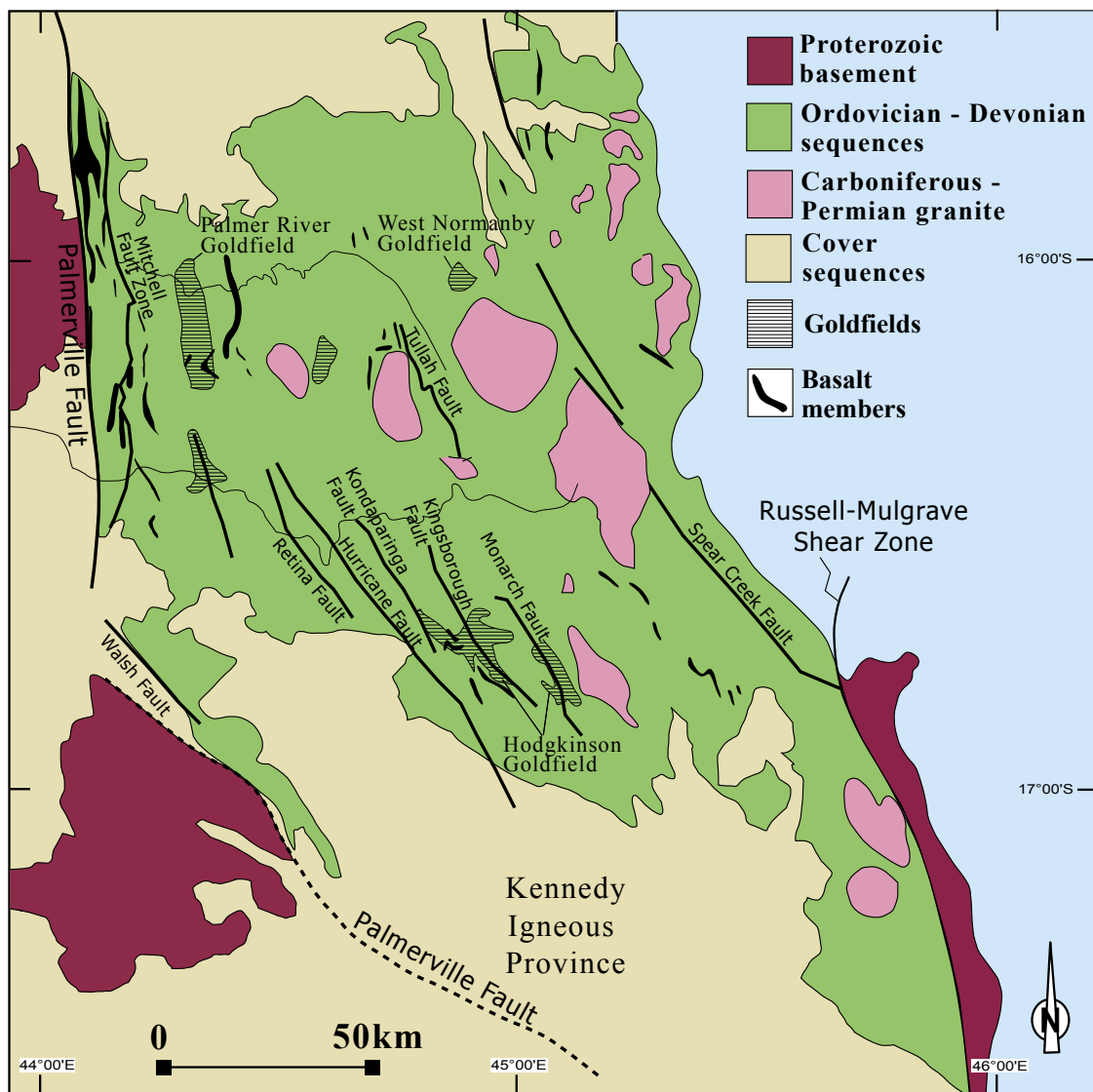


Fig. 1.6: General geology of the Hodgkinson Province, indicating main fault structures and basalt units as well as the location of major goldfields.

1.4). It forms a southwest-trending wedge of Palaeozoic lithologies that truncates the general north to northwesterly trend of the Tasman Fold Belt System. To the northwest it is separated from the Precambrian Georgetown Inlier by the Burdekin River Fault, and to the southeast from the Charters Towers Province by the Clarke River Fault (Fig. 1.4).

The physiography of the Broken River Province is comparable to that of the Hodgkinson Province and is mainly characterised by small ridges and valleys in a generally undulating landscape.

The general geology of the Broken River Province is illustrated in Figure 1.8 and a comprehensive summary of geological characteristics is given in Withnall & Lang (1993) and Withnall *et al.* (1997). The main geological events are summarised in Figure 1.7, while additional detail is provided in the relevant chapters in this dissertation.

The Broken River Province can be divided into the Graveyard Creek and Camel Creek subprovinces separated by the Gray Creek Fault Zone (Arnold & Henderson 1976). The Graveyard Creek Subprovince (GCSP)

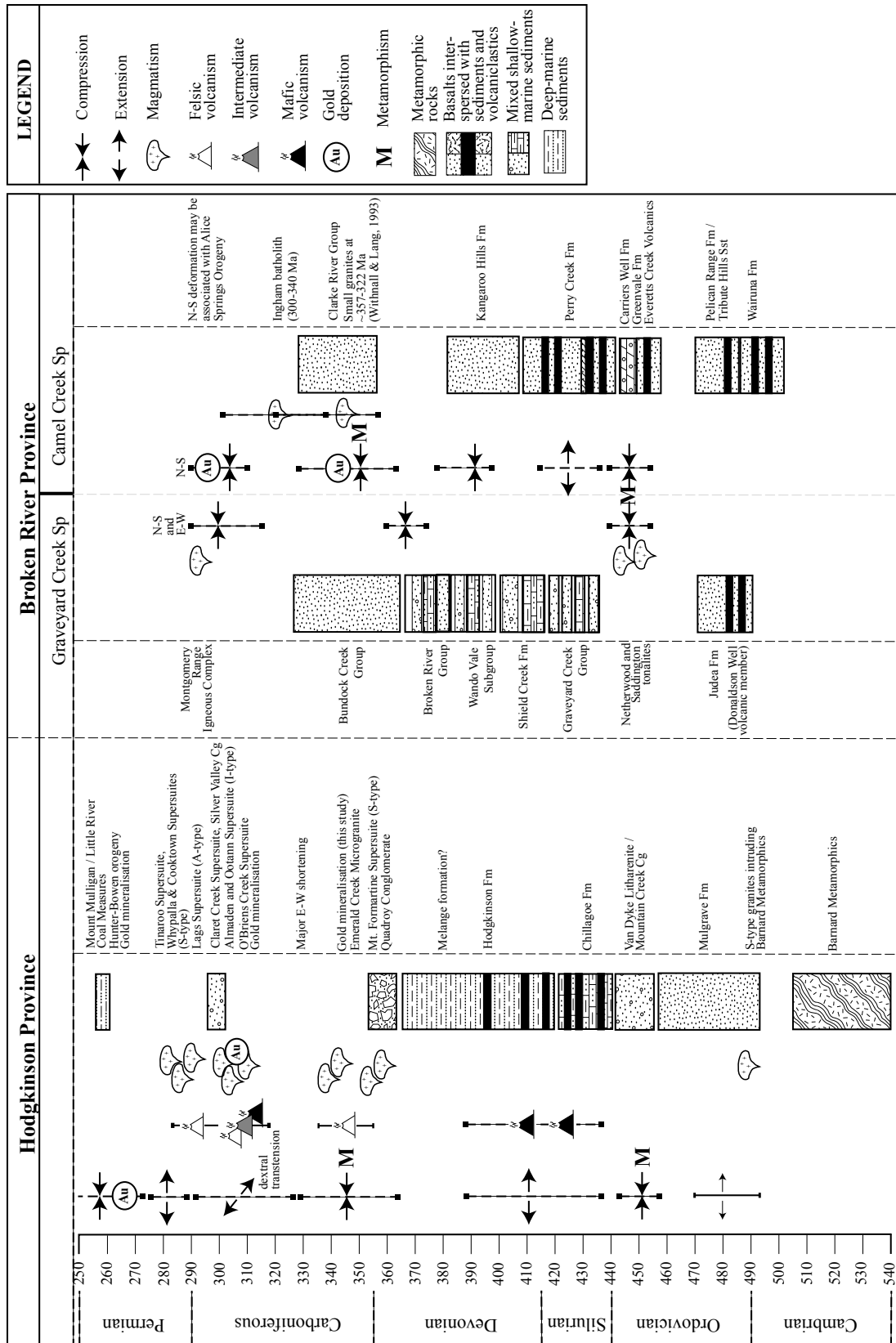


Fig. 1.7: Overview of stratigraphic units, deformation history and volcano-intrusive events in the Palaeozoic evolution of the Hodgkinson and Broken River provinces.

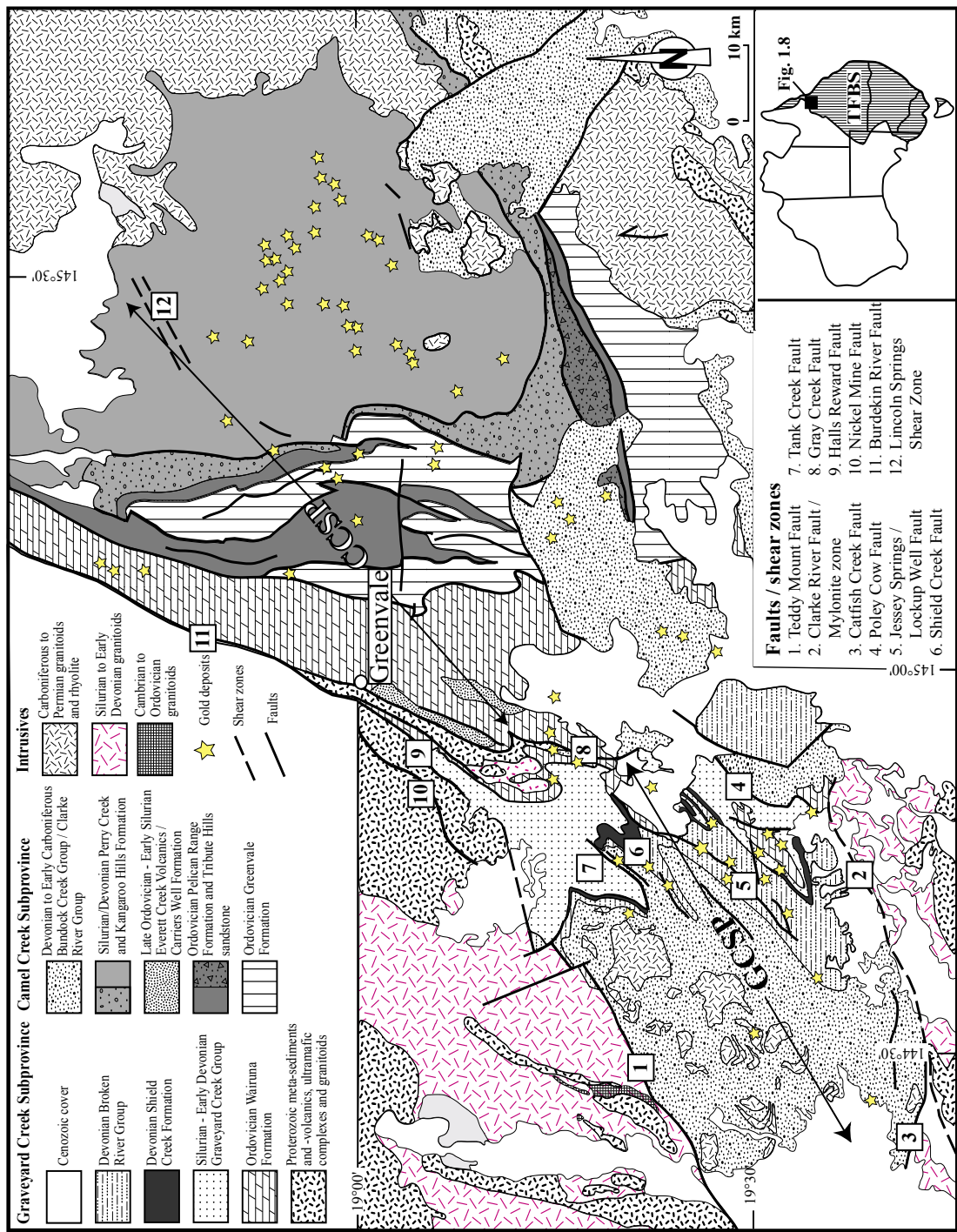


Fig. 1.8: General geology of the Broken River Province indicating the main fault structures and location of gold deposits. Figure modified from Withnall *et al.* 1997.

forms the western part of the Broken River Province and comprises mainly multiply-deformed, greenschist-metamorphosed, Ordovician to Early Carboniferous sedimentary and volcanic rocks.

Metamorphosed Precambrian mafic and ultramafic rocks of the Gray Creek Complex are considered as the basement rocks in the western part of this province and are overlain by the Judea Beds, which, in turn, are unconformably overlain by rocks of the Middle Silurian to Early Carboniferous Graveyard Creek, Broken River and Bundock Creek groups (e.g. Withnall & Lang 1993; Withnall *et al.* 1997).

Focus in this introduction lies on the Camel Creek Subprovince, since selected study areas were located in this subprovince (Fig. 1.3). The Camel Creek Subprovince (CCSP) forms the eastern part of the Broken River Province and represents an Ordovician to Devonian turbidite basin dominated by the meta-sedimentary rocks of the Greenvale, Pelican Range, Perry Creek and Kangaroo Hills formations. The CCSP contains a sequence of stacked thrust sheets that overall young to the east and formed during a number of deformation phases associated with greenschist metamorphism (e.g. Withnall *et al.* 1997). Details on the timing and characteristics associated with these deformation phases are provided in Chapters 2 and 7. In the east of the CCSP, Carboniferous to Permian I- and S-type granites of the Kennedy Igneous Province intrude the Palaeozoic volcano-sedimentary successions.

In terms of mineralisation, the Broken River Province is host to a variety of economic and sub-economic deposits, including gold, antimony, nickel, chromium, tin and base metals. Much of the mineralisation is spatially or genetically associated with either Early Palaeozoic

(ultra-)mafic rocks or Late Palaeozoic granites. A detailed description of gold and other deposits in the Broken River Province is provided later in this dissertation. For a complete description of known mineralisation and resources, the reader is referred to Tate *et al.* (1990).

1.4 DISSERTATION OUTLINE

This dissertation investigates the Palaeozoic tectono-metallogenic evolution of the northern Tasman Fold Belt System in northeastern Australia. It has been written as a series of journal-style articles that are published or submitted for publication in international journals, in line with current Monash University policies. Publication details are provided at the beginning of each chapter. This chapter is followed by six chapters that each provide information on either or both tectonic and metallogenic processes in various parts of the northern Tasman Fold Belt System during the Palaeozoic. Chapter 8 deals with large-scale tectonic processes that could control the formation of large ore bodies. The dissertation ends with closing remarks in chapter 9. Below is a general outline of chapters 2 to 9:

Chapter 2 deals with the characterisation of gold deposits in the Amanda Bel Goldfield in the Broken River Province based on results of metallogenic, structural, petrological and fluid inclusion studies. The structural framework for gold deposition in this goldfield is defined and implications for the tectonic evolution of the Broken River Province are explored.

Chapter 3 deals with the characterisation of gold deposits in the Northcote District in the Hodgkinson Goldfield of the Hodgkinson

Province based on results of metallogenic, structural, petrological and fluid inclusion studies. The structural framework for gold deposition in this goldfield is defined and implications for the tectonic evolution of the Hodgkinson Province are explored.

Chapter 4 is concerned with the geochemistry of Late Ordovician to Devonian mafic rock assemblages in the Hodgkinson Province. Petrogenetic and Sm-Nd isotope characteristics of these mafic volcanic rocks are investigated and used to constrain the tectonic setting in which they erupted.

In *Chapter 5* the nature and subsurface expression of the Palmerville Fault are investigated. This fault plays an important role in the Palaeozoic tectonic evolution of the Hodgkinson Province and insight from structural field and microscopic observations, as well as multi-scale wavelet edge analysis ('worming'), forward modelling of regional magnetic and gravity data, and geochemical data sets have been used to improve the understanding of the nature and subsurface geometry of this fault.

Having obtained insight into the nature and geometry of the Palmerville Fault and its role in the tectonic evolution of the Hodgkinson Province, *Chapter 6* deals with the role of the Palmerville Fault in mineralisation processes throughout the Hodgkinson Province using mechanical-fluid flow coupled numerical simulations. Predictions from our modelling are of significant value for future exploration in the Hodgkinson Province and similar terranes elsewhere.

Chapter 7 presents results from absolute age dating of gold deposits in the Hodgkinson and Broken River provinces and petrogenetic investigations of volcano-intrusive rocks in the Amanda Bel Goldfield. These are integrated with available geological data from the northern Tasman Fold Belt System including the knowledge accumulated from the Hodgkinson and Broken River provinces as presented in the previous chapters. Based on these, a geodynamic model for the tectonic evolution of the northern Tasman Fold Belt System is developed and linked with the genesis of various types of ore deposits within the system.

Chapter 8 reviews contemporaneous metallogenic, tectonic, magmatic and sedimentological events in central and eastern Australia around 440 Ma. A model of slab break-off along a mega-subduction system that existed outboard of the Gondwanan margin of Australia is proposed to explain the temporal coincidence of events. This scenario is considered of great importance to the generation of large ore deposits.

Chapter 9 presents the closing remarks for this dissertation, summarises the general outcomes, implications for exploration and lists suggestions for future work.

REFERENCES

- AGRICOLA G. 1556. *De Re Metallica*. Translated from Latin in 1950 by Hoover H.C. & Hoover L. H. New York, Dover Publications Inc.
- ARNOLD G. O. & FAWCKNER J. F. 1980. The Broken River and Hodgkinson Provinces. In: Stephenson H. ed. The geology and geophysics of northeastern Queensland, pp175-189

- James Cook University, Department of Geology, Townsville, Australia.
- ARNOLD G.O. & HENDERSON R.A. 1976. Lower Palaeozoic history of the southwestern Broken River Province, north Queensland. *Journal of the Geological Society of Australia* 23, 73-93.
- BULTITUDE R. J., DONCHAK P. J., DOMAGALA J. & FORDHAM B. G. 1993 The Pre-Mesozoic stratigraphy and structure of the western Hodgkinson Province and environs. *Queensland Geological Record* 29. Department of Minerals and Energy, Queensland, 1-259.
- BULTITUDE R. J., GARRAD P. D., DONCHAK P. J. T., DOMAGALA J., CHAMPION D. C., REES I. D., MACKENZIE D. E., WELLMAN P., KNUTSON J., FANNING C. M., FORDHAM B. G., GRIMES K. G., OVERSBY B. S., RIENKS I. P., STEPHENSON P. J., CHAPPELL B. W., PAIN C. F., WILFORD J. R., RIGBY J. F. & WOODBURY M. J. 1997. Cairns region. In: Bain J. H. C. & Draper J. J. eds. North Queensland Geology. *Australian Geological Survey Organisation Bulletin* 240, 225-325.
- CAWOOD P. A. 2005. Terra Australis Orogen: Rodinia breakup and development of the Pacific and Iapetus margins of Gondwana during the Neoproterozoic and Paleozoic. *Earth-Science Reviews* 69, 249-279.
- CONEY P. J., EDWARDS A., HINE R., MORRISON F. & WINDRIM D. 1990. The regional tectonics of the Tasman orogenic system, eastern Australia. *Journal of Structural Geology* 12, 519-543.
- FEARY D. A., CHAMPION D. C., BULTITUDE R. J. & DAVIES P. J. 1993. Igneous and metasedimentary basement lithofacies of the Queensland Plateau (sites 824 and 825); *Proceedings of the Ocean Drilling Program, Scientific Results* 133, 535-540.
- FOSTER D. A., GRAY D. R. & BUCHER M. 1999. Chronology of deformation within the turbidite-dominated Lachlan Orogen: implications for the tectonic evolution of eastern Australia and Gondwana. *Tectonics* 18, 452-485.
- HENDERSON R. A. 1987. An oblique subduction and transform faulting model for the evolution of the Broken River Province, northern Tasman Orogenic System. *Australian Journal of Earth Sciences* 34, 237-249.
- HILL D. 1951. *Geology Handbook of Queensland*, pp.12-24. Australasian Association for the advancement of Science, Brisbane.
- HRONSKY J. 2004. The science of exploration targeting. In: Muhling J., Goldfarb R., Vielreicher N., Bierlein F., Stumpfl E., Groves D.I. & Kenworthy S. eds. SEG 2004: Predictive Mineral Discovery Under Cover; extended abstracts. Centre for Global Metallogeny, *University of Western Australia Publication* 33, 120-134.
- SCHEIBNER E. & VEEVERS J. J. 2000. Tasman Fold Belt System. In: Veevers, J. J. ed. Billion-year earth history of Australia and neighbours in Gondwanaland. GEMOC press, Sydney, 154-234.
- SCHODDE R.C. 2004. Discovery performance of the western world gold industry over the period 1985-2003. Pacific Rim Conference 2004 Proceedings, pp. 367-381. Australian Institute of Mining and Metallurgy.
- TATE N. M. MORRISON G. W., SEARSTON S. & COOPER R. 1990. Gold mineralisation in the Broken River Province, North Queensland. *AMIRA Gold Metallogenic Bulletin* 15, 1-65.
- WITHNALL I.W. & LANG S.C. 1993. Geology of the Broken River province, north Queensland. *Queensland Geology* 4, Department of Resource Industries, Queensland.
- WITHNALL I. W., LANG S. C., LAM J. S., DRAPER J. J., KNUTSON J., GRIMES K. G. & WELLMAN P. 1997. Clarke River Region. In: Bain J. H. C. & Draper J. J. eds. North Queensland Geology. *Australian Geological Survey Organisation Bulletin* 240, 327-363.

GENESIS OF OROGENIC GOLD DEPOSITS IN THE BROKEN RIVER PROVINCE, NORTHEAST QUEENSLAND, AUSTRALIA

I.M.A. Vos, F.P. Bierlein and G.S. Teale

Australian Journal of Earth Sciences, in press

ABSTRACT

We report results of metallogenic, structural, petrological and fluid inclusion studies that characterise the nature of gold mineralisation in the Amanda Bel Goldfield, the most significant gold producer in the Palaeozoic Broken River Province of northeastern Queensland, Australia. Gold-antimony-arsenic and gold-arsenic deposits in the Amanda Bel Goldfield occur along distinctive northeastern trends suggesting a strong structural control for their development during several phases of deformation in the Devonian to Carboniferous. Field evidence, as well as petrographic, scanning electron microscope and fluid inclusion analysis of mineralised samples, indicate the presence of two main stages of gold genesis. These are distinguished by the coarse-grained versus invisible nature of gold particles and their association with particular sulphide phases. A third stage of gold deposition is attributed to introduction of antimony±gold-rich ore fluids. Fluid inclusion studies record minimum trapping temperatures between 140° and 380°C, and salinities of up to 6.5 weight percent NaCl equivalent for the two main gold-forming stages. Our analyses further indicate that mineralising solutions for the earlier of the two main gold-forming stages were slightly more saline, and that the ore-hosting veins formed at higher temperatures. The style of gold mineralisation in the Amanda Bel Goldfield is compatible with ‘orogenic’ gold deposits that form primarily during compressional and transpressional deformation along convergent plate margins in accretionary and collisional orogens. The increased understanding gained from our studies on the origin and nature of the deposits aids predictive mineral discovery elsewhere in the Broken River Province, and also in analogous terranes throughout the Tasman Fold Belt System of eastern Australia.

2.1 INTRODUCTION

The Neo-Proterozoic to Mesozoic Tasman Fold Belt System (TFBS; see inset in Fig. 2.1) in eastern Australia is host to a several world-class orogenic gold-producing areas (e.g. Walshe *et al.* 1995). Some of the best-documented gold-producing areas include the central Victorian goldfields (e.g. Ramsay *et al.* 1998) and the Charters Towers Province (e.g. Peters 1987a). Other areas that have produced less gold and have received significantly less attention, include the Hodgkinson and Palmer River goldfields (e.g. Morrison 1988) in the Hodgkinson Province. In view of the geological similarities with analogous terrains elsewhere in the TFBS, there is a considerable likelihood for the presence of as yet undiscovered gold resources in the relatively unexplored northern parts of the TFBS like the Broken River Province (Fig. 2.1).

The Amanda Bel Goldfield (Fig. 2.2), situated in the Camel Creek Subprovince of the Broken River Province in northeastern Queensland, represents a ‘greenfields’ discovery made in the 1980s (Fig. 2.1; Teale *et al.* 1989). Over 2.8t of gold was produced (shallow oxide-zone only) from the goldfield between 1989 and 1994 (Withnall *et al.* 1997) with resource drilling by Lynch Mining Pty Ltd indicating that the known occurrences remain open at depth. The nature and style of gold (-arsenic \pm antimony) deposits in this goldfield are poorly constrained and, apart from regional studies (e.g. Withnall *et al.* 1997), the region has received relatively little research and exploration attention compared to gold deposits in the Hodgkinson Province that were discovered in the gold rushes of the late 1800s.

In this paper, we describe the characteristics,

timing, structural control and style of gold mineralisation in the Amanda Bel Goldfield. Fieldwork concentrated on several abandoned mine sites and resulted in the construction of a structural framework for mineralisation. Petrographic, Scanning Electron Microscope (SEM), electron microprobe and fluid inclusion studies were conducted to resolve the sulphide paragenesis, and temperature and chemical composition of the mineralising fluids at the various deposits.

The Palaeozoic tectonic setting of the Broken River Province and the Camel Creek Subprovince has been the subject of several studies (e.g. Arnold & Fawckner 1980; Bell 1980; Henderson 1987; Withnall & Lang 1993; Withnall *et al.* 1997) but remains contentious. Understanding the genesis and origin of poorly constrained gold deposits in the Broken River Province can provide insight into the tectonic framework for gold mineralisation in the Amanda Bel Goldfield and also contributes as an aid for further exploration in the province. Furthermore, characterisation of the gold deposits in the Amanda Bel Goldfield allows for comparisons with other gold deposits of similar association throughout the remainder of the TFBS in Queensland (i.e. Hodgkinson Goldfield; Charters Towers Province).

2.2 REGIONAL GEOLOGY

The TFBS is a composite of orogenic belts that makes up most of eastern Australia and resulted from the interaction between the proto-Pacific plate and the Australian continent in the Palaeozoic (e.g. Coney 1990). The Broken River Province, together with the Hodgkinson Province to the north, forms the northern part of the TFBS. The Broken River Province

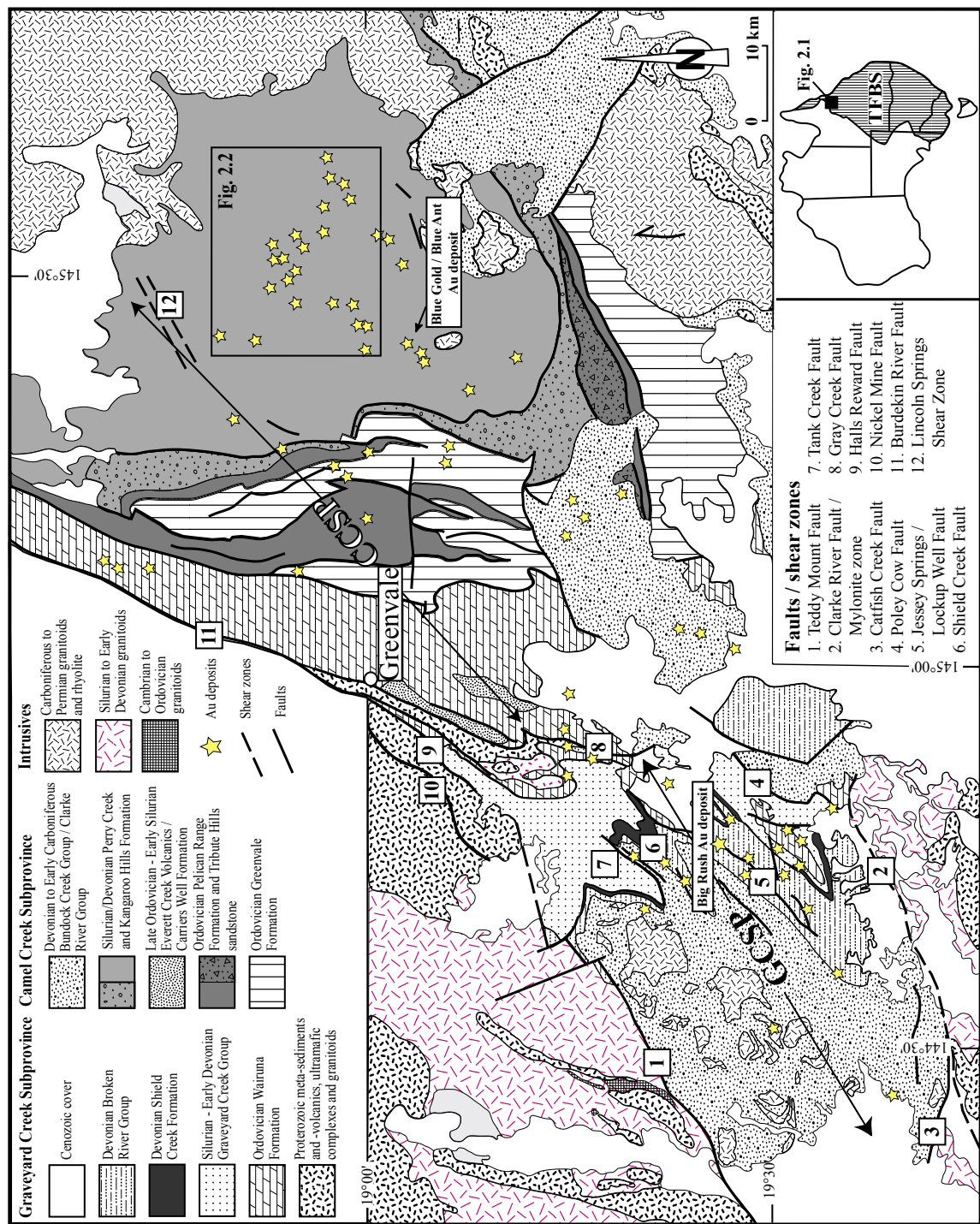


Fig. 2.1: Geological map of the Broken River Province showing the location of the Amanda Bel Goldfield. Major faults, shear zones and gold deposits are indicated, and locations of the Big Rush, Blue Gold and Blue Ant gold deposits are specified on the map. GCSP = Graveyard Creek Subprovince, CCSP = Camel Creek Subprovince. Inset shows the extent of the Tasman Fold Belt System in eastern Australia, with the study region indicated by black square. Modified from Withnall *et al.* (1997).

is dominated by an open to tightly-folded sequence of sedimentary and volcanic rocks of Late Ordovician to Early Carboniferous age that are structurally juxtaposed in the northwest against the Precambrian Georgetown Inlier. The province can be divided into the Graveyard Creek and Camel Creek subprovinces separated by the Gray Creek Fault Zone (Arnold & Henderson 1976; Fig. 2.1). Although interfingering stratigraphic relationships occur locally within the subprovinces, most contacts between lithological units are of tectonic nature.

The Camel Creek Subprovince (CCSP) forms the eastern part of the Broken River Province and represents a multiply deformed Ordovician to Devonian turbidite basin. According to Withnall *et al.* (1997), the CCSP contains an Ordovician to Early Devonian sequence of stacked thrust sheets that overall young to the east. The individual quartz-rich and quartz-intermediate thrust units internally display westward younging with rare large-scale fold closures. Withnall *et al.* (1997) interpreted the tectonic setting of the CCSP as an inverted extensional basin, while other authors (e.g. Arnold & Fawckner 1980; Henderson 1987) suggested that the subprovince represents an accretionary wedge oversteepened by ramping and later shortening.

The CCSP is host to the Amanda Bel Goldfield (Fig. 2.2) that covers an area of approximately 1000 km². Gold mineralisation occurs in open to tightly-folded lower greenschist facies meta-sedimentary rocks of the Silurian Greenvale Formation and the Early Devonian Kangaroo Hills Formation. To the east and northeast, Carboniferous to Permian granites intrude the meta-sedimentary rocks. Table 2.1 presents

the deformation history in the Amanda Bel Goldfield and its relationship to the regional deformation framework for the CCSP. During $_{ab}D_1$ imbricate thrusting and *mélange* formation is linked to the development of pervasive mesoscopic, isoclinal folds and slaty cleavage, as observed throughout the CCSP ($_{cc}D_1$; Withnall *et al.* 1997). Arnold & Fawckner (1980) associated this event with heterogeneous faulting, boudinage and chaotic disarray of bedding resulting from large-scale imbrication of thrust sheets. These $_{ab}D_1$ -structures are overprinted by NE-SW trending, upright chevron folds ($_{ab}D_2$). The latter can be related to a NE-SW regional and mesoscopic fold event in the CCSP ($_{cc}D_2$), during which greenschist facies peak metamorphic conditions were reached (Arnold & Fawckner 1980). A weakly-developed, third deformation event, observed in the Amanda Bel Goldfield ($_{ab}D_3$) is related to NW-SE striking thrust faults and minor mesoscopic open folds. Although regional-scale relationships remain unclear, this event could be related to an E-W folding event in the CCSP ($_{cc}D_3$), which occurred in response to N-S contraction in the mid to Late Carboniferous (Withnall *et al.* 1997). Locally, the $_{ab}D_3$ event led to plunge reversals along major $_{ab}D_2$ folds. This three-stage structural evolution has been corroborated by our field observations in the Amanda Bel Goldfield. The $_{ab}D_1$ and $_{ab}D_2$ inter-relationships are abundant at the outcrop scale, where refolded, recumbent folds mainly represent $_{ab}D_1$ -structures. These structures are transected by a strongly developed $_{ab}S_2$ -cleavage, which is also found associated with cm-scale fold closures. Fold axes and cleavage related to these phases of deformation have similar pre-dominantly NE-SW orientations,

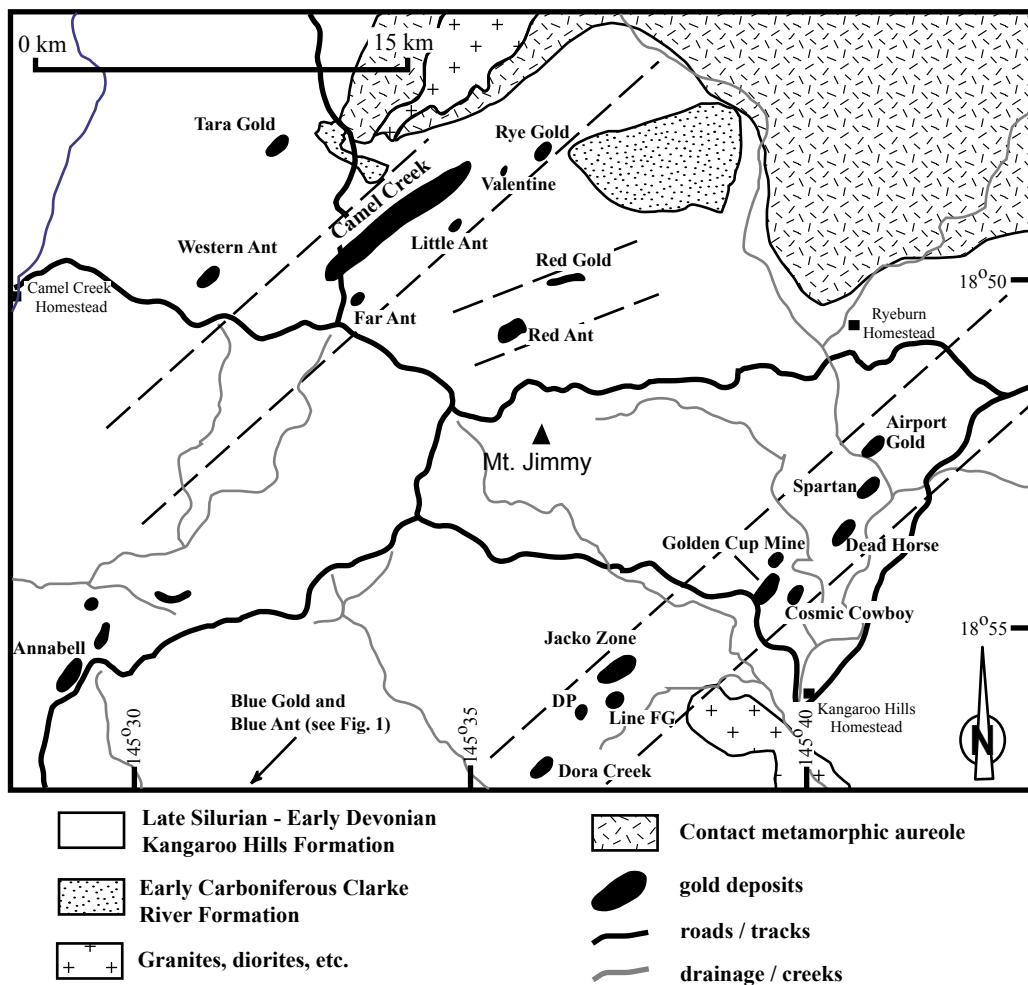


Fig. 2.2: Generalised geology of the Amanda Bel Goldfield indicating the location and names of the major gold deposits. The dashed lines indicate distinctly NE-trending (structural) corridors in which the gold deposits are situated. The location of the Blue Gold and Blue Ant deposits, situated along a NW strike, are indicated on Figure 2.1.

where $_{ab}S_2$ cuts $_{ab}S_1$ at a high angle. Figure 2.3a gives an indication of the pre-dominant NE-SW strike of $_{ab}S_2$ in the Amanda Bel Goldfield that can be found throughout the region. In addition, an example of the interrelationship between the two deformation phases is illustrated in Figure 2.4. At a mesoscopic scale, $_{ab}D_1/D_2$ -structures are commonly crosscut by NW-SE-striking reverse faults and associated (poorly developed) cleavage. Buck quartz veins, up to 10cm thick, commonly occur in similar NW-SE orientations and are often hosted by these reverse faults. Strike measurements of $_{ab}S_3$, reverse faults and shear planes in the Amanda Bel Goldfield are presented in Figure 2.3b and

reflect the regional trend. An example of a D_3 -reverse fault, as indicated by fault drag, hosting a quartz vein is shown in Figure 2.5.

2.3 GOLD DEPOSITS IN THE AMANDA BEL GOLDFIELD

On the basis of field observations and our analytical work we have distinguished three phases of gold mineralisation in the Amanda Bel Goldfield, confirming previous observations by Teale *et al.* (1989) and Tate *et al.* (1990). Syn- $_{ab}D_1$ mineralisation occurred primarily as fold repetitions of quartz-stibnite-carbonate-arsenopyrite lenses and boudin necks in auriferous, commonly quartz-veined,

Table 2.1: Comparison of deformation event history for the Camel Creek Subprovince (CCSP) and the Amanda Bel Goldfield (ABG). Abbreviations: CC = Camel Creek deposit; AP = Airport deposit; RG = Red Gold deposit; GC = Golden Cup deposit; BG = Blue Gold deposit; ccDm = deformation event related to melange formation in the CCSP.

Deformation event (CCSP)	Orientation (ABG)	Style	Fabrics	Distribution in ABG	Age and correlation	Reference
ccDm			bedding disarray / boudinage	CC, RG	probably syn-D1	Withnall <i>et al.</i> 1997
ccD1	abD1	north-striking?	isoclinal folding and thrusting	minor slaty cleavage / boudinage	CC, AP, RG, GC	(?Early) Devonian Withnall <i>et al.</i> 1997; this paper
ccD2	abD2	NE-SW	close to tight upright folding	slaty / crenulation cleavage	CC, AP, RG, GC	(?Late) Devonian Withnall <i>et al.</i> 1997; this paper
	abD3	NW-SE	thrusting and minor folding	minor cleavage	CC, AP, RG, GC, BG	Mid- to Late Carboniferous Withnall <i>et al.</i> 1997; this paper
ccD3	E-W	open folding	sporadic folds / cleavage	not observed	Mid- to Late Carboniferous	Withnall <i>et al.</i> 1997

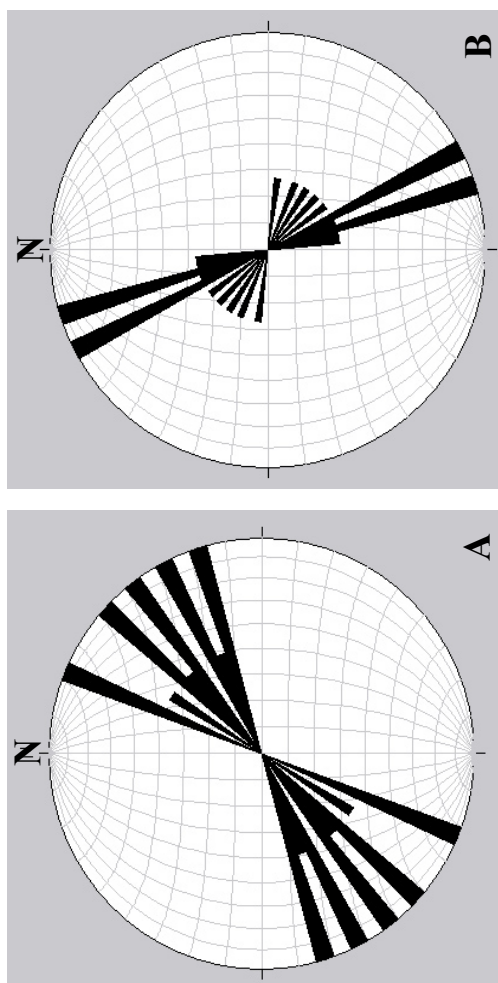


Fig. 2.3: Rose diagrams illustrating a) the pre-dominant NE-SW strike of structures associated with D_3 ($n=13$), and b) the pre-dominant NW-SE strike associated with D_3 structures ($n=14$) in the Amanda Bel Goldfield.

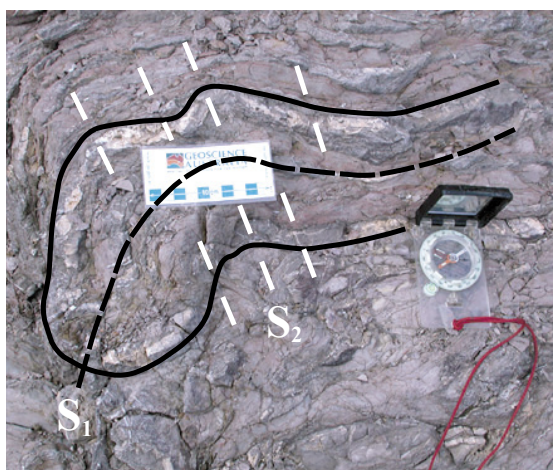


Fig. 2.4: Refolded recumbent $_{ab}F_1$ -fold in weathered shales at the Camel Creek deposit. Traces of $_{ab}S_1$ and $_{ab}S_2$ are indicated on the photograph, where $_{ab}S_2$ cleavage is trending NE-SW. Scale bar is 10 cm long.

arsenopyrite-rich carbonaceous shales. Stibnite-rich domains in the lenses and boudins can contain some gold, pyrite, sphalerite, boulangerite, alledmontite, aurostibite and native antimony. Subsequent $_{ab}D_2$ -mineralisation (gold - arsenopyrite - pyrite) comprises boudinaged quartz veins and stockworks that parallel NE-trending $_{ab}F_2$ axial planes in sheared, carbonaceous shales. The third phase of mineralisation ($_{ab}D_3$) is associated with numerous generations of breccia veins and injection of silica (-Au-As)-rich fluids along NW-trending fault zones. Tate *et al.* (1990) suggested that the first two

phases of mineralisation were of metamorphic origin, because of the lack of intrusives during $_{ab}D_1$ and $_{ab}D_2$. These authors considered the third phase of mineralisation to be associated with intrusive emplacement, because of the paragenetic similarities with porphyry-hosted mineralisation elsewhere in the Broken River Province (e.g. Picklebottle Camp; e.g. Tate *et al.* 1990).

Field investigations were conducted at the abandoned mine sites of the Camel Creek, Golden Cup and Red Gold deposits (for locations see Fig. 2.2). Due to the removal of the primary ore zones at the study sites, additional observations to determine metallogenic relationships were made on samples collected by the third author during the active mining stage from the primary ore zones in these and other deposits



Fig. 2.5: Outcrop photograph of NW-striking, quartz-filled $_{ab}D_3$ reverse fault in pit wall at the Camel Creek deposit. Dashed lines represent fault drag. Hammer for scale.

Table 2.2: Summary of deposit location, sulfide mineralogy and production. Cpy = chalcopyrite; Tth = tetrahedrite, Py = pyrite; Au = gold; Sph = sphalerite; Aspy = arsenopyrite; Sb = Stibnite; Gl = galena. Production figures courtesy of Lynch Mining Pty. Ltd.

	Locality (UTM)	Sulfide mineralogy	Dominant lithology	production (t)
Red Gold	353528 7917139	Cpy, Tth, Py, Au	greywacke / shale	0.3
Airport Gold	363063 7912500	Sph, Py, Aspy, Au, Sb	siltstone / shale	0.2
Camel Creek	348148 7918209	Sph, Py, Aspy, Au, Sb	greywacke / shale	2.5
Golden Cup	358915 7909611	Cpy, Tth, Sph, Gl, Py, Aspy, Au	greywacke / shale	1.6
Blue Gold	338750 7902420	Py, Aspy, Au, Gl, Sb	siltstone / shale	0.16

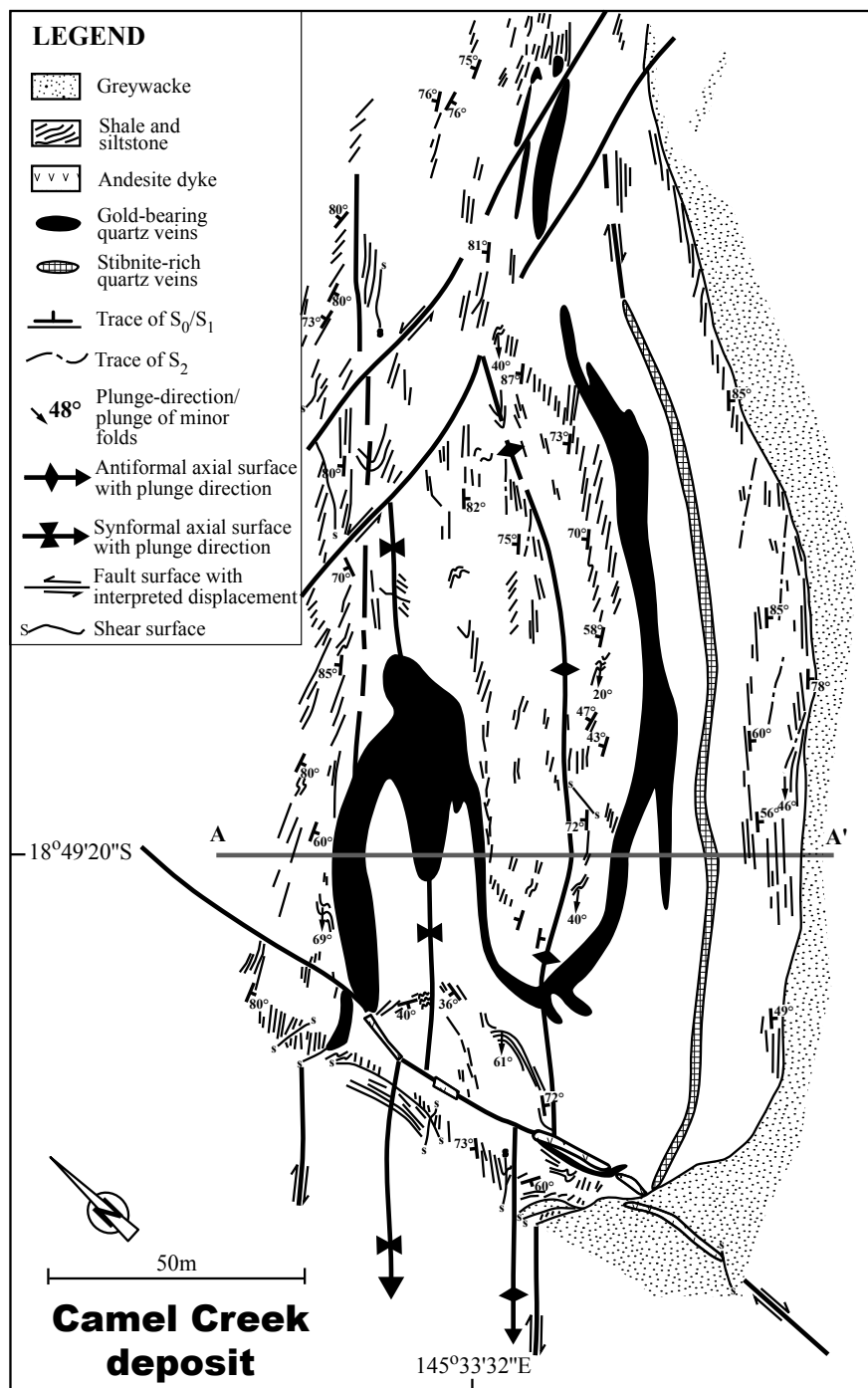


Fig. 2.6: Detailed geology of pit 1/6 at the Camel Creek deposit modified from field map. Note the orientation of refolded ore lenses along a distinct NE strike. Location of cross-section (Fig. 2.7) is indicated A-A'.

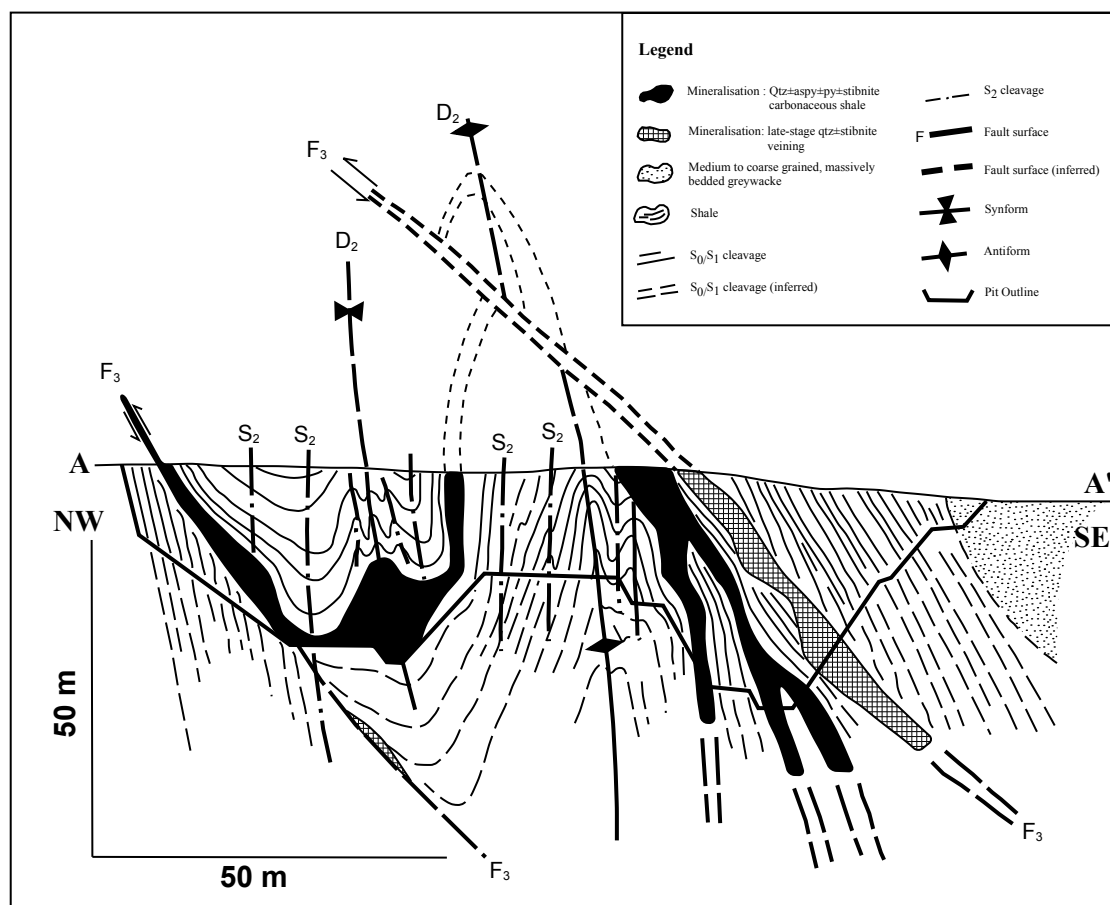


Fig. 2.7: Geological cross-section through pit 1/6 in the Camel Creek deposit indicating the overprinting relationships between the main deformation phases and the refolded nature of the ore lenses. Section based on mapping by S. Sullivan and G. Teale

(Blue Gold and Airport Gold deposits) in the Amanda Bel Goldfield. These five gold deposits represent a cross-section of mineralisation styles in the Amanda Bel Goldfield. Their main characteristics are outlined below and in Table 2.2.

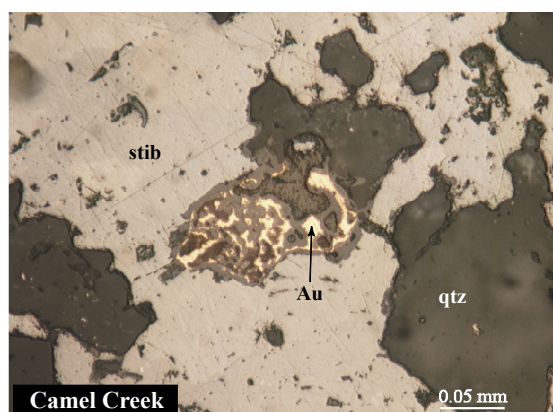


Fig. 2.8: Photomicrograph (reflected light) of free gold (Au) and aurostibite (contact zone between gold and stibnite) in stibnite (stib) from the Camel Creek deposit.

2.3.1 Camel Creek deposit

The ore zone in the Camel Creek deposit (Figs. 2.6 and 2.7) lies along a NE strike in tightly folded Greenvale Formation meta-sedimentary rocks. Lenses and boudins of quartz veins up to a meter thick in arsenopyrite-rich carbonaceous shale horizons are associated with $_{ab}D_1$ -deformation and host stibnite, arsenopyrite, sphalerite, pyrite, boulangerite and gold. Gold can form complex intergrowths with stibnite, presumably after aurostibite (Fig. 2.8) and can contain up to 11 wt percent silver. Narrow and stockwork mineralised quartz veins associated with $_{ab}D_2$ strike consistently around 050. This type of mineralisation is best developed at the intersection of local shear zones and $_{ab}D_1$ mineralisation. The main shear zones are

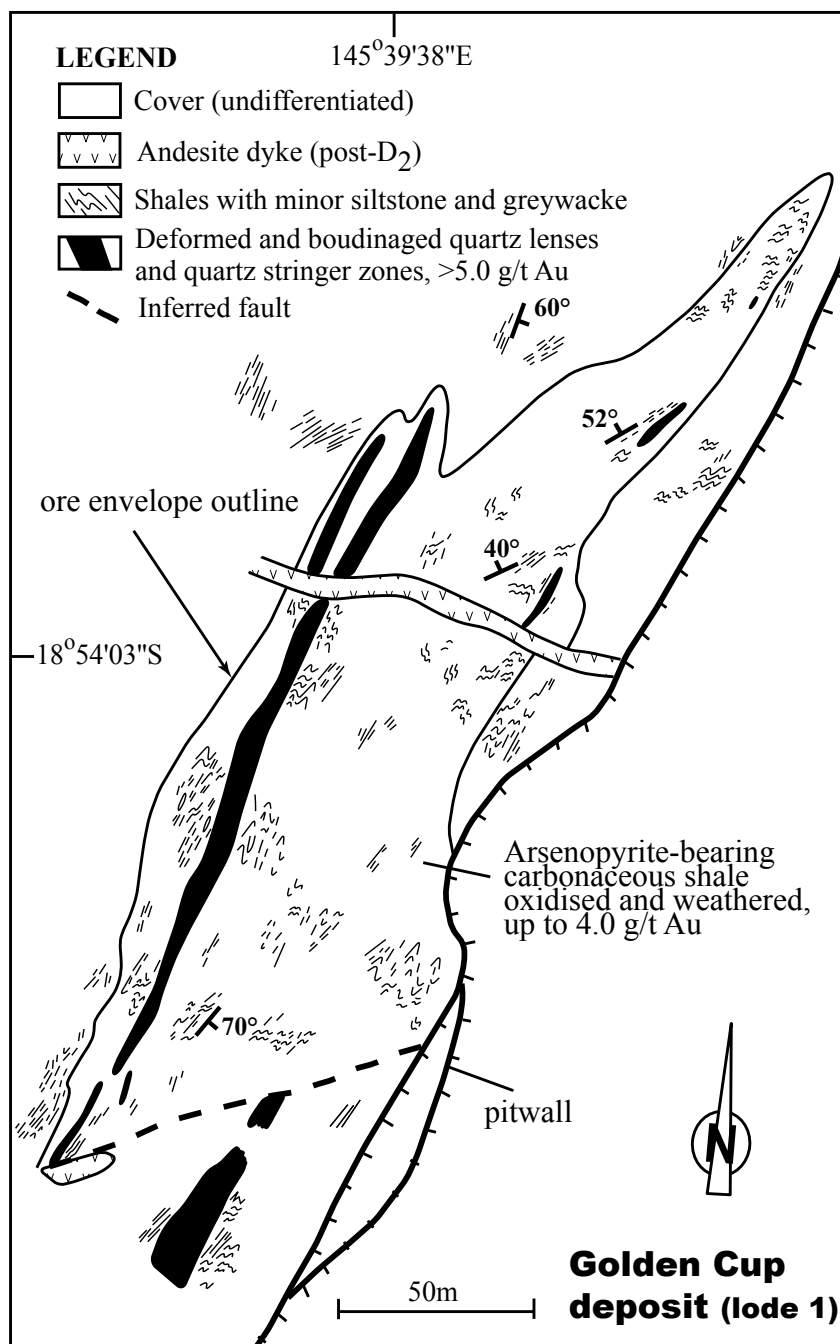


Fig. 2.9: Detailed geology of the Golden Cup deposit modified from field map. Note the orientation of ore lenses along a distinct NE strike associated with $_{ab}D_2$.

localised along the main lithological boundary between shale and sandstone, forming a zone of high competency contrast. The $_{ab}D_2$ veins host arsenopyrite, pyrite, chalcopyrite and sphalerite. Gold can be found in solid solution within the arsenopyrite and pyrite as indicated by SEM analysis (see next section). Later-stage $_{ab}D_3$ mineralisation is associated with NW-

striking, SE-dipping thrust faults and consists mainly of discrete stibnite pods and lenses in quartz veins that may contain some gold (see Fig. 2.8). Wallrock alteration comprises mainly quartz, sericite, ankerite and chlorite (\pm illite) along vein margins.

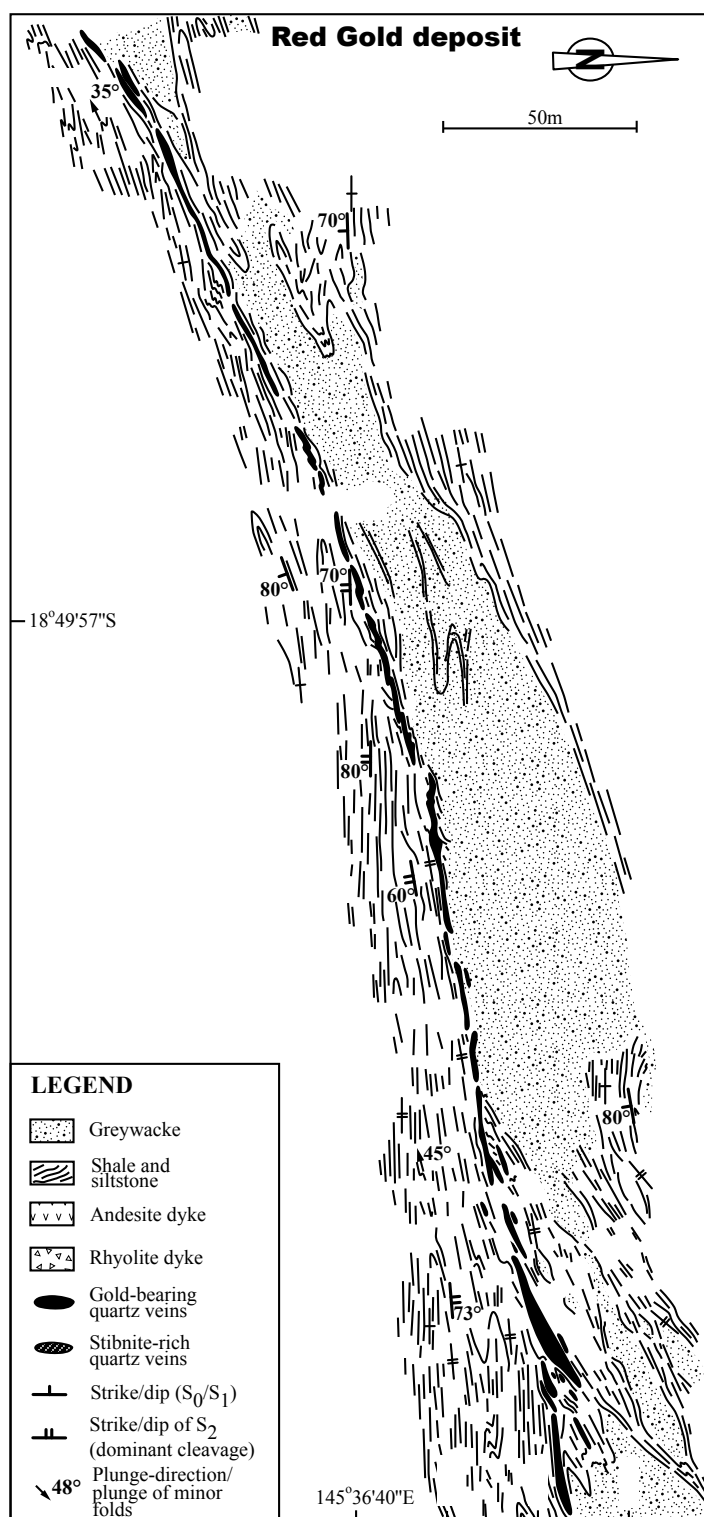


Fig. 2.10: Detailed geology of the Red Gold deposit modified from field map. Ore lenses strike slightly off NE-SW. Legend applies to Figures 2.11 and 2.12 as well.

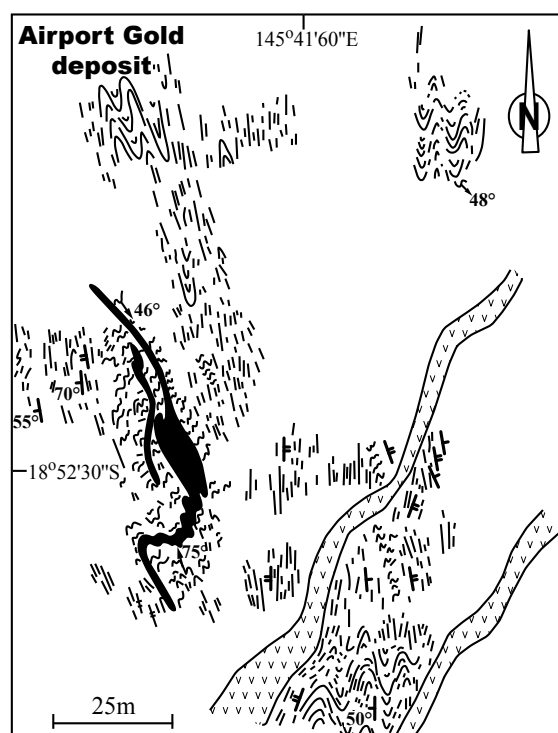


Fig. 2.11: Detailed geology of the Airport Gold deposit modified from field map. Ore lenses are refolded along a NNW trend. See Figure 2.10 for legend.

2.3.2 Golden Cup deposit

The Golden Cup deposit consists of three main lodes with several offshoots. The NE-SW trending lodes (Fig. 2.9) are located along a major regional fold hinge. This hinge zone is characterised by boudinaged sandstone beds and quartz veins within strongly sheared shales, and is flanked by planar-bedded greywackes and siltstones. The location of the lodes is controlled by a competency contrast represented by phyllic fracture zones in strongly deformed carbonaceous shales and feldspathic greywackes. Generally NE-SW striking cleavage ($_{ab}S_2$) forms the dominant foliation. Undulating shear zones have formed parallel to the dominant NE-SW-trending $_{ab}F_2$ axial planar cleavage, and are host to quartz veins and stockworks. These contain mainly arsenopyrite and pyrite, with minor chalcopyrite and other accessory sulphides. Veins can be boudinaged and are generally

up to 2m thick. Breccia veins, consisting of quartz (\pm carbonate) matrix with host rock fragments, are also common. Barren laminated quartz spur veins are oriented along a NW trend. These are slightly deformed and can be related to $_{ab}D_3$. Quartz veins are associated with alteration envelopes comprising sericite, ankerite and chlorite within sulphide-rich carbonaceous shales. Andesitic dykes traverse the deposits along a mainly E-W trend. In lode 2, a rhyolitic dyke crosscutting the major lode trend was observed as well. Two generations of dykes can be distinguished that intersect the main $_{ab}D_2$ trend. The relative timing of dyke emplacement can be constrained on the basis of crosscutting interrelationships.

2.3.3 Red Gold deposit

The Red Gold deposit (Fig. 2.10) has a generally WSW-ENE strike. Mineralisation is hosted along the contact between a massive

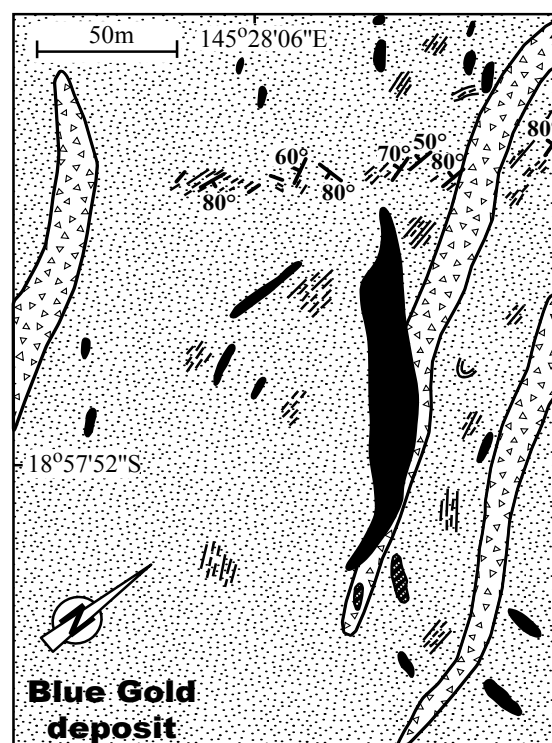


Fig. 2.12: Detailed geology of the Blue Gold deposit modified from field map. Ore lenses are situated along a NW-SE trend associated with $_{ab}D_3$. See Figure 2.10 for legend.

coarse-grained greywacke unit and red-coloured, ferruginous shales and siltstones. Within the ore zone, $_{ab}S_1$ and $_{ab}S_2$ foliations are almost co-planar where $_{ab}S_2$ is the most pervasive cleavage. Away from the ore zone, $_{ab}S_1$ is transposed by $_{ab}S_2$. Mineralisation is dominated by arsenopyrite, pyrite with minor tetrahedrite and chalcopyrite, and occurs along a quartz-inundated shear zone that follows the lithological contact. Abundant en-echelon fractures strike NE-SW and are associated with silica flooding. Chlorite-alteration selvages can be found around late-stage $_{ab}D_2$ quartz veins.

2.3.4 Airport Gold deposit

Mineralisation at the Airport gold deposit (Fig. 2.11) consists of gold-bearing quartz and stibnite veins within strongly deformed arsenic (\pm gold)-rich shales. Mineralised quartz veins are intensely transposed and boudinaged, leading to breccia development. The mineralised quartz veins are refolded along minor $_{ab}D_2$ -folds. NE-trending andesitic dykes that dip steeply towards the NW and crosscut mineralised quartz veins were emplaced post- $_{ab}D_2$. Their relative age is mainly derived from crosscutting relationships and observations at other deposits such as Golden Cup.

2.3.5 Blue Gold deposit

The Blue Gold deposit (Fig. 2.12) is located along a NW-SE trending fault zone that has been intensely silicified and parallels rhyolitic dykes in the area. Numerous generations of veins have brecciated the wallrock and resulted in rotation and silicification of wallrock fragments in the quartz veins. Quartz veins are hosted by brittle sandstones rather than carbonaceous shales, and commonly contain pyrite and free gold that is rarely found intergrown. Additionally,

isolated non-auriferous veins show late, open-space fillings of stibnite. Teale *et al.* (1989) reported stibnite-bearing quartz veins from the nearby Blue Ant prospect. These veins occur along fractures and the stibnite crystals are undeformed. The latter feature combined with open-space growth in the quartz veins from the Blue Ant prospect support a late-stage ($_{ab}D_3$) phase of minor gold and stibnite mineralisation. Open-space filling textures and the abundance of stibnite as observed at these deposits are often characteristic of shallow formation levels (e.g. Ashley & Craw 2004).

2.4 SULPHIDE PARAGENESIS

2.4.1 Sampling methods and analytical techniques

Due to oxidation depths locally reaching up to 30m and weathering of exposed ore-bearing rocks, material within the studied deposits has been largely oxidised. Nonetheless, unweathered sulphide-rich samples have been obtained from mine dumps and exploration drillcores at the various mine sites. Around 60 polished thin sections were petrographically examined. Additionally, 15 thin sections were analysed by SEM (JEOL 6300) at the University of Ballarat. Energy-dispersive spectra were obtained operating at 15kV and a beam current of approximately 1nA using an Oxford Instruments Link UTW Si detector. Wavelength-dispersive spectra and maps ($AuL\alpha$) were obtained operating at 30kV and a beam current of approximately 600nA using a Microspec WDX 3PC spectrometer. Sulphide phases from representative samples from each of the studied deposits were analysed for major and trace elements using a CAMECA SX50 electron microprobe

Deposit	Minerals	D ₁	D ₂	post-D ₂ /D ₃
Airport Gold	Sphalerite Pyrite Arsenopyrite Gold			
Blue Gold	Arsenopyrite Galena Gold Pyrite Stibnite			
Camel Creek	Sphalerite Pyrite Arsenopyrite Stibnite Gold Aurostibite			
Golden Cup	Chalcopyrite Tetrahedrite Sphalerite Galena Pyrite Arsenopyrite Gold			
Red Gold	Chalcopyrite Tetrahedrite Pyrite Gold			

Fig. 2.13: Generalised ore paragenetic sequence for selected deposits in the Amanda Bel Goldfield.

with 4 WDS spectrometers at the School of Earth Sciences, University of Melbourne. Instrument settings used were voltage of 20 kV, beam current of 20 nA, a sharply focused probe, and counting times of 30 seconds.

2.4.2 Results

Petrographic, SEM and electron microprobe analyses of mineralised quartz vein samples and adjacent wallrock enable the unravelling of the paragenesis in gold deposits in the Amanda Bel Goldfield. The paragenetic sequence of mineralisation in each of the deposits is summarised in Figure 2.13. An overview of the main sulphide and accessory phases at each of the studied deposit is presented below and examples of the sulphide association at the various deposits are presented in Figure 2.14. Sulphide mineralisation in the Camel Creek

deposit is of two types. Samples from the primary ore zones are commonly stibnite-dominated, quartz-rich, and contain some gold (\pm berthierite \pm arsenopyrite \pm pyrite \pm sphalerite \pm aurostibite). Pyrite (\pm arsenopyrite) assemblages occur mainly within stylolitic fractures in the quartz veins, where pyrite regularly forms polyform aggregates (Fig. 2.14a). In contrast, the carbonaceous shales hosting the ore zones contain mainly prismatic pyrite and arsenopyrite (Fig. 2.14b).

The vein-hosted sulphide assemblage at the Golden Cup deposit is more complex.

Galena, tetrahedrite, stibnite, chalcopyrite, sphalerite and freibergite can be observed as accessory sulphide minerals together with monazite, zircon and rare gold within the quartz lodes (Fig. 2.14d). The Golden Cup ore zone further consists of carbonaceous shales and siltstones that host arsenopyrite and pyrite (Fig. 2.14c). Arsenopyrite tends to be corroded, and rhomboid-shaped crystals are chemically-zoned and preferentially contain gold in solid solution.

In the Red Gold deposit, the sulphide assemblage consists mainly of pyrite with minor tetrahedrite and chalcopyrite, whereas in the Blue Gold deposit, the sulphide assemblage is dominated by pyrite, minor arsenopyrite, gold (\pm silver) and galena. Gold in the Blue Gold deposit can be found as single grains, in some cases intergrown with pyrite, and containing up

Table 2.3: Chemical analyses (electron microprobe WDS) of representative pyrite and arsenopyrite from selected deposits in the Amanda Bel Goldfield. Except where otherwise indicated, concentrations are in ppm. Blanks represent analyses below detection limit. Abbreviations: AP = Airport deposit, CC = Camel Creek deposit, GC = Golden Cup deposit, BA = Blue Ant deposit.

Py = Pyrite, Aspy = Arsenopyrite; I, II and III for stage I, II and III mineralisation respectively.

Analysis no.	Mineral	S wt%	Fe wt%	As wt%	Sb	Au	Ag	Co	Ni	Si wt%
AP_1	Py I	53.3	46.6							
AP_2	Py I	53.4	46.2	1.0						
AP_3	Py I	52.7	46.4						1143	
AP_1	Aspy I	19.7	34.6	45.3				1134		
AP_2	Aspy I	19.1	34.5	46.0						
AP_3	Aspy I	20.6	34.9	43.3	7215					
AP_line_1-2	Py I	53.0	46.1							
AP_line_1-3	Py I	53.2	46.7							
AP_line_1-4	Py I	53.3	46.9							
AP_line_1-5	Py I	53.3	46.3							
AP_line_1-6	Py I	52.2	46.3	1.3						
AP_line_1-7	Py I	52.6	45.8	1.2						
CC_1	Py I	52.2	46.1	2.0						
CC_2	Py I	52.4	45.6	1.5						
CC_3	Py I	53.0	45.8	1.2						
CC_4	Py I	52.1	45.6	2.8						
CC_1	Aspy I	19.4	34.8	44.7	8756					
CC_2	Aspy I	20.0	34.0	44.0	6952				2078	
CC-PE2-A	Aspy I	19.6	34.3	44.7	2385	6453				
CC-PE2-B	Aspy I	21.0	34.7	43.7	5217	1013				
CC_line_1-1	Py I	53.1	45.6							
CC_line_1-2	Py I	51.9	45.4	2.9		3417				
CC_line_1-3	Py I	51.4	45.7	2.6						
CC_line_1-6	Py I	51.8	45.4	3.3						
CC_line_1-7	Py I	51.7	45.5	3.6		2268				
CC_line_1-8	Py I	53.4	46.4							
GC_2	Py II	51.9	45.6	2.3						
GC_3	Py II	53.3	45.9							
GC_1	Aspy II	19.3	34.2	46.1						
GC_2	Aspy II	19.2	34.0	45.8						
GC_3	Aspy II	18.6	32.4	44.1						
GC_line_1-3	Py II	52.6	45.6	1.4						
GC_line_1-4	Py II	54.1	46.0							
GC_line_1-5	Py II	52.8	45.6	1.6						
GC_line_1-6	Py II	53.4	45.4	1.3						
BA_1	Py III	53.4	46.0		2872					
BA_1	Stib III	28.1		2.4	717411					
BA_2	Stib III	28.0		2.5	706990					
BA_3	Stib III	28.0		2.6	712842					
BA_4	Stib III	28.3		2.4	716875					

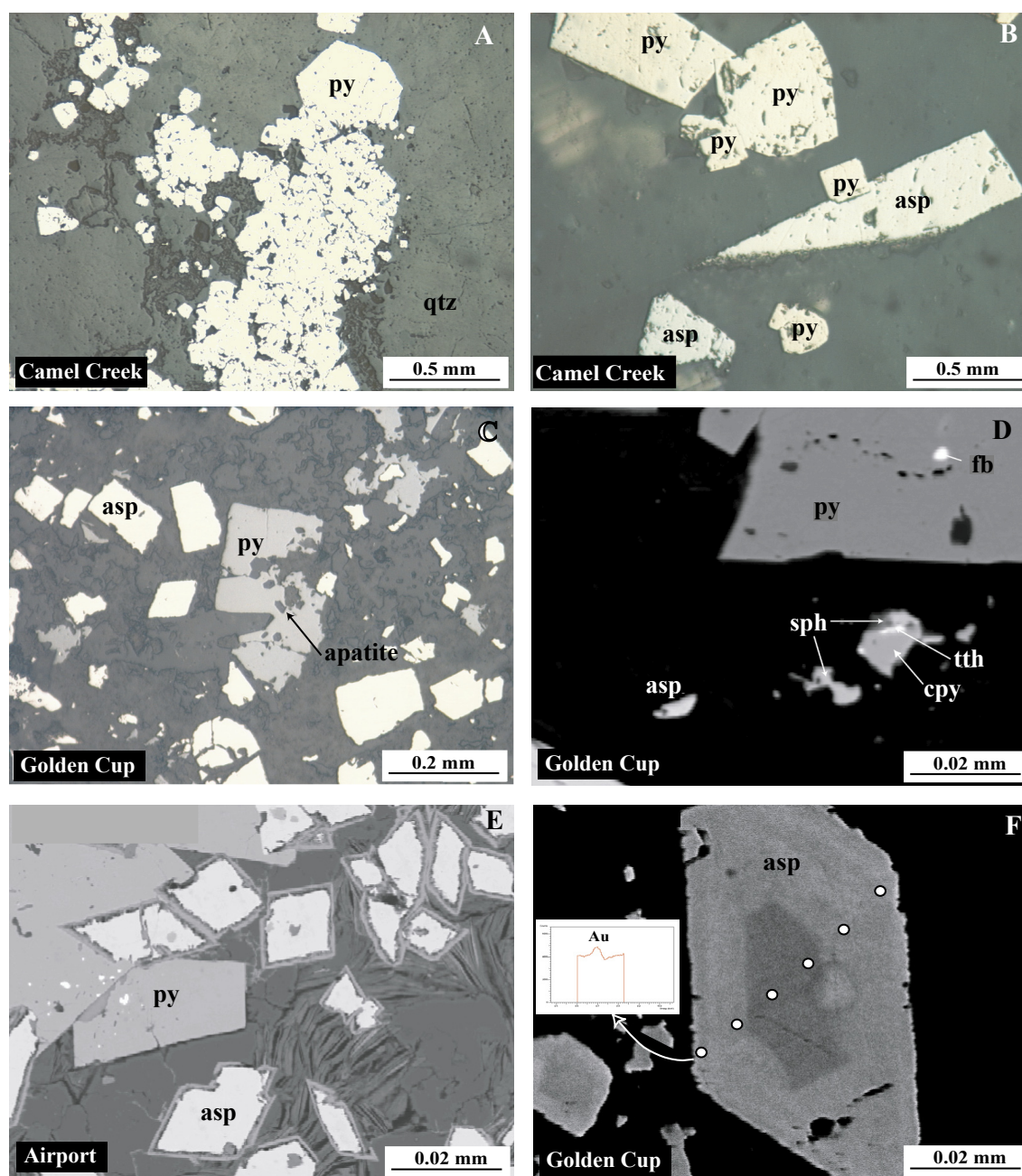


Fig. 2.14: Examples of sulphide associations from selected deposits in the Amanda Bel Goldfield. a) Photomicrograph (reflected light) of aggregates of framboidal pyrite filling fractures in quartz vein from the Camel Creek deposit; b) Photomicrograph (reflected light) of arsenopyrite-pyrite association in shales at the Camel Creek deposit; c) Photomicrograph (reflected light) of pyrite with apatite inclusions intergrown with arsenopyrite in quartz-rich shales from the Golden Cup deposit; d) SEM photomicrograph of complex sulphide mineralogy at Golden Cup deposit; tth=tetrahedrite, sph=sphalerite, fb=freibergite, cpy=chalcopyrite, py=pyrite, asp=arsenopyrite; e) SEM photomicrograph of typical scorodite-rimmed arsenopyrite (asp) intergrown with pyrite (py) in quartz-chlorite matrix from the Airport deposit; f) SEM photomicrograph of arsenopyrite grain from the Golden Cup deposit. Gold was detected at the rim of the grain as indicated by the Au α -peak in the inset for detection point at the arsenopyrite rim reflecting number of counts on the vertical axis and energy (keV) on the horizontal axis.

to around 11 weight percent silver.

The sulphide mineralogy in the Airport Gold deposit is dominated by pyrite and arsenopyrite. Arsenopyrite is generally oxidised and surrounded by a rim of scorodite (Fig. 2.14e). Pyrite inclusions can be found within arsenopyrite and vice versa. Minor inclusions of rutile, galena, apatite, white mica, zircon and gold are associated with both pyrite and arsenopyrite. Stibnite \pm gold \pm sphalerite assemblages occur mainly in boudinaged and in strongly deformed quartz veins, whereas later generations of less deformed veins remain barren. The location of the Airport gold deposit within the contact aureole of a nearby granitoid appears to have resulted in the exsolution of gold from arsenopyrite and pyrite (Cabri *et al.* 2000).

A representative portion of the microprobe analyses is summarised in Table 2.3. The results support the occurrence of two main mineralising episodes and one later mineralising episode (e.g. Teale *et al.* 1989; Tate *et al.* 1990; Vos *et al.* 2004). Gold was introduced late during the first mineralising episode associated with D_1 and is represented by minute free gold grains mostly associated with stibnite (Fig. 2.8). Minor amounts of gold can be found in solid solution within arsenopyrite, and in pyrite that is characterised by relatively elevated arsenic contents (Table 2.3; CC-line_1-7). Elevated amounts of antimony were detected in arsenopyrite (e.g. Table 2.3; Ap_3), where the elevated antimony reflects the occurrence of stibnite during the final stages of D_1 .

Gold deposited during the second mineralisation phase can mainly be found in solid solution within arsenopyrite. An example of the gold association with arsenopyrite is presented in

Figure 2.14f showing an SEM transect across an arsenopyrite grain from the Golden Cup deposit that detected elevated gold concentrations (represented by Au-peak in inset) at the rim of the grain. No detectable levels of gold were found in pyrite and no free gold or stibnite was observed in samples associated with this second phase of mineralisation.

The third phase of mineralisation is represented by a strong increase of antimony concentrations. Petrographic observations and microprobe analyses indicate that antimony is the dominant phase during this mineralising episode. Very little arsenopyrite and pyrite is found associated with this final stage. Stibnite grains associated with this phase of mineralisation are clearly distinguished as having formed late in the paragenetic history by their undeformed nature characteristic of open space growth. Minor amounts of gold have been detected within stibnite, usually in the close vicinity of visible gold grains.

2.5 FLUID INCLUSIONS

2.5.1 Analytical methods

Fluid inclusion analyses were carried out on a selection of vein quartz samples to determine the pressure, temperature and composition of mineralising fluids in the Amanda Bel Goldfield. Microthermometric measurements were conducted using the fully-automated Linkam THMSG 600 heating and freezing stage equipped with a TMS 93 temperature programmer at Geoscience Australia, Canberra. Measurements were collected from two-phase (liquid-vapour) fluid inclusions in mineralised quartz vein samples from the Camel Creek, Golden Cup and Red Gold deposits. Two types

Table 2.4: Summary of microthermometric data from fluid inclusions in the Amanda Bel Goldfield.						
Inclusion type	Analyses (n)	Tm ice (°)	Wt.% NaCl equivalent	Th total (°)	Vapour range (vol.%)	Size (microns)
i	19	-3.6 to -0.7	0.4 to 6.0	164 to 376	3 to 8	5 to 10
ii	83	-4.1 to 0.0	0.0 to 6.5	116 to 297	2 to 5	3 to 5

of primary inclusions could be distinguished (Table 2.4 and Figure 2.15) in all samples: (i) rare, isolated inclusions ranging from 5 to 10µm with between 3 to 8 volume% vapour, and (ii) abundant elongated and irregular inclusions ranging from 3 to 5µm with between 2 to 5 volume% vapour. In addition, Laser Raman spectra of fluid inclusions were recorded on a Dilor SuperLabram spectrometer at Geoscience Australia to qualitatively constrain the presence of volatile phases such as CO₂, CH₄ and N₂.

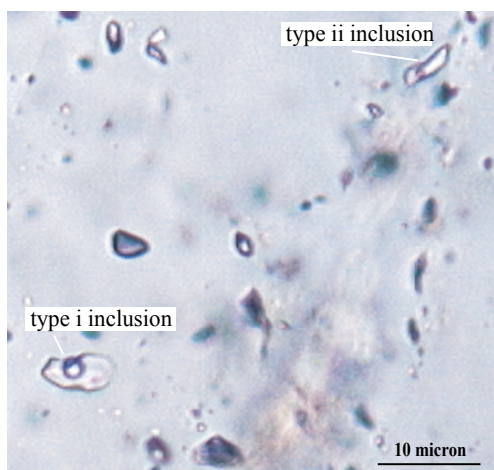


Fig. 2.15: Photomicrograph of representative fluid inclusions i and ii from the Golden Cup deposit. For discussion, see text.

2.5.2 Results

Microthermometric results from our fluid inclusion study are presented in Table 2.4 and Figure 2.16a and b. These indicate relatively low fluid salinities of up to 6.5 weight percent NaCl equivalent as determined from ice melting temperatures ranging between -4.1 and 0.0 °C (average -2.3 ± 0.3°C; n=82). Homogenisation temperatures range generally between

140 and 360°C (average 218 ± 52°C; n=70), and all inclusions homogenise into the liquid phase. After pressure correction (using a 35°C/km thermobaric gradient), this suggests minimum fluid trapping temperatures between 180 and 380°C (e.g. Roedder 1984). In turn, this implies that fluids were trapped at rather shallow crustal levels at pressures between

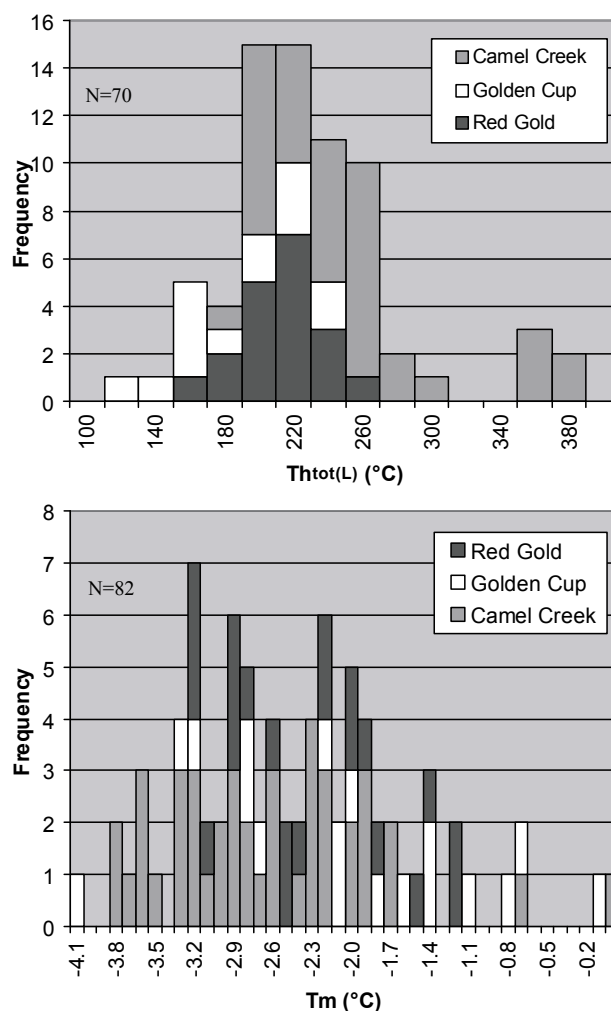


Fig. 2.16: a) Histogram of ice melting temperatures representing fluid salinity from primary aqueous fluid inclusions from the Golden Cup, Red Gold and Camel Creek deposits. N indicates number of measurements; b) Histogram of temperatures for homogenisation into liquid phase from primary aqueous fluid inclusions from the Golden Cup, Red Gold and Camel Creek deposits.

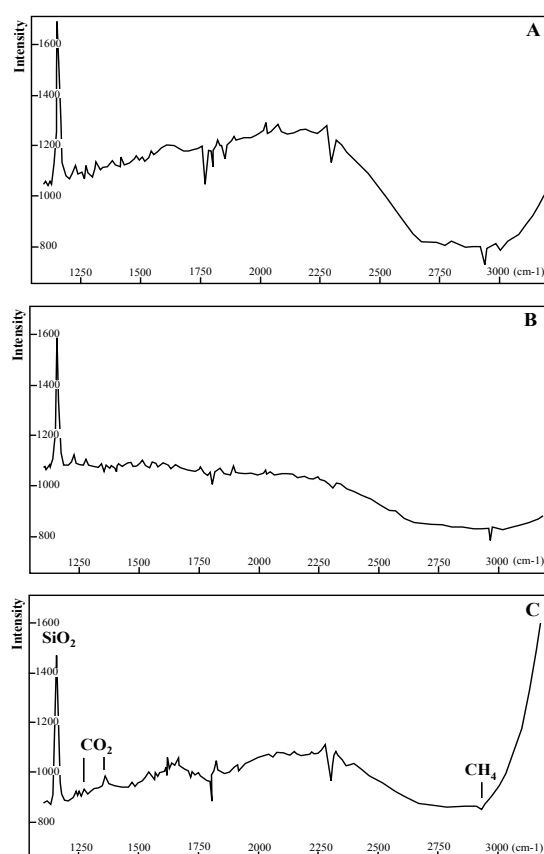


Fig. 2.17: Results from laser Raman spectroscopy indicating very minor levels of CO_2 and CH_4 (<5 vol.%) in fluid inclusions trapped in veins from deposits from the Amanda Bel Goldfield; a) type i aqueous inclusion, Camel Creek deposit; b) type ii aqueous inclusion Camel Creek deposit; c) type i aqueous inclusion, Golden Cup deposit. Position for peaks for volatile phases are indicated and applicable to Fig. 2.17a and b as well.

0.5 and 1 kbar (Goldstein & Reynolds 1994), which is consistent with our field observations (e.g. metamorphic grade, style of veining, relative timing of vein formation). Furthermore, the results indicate that salinities and homogenisation temperatures for fluids associated with $_{ab}D_1$ mineralisation (i.e. Camel Creek deposit) are slightly higher than those associated with $_{ab}D_2$ mineralisation (i.e. Red Gold and Golden Cup deposits). Results of Laser Raman spectroscopy are presented in Figure 2.17a-c. These suggest the presence of very small (i.e. <5 vol.%) concentrations of CO_2 based on very minor peaks in the laser Raman spectra.

2.6 DISCUSSION

2.6.1 Temporal framework for gold-forming episodes

Previous work undertaken by the Geological Survey of Queensland used stratigraphic relationships and conodont dating to construct a relative temporal framework for deformation in the Camel Creek Subprovince of the Broken River Province (see Table 2.1; Withnall *et al.* 1997). This stratigraphic framework constrained the timing of the three deformation phases as observed in the Amanda Bel Goldfield between the Early Devonian and the mid to Late Carboniferous. Withnall *et al.* (1997) stated that the ages of $_{cc}D_1$ and $_{cc}D_2$ are constrained by the early Devonian conodont age of the Kangaroo Hills Formation and the early Tournaisian age of the overlying basal Clarke River Group. These authors further mention that $_{cc}D_1$ is generally regarded to have occurred in the Early Devonian (~ 410 Ma) and could correlate with an apparent unconformity in the Graveyard Creek Subprovince between the Graveyard Creek Group and Shield Creek Formation. Subsequent $_{cc}D_2$ was considered Late Devonian (~ 370 Ma) by Withnall *et al.* (1997), where its upper limit was interpreted to be constrained by the weak angular unconformity in the Graveyard Creek Subprovince at the base of the Bundock Creek Group as well as an angular unconformity beneath the Clarke River Group. However, Withnall *et al.* (1997) could not rule out that $_{cc}D_1$ and $_{cc}D_2$ are separate phases of the same deformation event in the Late Devonian during which opening of a pull-apart basin (Bundock Creek Group deposition) may have been simultaneous with thrusting in the Camel Creek Subprovince and movement

on the Clarke River Fault.

Our field observations indicate a close relationship between deformation and mineralisation in the Amanda Bel Goldfield and further consolidate the findings of Teale *et al.* (1989) who assigned syn-_{cc}D₁, syn-_{cc}D₂ and syn-_{cc}D₃ ages to the mineralisation events, placing them in the Early Devonian, Late Devonian and mid to Late Carboniferous, respectively. The following observations strongly rule in favour of a three-stage mineralisation model: (1) the occurrence of folded ore lenses along a NE strike in the Camel Creek deposit suggests deposition during _{ab}D₁ and deformation of these lenses during _{ab}D₂ deformation; (2) the occurrence of gold as minute free grains associated with _{ab}D₁ and as invisible gold (solid solution in arsenopyrite and pyrite) associated with _{ab}D₂; (3) the distinctive undeformed, open-space growth of stibnite characteristic of a _{ab}D₃ mineralisation in contrast to the earlier deformed stibnite mineralisation. These observations collectively imply that gold in the Amanda Bel Goldfield was deposited at a relatively shallow crustal level and evolved from an early gold-stibnite-quartz stage to a stage in which Au-bearing arsenopyrite and minor pyrite was deposited. A final stage of stibnite-quartz ± gold veining dominated by open-space infill textures was associated with introduction of antimony ± gold-rich ore fluids.

2.6.2 Classification of deposit style

The results from our study indicate that the deposits in the Amanda Bel Goldfield can be classified as ‘orogenic’ gold deposits (Groves *et al.* 1998; Bierlein & Crowe 2000). The occurrence of two mineralising episodes that took place prior to major magmatic activity in

the Carboniferous and Permian suggests that mineralising fluids were not magmatic in origin. This notion is supported by the results from our fluid inclusion study that are compatible with mineralising fluids of metamorphic origin trapped at epizonal conditions. Ridley & Diamond (2000) illustrated that ore-bearing fluids in most orogenic gold deposits are dominated by low-salinity, mixed aqueous-carbonic fluid with low to moderate CO₂ contents. These authors stated that typically one or two fluid types can be recognised in meso- to epizonal orogenic gold deposits: a carbonic fluid with low H₂O content and a low-to moderate salinity, almost CO₂-‘free’, aqueous fluid. The fluids responsible for mineralisation in the Amanda Bel Goldfield fit the latter description. The close relationship between structurally-controlled mineralisation and deformation in an overall eastward younging fold-and-thrust belt further supports the orogenic nature of the gold deposits.

It is well recognised that the ore in orogenic gold systems is predominantly transported as a hydrosulphide complex (Seward 1973; Seward & Barnes 1997). Conditions of mineralisation in the Amanda Bel Goldfield are analogous to orogenic gold-antimony-dominated deposits in equivalent settings in eastern Australia and elsewhere that formed at low to moderate temperature (e.g. ~140-300°C) and low pressure (<1 kbar) and from minor CO₂-bearing fluids. Examples of similar epizonal type, Au ± Sb style of mineralisation in eastern Australia include Hillgrove (Ashley *et al.* 2000) and Fosterville (Zurkic 1998). Ashley *et al.* (2000) suggested that deposition of gold at Hillgrove may have been due to several factors including (a) temperature decrease, (b) rapid pressure

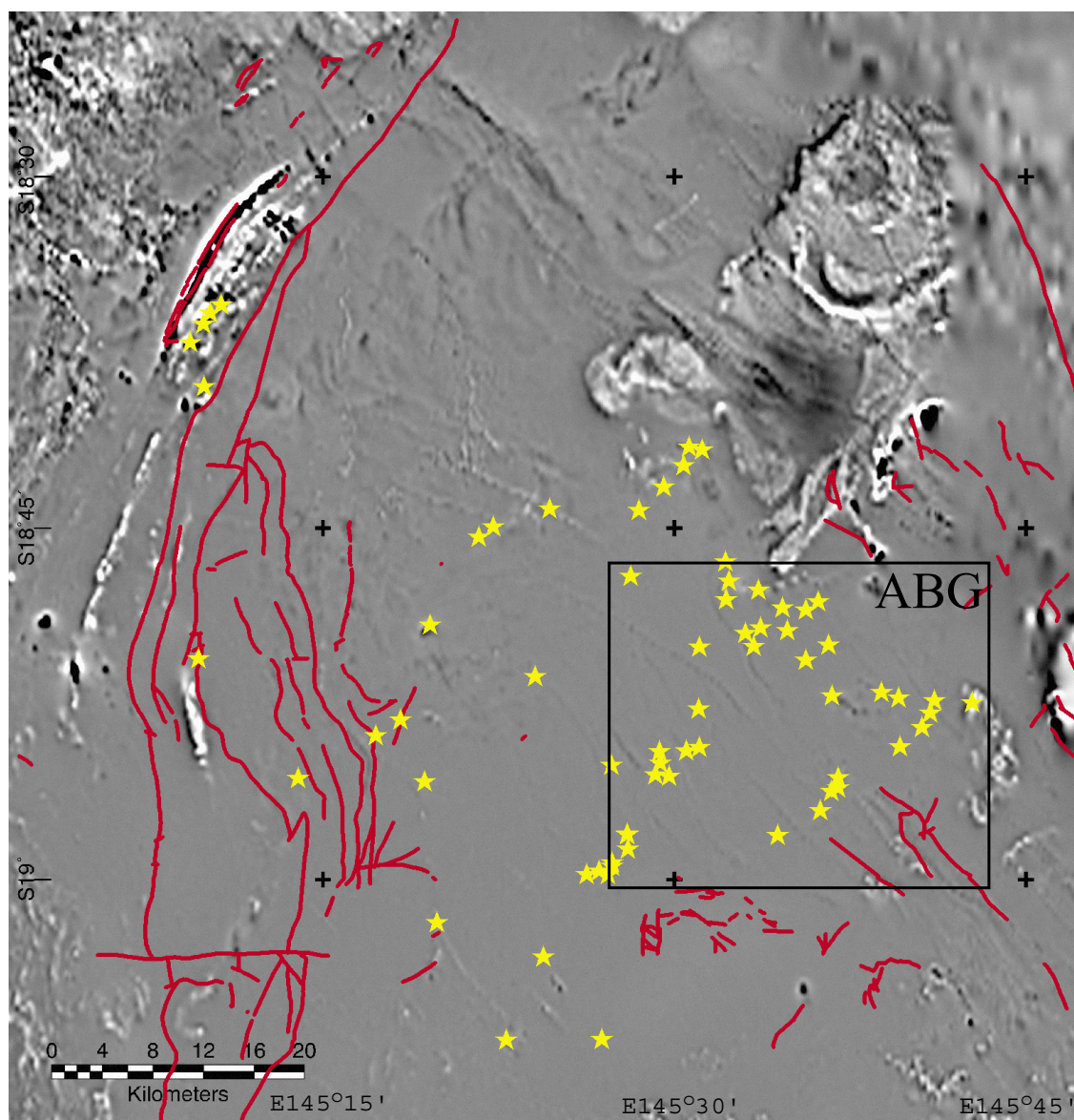


Fig. 2.18: Total magnetic intensity image of a portion of the Broken River Province illustrating the occurrence of the gold-antimony resources of the Amanda Bel Goldfield (ABG) away from recognised fault structures. The image approximately covers the upper right quadrant of Figure 2.1. Image constructed from Queensland Department of Natural resources and Mines data that was accessed from Geoscience Australia web databases.

decrease along fluid conduits caused by dilation during fault movement, resulting in fluid phase separation and mineral precipitation, (c) fluid mixing and (d) wall-rock carbonatisation and sulphidation. At Hillgrove, initial deposition of gold commonly occurred within arsenopyrite and pyrite, with minor deposition of sphalerite, chalcopyrite, galena and tetrahedrite (Ashley *et al.* 2000). The initial mineralisation at Hillgrove phase shows analogies with syn-_{ab}D₂

mineralisation (e.g. Golden Cup) in the Amanda Bel Goldfield. The second, most dominant phase of mineralisation at Hillgrove is characterised by quartz-stibnite-gold veins displaying open-space filling textures (Ashley & Craw, 2004). As such, this phase of mineralisation also shows analogies with syn-_{ab}D₃ mineralisation in the Amanda Bel Goldfield. The analogy between the gold deposits in the Amanda Bel Goldfield and at Hillgrove suggests that similar processes

could have controlled mineral deposition at both sites.

2.6.3 Structural control on mineralisation in the Amanda Bel Goldfield

In the central part of the Broken River Province, a close spatial association exists between gold deposits and major faults structures (e.g. Big Rush Au deposit; see Fig. 2.1 for location). However, the recognised gold occurrences in the Amanda Bel Goldfield appear to be located in areas without mapped fault structures. This notion is illustrated by a total magnetic intensity (TMI) image of a portion of the Broken River Province draped with known fault structures and gold occurrences (Fig. 2.18). The orogenic nature of the gold deposits and their alignment along distinct NE trends, however, almost postulate that the location of mineralisation is controlled by structural elements. Although no faults can be recognised in TMI images of the area, the distinct NE trend of the gold deposits follows the strike of the dominant D_2 upright folds and shear zones along the same orientation. We suggest that subsurface structures exist in the Amanda Bel Goldfield that may have provided the conduits for metal-bearing fluids during one or more mineralising episodes. The absence of lithological contrasts (potentially giving rise to magnetic gradients) as a result of a relatively monotonous turbidite stratigraphy together with the limited presence of exposed rocks in the study region may explain why such structures have not been documented previously. Recognition of these features implies the potential for the existence of gold deposits away from recognised fault structures elsewhere in the Palaeozoic of northeastern Queensland and provides a challenge for future

exploration in this region.

2.6.4 Significance for the (northern) Tasman Fold Belt System

Understanding the generation and origin of the Amanda Bel gold deposits is crucial to constraining the processes that controlled mineralisation in the northern part of the TFBS, and also allows comparison with analogous gold deposits elsewhere in the TFBS. Strong similarities of the Amanda Bel gold deposits exist with orogenic gold deposits in central Victoria (e.g. Fosterville), New South Wales (e.g. Hillgrove), and elsewhere in Queensland (e.g. Hodgkinson Goldfield). The orogenic nature of the gold deposits in the Amanda Bel Goldfield suggests that orogenic processes controlled their generation in the Devonian to Carboniferous and supports previously proposed tectonic models that have invoked the occurrence of subduction to the east of the province outboard of the Australian craton (e.g. Coney 1990). The widespread presence of turbidite deposits and reverse faults in an eastward younging fold-and-thrust belt associated with gold deposits in the Camel Creek Subprovince further substantiates the occurrence of subduction-related orogenic processes. Structural constraints, together with findings from our fluid inclusion study, imply an evolving three-stage mineral deposition sequence for deposits in the Amanda Bel Goldfield. Based on higher temperatures associated with syn- D_1 mineralisation compared to syn- D_2 mineralisation, as inferred from our fluid inclusion data (Fig. 2.16a), we propose that these episodes of gold mineralisation took place in decreasing temperature (and pressure) conditions. These

could potentially be inferred to represent uplift and exhumation associated with orogenesis in the Devonian and Carboniferous. Apart from a more protracted relative age range for the gold deposits in the Amanda Bel Goldfield, the three-stage evolution is similar to the evolution of the Hillgrove deposit, which has been related to orogenic uplift and subsequent exhumation in a collisional tectonic regime (Ashley *et al.* 2004). Gold deposits in the Hodgkinson Goldfield in the Hodgkinson Province north of the Broken River Province (Peters 1987b; Morrison 1988; Davis *et al.* 2002) also show strong similarities in terms of their nature and timing with the gold deposits in the Amanda Bel Goldfield and an analogous tectonic setting may potentially be inferred for both goldfields.

2.7 CONCLUSIONS

The Amanda Bel Goldfield in the Camel Creek Subprovince of the Broken River Province contains an array of vein/stockwork-hosted and disseminated, mesozonal to epizonal gold-antimony deposits that occur in lower-greenschist facies greywacke and shale assemblages. Three generations of gold-quartz vein assemblages can be closely linked to the structural history of the host rocks from the Early Devonian to Late Carboniferous. The first two are considered the main mineralising episodes, with the third episode the result of addition of antimony \pm gold-rich mineralising fluids. The earliest mineralising episode (i.e. Camel Creek and Airport deposits) occurred contemporaneously with $_{ab}D_1$ deformation associated with mesoscale, isoclinal recumbent folds. A second stage of mineralisation occurred contemporaneously with $_{ab}D_2$ deformation characterised by NE-SW striking upright folds.

This event is represented by the occurrence of gold in solid solution in sulphide phases (e.g. Golden Cup and Red Gold deposits). A third phase of mineralisation is dominated by the influx of antimony \pm gold-rich fluids (e.g. Blue Gold deposit) during a weak NW-SE deformation event ($_{ab}D_3$).

The formation of gold deposits in the Amanda Bel Goldfield is structurally controlled and it is postulated that sub-surface faults along a northeastern trend provided conduits for mineralising fluids. Together with this strong structural control, paragenetic relationships and the mesozonal to epizonal, low- to mid-temperature and metamorphic origin for mineralising fluids, an ‘orogenic’ style of gold deposition in the Amanda Bel Goldfield can be inferred.

The results from our study, in particular the strong structural control on mineralisation, have implications for the interpreted tectonic setting for the Camel Creek Subprovince during the genesis of the gold deposits. Subduction processes, outboard of the Australian craton, and associated orogenesis controlled the mineralisation in the Camel Creek Subprovince in the Devonian and Carboniferous. More research is needed to constrain the location and timing of subduction processes in the Camel Creek Subprovince and to compare these results with regions elsewhere in the northern part of the Tasman Fold Belt System.

ACKNOWLEDGEMENTS

Research has been funded by the Cooperative Research Centre for predictive mineral discovery (pmd*CRC) and this paper is published with the permission of the CEO, pmd*CRC. Field research was in part subsidised by a Newmont-

SEG student research grant. An International Postgraduate Research Scholarship from Monash University is gratefully acknowledged. Lynch Mining Pty Ltd is thanked for allowing access to mine sites in the Amanda Bel Goldfield. S. McKnight, T. Mernagh and A. Priymak are thanked for their support with the analytical work as part of this study, as is Werrie Gold Ltd for in-kind support. M. Barlow is acknowledged for valuable discussions on the geophysics of the study region. Support by P. Betts in constructing the image from geophysics is appreciated. We are grateful for constructive reviews by R. Henderson, S. Hagemann and I. Withnall as well as comments by G. Rosenbaum and M. Hannington.

REFERENCES

- ARNOLD G. O. & FAWCKNER J. F. 1980. The Broken River and Hodgkinson Provinces. In: Stephenson H. ed. *The geology and geophysics of northeastern Queensland*, pp. 175-189. James Cook University, Department of Geology, Townsville, Australia.
- ARNOLD G. O. & HENDERSON R. A. 1976. Lower Palaeozoic history of the southwestern Broken River Province, North Queensland. *Journal of the Geological Society of Australia* 23, 73-93.
- ASHLEY P. M. & CRAW D. 2004. Structural controls on hydrothermal alteration and gold-antimony mineralisation in the Hillgrove area, NSW, Australia. *Mineralium Deposita* 39, 223-239.
- ASHLEY P. M., CREAGH C. J. & RYAN C. G. 2000. Invisible gold in ore and mineral concentrates from the Hillgrove gold-antimony deposits, NSW, Australia. *Mineralium Deposita* 35, 285-301.
- BELL T. H. 1980. The deformation history of northeastern Queensland - a new framework. In: Stephenson H. ed. *The geology and geophysics of northeastern Queensland*, pp. 307-313. James Cook University, Department of Geology, Townsville, Australia.
- BIERLEIN F. P. & CROWE D. E. 2000. Phanerozoic orogenic lode gold deposits. *Reviews in Economic Geology* 13, 103-139.
- CABRI L. J., NEWVILLE M., GORDON R. A., CROZIER E. D., SUTTON S. R., MCMANON G. & JIANG D-T. 2000. Chemical speciation of gold in arsenopyrite. *The Canadian Mineralogist* 38, 1265-1281.
- CONEY P. J. 1990. The regional tectonics of the Tasman orogenic system, eastern Australia. *Journal of Structural Geology* 12, 519-543.
- DAVIS B. K., BELL C. C., LINDSAY M. & HENDERSON R. A. 2002. A single late orogenic episode of gold mineralization in the Hodgkinson Province, North Queensland, Australia. *Economic Geology* 97, 311-323.
- GOLDSTEIN R. H. & REYNOLDS T. J. 1994. Systematics of fluid inclusions in diagenetic minerals. *SEPM short course* 31, 199p.
- GROVES D. I., GOLDFARB R. J., GEBRE-MARIAM M., HAGEMANN S. G. & ROBERT F. 1998. Orogenic gold deposits; a proposed classification in the context of their crustal distribution and relationship to other gold deposit types. *Ore Geology Reviews* 13, 7-27.
- HENDERSON R. A. 1987. An oblique subduction and transform faulting model for the evolution of the Broken River Province, northern Tasman Orogenic System. *Australian Journal of Earth Sciences* 34, 237-249.
- MORRISON G. W. 1988. Palaeozoic gold deposits of northeastern Queensland. In: Morrison G. W. ed. *Epithermal and porphyry style gold deposits in North Queensland. Contributions of the Economic Geology Research Unit* 29, 11-21. James Cook University, Townsville.
- PETERS S. G. 1987a. Geology and lode controls of the Charters Towers Goldfield, North-eastern Queensland. *Contributions of the Economic Geology Research Unit* 19. James

- Cook University of North Queensland.
- PETERS S. G. 1987b. Geology, lode descriptions and mineralization of the Hodgkinson Goldfield, northeastern Queensland. *Contributions of the Economic Geology Research Unit* 20. James Cook University of North Queensland.
- RAMSAY W. R. H., BIERLEIN F. P., ARNE D. C. & VANDENBERG A. H. M. 1998. Turbidite-hosted gold deposits of Central Victoria, Australia: their regional setting, mineralising styles, and some genetic constraints. *Ore Geology Reviews* 13, 131-151.
- RIDLEY J. R. & DIAMOND L. W. 2000. Fluid chemistry of orogenic lode gold deposits and implications for genetic models. *Reviews in Economic Geology* 13, 141-162.
- ROEDDER E. 1984. Fluid inclusions. *Reviews in mineralogy* 12, p. 644. Mineralogical Society of America, Washington DC, United States.
- SEWARD T. M. 1973. Thio complexes of gold and the transport of gold in hydrothermal ore solutions. *Geochimica et Cosmochimica Acta* 37, 379-399.
- SEWARD T. M. & BARNES H. L. 1997. Metal transport by hydrothermal ore fields. In: Barnes H. L. ed. *Geochemistry of hydrothermal ore deposits*, pp. 435-486. Pennsylvania State University, Ore Deposits Research Section, University Park, United States.
- TATE N. M., MORRISON G. W., SEARSTON S. & COOPER R. 1990. Gold mineralisation in the Broken River Province, North Queensland. *AMIRA Gold Metallogenic Bulletin* 15, 1-65.
- TEALE G. S., PLUMRIDGE C. L., LYNCH J. E. & FORREST R. J. 1989. The Amanda Bel Goldfield: a significant new gold province. *North Queensland Gold '89 Conference*, Townsville, Australia, Australasian Institute of Mining and Metallurgy, 103-109.
- VOS I. M. A., BIERLEIN F. P. & TEALE G. S. 2004. Timing, nature and characteristics of orogenic gold deposits in the Broken River Province, NE Queensland, Australia. Australian Geological Convention, Hobart, *Geological Society of Australia Abstracts* 73, 133.
- WALSHE J. L., HEITHERSAY P. S. & MORRISON G. W. 1995. Toward an understanding of the metallogeny of the Tasman Fold Belt System. *Economic Geology* 90, 1382-1401.
- WITHNALL I. W. & LANG S. C. 1993. Geology of the Broken River Province, North Queensland. *Queensland Geology* 4. Department of Resource Industries, Queensland.
- WITHNALL I. W., LANG S. C., LAM J. S., DRAPER J. J., KNUTSON J., GRIMES K. G. & WELLMAN P. 1997. Clarke River region. In: Bain J. H. C. & Draper J. J. eds. *North Queensland geology*. Australian Geological Survey Organisation Bulletin 240, 327-364.
- ZURKIC N., 1998. Fosterville gold deposits. In: Berkman D. A. & Mackenzie D. H. eds. *Geology of Australian and Papua New Guinean mineral deposits* 22, pp. 507-510. Australasian Institute of Mining and Metallurgy, Melbourne.

CHARACTERISTICS OF OROGENIC GOLD DEPOSITS IN THE NORTHCOTE DISTRICT, HODGKINSON PROVINCE, NORTH QUEENSLAND, AUSTRALIA: IMPLICATIONS FOR TECTONIC EVOLUTION

I.M.A. Vos and F.P. Bierlein

Australian Journal of Earth Sciences, in press

ABSTRACT

We report results of metallogenic, structural, petrological and fluid inclusion studies that characterise the nature of gold mineralisation in the Northcote District of the Hodgkinson Goldfield, one of the major goldfields in the Palaeozoic Hodgkinson Province of northeastern Queensland, Australia. Gold-arsenic and gold-antimony-arsenic deposits in the Northcote District are spatially associated with distinctive northwest-trending faults and shear zones suggesting a strong structural control on their development during several phases of deformation in the Late Devonian to Carboniferous. Field evidence, as well as petrographic, scanning electron microscope and fluid inclusion analysis of mineralised samples, indicate the occurrence of two stages of gold genesis. Gold associated with the earlier of the two mineralising episodes exists mainly in solid solution with acicular arsenopyrite. SEM analysis indicated that minor sphalerite, galena and tetrahedrite formed during this episode of mineralisation. Gold deposited during the second mineralising episode has a strong association with antimony. Fluid inclusion studies of quartz veins samples record minimum homogenisation temperatures between 108° and 312°C, and salinities of up to 13 weight percent NaCl equivalent. Little to no difference in the nature of the fluids is observed between samples related to the two gold-forming stages. The style of gold mineralisation in the Northcote District is compatible with 'orogenic' gold deposits that form primarily during compressional and transpressional deformation along convergent plate margins. Our studies increased the understanding on the origin and nature of the deposits and can aid predictive mineral discovery elsewhere in the Hodgkinson Province as well as analogous terranes throughout the remainder of the Tasman Fold Belt System of eastern Australia.

3.1 INTRODUCTION

The Hodgkinson Province in northeastern Queensland, Australia, forms the northernmost part of the dominantly Palaeozoic Tasman Fold Belt System in eastern Australia (Fig. 3.1). The Hodgkinson Province hosts several gold-rich regions, which include the Palmer River, West Normanby and Hodgkinson goldfields. Together these fields have produced more than 45t of gold from alluvial and lode workings over approximately the last 150 years (e.g. Garrad & Bultitude 1999; for location see Fig. 3.1). Although various studies have focussed on the goldfields in the Hodgkinson Province in the past (e.g. Peters 1987; Morrison 1988; Peters 1987; Peters *et al.* 1990; Davis *et al.* 2002), the timing of gold mineralisation and the regional geodynamic framework remain contentious. In view of the geological similarities with analogous terrains elsewhere in the Tasman Fold Belt System and as reflected by renewed exploration interest in the province, there is a considerable likelihood for the presence of as yet undiscovered gold resources in the

Hodgkinson Province.

The Northcote District in the Hodgkinson Goldfield (Fig. 3.2) is host to several gold and gold-antimony deposits. Mining in the Northcote District commenced as early as 1877 (Garrad & Bultitude 1999) and has continued intermittently ever since, with ongoing exploration in this area. In this paper, we describe the characteristics, timing, structural control and style of gold mineralisation in the Northcote District of the Hodgkinson Goldfield. Fieldwork concentrated on several mine sites and resulted in the construction of a structural framework for mineralisation. Petrographic, Scanning Electron Microscope (SEM), electron microprobe and fluid inclusion studies were conducted to resolve the sulphide paragenesis, and the temperature and chemical composition of the mineralising fluids at the various deposits.

Understanding the genesis and origin of the gold deposits in the Northcote District can provide insight into the tectonic framework for gold mineralisation in the Hodgkinson Province

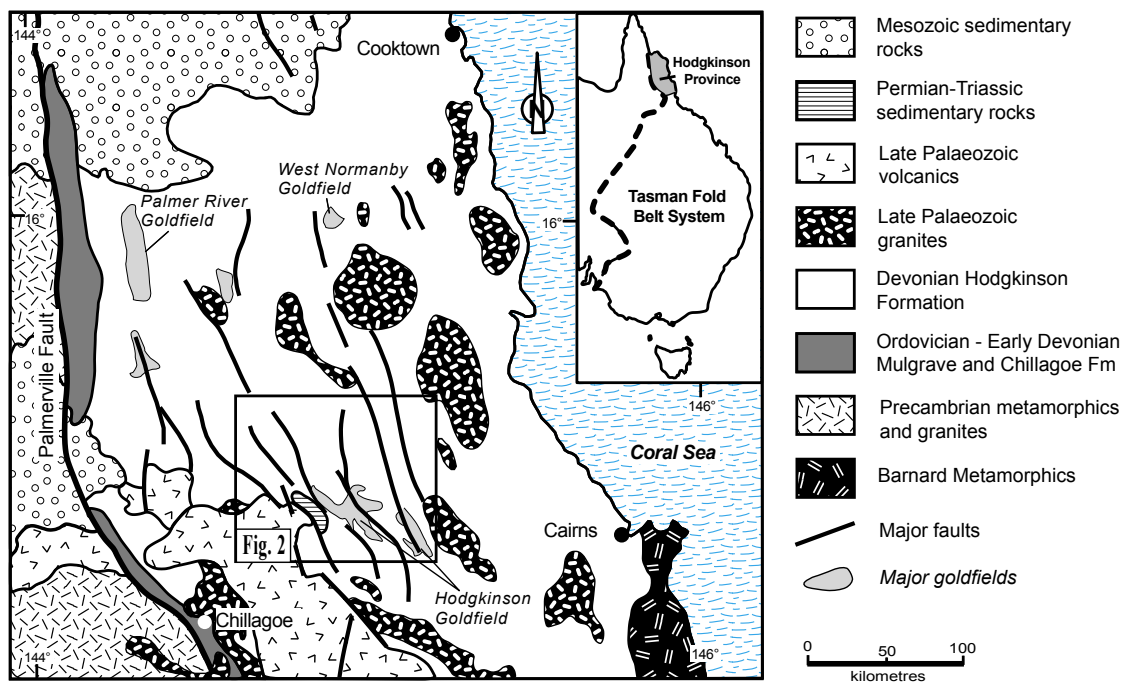


Fig. 3.1: General geology of the Palaeozoic Hodgkinson Province in northeastern Queensland, Australia.

and may provide an aid to future exploration in the province. Furthermore, the description of characteristics of gold deposits in the Northcote District allows for comparison with other gold deposits of similar association throughout the remainder of the Tasman Fold Belt System in Queensland (i.e. Amanda Bel Goldfield; Charters Towers Province) and elsewhere.

3.2 GEOLOGICAL SETTING

The Tasman Fold Belt System in eastern Australia forms a composite of predominantly Palaeozoic fold belts that have a closely interrelated tectonic evolution mostly

controlled by subduction-related processes that occurred outboard of the Australian craton (e.g. Veevers 1984; Coney *et al.* 1990). The Hodgkinson Province is situated in northeastern Queensland and, together with the Broken River Province to the south, forms the northern part of the Tasman Fold Belt System (Fig. 3.1). A comprehensive summary of the geology of the Hodgkinson Province is given in Bultitude *et al.* (1997). An overview of the geodynamic framework of the province that includes stratigraphy and main magmatic and tectonic events is compiled and presented in Figure 3.3.

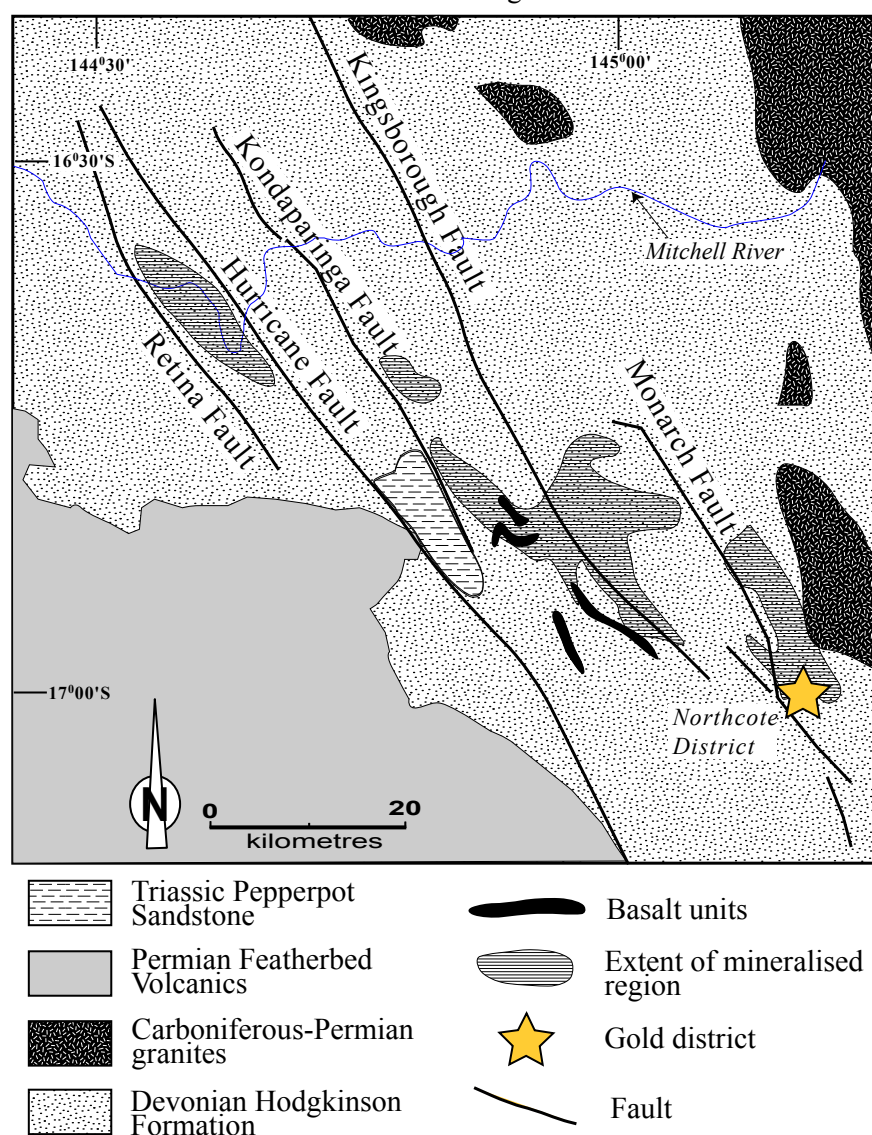


Fig. 3.2: Regional geology of the Hodgkinson Goldfield indicating the location of the Northcote District and outlining regional fault structures.

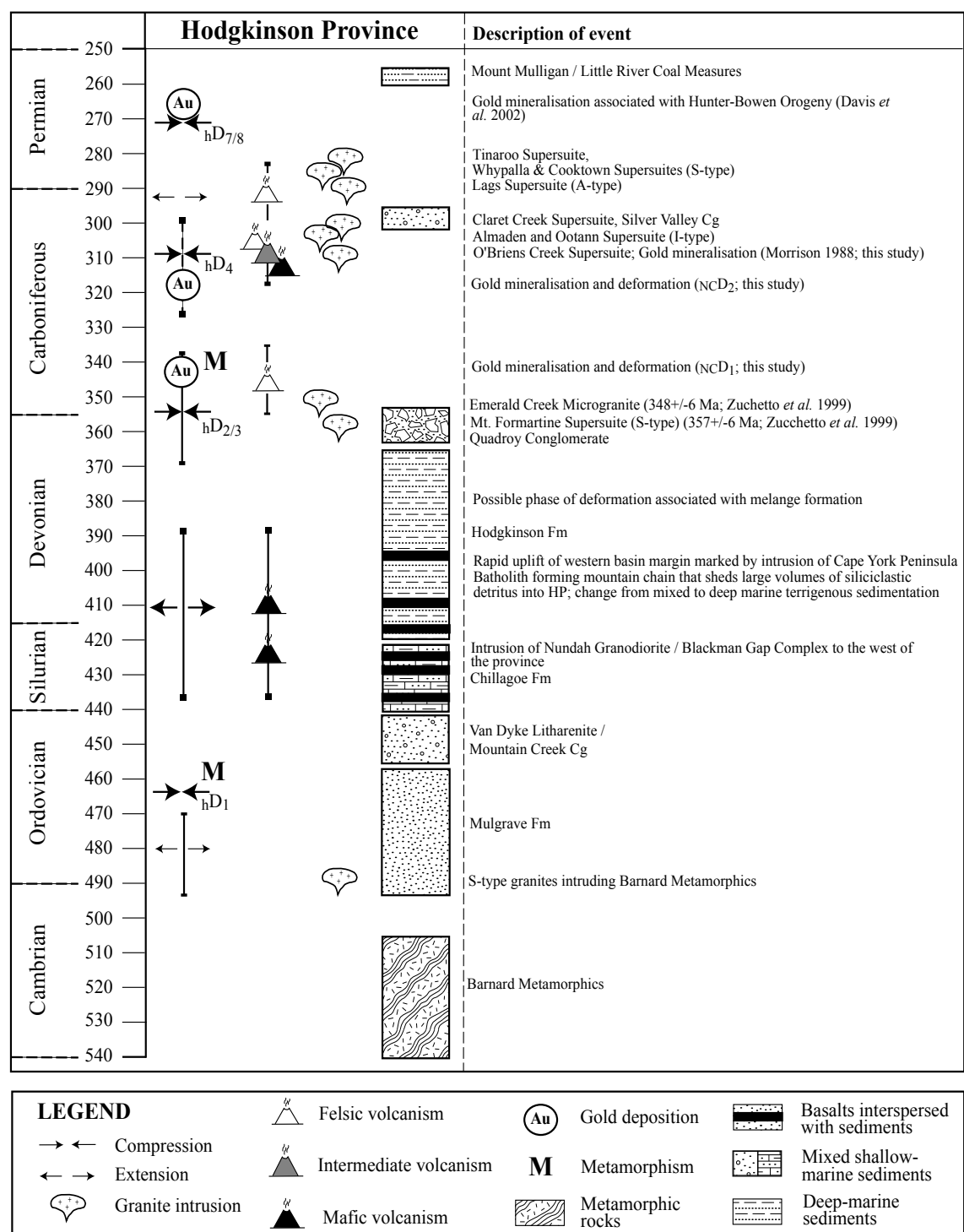


Fig. 3.3: Time-space diagram of Early Palaeozoic geological events across the Hodgkinson and directly adjacent provinces (compiled from Morrison 1988; Bultitude *et al.* 1997; Zuchetto *et al.* 1999; Davis *et al.* 2002).

In summary, the Hodgkinson Province is undergone mild, lower greenschist facies (chlorite zone) to upper greenschist facies (biotite zone) metamorphism (Bultitude *et al.* 1993; 1997). Numerous granites have intruded the stratigraphy during widespread magmatic activity in the province in the Late Ordovician to Late Devonian age. Rock sequences in the province have predominantly Carboniferous to Early Permian (Bultitude *et*



Fig. 3.4: Outcrop photograph of north-trending, isoclinal F_1 -fold in the Northcote District. These folds can be related to regional-scale D_2 deformation. Hammer for scale.

al. 1997), with minor magmatism possibly as early as 357 Ma (Zucchetto *et al.* 1999). The Palmerville Fault represents the main terrane-bounding structure that separates the province from the Precambrian Coen and Georgetown inliers (Bultitude *et al.* 1997; Vos *et al.* in review).

At least four deformation phases occurred during the evolution of the Hodgkinson Province (e.g. Bultitude *et al.* 1997). These resulted in the generation of a series of overprinting structures ranging from early isoclinal folds and *mélange* zones to later more open, steeply plunging folds and reverse faults. Deformation structures in the Hodgkinson Province have commonly formed co-planar to pre-existing ones and as a result produced regions that are characterised by composite cleavages and folds as well as multiply-reactivated fault structures (Davis *et al.* 2002). The deformed rock sequences of the Hodgkinson Province

now form a series of thrust packets that overall young eastward, but internally display westward younging (Bultitude *et al.* 1993, 1997). The complex structural relationships in the Hodgkinson Province have resulted in various interpretations on the nature and timing of deformation episodes within the province (Bultitude *et al.* 1997; Garrad & Bultitude 1999; Davis *et al.* 2002). These are illustrated in Table 3.1, which presents the characteristics of regional deformation events and relates these to the deformation events observed in the Northcote District. The first deformation event in the Northcote District (D_1) is characterised by thrusting together with the development of slaty cleavage and regional north- to northwest-trending, tight to isoclinal folds (Fig. 3.4) in the lower greenschist facies meta-sedimentary rocks of the Hodgkinson Formation (Figs. 3.2 and 3.5). Structural features associated with D_1 are characteristic of a Late Devonian – Early Carboniferous phase of regional deformation in the Hodgkinson Province ($D_{2/3}$; Table 3.1). Zucchetto *et al.* (1999) suggested that D_2 in the eastern Hodgkinson Province occurred prior to or contemporaneous with emplacement of the Mount Formartine Granite, for which these authors obtained an age of 357 ± 6 Ma from SHRIMP U-Pb analysis of zircon. The steepening and reactivation of fault zones and development of a weak slaty cleavage during a phase of sinistral transpression as evident from shear fabrics in the host rocks characterise the second deformation event in the Northcote District (D_2 ; Fig. 3.6). It is unclear whether this event correlates with the Early – middle Carboniferous regional D_4 event, or alternatively with the regional D_6 event (Table 3.1).

Table 3.1: Comparison of regional deformation history of the Hodgkinson Subprovince (HP) from several sources compared with locally observed deformation events in the Northcote District (NC).

HP	Deformation event				Orientation	Style	Fabrics	Age
	HP	HP	HP	NC				
	1	2	3	4				
hD1	hD1	D1			N	mesoscale folding	axial planar / slaty cleavage	middle? Ordovician
	hD2	D2			N-NW	isoclinal and open folding / thrusting	slaty cleavage	Late Devonian
	hD3	(D2)				shearing and faulting / melange zones	slaty and spaced solution cleavage	Late Devonian
hD2				ncD1		(similar to hD2 of Garrad & Bultitude, 1999 and Davis <i>et al.</i> 2002)		Late Devonian - early Carboniferous
hD3					N-NW	thrust reactivation and shearing	shear fabrics (s-c)	Early Carboniferous?
hD4	hD4			ncD2	N-NW	folding (chevron style / asymmetric)	fracture / slaty cleavage	Early - middle Carboniferous
hD5						doming (granite intrusion?)	differentiated crenulation cleavage	Early - middle Carboniferous?
hD6					E-W	minor small-scale folding	spaced crenulation / fracture cleavage	Middle Carboniferous
	hD5					(similar to hD5 of Bultitude <i>et al.</i> 1997)		Early Permian?
	hD6	D3				(similar to hD6 of Bultitude <i>et al.</i> 1997)		Early Permian?
	hD7				N	mesoscopic open to kink folding	slaty cleavage and foliation	Early Permian?
hD7		D4			N-NW	shearing and kink folding	differentiated crenulation cleavage	Late Permian - Early Triassic
	hD8				N-NW	shearing	slaty cleavage and foliation	Late Permian - Triassic

¹ Bultitude *et al.* 1997

² Garrad & Bultitude 1999

³ Davis *et al.* 2002

⁴ Vos and Bierlein, this study

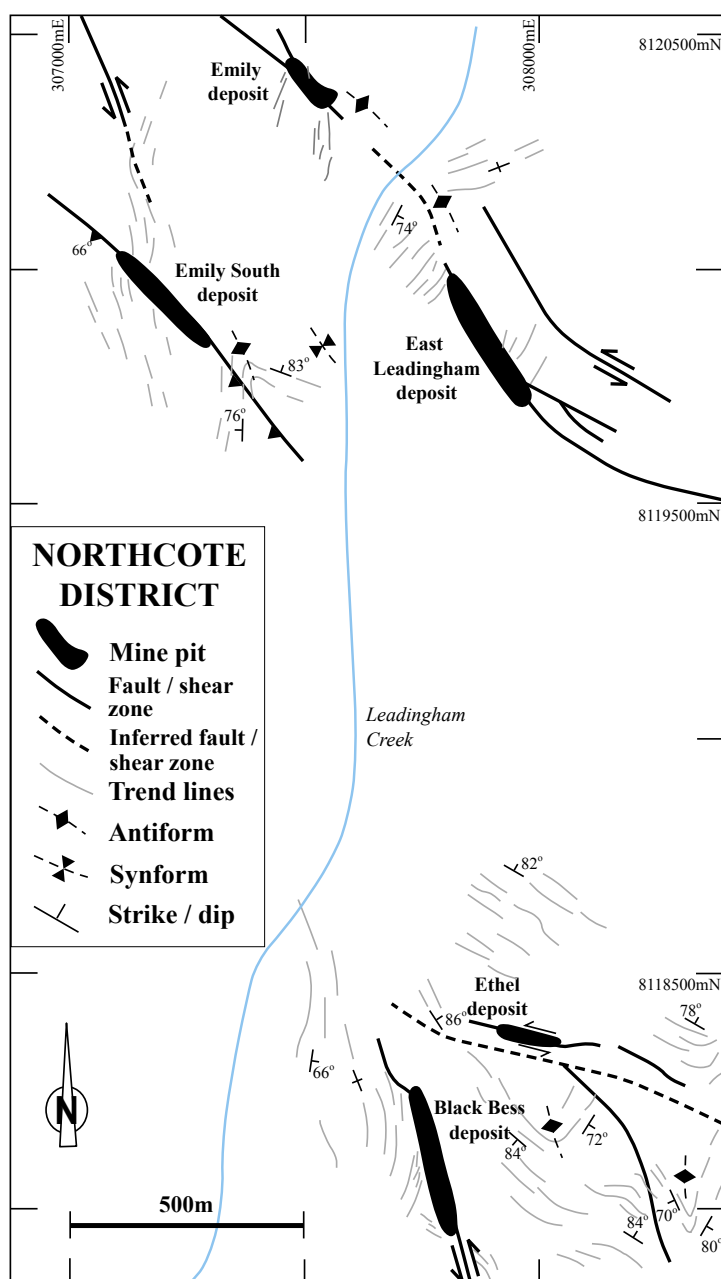


Fig. 3.5: Local geology of the Northcote District indicating location and structural make-up of known gold-antimony deposits. All deposits are hosted by strongly-folded Hodgkinson Formation sedimentary rocks.

3.3 GOLD ± ANTIMONY DEPOSITS IN THE NORTHCOTE DISTRICT

The Northcote District is part of the Hodgkinson Goldfield and is situated in the central south of the Hodgkinson Province. The Hodgkinson Goldfield further includes the Beaconsfield, Union, Thornborough and Kingsborough Districts. The Northcote District contains numerous gold and gold-antimony deposits from which a total gold reserve of ~244,000t (5.76g/t; Garrad & Bultitude 1999) has been determined. The deposits generally comprise several up to 1m wide, steeply-dipping, sulphide-poor quartz veins that contain silicified sulphide-bearing arenite fragments. The deposits generally strike northwest and are closely associated with northwest-trending shear and fault zones. These zones are parallel to and laterally connect with regional-scale shear and fault zones that show evidence for multiple

Table 3.2: Summary of deposit location, sulfide mineralogy and production. Production figures from Republic Gold Ltd. Annual Report 2004.

	Locality (UTM)	Sulfide mineralogy	Host lithology	Au production (t)
Emily	307919 8119540	Sph, Py, Aspy, Au, Sb, Gl	sst / slt / sh	21310
East Leadingham	307250 8120000	Sph, Py, Aspy, Au, Sb	sst / slt / sh	17844
Ethel	308140 8118421	Py, Aspy, Au, Sb	sst / slt	6338
Black Bess	307843 8118217	Py, Aspy, Au, Sb, Tth	sst / slt / sh	32714

Abbreviations: Tth = tetrahedrite; Aspy = arsenopyrite; Py = pyrite; Au = gold; Sph = sphalerite; Gl = galena; ; Sb = stibnite; sst/slt/sh = sandstone/siltstone/shale.

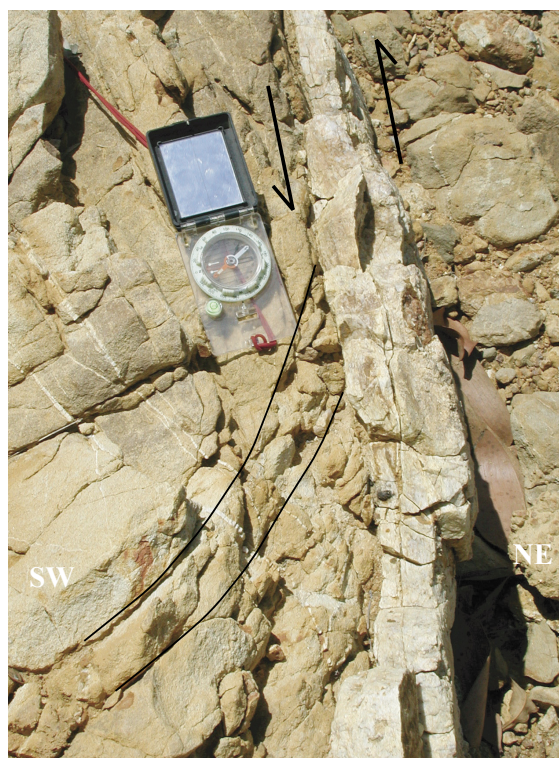


Fig. 3.6: Outcrop photograph (plan view) of NW-striking, silicified, sinistral shear in the Emily deposit crosscutting the ore zone and therefore related to $_{NC}D_2$. Lines represent fault drag. Compass for scale.



Fig. 3.7: Mineralised laminated quartz veins in drillcore from the Emily deposit.

episodes of deformation (Garrad & Bultitude 1999). Peters (1987) and Peters *et al.* (1990) showed that gold - antimony - bearing quartz veins in the Hodgkinson Goldfield are generally discontinuous with well-developed pinch and swell structures and commonly truncate gold-bearing quartz veins. Quartz veins in the Northcote District comprise a complex mixture of gouge and include abundant laminations, stylolites and clear quartz veinlets that show evidence of incremental quartz deposition (Garrad & Bultitude 1999; Fig. 3.7). Garrad & Bultitude (1999) reported that laminations of country rock and associated sulphides within quartz veins are commonly associated with higher gold grades. Poorly developed sericitic and argillic alteration selvages up to a few centimetres wide are associated with individual quartz veins, while locally ore zones may be accompanied by a sericite / ankerite alteration haloes that can extend for up to 2 m into the host rocks.

3.4 FIELD INVESTIGATIONS IN THE NORTHCOTE DISTRICT

Field investigations were conducted at the Emily, Ethel and Black Bess deposits (Fig. 3.5). Due to the removal of the primary ore zones at these sites, additional observations to determine metallogenic relationships were derived from analysis of core samples (courtesy of Republic Gold Ltd). The main characteristics of the studied gold deposits in the Northcote District are outlined below and summarised in Table 3.2.

3.4.1 Emily deposit

The Emily deposit consists of a number of northwest-trending gold-bearing lode structures including the Emily, Emily South and East Leasingham mineralised zones. The ore

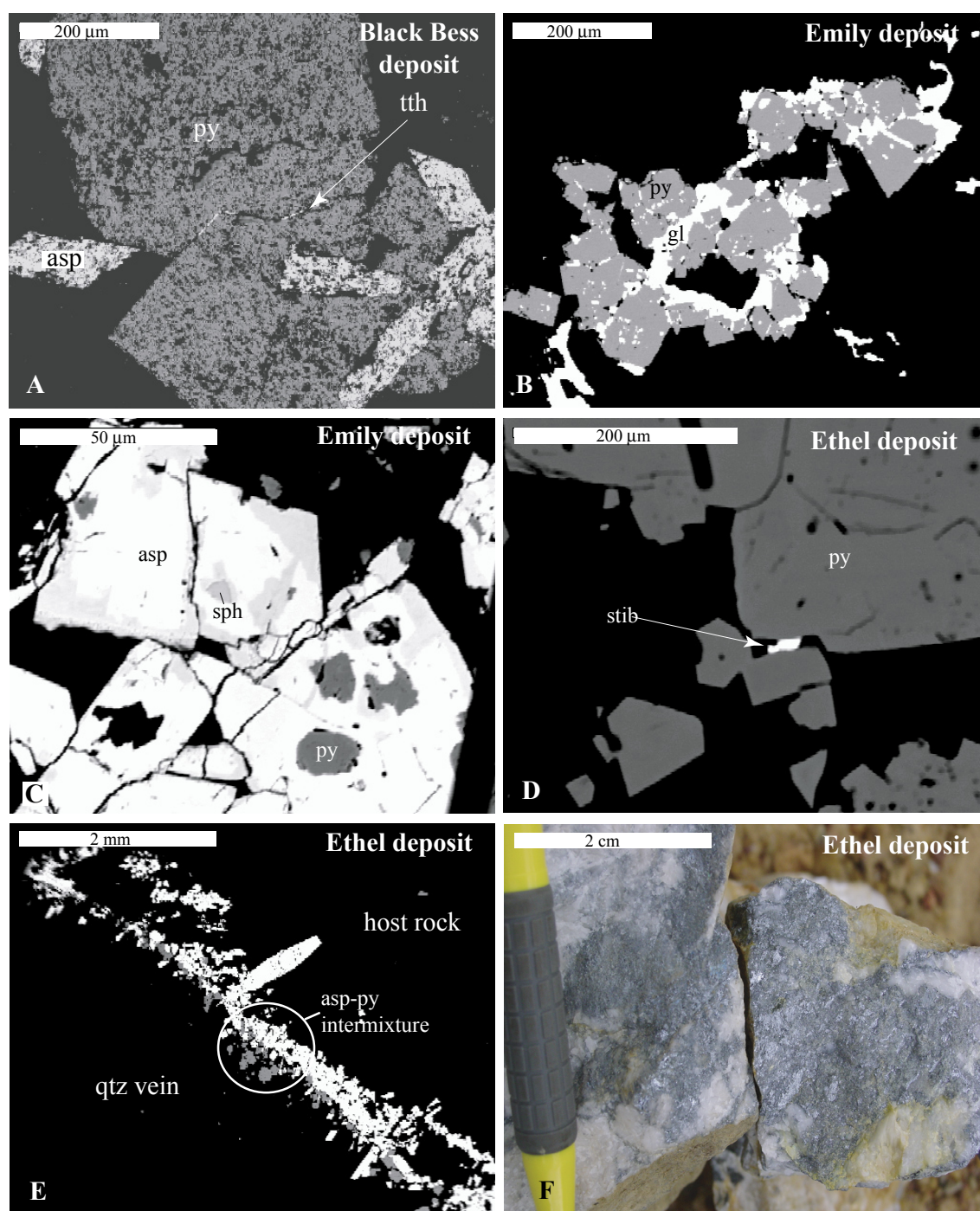


Fig. 3.8: Examples of sulphide associations in selected gold deposits in the Northcote District. A) SEM photomicrograph of pyrite and arsenopyrite intergrowth at the Black Bess deposit. Note tetrahedrite along crack in pyrite; B) SEM photomicrograph of pyrite and galena intergrowth at the Emily deposit; C) SEM photomicrograph of arsenopyrite, pyrite and sphalerite sulphide association in the Emily deposit; D) SEM photomicrograph of minor stibnite grain post-dating pyrite growth in the Ethel deposit; E) SEM photomicrograph of arsenopyrite-pyrite intermixture at the interface between quartz vein and host rock in the Ethel deposit; F) Stibnite-rich quartz vein sample from the Ethel deposit. Abbreviations: tth=tetrahedrite, sph=sphalerite, gl= galena, py=pyrite, asp=arsenopyrite.

zone can be up to several metres wide and is controlled by west-dipping, undulating fault and shear planes that are most probably associated with $_{NC}D_1$ as they are generally parallel to $_{NC}S_1$

foliation in the host rocks. Mineralisation comprises of arsenopyrite - pyrite \pm sphalerite \pm galena-bearing, laminated quartz veins (Figs. 3.7 and 3.8BC) and breccias in isoclinally

folded, subvertically dipping arkosic sandstones, micaceous siltstones and minor shales. Antimony mineralisation occurs as lenses within and along the margins of up to 1m wide brecciated quartz veins. A rhyodacite dyke cuts the gold-quartz veins in the Emily deposit. This dyke has been hydrothermally altered and brecciated, and contains antimony mineralisation, indicating that gold-antimony quartz veins post-date gold-quartz veins (Garrad & Bultitude 1999).

3.4.2 Ethel deposit

The Ethel deposit is situated ~1.5km south of the Emily deposit and consists of multiple quartz-breccia veins that together form an up to several metres wide ore zone. The veins are associated with a WNW-ESE trending, steeply SSW-dipping anastomosing shear plane that crosscuts dominantly NW-trending, upright arenites and siltstones. The quartz-breccia veins are characterised by sericitised arsenopyrite- and pyrite-rich sandstone fragments in a quartz matrix (Fig. 3.8E). Sinistral dragging of $_{NC}S_1$ foliation in the host rocks is noted along the main shear plane. Pods and lenses of stibnite occur within the quartz-breccia lodes (Fig. 3.8F).

3.4.3 Black Bess deposit

Mineralisation in the Black Bess deposit is hosted by a NW-SE trending, southwest-dipping reverse fault zone that truncates immature arenaceous sedimentary rocks. An up to 5m wide fault breccia hosts pyrite- and arsenopyrite-bearing quartz clasts in a sericitised pyrite - arsenopyrite \pm tetrahedrite-bearing host rock


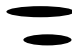





Deposit	Minerals	D ₁	D ₂
Emily	Sphalerite Pyrite Arsenopyrite Gold		
Black Bess	Pyrite Arsenopyrite Gold Tetrahedrite		
Leading-ham Creek	Pyrite Arsenopyrite Stibnite Gold		
Ethel	Pyrite Arsenopyrite Stibnite Gold		

Fig. 3.9: Generalised ore paragenetic sequence for selected deposits in the Northcote District of the Hodgkinson Goldfield. D₁ and D₂ refer to local deformation episodes in the Northcote District ($_{NC}D$ in Table 3.1).

assemblage. Minor undeformed quartz stibnite veins truncate the quartz-breccia veins.

3.5 SULPHIDE PARAGENESIS

3.5.1 Sampling methods and analytical techniques

Ore-bearing rocks in the studied deposits have been largely oxidised as a result of weathering (locally reaching depths up to 30 m). Nonetheless, unweathered ore-rich samples have been obtained from mine dumps and exploration drillcore. Around 30 polished thin sections have been examined petrographically and 10 thin sections were analysed by SEM (JEOL 6300) at the Department of Geology and Metallurgy, University of Ballarat. Energy-dispersive spectra were obtained operating at 15kV and a beam current of approximately 1nA using an Oxford Instruments Link UTW Si detector. Wavelength-dispersive spectra and maps (AuLa) were obtained operating at 30kV and a beam current of approximately 600vA using a Microspec WDX 3PC spectrometer.

Sulphide phases from selected samples were analysed for significant major and trace elements using a CAMECA SX50 electron microprobe with 4 WDS spectrometers at the School of Earth Sciences, University of Melbourne. Instrument settings used were voltage of 20 kV, beam current of 20 nA, a sharply focused probe, and counting times of 30 seconds.

3.5.2 Results

Petrographic, SEM and electron microprobe analyses of mineralised quartz vein samples and adjacent wallrock allowed determination of the sulphide paragenesis in the gold-antimony deposits in the Northcote District. The paragenetic sequence of mineralisation in each of the deposits is summarised in Figure 3.9. Based on paragenetic relationships, gold mineralisation in the Northcote District can be divided into two episodes. The first episode is characterised by relatively simple vein-hosted sulphide assemblages consisting of pyrite and arsenopyrite with minor galena, sphalerite and tetrahedrite (Fig. 3.8BC). In addition, intergrown pyrite and acicular arsenopyrite can be found disseminated in the sedimentary host rocks (Fig. 3.8A) that occur peripheral to zones of quartz veining and as fragments within the quartz veins. The second episode is dominated by stibnite pods and lenses (Fig. 3.8F) with minor arsenopyrite that contain minor gold and can be found intermingled with brecciated quartz.

A representative portion of the microprobe analyses is summarised in Table 3.3 and supports the occurrence of two distinct gold mineralising episodes. Gold introduced during the first mineralising episode can generally be found in solid solution with acicular arsenopyrite (e.g. EY_line_1-1; Table 3.3) and less commonly

with disseminated pyrite that is characterised by reduced sulphur concentrations (e.g. EY_line_2_1; Table 3.3). Pyrite occasionally may have detectable concentrations of silver (e.g. EY_3; Table 3.3). The second phase of mineralisation is characterised by high antimony concentrations. Gold has been detected within stibnite (EY_line_2; Table 3.3), which commonly occurs along the margins of quartz veins. Minor arsenopyrite overprinted by stibnite is found associated with this second stage. The extent of alteration and the characteristics of mineralisation at the Ethel deposits have been further investigated through geochemical analysis of samples collected from exploration drill core EL003 carried out by Republic Gold Ltd. in 2003-2004. This drill core intersects the ore-hosting structure, and samples from the footwall, ore zone and hanging-wall were selected to investigate the alteration characteristics associated with mineralisation. Results from this geochemical analysis are presented in Table 3.4 and Figure 3.10. These indicate that high gold concentrations in the mineralised samples correlate with high arsenic concentrations. The elevated gold concentrations in these samples are likely to reflect invisible gold in solid solution with arsenopyrite in host rocks that occur peripheral to quartz veins and as fragments incorporated in the veins. Furthermore, visible native gold grains are associated with stibnite-rich vein material that is related to the second episode of mineralisation.

Figure 3.10 illustrates that the fault-related character of the ore-zone in the Emily deposit resulted in the generation of a narrow hydrothermal alteration envelope in the host rocks. In addition, lithological control on element variation is observed, in particular in the case of shale units that are found intercalated

Table 3.3: Chemical analyses (electron microprobe WDS) of representative pyrite and arsenopyrite from selected deposits in the Northcote District, Hodgkinson Goldfield. Except where otherwise indicated, concentrations are in ppm. Blanks represent analyses below detection limit. Abbreviations: EY = Emily deposit, SEY = Emily South deposit, EL = Ethel deposit.; Py = Pyrite, Asp = Arsenopyrite.

Analysis no.	Mineral	S wt%	Fe wt%	As wt%	Sb wt%	Au	Ag	Co	Ni
EY_line_1-1	Asp	19.4	34.5	46.2		2423			
EY_line_1-2	Asp	18.7	34.7	47.2					
EY_line_1-3	Asp	19.1	34.8	46.9					
EY_line_1-4	Asp	18.5	33.3	46.6					
EY_line_1-5	Asp	18.4	34.4	48.1					
EY_line_1-6	Asp	18.6	34.4	47					
EY_line_1-7	Asp	18.5	34.4	47.1		2197			
EY_line_1-8	Asp	19.7	35.2	45.4		2322			
EY_line_1-9	Asp	18.9	34.5	46.6					
EY_line_1-10	Asp	18.5	34.4	48.3		1226			
EY_line_1-11	Asp	29.2	4.4	7.4					
EY_line_1-12	Asp	19.6	34.7	45.3					1456
EY_line_1-13	Asp	18.8	34.3	46.9					
EY_1	Py	52	46						
EY_2	Py	52.8	45.9						
EY_3	Py	51.9	45.9				1063		
EY_4	Py	51.9	45.6						
EY_line_2-1	Py	48.3	41.4			1322			
EY_line_2-2	Py	51.1	45.4						
EY_line_2-3	Py	50.4	45.1						
EY_line_2-4	Py	51.4	45.7						1714
EY_line_2-5	Stib	28.5	0		71.4	2241			
EY_line_2-6	Stib	28.1	0		72.1				
EY_line_2-7	Stib	26.6	0.1		69.3				
EY_line_2-8	Stib	27.7	0		71.9				
EY_line_2-9	Stib	28.4	0		71.6				
EY_line_2-10	Stib	27.9	0		72.1	1721			
EY_line_2-11	Stib	28.6	0		72.6	2383			
EY_line_2-12	Stib	27.8	0		72.1				
SEY_1	Asp	18.2	33	47.7					
SEY_2	Stib	27.9	0		71.7				
EL_1	Asp	19.2	34.8	46.3					1465
EL_2	Asp	19.6	35	45.6					
EL_3	Asp	17.7	29.1	44.1					
EL_4	Asp	18	34.5	47.6					

Table 3.4: Results of geochemical analysis of part of drillcore from the Ethel deposit

from (m)				66.4	76.5	81.35	86.7	88.75	90.65	93	105.8	106.55
to (m)				66.7	76.8	81.65	87	89.05	90.95	105.8	106.5	106.8
lithology				SST	SST	SST	SST	SST	INT	MIN	SST	SST
qtz veining				1%	1%	1%				2-5%	1%	1%
ore (py / asp)								trace	trace	1-2%	1-2%	
	units	method	DL									
SiO2	%	IC4	0.01	71.5	72	72.2	67.9	71.9	72	60.6	74	74
TiO2	%	IC4	0.005	0.5	0.6	0.5	0.5	0.5	0.6	0.8	0.5	0.6
Al2O3	%	IC4	0.01	11.4	12.3	11.2	12	12.5	12.4	17.7	10.5	10.9
Fe2O3	%	IC4	0.01	3.3	3.8	4.3	3.2	3.7	4.3	6.4	3.1	3.4
MgO	%	IC4	0.01	1.2	1.3	1.3	1.5	1.4	1.6	1.7	0.9	1.1
MnO	%	IC4	0.01	0.1	0.1	0.1	0.1	0.1	0.1	0.1	0.1	0.1
CaO	%	IC4	0.01	2.4	1.4	1.7	3.7	1.3	1.1	0.9	1.6	1.6
Na2O	%	IC4	0.01	1.8	2.5	2.1	1.3	1	0.1	0.1	0.1	0.1
K2O	%	IC4	0.01	2.3	2.8	2.3	2.7	2.7	3	4.9	2.7	2.7
P2O5	%	IC4	0.01	0.1	0.1	0.1	0.1	0.1	0.1	0.1	0.1	0.1
LOI	%	GRAV7	0.01	4.9	3	3.9	7	4.3	4.2	6.3	4.6	4.8
Cu	ppm	IC3E	2	13	24	17	26	23	18	46	7	17
Ni	ppm	IC3E	2	15	18	14	18	19	19	42	15	16
Pb	ppm	IC3E	5	24	22	20	20	28	26	28	18	14
Zn	ppm	IC3E	2	54	62	52	62	70	60	115	46	54
Sb	ppm	NAA	0.2	25	17	15	29	60	35	80	4600	43
As	ppm	NAA	1	17	5	7	16	61	101	429	1840	1670
Ba	ppm	NAA	100	353	492	198	279	249	262	549	300	269
Ce	ppm	NAA	2	79	101	65	77	73	94	99	64	89
Cs	ppm	NAA	1	7	9	6	10	9	9	19	bdl	10
Cr	ppm	NAA	5	74	48	91	47	51	105	72	108	46
Co	ppm	NAA	1	7	9	7	9	9	9	15	3	8
Eu	ppm	NAA	0.5	1	1	1	1	1	1	1	bdl	1
Au	ppb	NAA	5	bdl	33	bdl	34	43	24	171	1200	1580
Hf	ppm	NAA	0.5	6	8	5	5	6	8	6	bdl	7
La	ppm	NAA	0.5	40	51	33	38	38	49	51	33	46
Rb	ppm	NAA	20	120	120	100	156	148	179	283	134	123
Sm	ppm	NAA	0.2	6	7	5	6	5	7	8	5	7
Sc	ppm	NAA	0.1	9	10	9	10	10	10	17	7	9
Th	ppm	NAA	0.5	17	20	14	16	16	24	22	16	21
W	ppm	NAA	2	4	bdl	bdl	3	7	7	12	8	12
U	ppm	NAA	2	4	4	2	4	3	6	5	bdl	4
Yb	ppm	NAA	0.5	3	3	3	3	3	4	4	bdl	3
V	ppm	IC4	20	50	60	50	50	50	60	90	40	40
Ga	ppm	IC4M	1	15	16	13	14	16	14	23	11	12
Sr	ppm	IC4M	5	120	135	92	135	86	70	72	100	110
Y	ppm	IC4M	1	22	27	22	27	23	31	33	24	28
Zr	ppm	IC4M	15	210	240	170	190	200	280	220	190	220

Table 3.4 (continued)

from (m)				108.7	112.5	114.1	116	121	126.05	131	147.65	155.25
to (m)				109	112.75	114.85	116.3	121.25	126.4	131.3	147.95	155.55
lithology				SST	SST	SST	SST	SST	SHL	SST	SST	SHL
qtz veining					<1%	1%				2%	1%	
ore (py / asp)									trace	trace		
	units	method	DL									
SiO ₂	%	IC4	0.01	70.6	65.7	77.2	70.6	67.1	64.2	72	73.1	74.4
TiO ₂	%	IC4	0.005	0.4	0.7	0.4	0.5	0.6	0.5	0.5	0.6	0.5
Al ₂ O ₃	%	IC4	0.01	12.1	14.6	10.2	12.3	15.1	17	11.6	10.4	11.9
Fe ₂ O ₃	%	IC4	0.01	4.1	4.6	2.9	4	3.6	3.8	3.8	3	3.9
MgO	%	IC4	0.01	1.5	1.7	0.9	1.3	1.4	1.8	1.4	1	1.3
MnO	%	IC4	0.01	0.1	0.1	0	0.1	0.1	0	0.1	0.1	0.1
CaO	%	IC4	0.01	1.6	1.4	1.1	1.3	1.1	1.2	1.2	2.3	0.7
Na ₂ O	%	IC4	0.01	1.2	1.6	2.2	2.3	2	0.7	2.1	2.4	2.7
K ₂ O	%	IC4	0.01	2.7	3.5	2.1	2.7	3.8	5.1	2.6	2.4	2.5
P ₂ O ₅	%	IC4	0.01	0.1	0.1	0.1	0.1	0.1	0.1	0.1	0.1	0.1
LOI	%	GRAV7	0.01	5.2	5.8	2.8	4.7	5	5.7	3.6	4.1	2.2
Cu	ppm	IC3E	2	20	30	19	20	25	22	16	14	16
Ni	ppm	IC3E	2	15	26	10	20	17	19	19	15	16
Pb	ppm	IC3E	5	22	26	20	22	24	32	22	22	20
Zn	ppm	IC3E	2	56	92	39	64	66	70	62	46	54
Sb	ppm	NAA	0.2	39	43	37	29	19	118	14	5	5
As	ppm	NAA	1	24	24	11	13	8	16	7	6	4
Ba	ppm	NAA	100	234	279	279	383	513	566	288	436	410
Ce	ppm	NAA	2	67	93	72	76	85	88	72	93	71
Cs	ppm	NAA	1	11	15	6	9	13	23	8	6	6
Cr	ppm	NAA	5	78	59	82	47	90	41	56	47	68
Co	ppm	NAA	1	7	13	5	8	8	8	9	7	6
Eu	ppm	NAA	0.5	1	2	1	1	1	1	1	1	1
Au	ppb	NAA	5	bdl	22	bdl	32	bdl	bdl	bdl	31	bdl
Hf	ppm	NAA	0.5	5	7	6	5	7	5	6	8	5
La	ppm	NAA	0.5	34	49	37	39	43	48	37	47	36
Rb	ppm	NAA	20	149	189	86	129	191	296	116	109	117
Sm	ppm	NAA	0.2	5	7	5	5	6	6	5	7	5
Sc	ppm	NAA	0.1	8	13	7	10	11	11	10	8	9
Th	ppm	NAA	0.5	14	19	15	16	22	25	16	22	15
W	ppm	NAA	2	bdl	bdl	bdl	bdl	bdl	bdl	bdl	bdl	bdl
U	ppm	NAA	2	4	4	3	3	5	7	4	4	3
Yb	ppm	NAA	0.5	2	3	2	2	3	4	3	3	2
V	ppm	IC4	20	40	70	40	50	60	60	50	50	50
Ga	ppm	IC4M	1	12	19	4	11	16	20	11	7	11
Sr	ppm	IC4M	5	120	120	88	125	140	145	125	160	135
Y	ppm	IC4M	1	21	28	21	24	28	30	22	29	22
Zr	ppm	IC4M	15	160	220	190	170	210	170	170	250	170

Below detection limit for all samples: Sn, Nb, Bi, Te, Ta, Se, Mo, Lu, Ir, Br, Ag

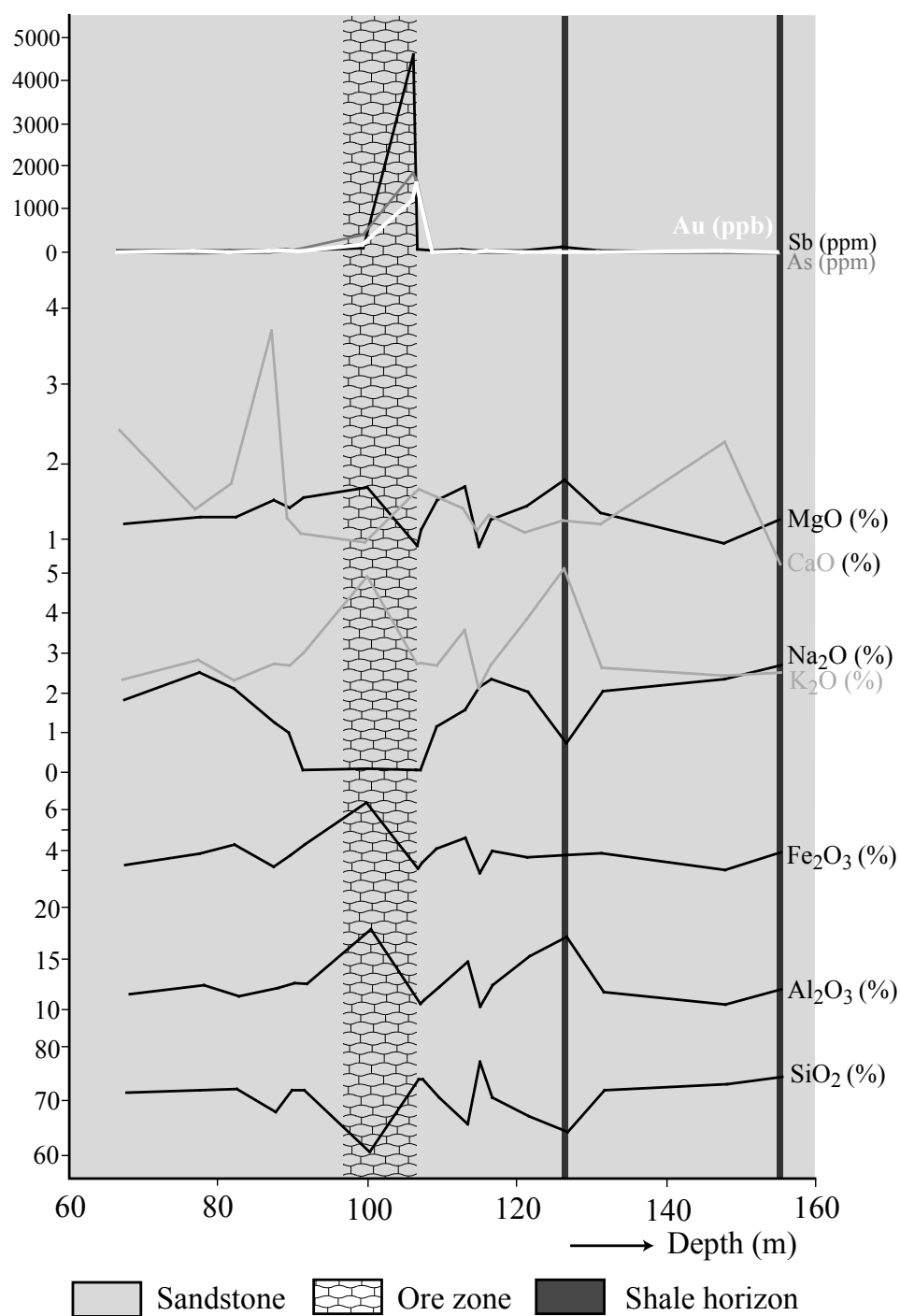


Fig. 3.10: Plot of selected major and trace element concentrations from drill core (EL003) geochemical analysis, indicating the intimate relationship between elemental trends in the ore zone of the Ethel deposit. Courtesy of Republic Gold Ltd.

with the sandstones.

FLUID INCLUSIONS

3.6.1 Analytical methods

Fluid inclusion analyses were carried out on a selection of quartz vein samples in order to determine the pressure, temperature

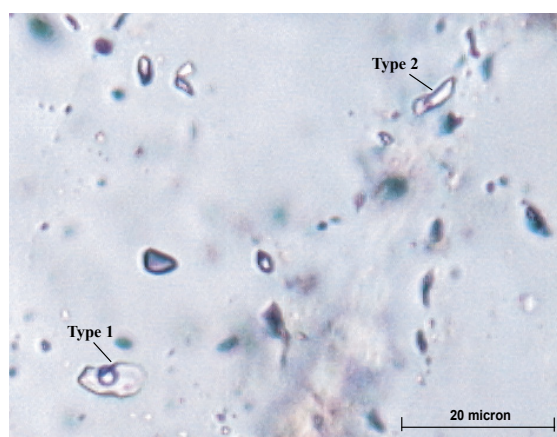


Fig. 3.11: Photomicrograph of representative type i and ii fluid inclusions from the Emily deposit. For discussion, see text.

and composition of mineralising fluids in the Northcote District. Microthermometric measurements were conducted using the fully-automated Linkam THMSG 600 heating and freezing stage equipped with a TMS 93 temperature programmer at Monash University. Measurements were collected from homogeneous, two-phase (liquid-vapour) fluid inclusions in mineralised quartz vein samples from the Emily, Leadingham and Ethel gold deposits. Two types of primary inclusions could be distinguished in all samples: i) rare, isolated inclusions ranging in size from 5 to 8 μm with between 3 to 8 volume% vapour, and ii) abundant elongated and irregular inclusions ranging in size from 3 to 5 μm with up to 8 volume% vapour (Fig. 3.11).

3.6.2 Results

Microthermometric results from our fluid inclusion study are summarised in Table 3.5 and Figure 3.12. Ice melting temperatures ranging between -8.4 and -0.3 $^{\circ}\text{C}$ (average -4.7 ± 2.0 $^{\circ}\text{C}$; $n=54$) indicated salinities that range up to 9 weight percent NaCl equivalent, with rare occurrences ($n=9$) of more saline, between 9 and 13 weight percent NaCl

equivalent, inclusions. No clathrates were observed in the rather small fluid inclusions, suggesting that high salinities may be the result of post-deposition modification of some of the inclusions, for instance, via necking down and/or escape of gas. Homogenisation temperatures range generally between 108 and 312 $^{\circ}\text{C}$ (average 197 ± 55 $^{\circ}\text{C}$; $n=70$), and all inclusions homogenise into the liquid phase. After pressure correction (using a 35 $^{\circ}\text{C}/\text{km}$ thermobaric gradient), this suggests minimum fluid trapping temperatures between ~ 150 and 400 $^{\circ}\text{C}$. These characteristics imply that fluids were trapped at mesozonal to epizonal crustal levels at pressures between 0.5 and 1.5 kbar (Goldstein

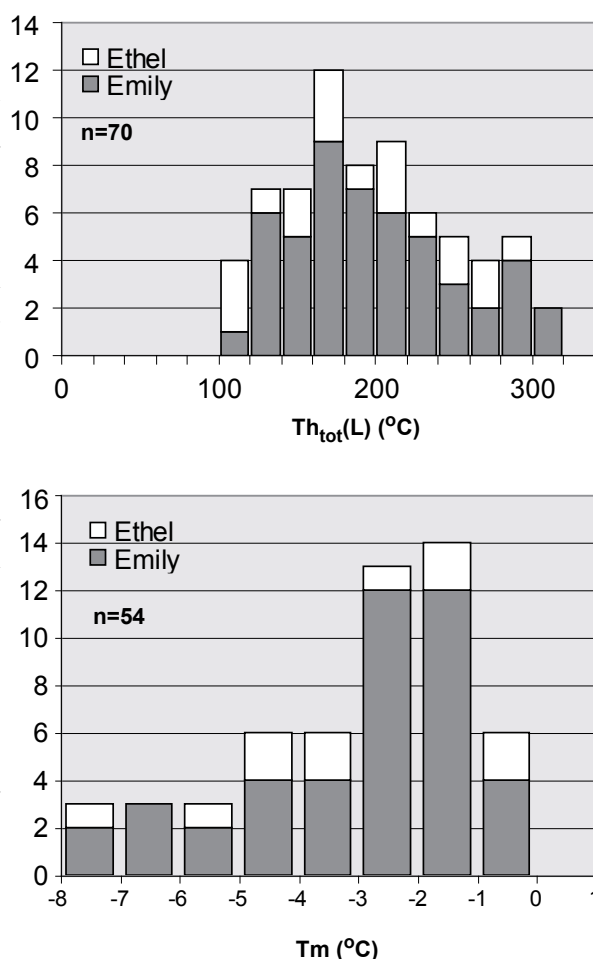


Fig. 3.12: Histogram of ice melting temperatures representing fluid salinity (bottom) and temperatures for homogenisation into liquid phase (bottom) from primary aqueous fluid inclusions from the Emily and Ethel deposits. Number of measurements (n) are indicated.

Table 3.5: Summary of microthermometric data from fluid inclusions in the Northcote District.

Inclusion type	No. of analyses (n)	Tm ice (°)	wt% NaCl equiv.	Th total (°)	vol% vapour	Size (micron)
i	23	-7.7 to -0.9	12 to 2	108 to 294	3 to 8	5 to 8
ii	62	-8.4 to -0.3	13 to 0.8	116 to 312	0 to 8	3 to 5

& Reynolds 1994), which is consistent with our field observations (e.g. metamorphic grade, style of veining, relative timing of vein formation). The range in homogenisation temperature and salinity is similar for gold-only (Emily deposit) and gold-antimony-bearing (Ethel deposit) quartz veins. Our results are in accord with previous fluid inclusion studies of gold-antimony deposits in the Hodgkinson Goldfield by Peters *et al.* (1990). These authors recorded minimum fluid trapping temperatures between 285 and 335°C, salinities of 3 to 11 wt% NaCl equivalent. Petrographic and microthermometric observations of our quartz veins samples suggest the presence of very small concentrations of gaseous phases (e.g. CO₂ / CH₄) in the fluid inclusions, although no phase changes indicative of CO₂ were observed. The presence of small volumes (<1%) of CO₂ would be in accordance with previous Laser Raman spectroscopy studies in the Hodgkinson Goldfield (Peters *et al.* 1990).

3.7 DISCUSSION

3.7.1 Temporal framework for gold-forming episodes

Previous studies by Morrison (1988) and Davis *et al.* (2002) postulated various ages for gold mineralisation in the Hodgkinson Province. Morrison (1988) constrained the age of mineralisation in the Hodgkinson Goldfield as Late Carboniferous (~300 Ma in most studies that reference Morrison 1988, but ~328 Ma in Morrison & Beams 1995) based on K-Ar dating of alteration muscovite from gold-quartz veins. Based on overprinting relationships

of deformational fabrics with isotopically dated igneous intrusions, Davis *et al.* (2002) postulated that gold mineralisation throughout the Hodgkinson Province was more likely to have occurred contemporaneous with 280-240 Ma contraction (i.e. Hunter-Bowen Orogeny). Our field investigations indicate that the gold deposits in the Northcote District formed during two episodes of mineralisation and that a close relationship exists between episodes of mineralisation and deformation. Based on the structural and metallogenic characteristics of gold deposits observed in the Northcote District, we infer that the two episodes of mineralisation occurred contemporaneously with regional $D_{2/3}$ and D_4 deformation in the Hodgkinson Province, placing them in the Late Devonian – Early Carboniferous and (middle?) Carboniferous, respectively (Table 3.1).

The Hodgkinson Province is considered to have once been continuous with the Broken River Province to the south, based on similar sedimentary and structural characteristics (e.g. Arnold & Fawcner 1980; Bultitude *et al.* 1997). Gold and antimony deposits in the Amanda Bel Goldfield in the Broken River Province have recently been shown to form during three mineralising episodes in the Early and Late Devonian and middle to Late Carboniferous respectively (Vos *et al.* in press). Structural and metallogenic characteristics associated with the second and third episode of mineralisation in the Amanda Bel Goldfield are strikingly similar to structural and metallogenic characteristics associated with the mineralising episodes in the Northcote

District. These include 1) the presence of gold in solid solution within acicular arsenopyrite and a strong relationship between quartz veins and regional fault structures associated with the earlier of the two mineralisation episodes, and 2) antimony mineralisation overprinting and disrupting earlier gold-quartz veins during the later of the two mineralisation episodes. The similarities between the deposits and their structural relationships in the Hodgkinson Province and Broken River Province suggest that these formed at the same stage and would thus strengthen the case for gold mineralisation in the Late Devonian and middle Carboniferous in the Northcote District. The association of gold-antimony quartz veins with sinistral shearing further suggests that these formed during regional fault reactivation, most likely represented by the regional D_4 event. Golding *et al.* (1990) indicated that tin-tungsten deposits associated with Late Carboniferous – Early Permian granites crosscut gold and gold-antimony deposits elsewhere in the Hodgkinson Province, implying that the gold mineralising episodes must have occurred prior to ~300 Ma major magmatism in the Hodgkinson Province. This would correlate with middle to Late Carboniferous mineralisation ages (Morrison & Beams 1995), which may reflect the timing of the second mineralisation episode associated with gold-antimony-quartz veins.

3.7.2 Nature of gold-bearing fluids in the Northcote District

Based on their temporal association, Morrison (1988) suggested that a genetic relationship may exist between gold deposits and Late Carboniferous granites in the Hodgkinson Province. In the Northcote District, a similar relationship may be inferred, since Late

Carboniferous – Early Permian granites intrude the meta-sedimentary rocks of the Hodgkinson Formation to the east and northeast of the district. Oxygen isotope studies on gold-quartz veins from the Hodgkinson Goldfield by Golding *et al.* (1990) and Peters *et al.* (1990) obtained $\delta^{18}\text{O}$ values of $16.6 \pm 0.9\text{‰}$ and $10 \pm 2\text{‰}$, respectively. Golding *et al.* (1990) pointed out that the higher $\delta^{18}\text{O}$ values of $19.2 \pm 0.8\text{‰}$ for fluids forming the gold-antimony-quartz veins in the Hodgkinson Goldfield may reflect distinctive flow paths and / or a distinct and separate proximal magmatic source for the antimony-bearing ore fluids.

The close relationship between deformation and mineralisation in the Northcote District as well as ore-forming fluid characteristics and the relative timing of mineralisation episodes prior to regional magmatism suggest that gold deposits in the district can be classified as ‘orogenic’ in terms of mineralisation style (Groves *et al.* 1998). We suggest that ore-forming fluids associated with gold and antimony mineralisation were derived from mid-crustal devolatilisation of sedimentary rocks with faults acting as the main conduits transporting the fluids to mesozonal to epizonal levels. Peters *et al.* (1990) previously suggested a (deep) metamorphic origin for ore-forming fluids based on isotopic and fluid inclusion studies of gold and gold-antimony deposits elsewhere in the Hodgkinson Goldfield.

Conditions of mineralisation in the Northcote District are analogous to orogenic gold-antimony-dominated deposits in equivalent settings in eastern Australia and elsewhere that formed at low to moderate temperatures (~120–320°C) and low pressure (~1kbar) from fluids that contained minor to moderate CO_2 . Examples of similar epizonal type, gold \pm antimony style

of mineralisation in eastern Australia include the previously mentioned gold \pm antimony deposits in the West Normanby Goldfield, the Amanda Bel Goldfield, the Hillgrove deposit in NSW (Ashley *et al.* 2000) and the Fosterville (Zurkic 1998) and Nagambie (Gao *et al.* 1995) deposits in Victoria. At each of these deposits, gold-antimony-quartz assemblages truncate earlier gold-quartz assemblages deposited at higher temperatures and pressures. It generally remains unresolved whether ore-forming fluids associated with each mineralisation phase are derived from similar fluid sources. Davis & Hippert (1998) speculated that the gold- and arsenic-rich fluids in the West Normanby Goldfield (Fig. 3.1) represented metamorphic fluids in equilibrium with graphite, whereas stibnite-bearing fluids could be sourced from magmatic vapours derived from nearby subsurface S-type intrusions. Gao *et al.* (1995) invoked scavenging of both gold and stibnite from host sediments at the Nagambie gold deposit in Victoria, rather than an association with nearby S-type intrusions, arguing that gold deposits are generally related to I-type intrusions. Based on metallogenic characteristics and analogies with gold-antimony deposits elsewhere, we postulate that the first episode of gold mineralisation in the Northcote District was associated with metamorphic devolatilisation during orogenesis. The subsequent antimony-rich episode of mineralisation may genetically be related to (initiation of) widespread magmatism in the Hodgkinson Province that could have instigated additional metamorphism (e.g. Gao *et al.* 1995) and provided antimony-rich fluids.

3.7.3 Significance for the (northern)

Tasman Fold Belt System

Understanding the generation and origin of gold \pm antimony deposits in the Northcote District provides insight into the processes that controlled gold mineralisation in the northern part of the Tasman Fold Belt System, and also allows comparison with similar gold deposits elsewhere in the system. The orogenic nature of the gold deposits in the Northcote District and their relationship to similar gold deposits throughout the Hodgkinson Province suggests that orogenic processes controlled their generation in the Late Devonian to Carboniferous. Their association with regional deformation episodes in the Hodgkinson Province suggests that their generation is intimately associated with subduction outboard of the Australian Craton (e.g. Coney 1990). The widespread presence of turbidites and reverse faults in an eastward younging fold-and-thrust belt associated with gold deposits in the Hodgkinson Province further substantiate the occurrence of orogenic processes most probably related to subduction outboard the northeast Australian continental margin, and which have also been inferred to control gold mineralisation in the Amanda Bel Goldfield in the Broken River Province to the south (Vos *et al.* in press).

3.8 CONCLUSIONS

The Northcote District in the Hodgkinson Goldfield of the Hodgkinson Province contains several vein-hosted and disseminated, mesozonal to epizonal, gold and gold-antimony deposits that occur in lower-greenschist facies sedimentary rocks of the Devonian Hodgkinson Formation. Two generations of mineralised vein assemblages can be closely linked to the Late Devonian to Carboniferous

regional deformation events. The first mineralising episode (i.e. Emily and Black Bess deposits) occurred contemporaneously with $_{NC}D_1$ deformation that is associated with north- to northwest-trending isoclinal folding and thrusting characteristic of regional $_{h}D_{2/3}$ deformation. This event is represented by gold-bearing quartz veins and the occurrence of gold in solid solution with acicular arsenopyrite in host rock assemblages peripheral to veins. The second stage of mineralisation (i.e. Ethel deposit) occurred contemporaneously with $_{NC}D_2$ deformation that is represented by sinistral shearing and fault reactivation most probably related to regional $_{h}D_4$ deformation. Mineralisation during this event is represented by brecciation of earlier quartz veins and the generation of lenses and pods of antimony mineralisation in dilational sites. The structural control on mineralisation, paragenetic relationships and the mesozonal to epizonal, low- to mid-temperature and metamorphic origin for mineralising fluids indicate that gold deposits in the Northcote District can be classified as orogenic gold deposits. These characteristics support the hypothesis that subduction processes outboard of the Australian craton and associated orogenesis, controlled the mineralisation in the Northcote District and most likely in the remainder of the Hodgkinson Goldfield (if not throughout the Hodgkinson Province) in the Devonian and Carboniferous.

ACKNOWLEDGEMENTS

Research has been funded by the Cooperative Research Centre for predictive mineral discovery (pmd*CRC) and this paper is published with the permission of the CEO, pmd*CRC. An International Postgraduate Research Scholarship from Monash University

is gratefully acknowledged. Jackson Gold Ltd. and Republic Gold Ltd. are thanked for access to mine sites in the Northcote District and providing drill core material. S. McKnight, A. Wilde and A. Priymak are thanked for support with analytical work. Input by P. Betts, D. Wood and A. Harwood is gratefully acknowledged, as is J. Nethery for logistical support and discussion of the Hodgkinson Province evolution. K. Dowling and P. Donchak are thanked for reviewing the manuscript.

REFERENCES

- ARNOLD G. O. & FAWCKNER J. F. 1980. The Broken River and Hodgkinson provinces. *In*: Stephenson H. ed. The geology and geophysics of northeastern Queensland, pp175-189, James Cook University, Department of Geology, Townsville, Australia.
- ASHLEY P. M., CREAGH C. J. & RYAN C. G. 2000. Invisible gold in ore and mineral concentrates from the Hillgrove gold-antimony deposits, NSW, Australia. *Mineralium Deposita* 35, 285-301.
- BULTITUDE R. J., DONCHAK P.J., DOMAGALA J. & FORDHAM B.G. 1993. The Pre-Mesozoic stratigraphy and structure of the western Hodgkinson Province and environs. 259p. *Queensland Geological Record* 29. Department of minerals and energy, Queensland.
- BULTITUDE R. J., GARRAD P. D., DONCHAK P. J. T., DOMAGALA J., CHAMPION D. C., REES I. D., MACKENZIE D. E., WELLMAN P., KNUTSON J., FANNING C. M., FORDHAM B. G., GRIMES K. G., OVERSBY B. S., RIENKS I. P., STEPHENSON P. J., CHAPPELL B. W., PAIN C. F., WILFORD J. R., RIGBY J. F. & WOODBURY M. J. 1997. Cairns region. *In*: Bain J. H. C. & Draper J. J. eds. North Queensland Geology. *Australian Geological Survey Organisation Bulletin* 240, 225-325.
- CONEY P. J., EDWARDS A., HINE R., MORRISON F. & WINDRIM D. 1990. The regional tectonics of the Tasman orogenic

- system, eastern Australia. *Journal of Structural Geology* 12, 519-543.
- DAVIS B. K., BELL C. C., LINDSAY M. & HENDERSON R. A. 2002. A single late orogenic episode of gold mineralization in the Hodgkinson Province, North Queensland, Australia. *Economic Geology* 97, 311-323.
- DAVIS B. K. & HIPPERT J. F. M. 1998. Relationships between gold concentration and structure in quartz veins from the Hodgkinson Province, northeast Australia. *Mineralium Deposita* 33, 391-405.
- GAO Z. L., KWAK T. A. P., CHANGKAKOTI A., HUSSEIN E. & GRAY J. 1995. Supergene ore and hypogene non-ore mineralization at the Nagambie sediment-hosted gold deposit, Victoria, Australia. *Economic Geology* 90, 1747-1763.
- GARRAD P. D. & BULTITUDE R. J. 1999. Geology, mining history and mineralisation assessment of the Hodgkinson and Kennedy Provinces, Cairns Region, North Queensland. *Queensland Minerals and Energy Review Series*. Department of Mines and Energy, Queensland.
- GOLDING S. D., BULTITUDE R. J., PETERS S. G., MYERS I. A. & DOWLING K. 1990. Stable isotope constraints on genetic models for gold-quartz, antimony-gold-quartz, tin and tungsten-tin mineralization, Hodgkinson Province, northern Queensland. *Proceedings of the Pacific Rim congress* 1990, 325-335.
- GOLDSTEIN R. H. & REYNOLDS T. J. 1994. Systematics of fluid inclusions in diagenetic minerals. *SEPM short course* 31, 199p.
- GROVES D. I., GOLDFARB R. J., GEBRE-MARIAM M., HAGEMANN S. G. & ROBERT F. 1998. Orogenic gold deposits; a proposed classification in the context of their crustal distribution and relationship to other gold deposit types. *Ore Geology Reviews* 13, 7-27.
- MORRISON G. W. 1988. Palaeozoic gold deposits of northeastern Queensland. In: Morrison G. W. ed. Epithermal and porphyry style gold deposits in North Queensland. *Contributions of the Economic Geology Research Unit* 29, 11-21.
- MORRISON G. W. & BEAMS S. D. 1995. Geological setting and mineralisation style of ore deposits of Northeast Queensland. In: Beams S. D. ed. Mineral deposits of Northeast Queensland. *Contributions of the Economic Geology Research Unit* 52, 1-32.
- PETERS S. G. 1987. Geology, lode descriptions and mineralization of the Hodgkinson Goldfield, northeastern Queensland. *Contributions of the Economic Geology Research Unit* 20, 1-16.
- PETERS S. G., GOLDING S. D. & DOWLING K. 1990. Melange- and sediment-hosted gold-bearing quartz veins, Hodgkinson gold field, Queensland, Australia. *Economic Geology* 85, 312-327.
- VEEVERS J. J. 1984. Phanerozoic Earth history of Australia. 418p. Macquarie University, North Ryde, NSW, Australia. *Oxford Geological Sciences Series* 2.
- VOS I. M. A., BIERLEIN F. P. & TEALE G. S. in press. Genesis of orogenic gold deposits in the Broken River Province, northeastern Queensland, Australia. *Australian Journal of Earth Sciences*. (Chapter 2 of this dissertation)
- VOS I. M. A., BIERLEIN F. P., BARLOW M. A. & BETTS P. G. in review. The Palmerville Fault, NE Queensland, Australia: A multi-disciplinary approach to understanding major fault systems. *Journal of Structural Geology*. (Chapter 5 of this dissertation)
- VOS I. M. A., BIERLEIN F. P., & PHILLIPS D. in prep. The Palaeozoic tectono-metallogenic evolution of the northern Tasman Fold Belt System, Australia: Interplay of subduction rollback and accretion. *Ore Geology Reviews*. (Chapter 7 of this dissertation)
- ZUCCHETTO R. G., HENDERSON R. A., DAVIS B. K. & WYSOCZANSKI R. 1999. Age constraints on deformation of the eastern Hodgkinson Province, north Queensland: new perspectives on the evolution of the northern Tasman

GEOCHEMISTRY OF EARLY-MIDDLE PALAEOZOIC BASALTS IN THE HODGKINSON PROVINCE: A KEY TO TECTONO-MAGMATIC EVOLUTION OF THE TASMAN FOLD BELT SYSTEM IN NORTHEASTERN QUEENSLAND, AUSTRALIA.

I.M.A. Vos, F.P. Bierlein and J. Webb

International Journal of Earth Sciences, in press.

ABSTRACT

The Palaeozoic Hodgkinson Province in northeastern Queensland, Australia, is host to Late Ordovician to Devonian rock assemblages that contain tholeiitic to calc-alkaline basalts. These basalts occur as massive fault-bounded units interspersed with marine sedimentary rocks and limestones that are metamorphosed to lower greenschist facies in the Ordovician Mulgrave, Silurian Chillagoe and Devonian Hodgkinson formations, respectively. The petrogenetic and Sm-Nd isotope characteristics of these mafic volcanic rocks were investigated to constrain the tectonic setting in which they erupted. Major, trace and rare earth element analyses were carried out on samples from these formations and intrusive dolerites. The mafic rocks can be classified as basalts and basaltic andesites with distinct MORB characteristics. Furthermore, the basalts are characterized by a slight to moderate enrichment in Th and concomitant depletion in Nb, both of which become less pronounced with basalt evolution through time. These features are consistent with decreasing volcanic arc affinity of Silurian and Devonian MORB-type basalts in the Hodgkinson Province. Sm-Nd isotope characteristics of these basalts indicate a change in source region from dominantly sub-continental lithospheric mantle in the Silurian to asthenospheric input in the Devonian. Collectively, the geochemical and isotopic characteristics of the Hodgkinson Province basalts are interpreted to reflect deposition in an evolving back-arc basin setting. The onset of basin extension was initiated in the Silurian. Accelerated basin subsidence occurred throughout the Devonian and was halted by basin inversion in the Late Devonian. Basin evolution was controlled by an eastward stepping subduction zone outboard of the Australian Craton.

4.1 INTRODUCTION

The Early-Middle Palaeozoic tectono-magmatic evolution of the Hodgkinson Province in northeastern Queensland, Australia (Fig. 4.1) remains controversial. Several scenarios have been proposed that discuss the nature of the basement and the presence of subduction-related tectonic elements (White 1978; Arnold & Fawcner 1980; Henderson 1987; Withnall *et al.* 1987; Bultitude *et al.* 1990, 1993; Blewett & Wellman 1994). Similar controversies surround other parts of the Tasman Fold Belt System (Fig. 4.1) in eastern Australia (e.g. Dadd 1998; Foster & Gray 2000; Taylor & Cayley 2000). In the western part of the Hodgkinson Province, a number of Late Ordovician to Middle Devonian mafic volcanic units representing intermittent volcanism over a period of ~100 m.y., have been structurally disrupted and intermixed with chert, limestone and marine siliciclastic units within a regional thrust system (Fig. 4.2). The occurrence of these mafic volcanic units offers

an opportunity to evaluate tectonic processes that occurred along the Pacific margin of the Australian Craton. This paper investigates the petrogenesis of these mafic volcanic rocks as this method is commonly used to infer the tectonic setting in which volcanic rocks have originated (e.g. Pearce & Cann 1973; Floyd & Winchester 1975; Winchester & Floyd 1977; Meschede 1986). We have studied and sampled a number of mafic volcanic units from the western part of the Hodgkinson Province. The samples were subjected to major, trace and rare earth element (REE) analyses. In contrast to earlier studies (e.g. Arnold & Fawcner 1980), our investigation includes REE and Sm-Nd isotope analyses, as these generally prove more useful as an aid to interpreting the tectonic setting of extensively altered mafic volcanic rocks. Specifically, we address the petrogenesis of the Hodgkinson Province basalt units, the characterisation of their sources, and attempt to constrain the geodynamic setting in which

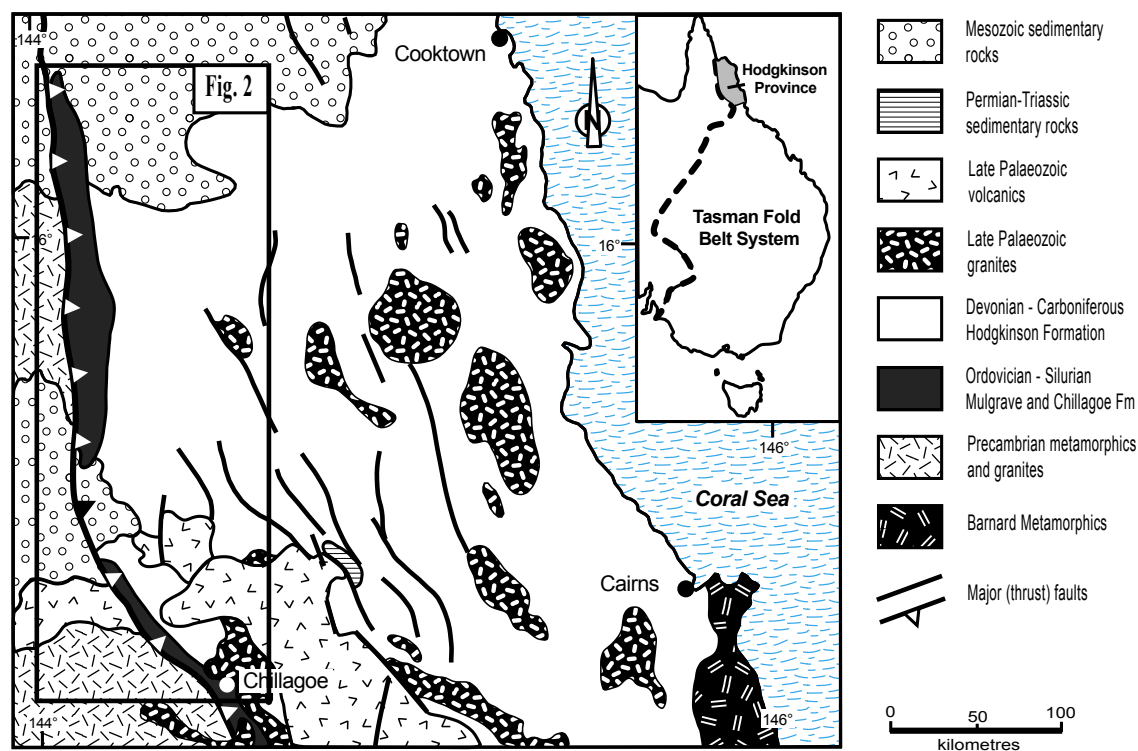


Fig. 4.1: Simplified geology of the Hodgkinson Province; inset shows the location of the province in the Tasman Fold Belt System of eastern Australia.

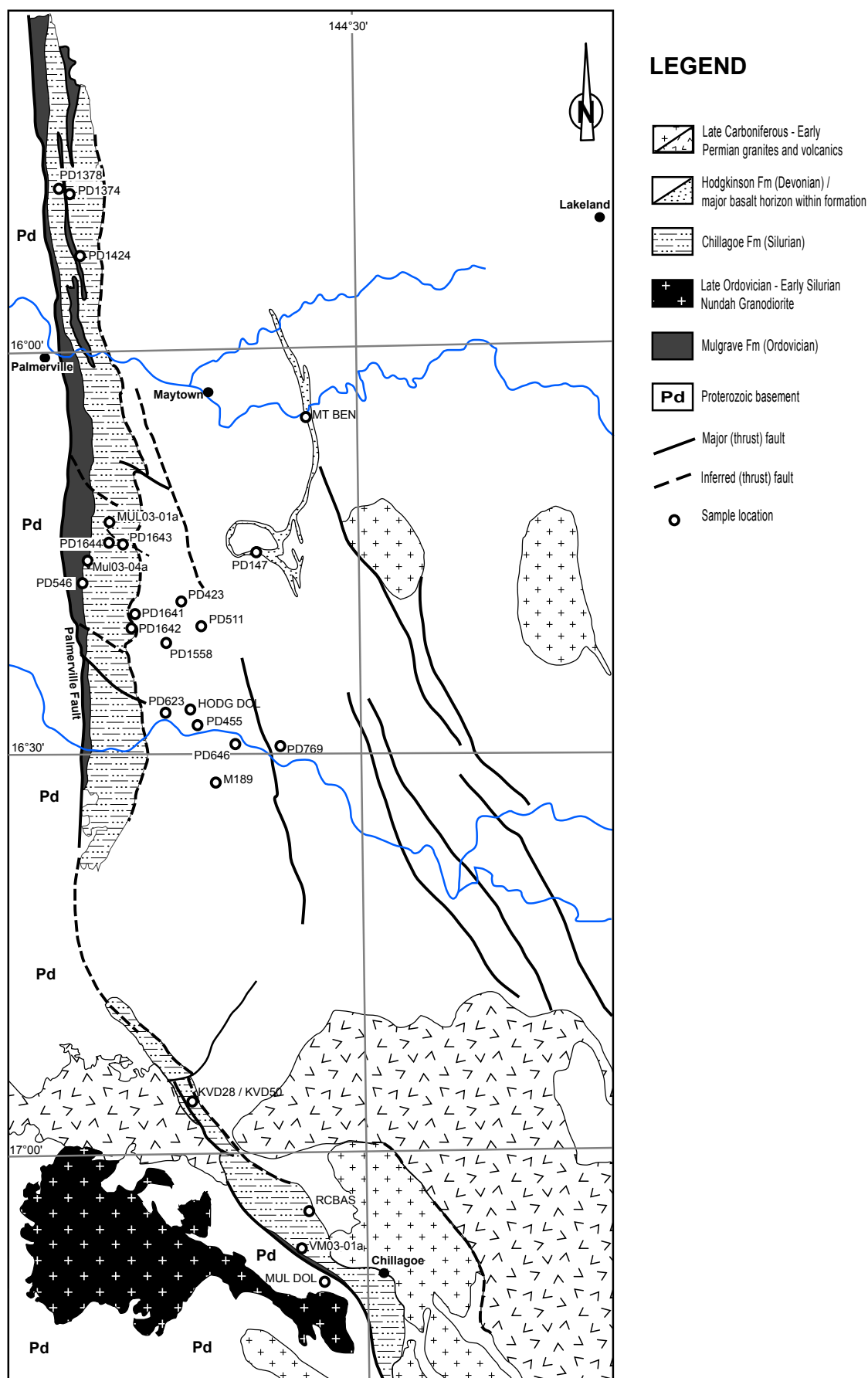


Fig. 4.2: Detailed geology of the western part of the Hodgkinson Province indicating sample locations.

they originated. Results from this study can be used to gain insight in the tectonic setting of the northern part of the Tasman Fold Belt System and comparison with analogous terranes in other parts of this system and elsewhere can be made.

4.2 GEOLOGICAL SETTING

The Hodgkinson Province is situated in northeastern Queensland and forms the northernmost part of the predominantly Palaeozoic Tasman Fold Belt System (Fig. 4.1) in eastern Australia. The Tasman Fold Belt System forms a composite of fold belts that have

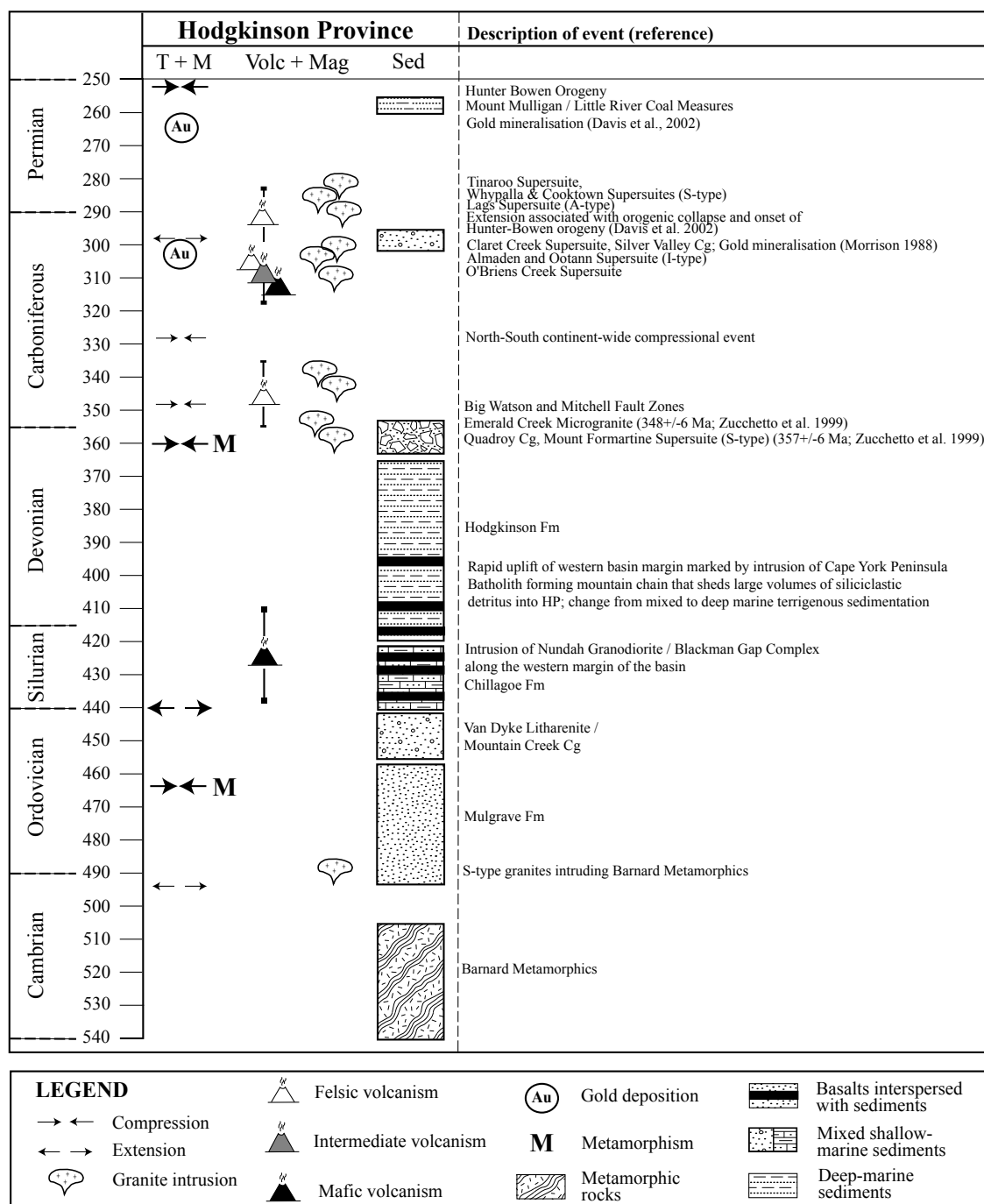


Fig. 4.3: Time-space diagram of Early Palaeozoic geological events across the Hodgkinson and adjacent provinces (compiled from Morrison 1988; Withnall & Lang 1993; Bultitude *et al.* 1997; Zucchetto *et al.* 1999; Davis *et al.* 2002). Abbreviations: T+M = Tectonic framework and mineralisation, Volc + Mag = volcanism and magmatism, Sed = sedimentation.

a closely interrelated tectonic evolution mostly controlled by subduction-related processes that occurred outboard of the Australian craton (e.g. Veevers 1984; Coney *et al.* 1990). A comprehensive summary of the geology of the Hodgkinson Province is given in Bultitude *et al.* (1997). An overview of the stratigraphy together with the main magmatic and tectonic events is compiled from selected literature sources and presented in Figure 4.3. In summary, the Hodgkinson Province has been affected by at least four deformation phases and is intruded by numerous Carboniferous to Permian, I- and S-type granites. Palaeozoic sedimentation started with the quartzose sedimentary rocks of the Early to Middle Ordovician Mulgrave Formation in a passive continental margin setting (e.g. Bultitude *et al.* 1997). The Mountain Creek Conglomerate and the Van Dyke Litharenite unconformably overlie the Mulgrave Formation and were deposited in the Late Ordovician. They have been interpreted as the products of arc magmatism during a major eustatic episode (Bultitude *et al.* 1997). The Silurian and Devonian mark a period of basin formation and infill, with deposition of the Chillagoe and Hodgkinson formations that represent mainly mixed-shallow marine to deep-marine terrigenous sedimentation, respectively.

4.3 BASALT UNITS IN THE HODGKINSON PROVINCE

The mafic volcanic units in the Hodgkinson Province are part of the Early-Middle Palaeozoic stratigraphy and can be found interleaved with the Mulgrave, Chillagoe and Hodgkinson Formation stratigraphy. The mafic volcanic rocks are more abundant towards the western margin, where they form a significant proportion

of the Chillagoe Formation. Additionally, the Hodgkinson Province stratigraphy is intruded by a number of dolerite dykes and sills of undetermined age. The mafic volcanic rocks generally occur as massive units conformably interbedded with marine sedimentary rocks. In the Chillagoe Formation, they are typically associated with chert intervals. Within the Hodgkinson Formation, a number of distinct belts, including the ~3km wide Larramore Metabasalt Member, consists mainly of metabasalt flows and interlayered chert lenses that commonly show a weak to prominent tectonic foliation (Bultitude *et al.* 1996a). In most cases the mafic units are part of structurally disrupted thrust packages, but slivers of basalts may also occur as inclusions within mélangé zones. Mafic units almost exclusively occur as fault-bounded units. The basalt units generally comprise metamorphosed, fine-grained, occasionally pillowed and brecciated rocks. Some basalt units are host to massive sulphide deposits (e.g. the King Vol deposit hosted by the Chillagoe Formation; Morrison 2004).

The occurrence of basalt units in the mature sedimentary rocks of the Mulgrave Fm representing a passive margin setting is difficult to explain. The fault-bounded nature of these basalt units may suggest that they have been tectonically juxtaposed with Mulgrave Formation sedimentary rocks. The spatial distribution of basalt units throughout the Hodgkinson Province seems to be a reflection of emplacement age overall younging to the east. Therefore the basalt units interleaved with the Mulgrave Formation are considered structurally emplaced and of Latest Ordovician to Earliest Silurian age and will be treated as a separate entity in this paper.

4.3.1 Sample description, petrography and alteration

Sample localities for basalt units in the Mulgrave, Chillagoe and Hodgkinson Formations are outlined in Figure 4.2. Most surface samples were collected from massive mafic flows characterized by the presence of pillow structures. Two samples were collected from drillcore (KVD28 / KVD50) and their origins (intrusive or extrusive) are undetermined.

Petrographic examination of the mafic volcanic units indicates that all samples have been metamorphosed to sub-greenschist facies and now consist of assemblages containing mainly carbonate, albite and chlorite, with minor actinolite, epidote, calcite, quartz and sphene (Fig. 4.4a-c). Some remnant grains of pyroxene occur, but generally the pyroxene is altered to carbonate and epidote. Samples are variably deformed and characterised by the presence of

one or more deformation and/or shear fabrics (e.g. PD1378 shows well-developed shear planes, see Fig. 4.4d). Most samples have an aphyric texture, but several are basalts with calcite-chlorite-clay-filled vesicles.

4.4 GEOCHEMISTRY

Eighteen altered and deformed basalt samples from the various units described above were analysed for major and selected trace elements at LaTrobe University in the late 1990s using XRF (Siemens SRS 303AS with Rhodium tube). Results from these analyses have been incorporated in this study. Another batch of samples was collected in 2003 by the first author to form a total of 26 samples that were then dried, jaw crushed, and milled in a plain carbon steel pulveriser to a nominal 90% passing 106 μm at Amdel Laboratories (Thebarton, South Australia). For the second batch of samples

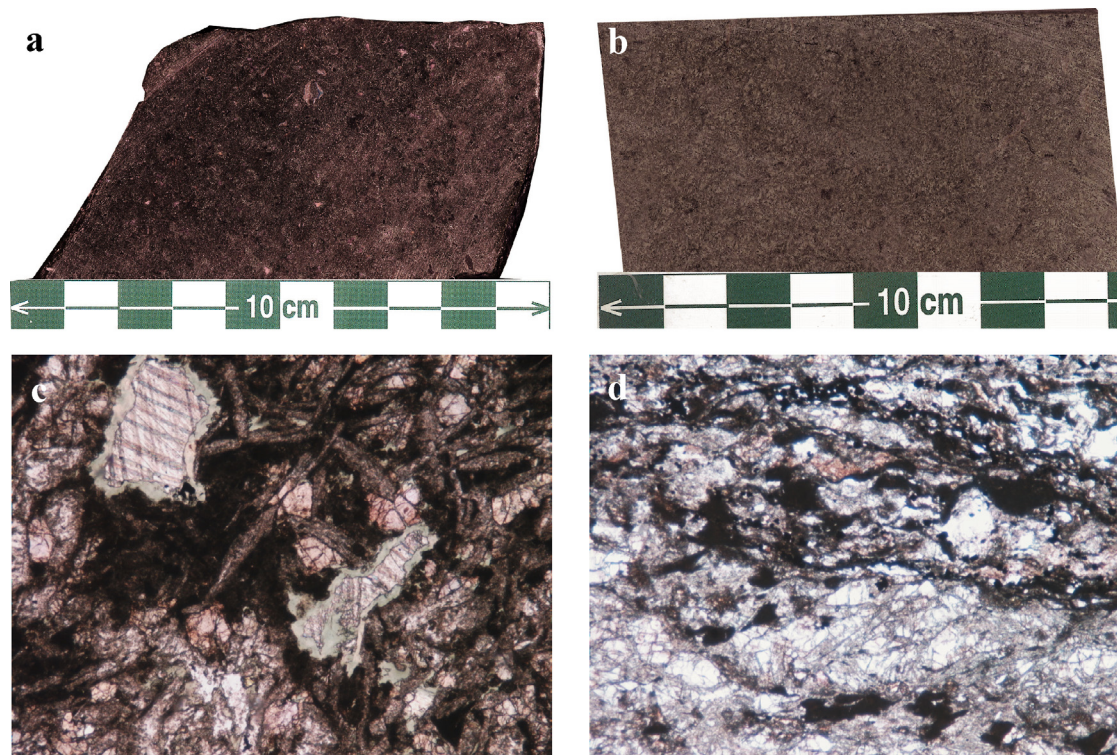


Fig. 4.4: Hand specimen and thin section photographs. (a) Chloritised basalt sample from the Chillagoe Formation (PD1643). (b) Albitised basalt sample from the Hodgkinson Formation (PD1558). (c) Microphotograph (plane polarised light) showing intense carbonate and chlorite alteration of basalt (PD1643); field of view = 1.4 cm. (d) Microphotograph (plane polarised light) of shear bands (near-horizontal) in microfractured basalt (PD1378), field of view = 1.4 cm.

analyses were carried out at Amdel Laboratories using ICP-OES (major elements and Ag, Ni, Cu, Pb, Mo, Zn, Zr and Sn) and ICP-MS (Bi, Ga, Nb, Sr, V and Y). In addition, all samples were quantified by Neutron Activation Analysis (NAA) for Au, As, Sb, W, Ag, Se, Te, Zn, La, Ce, Sm, Eu, Yb, Lu, Ca, Co, Cr, Fe, Ir, Sc, Ba, Br, Cs, Hf, K, Mo, Na, Rb, Ta, Th, U, Zr at Becquerel Laboratories (Lucas Heights, NSW, Australia). Eight representative samples were selected for Sm-Nd analysis at the University of Melbourne with a multi-collector LAM-ICP-MS. Two samples, selected on the basis of the least amount of deformation and / or alteration observed, from each formation studied were used in these analyses. The use of REE and Sm/Nd analyses prove particularly useful for basalts that are altered to the extent observed in this study.

Although no absolute ages have been determined for the basalt units and the samples studied herein, each sample was assigned an

estimated age based on field observations and the age of the formation they are presumed to be part of. The two samples from dolerite intrusions represent dykes that were emplaced to the west of the Hodgkinson Province in the Early Palaeozoic (MulDol) and in the Hodgkinson Province (HodgDol) respectively. HodgDol represents a sample from a dyke that crosscuts the Hodgkinson Formation stratigraphy and is therefore considered to be of post-Devonian age and may be associated to Carboniferous-Permian magmatism.

4.4.1 Results and interpretation

Major, trace and rare earth element analyses are presented in Table 4.1. The mafic volcanic units investigated are subdivided into four groups, namely those found interleaved with the Mulgrave, Chillagoe and Hodgkinson formations, and the dolerite intrusions. A total alkali-silica (TAS) diagram after LeMaitre *et al.* (1989) in Figure 4.5 demonstrates

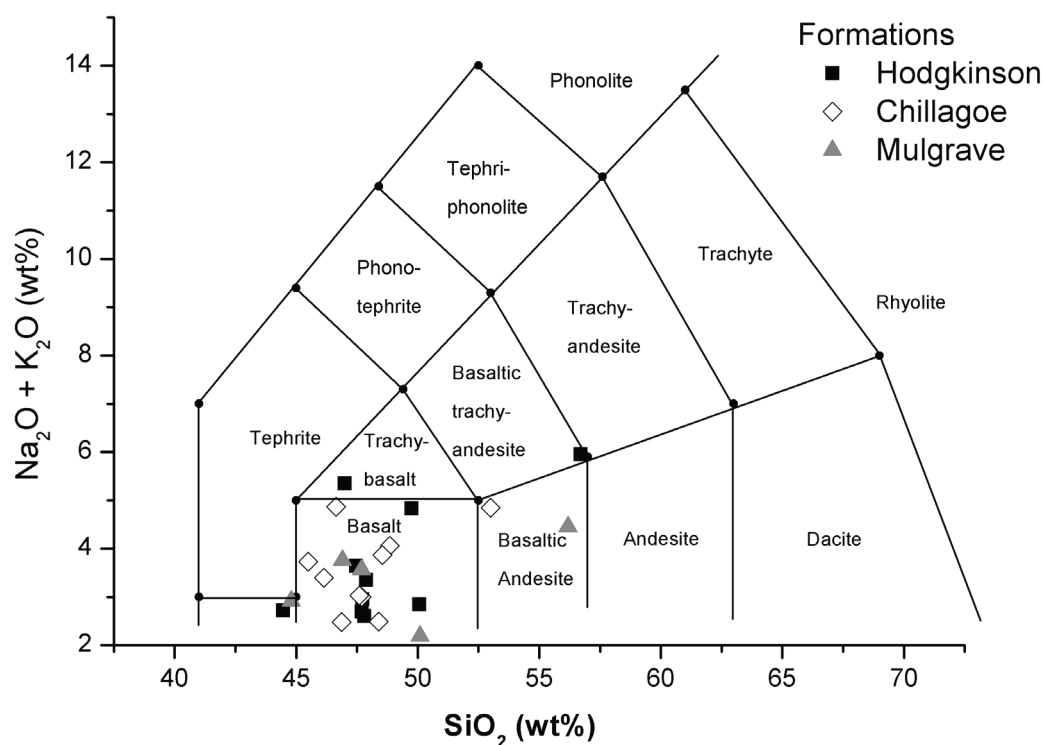


Fig. 4.5: Total alkali vs. silica diagram (after Le Maitre *et al.*, 1989) classifying the Hodgkinson Province samples as basalts and andesitic basalts; see text for discussion.

Table 4.1: Major, trace and rare earth element data for basalt units in the Hodgkinson Province. Where more than one analysis method has been used, these are listed together with their respective detection limit. In this case, the most reliable value has been listed in the table. Sample locations can be found on Fig. 2. The last two analyses concern dolerite intrusions in the Dargalong Metamorphics (MulDol) and Hodgkinson Fm (HodgDol).

Sample				PD1644	PD546	Mul03-01a	Mul03-04a	PD1641	PD1642	PD1643	PD1378
Basalt unit				MF	MF	MF	MF	CF	CF	CF	CF
UTM Easting				191600	189230	132591	192087	192800	192900	192300	185460
UTM Northing				8206200	8199210	8203863	8199223	8194000	8193400	8205800	8250940
Major elements	Method	DetLim									
SiO ₂	(wt%)	XRF	0.01	47.69	56.18	44.8	46.9	46.14	48.85	46.64	46.87
TiO ₂	(wt%)	XRF	0.01	0.81	1.63	2.13	1.29	1.87	1.74	2.01	1.19
Al ₂ O ₃	(wt%)	XRF	0.01	18.46	12.93	14.7	14.6	14.67	15.02	15.93	13.57
Fe ₂ O ₃	(wt%)	XRF	0.01	0.95	3.54	11.8	13.4	2.43	3.86	2.64	3.08
FeO	(wt%)	XRF	0.01	6.09	7.59	na	na	8.4	7.57	7.68	8.36
MnO	(wt%)	XRF	0.01	0.13	0.17	0.17	0.2	0.24	0.19	0.18	0.2
MgO	(wt%)	XRF	0.01	5.97	1.5	8.5	6.7	6.86	5.78	6.21	7.32
CaO	(wt%)	XRF	0.01	11.29	6.28	9.33	8.18	10.19	9.06	9.23	10.76
Na ₂ O	(wt%)	XRF	0.01	3.39	2.45	2.71	2.95	2.74	3.91	3.56	2.24
K ₂ O	(wt%)	XRF	0.01	0.18	2.01	0.21	0.81	0.66	0.15	1.31	0.24
P ₂ O ₅	(wt%)	XRF	0.01	0.08	0.69	0.32	0.12	0.19	0.18	0.22	0.14
LOI				4.96	4.9	5.05	4.56	5.52	3.42	4.67	6.11
Total	(wt%)	XRF		100	99.9	99.7	99.7	99.9	99.7	100.3	100.1
Trace elements											
Ba	(ppm)	XRF / NAA	2 / 100	44	355	114	bdl	144	70	193	72
Cr	(ppm)	NAA	2	8	6	268	108	136	152	48	106
Cu	(ppm)	IC3E	2	51	11	165	58	204	148	155	190
Nb	(ppm)	XRF / IC4M	1.0 / 10	bdl	10	bdl	bdl	4	7	9	5
Ni	(ppm)	IC3E	2	65	2	165	120	82	59	67	68
Pb	(ppm)	XRF / IC3E	1.0 / 5	bdl	18	bdl	bdl	bdl	1	bdl	2
Rb	(ppm)	XRF / NAA	1.0 / 20	2	72	bdl	bdl	11	3	16	4
Sr	(ppm)	XRF / IC4M	5	135	176	160	145	250	207	1914	251
Th	(ppm)	NAA	0.2	13	12	1	0.4	0.4	1	1	1
V	(ppm)	XRF / IC4	20	181	91	240	290	306	275	300	271
Y	(ppm)	XRF / IC4M	1	18	52	21	22	30	29	29	25
Zr	(ppm)	XRF / IC3E	5	46	549	84	60	106	113	128	71
Sc	(ppm)	NAA	0.1	38	42	30	40	40	42	39	51
Hf	(ppm)	NAA	0.2	12	na	3	2	3	3	2	2
Co	(ppm)	NAA	0.5	17	na	53	57	42	48	47	53
Zn	(ppm)	XRF / IC3E	2	61	115	96	92	108	110	108	94
Ga	(ppm)	IC4M	1	14	22	21	20	19	21	19	17
As	(ppm)	NAA	1	10	na	2	3	2	1	2	2
Br	(ppm)	NAA	1	bdl	na	bdl	bdl	bdl	bdl	bdl	bdl
Mo	(ppm)	IC3E	3	na	na	6	bdl	na	na	na	na
Sn	(ppm)	IC3E	5	na	na	14	6	na	na	na	na
Sb	(ppm)	NAA	0.2	0.4	na	1	2	bdl	bdl	1	0.5
Cs	(ppm)	NAA	0.5	3	na	1	bdl	1	bdl	bdl	1
U	(ppm)	XRF / NAA	1	bdl	2	bdl	bdl	1	2	bdl	1
Ta	(ppm)	NAA	0.5	1	na	1	bdl	bdl	1	1	bdl
Au	(ppm)	NAA	5	11	na	bdl	bdl	bdl	bdl	9	9
Rare-earth elements											
La	(ppm)	NAA	0.5	33	32	14	5	7	10	6	3
Ce	(ppm)	NAA	2	75	74	36	13	19	24	13	9
Sm	(ppm)	NAA	0.2	9	na	6	3	4	4	3	2
Eu	(ppm)	NAA	0.5	3	na	2	1	1	2	1	1
Tb	(ppm)	NAA	0.5	2	na	bdl	bdl	bdl	bdl	bdl	bdl
Yb	(ppm)	NAA	0.5	5	na	2	2	2	2	2	3
Lu	(ppm)	NAA	0.1	1	na	0.3	0.4	0.3	0.3	0.4	0.4

Table 4.1: continued												
Sample			PD1424	KVD28	KVD50	RCBAS	VM03-01a	PD147	MT BEN	PD769B	PD623	
Basalt unit			CF	CF	CF	CF	CF	HF	HF	HF	HF	
UTM Easting			188700	206828	206828	225521	224107	219650	225088	220490	202740	
UTM Northing			8240460	8125652	8125652	8109263	8105529	8201300	8219724	8174190	8179330	
Major elements	Method	DetLim										
SiO ₂	(wt%)	XRF	0.01	48.55	45.5	53	48.4	47.6	47.69	44.46	49.74	47
TiO ₂	(wt%)	XRF	0.01	1.57	1.89	1.19	1.61	1.41	1.43	1.42	1.42	2
Al ₂ O ₃	(wt%)	XRF	0.01	13.42	14.2	14.2	14.6	14.3	16.08	14.73	14.32	16.94
Fe ₂ O ₃	(wt%)	XRF	0.01	3.39	13.9	10.2	11.2	10.7	3.38	1.21	0.86	3.4
FeO	(wt%)	XRF	0.01	10.13	na	na	na	na	6.44	9.21	8.64	5.95
MnO	(wt%)	XRF	0.01	0.3	0.12	0.12	0.35	0.15	0.16	0.21	0.2	0.17
MgO	(wt%)	XRF	0.01	6.95	8	6.19	6.43	9.22	6.52	8.36	8.32	6.92
CaO	(wt%)	XRF	0.01	8.52	6.79	5.65	13.4	10.5	11.92	7.06	5.52	5.83
Na ₂ O	(wt%)	XRF	0.01	3.46	3.63	4.2	2.05	2.2	2.61	2.64	4.77	3.13
K ₂ O	(wt%)	XRF	0.01	0.41	0.1	0.65	0.44	0.83	0.09	0.08	0.06	2.22
P ₂ O ₅	(wt%)	XRF	0.01	0.19	0.13	0.18	0.16	0.14	0.14	0.15	0.16	0.34
LOI				3.41	6.31	3.59	1.41	3.21	3.79	10.52	5.82	6.06
Total	(wt%)	XRF		100.3	100.6	99.2	100.1	100.3	100.3	100.1	99.8	100
Trace elements												
Ba	(ppm)	XRF / NAA	2.0 / 100.0	55	bdl	2530	162	120	3	95	128	197
Cr	(ppm)	NAA	2	237	302	121	329	431	192	190	320	221
Cu	(ppm)	IC3E	2	145	150	140	36	230	67	83	59	200
Nb	(ppm)	XRF / IC4M	1.0 / 10.0	3	bdl	bdl	bdl	bdl	3	3	2	10
Ni	(ppm)	IC3E	2	50	150	82	120	140	60	74	62	186
Pb	(ppm)	XRF / IC3E	1.0 / 5	1	bdl	bdl	8	bdl	2	3	1	3
Rb	(ppm)	XRF / NAA	1.00 / 20.0	8	bdl	33	bdl	bdl	1	2	bdl	41
Sr	(ppm)	XRF / IC4M	5	134	430	550	260	300	187	120	208	121
Th	(ppm)	NAA	0.2	0.3	bdl	2	1	1	0.3	1	bdl	0.3
V	(ppm)	XRF / IC4	20	328	240	200	310	280	214	222	220	278
Y	(ppm)	XRF / IC4M	1	38	20	25	22	18	24	25	35	29
Zr	(ppm)	XRF / IC3E	5	93	72	110	80	74	92	96	123	134
Sc	(ppm)	NAA	0.1	32	30	30	40	40	40	45	35	41
Hf	(ppm)	NAA	0.2	1	2	3	3	2	2	3	3	2
Co	(ppm)	NAA	0.5	34	55	39	43	52	19	50	67	42
Zn	(ppm)	XRF / IC3E	2	121	120	68	135	155	83	88	155	119
Ga	(ppm)	IC4M	1	18	24	17	21	20	20	19	17	18
As	(ppm)	NAA	1	18	3	23	51	2	24	1	7	17
Br	(ppm)	NAA	1	bdl	bdl	bdl	3	bdl	1	bdl	bdl	bdl
Mo	(ppm)	IC3E	3	na	4	4	6	4	na	na	na	na
Sn	(ppm)	IC3E	5	na	16	6	8	8	na	na	na	na
Sb	(ppm)	NAA	0.2	0.3	4	6	3	1	1	1	0.5	1
Cs	(ppm)	NAA	0.5	1	8	7	5	bdl	2	2	3	bdl
U	(ppm)	XRF / NAA	1	bdl	bdl	bdl	bdl	bdl	2	1	bdl	na
Ta	(ppm)	NAA	0.5	bdl	bdl	1	bdl	bdl	bdl	bdl	bdl	bdl
Au	(ppm)	NAA	5	bdl	bdl	bdl	bdl	bdl	bdl	bdl	18	16
Rare-earth elements												
La	(ppm)	NAA	0.5	2	4	11	8	6	4	7	7	4
Ce	(ppm)	NAA	2	6	12	25	19	16	11	18	20	13
Sm	(ppm)	NAA	0.2	2	4	4	4	3	3	4	4	3
Eu	(ppm)	NAA	0.5	1	1	1	1	1	1	2	1	1
Tb	(ppm)	NAA	0.5	bdl	bdl	bdl	bdl	bdl	bdl	bdl	bdl	bdl
Yb	(ppm)	NAA	0.5	2	2	3	3	2	2	3	2	2
Lu	(ppm)	NAA	0.1	0.2	0.3	0.4	0.4	0.3	0.3	0.4	0.3	0.3

Table 4.1: continued											
Sample			PD1588	PD423	PD511	M189	PD455	PD646	MULDOL	HODGDOL	
Basalt unit			HF	HF	HF	HF	HF	HF	dolerite	dolerite	
UTM Easting			200800	203420	207000	206073	208580	212450	<i>231247</i>	<i>208380</i>	
UTM Northing			8185200	8193610	8191230	8170466	8178970	8175340	<i>8096110</i>	<i>8176889</i>	
Major elements	Method	DetLim									
SiO ₂	(wt%)	XRF	0.01	43.54	50.06	47.88	47.8	47.47	47.72	50.1	56.7
TiO ₂	(wt%)	XRF	0.01	1.04	1.2	1.33	1.2	1.47	1.3	0.82	1.83
Al ₂ O ₃	(wt%)	XRF	0.01	15.56	14.4	15.06	14.25	15.09	15.36	13.4	13.2
Fe ₂ O ₃	(wt%)	XRF	0.01	3.83	2.9	2.12	4.39	1.91	2.32	13.9	11.1
FeO	(wt%)	XRF	0.01	5.75	7.16	7.42	7	7.72	7.33	na	na
MnO	(wt%)	XRF	0.01	0.19	0.18	0.17	0.28	0.16	0.16	0.22	0.17
MgO	(wt%)	XRF	0.01	10.22	7.44	7.85	7.05	7.99	8.04	7.69	2.35
CaO	(wt%)	XRF	0.01	11.28	11.27	10.74	10.33	10.26	11.16	9.67	3.97
Na ₂ O	(wt%)	XRF	0.01	1.46	2.75	3.34	2.28	3.63	2.91	0.75	3.77
K ₂ O	(wt%)	XRF	0.01	0.05	0.1	0.02	0.33	0.02	0.04	1.44	2.19
P ₂ O ₅	(wt%)	XRF	0.01	0.12	0.14	0.14	0.12	0.14	0.13	0.07	0.83
LOI				7	2.79	4.14	5.18	4.03	3.63	1.42	3.44
Total	(wt%)	XRF		100	100.4	100.2	100.2	99.9	100.1	99.5	99.6
Trace elements											
Ba	(ppm)	XRF / NAA	2.0 / 100	10	21	7	65	16	9	bdl	611
Cr	(ppm)	NAA	2	204	285	295	270	389	871	145	10
Cu	(ppm)	IC3E	2	83	89	83	90	102	91	68	28
Nb	(ppm)	XRF / IC4M	1.0 / 10	bdl	2	3	bdl	bdl	2	bdl	bdl
Ni	(ppm)	IC3E	2	370	34	70	102	57	86	100	9
Pb	(ppm)	XRF / IC3E	1.0 / 5	1	bdl	2	bdl	bdl	4	bdl	18
Rb	(ppm)	XRF / NAA	1.00 / 20	bdl	1	1	11	1	bdl	93	110
Sr	(ppm)	XRF / IC4M	5	326	487	347	79	97	114	52	210
Th	(ppm)	NAA	0.2	0.4	bdl	0.4	0.4	0.3	bdl	1	10
V	(ppm)	XRF / IC4	20	216	244	227	304	255	235	320	110
Y	(ppm)	XRF / IC4M	1	23	24	27	27	30	27	19	52
Zr	(ppm)	XRF / IC3E	5	64	73	87	53	95	79	16	230
Sc	(ppm)	NAA	0.1	44	41	49	39	45	43	50	26
Hf	(ppm)	NAA	0.2	2	2	2	3	3	2	1	6
Co	(ppm)	NAA	0.5	46	44	55	37	49	54	61	23
Zn	(ppm)	XRF / IC3E	2	78	85	78	100	84	84	105	120
Ga	(ppm)	IC4M	1	15	17	16	15	18	16	15	25
As	(ppm)	NAA	1	15	6	3	1	5	2	4	10
Br	(ppm)	NAA	1	bdl	bdl	bdl	bdl	bdl	bdl	bdl	bdl
Mo	(ppm)	IC3E	3	na	na	na	na	na	na	bdl	4
Sn	(ppm)	IC3E	5	na	na	na	na	na	na	14	10
Sb	(ppm)	NAA	0.2	5	4	1	1	0.4	2	3	9
Cs	(ppm)	NAA	0.5	1	1	bdl	1	1	bdl	2	2
U	(ppm)	XRF / NAA	1	bdl	1	bdl	bdl	bdl	bdl	bdl	4
Ta	(ppm)	NAA	0.5	bdl	bdl	bdl	bdl	1	bdl	bdl	1
Au	(ppm)	NAA	5	bdl	bdl	bdl	bdl	bdl	bdl	8	bdl
Rare-earth elements											
La	(ppm)	NAA	0.5	5	5	3	5	3	2	3	31
Ce	(ppm)	NAA	2	13	13	8	16	11	6	9	68
Sm	(ppm)	NAA	0.2	3	3	2	4	3	2	2	9
Eu	(ppm)	NAA	0.5	1	bdl	1	1	1	1	1	3
Tb	(ppm)	NAA	0.5	bdl	bdl	bdl	bdl	bdl	bdl	bdl	2
Yb	(ppm)	NAA	0.5	2	2	3	4	3	3	2	4
Lu	(ppm)	NAA	0.1	0.3	0.3	0.4	1	0.4	0.3	0.4	1
Abbreviations: MF = Mulgrave Formation, CF = Chillagoe Formation, HF = Hodgkinson Formation; bdl = below detection limit; na = not analysed. UTM coordinates in italics are AMG84, others in AGD66, all in UTM Zone 51.											

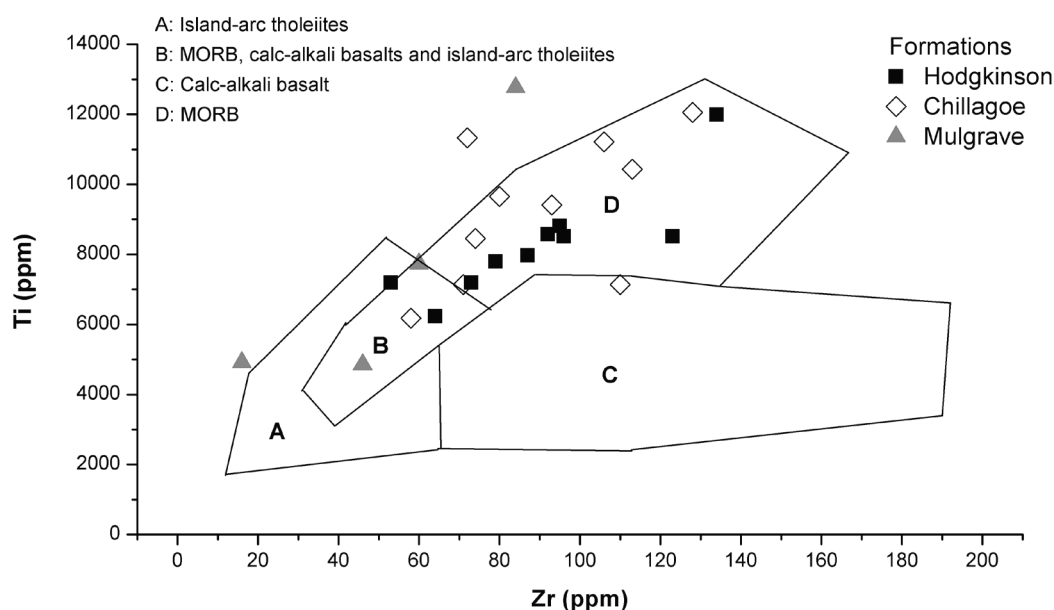


Fig. 4.6: Ti vs. Zr diagram after Pearce & Cann (1973) indicating overall the MORB affinity of Hodgkinson Province basalt samples.

classification of the studied samples as basalts and basaltic andesites. The basalts have a range from 44 to 56 wt% SiO_2 and MgO spanning 1.5 to 10 wt%. To better understand the tectonic setting and origin of the basaltic rocks, Ti and Zr values from Table 4.1 have been plotted in a tectonic discrimination diagram (Fig. 4.6; after Pearce & Cann 1973), which shows that the most basaltic rocks from the Hodgkinson

Province plot within the MORB field. Samples from the Mulgrave Formation notably plot either in field B (MORB, calc-alkali basalts and island-arc tholeiites) or outside any of the fields. Additionally, two samples from the Chillagoe Formation have anomalous Ti values that plot outside the MORB fields. No coherent linear relationships could be observed between samples of the same formation, although an overall relative decrease in Ti values can be implied for the Hodgkinson Fm samples when compared to

the Chillagoe Fm samples. Samples analysed for Th, Ta and Yb have been plotted on a Th/Yb vs. Ta/Yb diagram (Fig. 4.7) indicating that most samples fall within the mantle array. The samples that fall outside the mantle array indicate that the composition of some basalt samples in the Hodgkinson Province has been affected by crustal contamination (Pearce 1996).

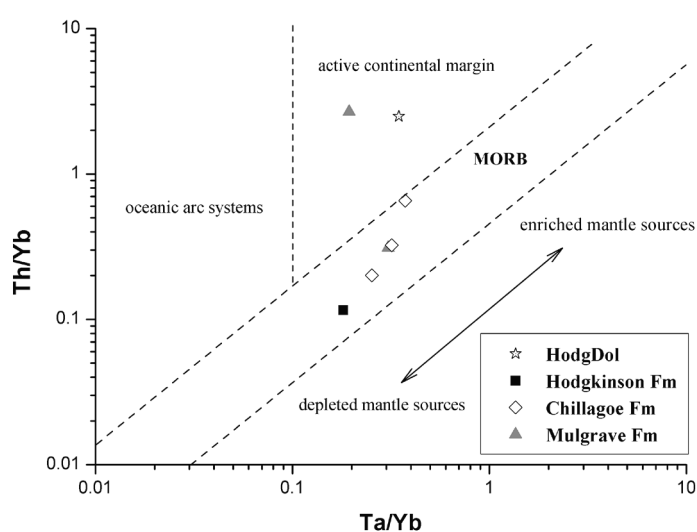


Fig. 4.7: Th/Yb vs. Ta/Yb diagram showing the derivation of representative Hodgkinson Province mafic rocks from the mantle array, with the exception of the HodgDol and PD1644 samples which plot in the active continental margin field.

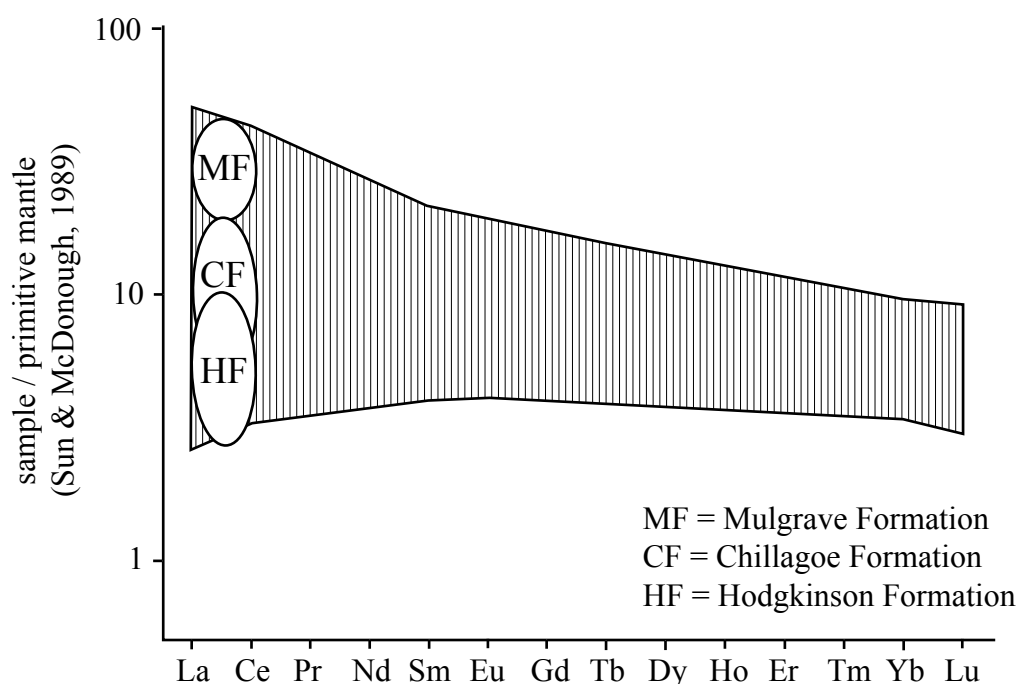


Fig. 4.8: REE diagram for Early-Middle Palaeozoic Hodgkinson basalts normalized to primitive mantle composition (Sun & McDonough, 1989). Envelope shows a relatively flat pattern shifting from slight enrichment in LREE for Late Ordovician-Early Silurian Mulgrave Formation basalts to slight depletion in LREE for Devonian Hodgkinson Formation basalts.

The envelope on the discrimination diagram for REE normalized to primitive mantle composition (Sun & McDonough 1989) represents the composition of Hodgkinson Province basalts (Fig. 4.8). This diagram shows that Mulgrave Formation basalts are enriched in LREE, while the Chillagoe and Hodgkinson Formation basalts show a relatively flat pattern, with depletion in LREE more common for the Hodgkinson Formation basalts. To further identify the most plausible tectonic environment in which these basalt samples originated, geochemical discrimination diagrams (spiderplots) based on basalt analyses normalized to an average tholeiitic (N-type) MORB (representing the composition a magma would attain without mantle source enrichment; for normalizing values refer to Pearce 1996) are shown in Figure 4.9. In the construction of these diagrams and where analyses remained below detection limit, we have normalized the detection limit and plotted the resulting

value as an indication of where a maximum value would plot. Figure 4.9a shows the pattern for the basalts interleaved with Mulgrave Formation sedimentary rocks and most strongly resembles a pattern of oceanic volcanic arc basalts (e.g. Pearce 1996) for three of the four samples. The samples from this formation are clearly more enriched in Th compared to the Chillagoe and Hodgkinson Fm, for which the patterns are shown in Figures 4.9b and 4.9c. In these figures the envelope is plotted for all of the analyses and representative analyses from both formations are shown. The patterns for the Chillagoe and Hodgkinson formation samples most closely resemble a pattern of (transitional) tholeiitic MORB. Several samples from the Chillagoe Formation show some volcanic arc basalt affinity or contamination by crustal sources illustrated by the positive Th and negative Nb anomalies (e.g. Pearce 1996). Figure 4.9d presents the geochemical pattern for the investigated dolerite samples.

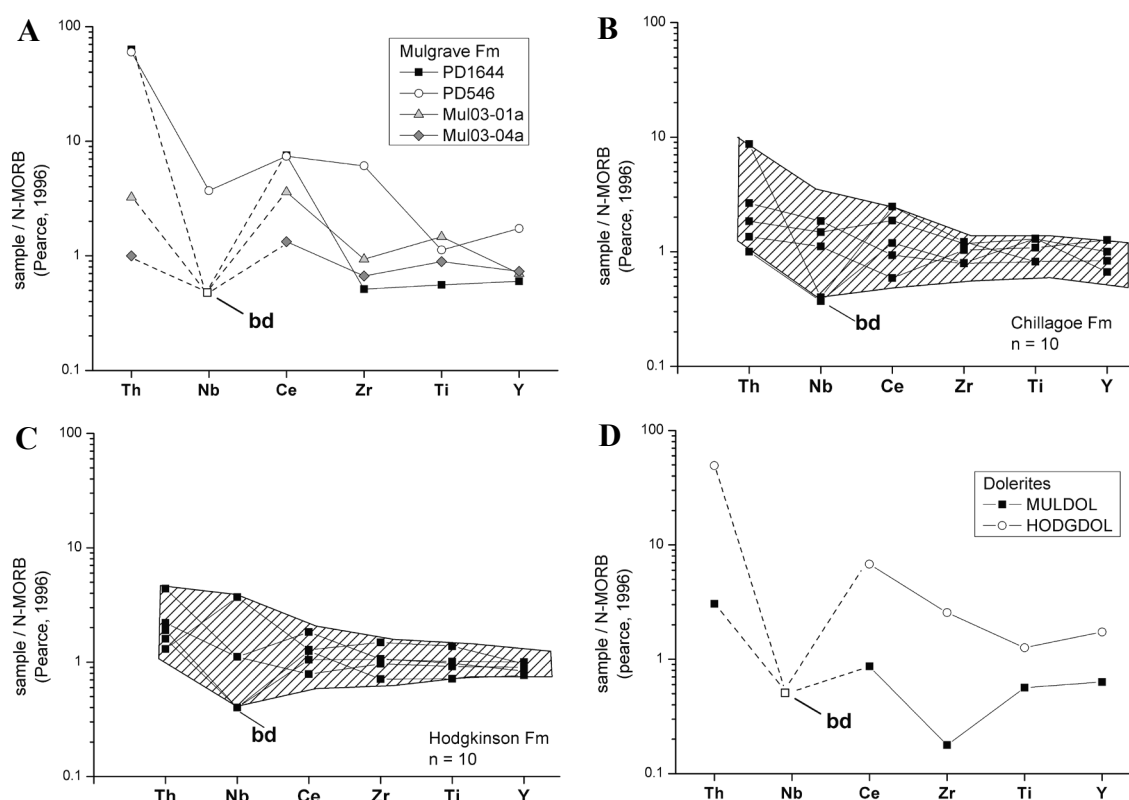


Fig. 4.9: Geochemical patterns based on basalt analyses normalized to an average tholeiitic (N-type) MORB. (a) Mulgrave Formation. (b) Chillagoe Formation. (c) Hodgkinson Formation. (d) dolerite intrusions; bd = below detection limit.

Strong Th enrichment for sample HodgDol reflects continental crustal derivation along an active continental margin (see also Fig. 4.7), whereas the pattern for sample MulDol closely resembles that of (transitional) MORB tholeiites, or tholeiitic volcanic arc basalts (Pearce 1996).

Results from Sm-Nd analysis of representative samples are presented in Table 4.2. Figure 4.10 shows the (age-corrected) ϵ_{Nd} values plotted against sample age. Since the absolute ages for the samples are not known, a dashed line indicates an age frame around our best estimate for the sample age (i.e. samples from the Chillagoe Fm are aged between 450 and 400 Ma). Depleted Mantle MORB (DMM) and sub-continental lithospheric mantle (SCLM) model age reference lines are indicated on Figure 4.10 and for comparison age corrected $\epsilon_{\text{Nd}}_{(420)}$ values for Proterozoic basement rocks adjacent

to and potentially underlying the Hodgkinson Province have been plotted on the figure with an average value of -13.7 (from Blewett *et al.* 1998). A distinct clustering is evident from this figure, where samples interleaved with the Mulgrave and Chillagoe Formations (and potentially MulDol) plot together, and samples from the Hodgkinson Formation plot together. One dolerite sample (HodgDol) forms a separate data point on this diagram.

The REE spiderplot for the Early-Middle Palaeozoic basalts (Fig. 4.8) suggests that the Mulgrave Formation basalts in the Hodgkinson Province are derived from an enriched mantle source (i.e. close to a volcanic arc; Pearce 1996). The Chillagoe Formation basalts represent a transition between the Mulgrave Formation basalts and the Hodgkinson Formation basalts of which the latter more closely resemble typical N-MORB composition (Pearce 1996).

Table 4.2: Results from Sm-Nd analysis.

Sample	Formation	Age (Ma)	Sm (ppm)	Nd (ppm)	$^{147}\text{Sm}/^{144}\text{Nd}$	$^{143}\text{Nd}/^{144}\text{Nd}$	eNd	eNd(t)	T(DM)
PD769B	Hodgkinson	370	4.07	12.55	0.196	0.513	7.45	7.48	498
Mt Ben	Mt. Bennett	400	3.01	9.37	0.194	0.513	7.39	7.53	519
PD1374	Chillagoe	420	2.23	6.39	0.211	0.513	7.06	6.28	629
PD1378	Chillagoe	420	2.43	8.28	0.177	0.513	4.33	5.37	698
MUL03-04A	Chill / Mulg	430	2.68	8.51	0.190	0.513	5.37	5.74	741
MUL03-01A	Mulgrave	450	5.05	23.08	0.132	0.513	1.41	5.12	678
HODG DOL	dolerite	300	8.87	36.71	0.146	0.512	-5.32	-3.39	1253
MUL DOL	dolerite	420	1.77	5.11	0.210	0.513	5.07	4.39	771

All $^{143}\text{Nd}/^{144}\text{Nd}$ relative to La Jolla standard = 0.511860; eNd(0) calculated using modern CHUR = 0.512638.

Depleted mantle Nd model age (TDM) calculated using a linear Sm-Nd isotope evolution from $eNd=0$ at 4.57 Ga to $eNd=+10$ at 0 Ga, resulting in present DM with $^{147}Sm/^{144}Nd=0.2136$ and $^{143}Nd/^{144}Nd=0.513141$

TDM considered meaningless because of high $^{147}\text{Sm}/^{144}\text{Nd}$; Estimated ages are based on stratigraphic position and field observations. Internal precision (2smean) and external precision (2sd) for $^{143}\text{Nd}/^{144}\text{Nd}$ $\leq \pm 0.00001$ and ± 0.00002 respectively. External precision (2sd) for $^{147}\text{Sm}/^{144}\text{Nd}=0.2\%$.

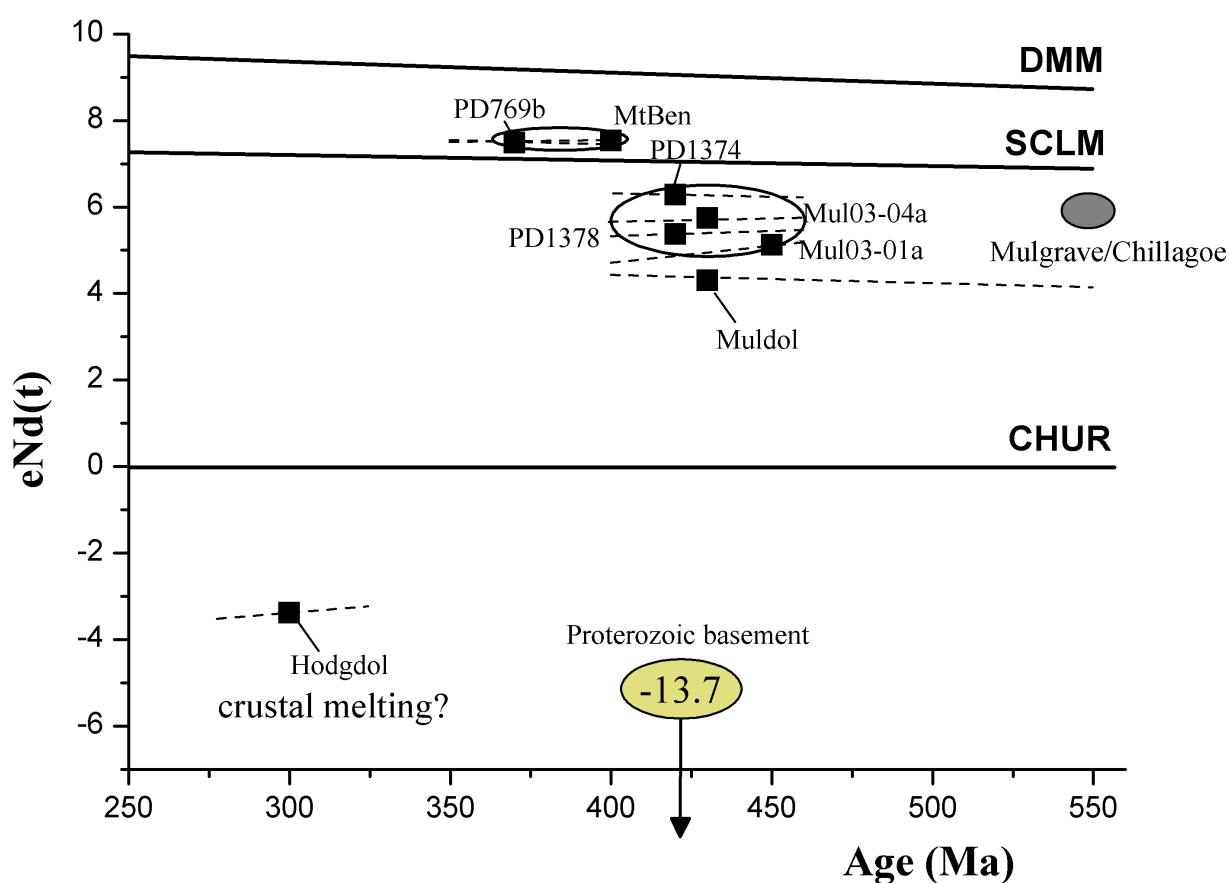


Fig. 4.10: ϵ_{Nd} values plotted against estimated ages for analysed samples from the Hodgkinson Province. See text for discussion.

In addition, the discrimination diagram for Mulgrave Formation basalts (Fig. 4.9a) shows distinct negative Nb anomalies that further support their generation in a volcanic arc-related setting (Pearce 1996). The discrimination diagrams for the Chillagoe and Hodgkinson formations (Figs. 4.9b and c) as well as the abundances of Y, Zr and REE in the majority of basaltic rocks from these formations are more characteristic for tholeiitic MORB. The positive Th and relatively minor negative Nb anomalies can be interpreted to indicate a volcanic arc affinity, but may also reflect crustal contamination. The patterns observed for the Chillagoe and Hodgkinson formation basalts most closely resemble back-arc basin rocks erupted in an incipient to slightly evolved rift setting (Pearce 1996; Dadd 1998).

4.5 DISCUSSION

4.5.1 Hodgkinson Province basalts: source characteristics

The clustering of Mulgrave and Chillagoe Formation samples on Figure 4.10 below the SCLM reference line indicates that these basalts may have been derived from a single source in the sub-continental lithospheric mantle and were partially contaminated by continental crust in their trajectory to the surface. The Muldol dolerite sample displays similar characteristics, but we do not necessarily consider it to be derived from the same source based on its model age trajectory (dashed line) diverging from the Mulgrave – Chillagoe Formation basalts. In addition, the Mulgrave – Chillagoe formation cluster, excluding MulDol gives a Sm-Nd model age of 555 ± 130 Ma (MSWD=0.13) as indicated by the errorchron in Figure 4.11.

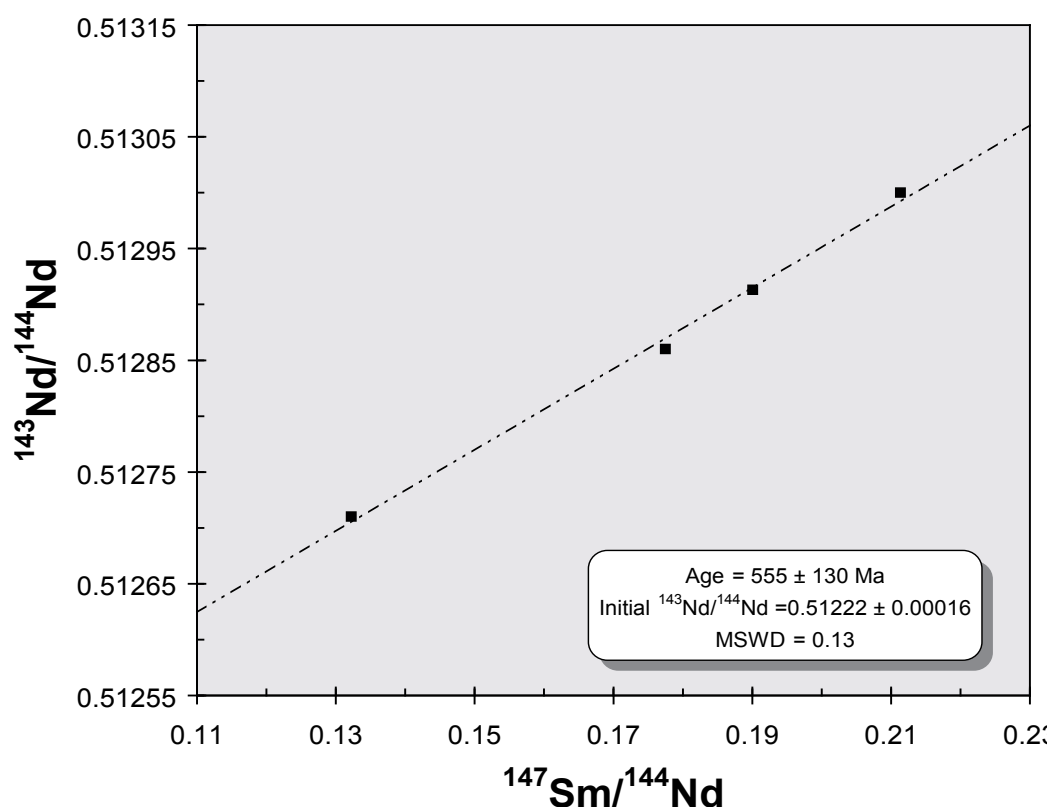


Fig. 4.11: Errorchron constructed for Mulgrave - Chillagoe Formation basalt cluster as indicated on Figure 4.10.

This model age may potentially infer that these basalts were co-magmatic at ~555 Ma. The clustering of Hodgkinson Formation samples between DMM and SCLM (Fig. 4.10) suggests that in contrast to the Silurian basalts, the Devonian basalts, may have been derived from an asthenospheric source and were contaminated by continental crust and / or lithospheric mantle. These results differ from Fawcckner (1981), who, on the basis of geochemical interpretations, argued that basalts from the Chillagoe and Hodgkinson formations were relatively uniform and sourced from a single, slightly differentiated tholeiitic magma source.

4.5.2 Hodgkinson Province basement

Based on Sm-Nd isotope data presented in this paper it is inferred that Early-Middle Palaeozoic basalts emplaced throughout the Hodgkinson Province were contaminated by a crustal source during their ascent through the lithosphere. The available data suggest that these mafic melts ascended through an attenuated and fractured continental Proterozoic crust. Crustal contamination became less pronounced with further attenuation of the crust through time. Such a model is consistent with previous findings by Champion & Bultitude (1994) who suggested that geochemical and Nd and Sr isotope characteristics of Carboniferous-Permian S- and I-type granites in the Hodgkinson Province reflect the presence of Proterozoic basement underneath the Palaeozoic Hodgkinson succession. Strontium and Nd isotopic data from I-type granites reported by Champion & Chappell (1992) indicate that the protolith for these granites was underplated beneath pre-existing crust at some time in the Middle Proterozoic. Therefore, the extent of

Carboniferous I-type granites may be used to indicate the minimum extent of Proterozoic basement beneath the Hodgkinson Province. The Barnard Metamorphics situated east of the Hodgkinson Province consist of mainly pre-Ordovician, middle to upper amphibolite facies schist and gneiss that are locally migmatitic (Bultitude *et al.* 1996b). Rocks of the Barnard Metamorphics may represent an exposed inlier of the basement underlying the Hodgkinson Province, as Sr and Nd isotopic data for Ordovician I-type granites that intruded the Barnard Metamorphics have $\epsilon_{\text{Nd}}(280-260 \text{ Ma})$ values identical to Permian I- and S-type granites in the Hodgkinson Province and near-identical $\epsilon_{\text{Nd}}(400 \text{ Ma})$ values to the Dido tonalite of the Georgetown Province (Black & McCulloch 1990).

4.5.3 Presence of a volcanic arc underneath the Hodgkinson Province

On the basis of geochemical and isotopic signatures, Champion & Bultitude (1994) argued that neither basaltic nor meta-sedimentary rocks in the Hodgkinson Province could have been the sole source for the Permian S-type granites present throughout the Province. According to Champion & Bultitude (1994) significant differences in ϵ_{Nd} values between the dominant quartz-lithic greywackes (ranging from -15 to -11) in the Hodgkinson Province and S-type granites (ranging from -2.5 to 6) necessitated considerable contributions from mafic magma to produce the ϵ_{Nd} values that characterise S-type granites in the Hodgkinson Province. On the other hand, geochemical characteristics of these granites are not consistent with a mixed basalt-sedimentary protolith. Champion & Bultitude (1994) therefore suggested that more suitable source rocks for these S-type granites,

as well as the I-type granites from the Yates and Cape Melville supersuites in the eastern part and to the northeast of the Hodgkinson Province, might be of early Palaeozoic volcanogenic provenance. The notion of an Early Palaeozoic volcanic arc is supported by the recognition of rare dacite clasts with SHRIMP crystallisation ages of 455 ± 5 Ma in the Mountain Creek Conglomerate in the western part of the Hodgkinson Province (Bultitude *et al.* 1993). These authors also suggested that the scarcity of these clasts might reflect burial of (a portion of) a volcanic arc underneath the cover sequence of the Hodgkinson Province rather than its erosion. This arc may have been active in the Middle to Late Ordovician as suggested by Withnall & Lang (1990, 1993) who suggested a change from a passive margin to an active arc environment at this time in the Broken River Province south of the Hodgkinson Province. The absence of post-Ordovician volcanoclastic arc-related rocks in the Hodgkinson Province suggests that the Silurian to Devonian arc system was spatially separated from the

Hodgkinson Province. We suggest that the subduction system that controlled the evolution of the Hodgkinson Province moved away from the Australian continental margin in the Silurian and thus removed any potential sources for arc-related rocks. In this regard, we emphasize that the Hodgkinson Province evolved on the landward side of a subduction-volcanic arc system and that the Early-Middle Palaeozoic basalts can therefore be regarded to have developed in a back-arc basin setting.

4.5.4 Implications for the Early-Middle Palaeozoic tectono-magmatic evolution of the Hodgkinson Province

Our findings indicate that the Early-Middle Palaeozoic Hodgkinson Province basalts record a transition from subduction related in the sub-continental lithospheric mantle to N-MORB-like basalts that are derived from sources in the asthenosphere. These characteristics support formation of the studied basalts in an extensional setting. Based on the strong petrogenetic similarity that exists between the Hodgkinson Province basalts and

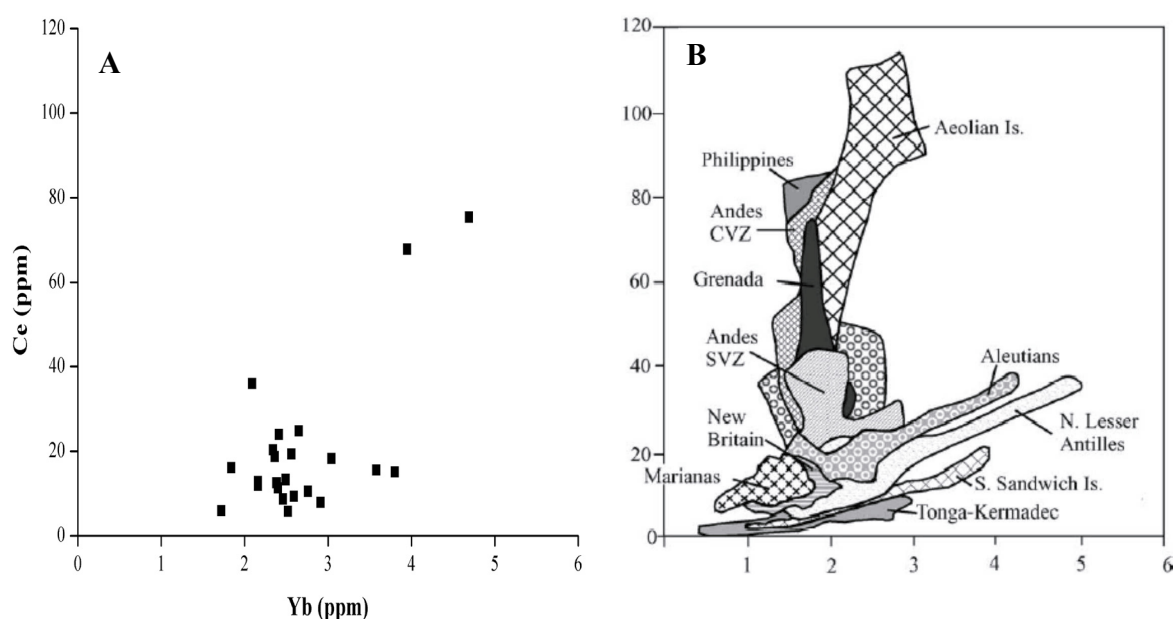


Fig. 4.12: Plots of Ce vs. Yb comparing result from Hodgkinson basalt analyses to modern arc systems (A) Hodgkinson Province basalts with outliers representing HodgDol and PD1644 respectively. (B) Oceanic and continental margin arc basalts. Fields from Hawkesworth *et al.* (1993).

modern back-arc basalts as indicated in Figure 4.12, we infer that the basalts were emplaced in an extensional back-arc basin setting. Although bimodal volcanism commonly occurs in extensional back-arc settings, no felsic volcanism is recorded in the Hodgkinson Province itself. However, the felsic Blackman's Gap Complex, Nundah Granodiorite and Cape York Peninsula Batholith were emplaced in the Georgetown region (Bultitude *et al.* 1997) contemporaneous with basalt volcanism in the Hodgkinson Province. Bultitude *et al.* (1997) also stated that the intrusion of these granites further supports an extensional model for the Hodgkinson Province.

Patterns of large-ion lithophile element enrichment in basaltic rocks are a function of age relative to basin evolution and commonly reflect the extent of spreading, with volcanogenic products formed during the early stages of rifting tending to have a marked enrichment in LILE due to crustal contamination, whereas products of more established back-arc spreading tend towards more typical MORB compositions less affected by crustal contamination (Saunders & Tarney 1984). Therefore, the geochemical characteristics of Hodgkinson Province basalts together with the transition of basalt sources as indicated in Figure 4.10 from sub-continental lithosphere (i.e. Mulgrave and Chillagoe formation basalts) to asthenosphere (i.e. Hodgkinson Formation basalts) may reflect enhanced crustal attenuation and accelerated extension rates in a widening back-arc basin. Accelerated widening of the back-arc basin led to rapid basin subsidence, crustal thinning and asthenospheric upwelling. This is supported by sedimentary records that indicate a change from mixed shallow marine sedimentation of the Chillagoe Formation to predominantly

deep-marine flysch-type sedimentation of the Hodgkinson Formation at ca. 400 Ma (Bultitude *et al.* 1993).

Previously proposed models for the tectonic evolution of the Hodgkinson Province revolved around two general types of tectonic settings: a subduction-related convergent regime (e.g. Cooper *et al.* 1975; Day *et al.* 1978; White 1978; Arnold & Fawcner 1980; Henderson 1980; Powell 1984) and a rifted continental margin regime (Fawcner 1981; Withnall *et al.* 1987; Bultitude *et al.* 1990, 1993, 1996a; Blewett & Wellman 1994; Blewett & Black 1998). We recognize that it is difficult to distinguish between continental rifting and back-arc models, since geochemical characteristics of basalts generated in both settings are very similar. In the case of the Hodgkinson Province basalts, petrogenetic similarities with modern back-arc basalts as illustrated in Figure 4.12 and the absence of oceanic crust in the Hodgkinson Province nevertheless favour a back-arc basin setting. We note, however, that the Hodgkinson basalts formed on an attenuated continental margin, which suggests their formation in a setting transitional between continental rifting and back-arc basin extension. This entails extension of the Australian continental margin on the landward side of, and spatially separated from a volcanic arc-subduction system similar to Palaeozoic back-arc basins in the central Andes (Bahlburg & Breiterkreuz 1991).

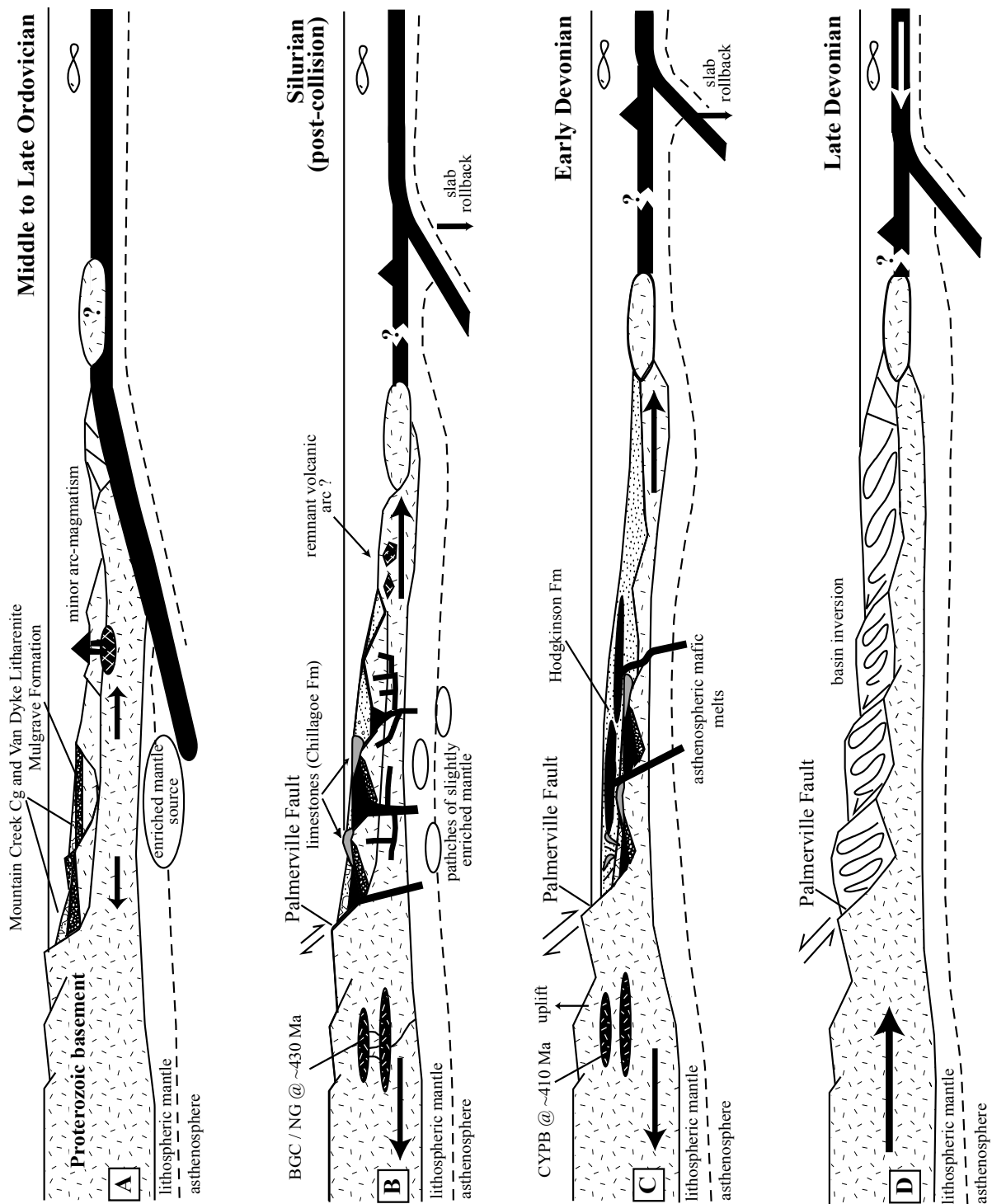
We propose that the petrogenetic evolution of basalts in the Hodgkinson Province reflects gradually decreasing input from an evolved magmatic arc-like source in the Late Ordovician and Silurian towards input of depleted primitive mantle sources in the Devonian controlled by an eastward stepping subduction system. This petrogenetic trend is reflected by an increase in

MgO content in these basalts through time, as the influence of the arc-like source decreases. The overall diminishing enrichment in Th and Ce in the basalt units in the Hodgkinson Province illustrated in the spiderplots further supports this notion. Rare earth element and Sm-Nd data from basalts incorporated in the Mulgrave and Chillagoe Formation support derivation from a melt source with a mixed MORB – arc signature in the sub-continental lithospheric mantle (possibly reflecting a previous episode of arc magmatism in the region). The arc signature diminishes with time as the back-arc basin widens and the source for the back-arc basin basalts becomes replenished by more primitive asthenospheric material in the Devonian. Mafic magmatism associated with back-arc basin development ceased during inversion of the Hodgkinson Basin in the Late Devonian.

4.6 A REVISED GEODYNAMIC MODEL FOR THE EVOLUTION OF THE HODGKINSON PROVINCE

Taking into account the findings of previous workers and geological studies, we have utilised the petrogenetic characteristics of basalts in the Hodgkinson Province as a key to tectonic setting and constructed a geodynamic model for the Early-Middle Palaeozoic evolution of the Hodgkinson Province. We suggest that the Late Ordovician to Late Devonian tectonic evolution of the Hodgkinson Province can be described in terms of four main events that followed deposition of the Mulgrave Formation in a passive margin environment in the Early to Middle Ordovician (Bultitude *et al.* 1997). We consider this part of the tectonic evolution of the Hodgkinson Province to be controlled by eastward stepping and rollback of a long-lived subduction system outboard of

the Palaeozoic Australian Craton (Coney *et al.* 1990). The Early-Middle Palaeozoic evolution of the Hodgkinson Province is illustrated in Figure 4.13 and includes: (a) Middle to Late Ordovician subduction along the eastern margin of the Australian Proterozoic Craton, minor arc magmatism that includes mantle enrichment and deposition of the Mountain Creek Conglomerate and Van Dyke Litharenite; (b) Oceanward stepping and rollback of the subducting slab followed ridge subduction (or docking of a microcontinent) around the Ordovician – Silurian transition. Renewed arc volcanism became spatially separated from the Hodgkinson Province, where incipient back-arc basin opening and attenuation of the Proterozoic crust occurred in the Silurian. The latter is represented by shallow marine deposition of the Chillagoe Formation as well as bimodal volcanism that includes the emplacement of Chillagoe Formation basalts and the intrusion of the Blackmans Gap Complex and Nundah Granodiorite in the Proterozoic hinterland west of the Hodgkinson Province (Bultitude *et al.* 1997); (c) Accelerated back-arc basin extension and crustal attenuation associated with continued rollback of the subducting slab causes further basin subsidence and deposition of the deep marine sediments of the Hodgkinson Formation in the Early Devonian. Bimodal volcanism continues and changes character to the asthenosphere-derived Hodgkinson Formation basalts and intrusion of the Cape York Peninsula Batholith contemporaneous with uplift in the Proterozoic hinterland; (d) Cessation of back-arc basin development and basalt generation with basin inversion and development of reverse faults and folds in the Early-Middle Palaeozoic stratigraphy caused by the overall eastward propagation



of the Australian craton overriding the proto-Pacific plate (Coney *et al.* 1990) probably in conjunction with collision with the outboard arc system and closure of the marginal sea basin.

4.6.1 Implications for the Early-Middle Palaeozoic evolution of the Tasman Fold Belt System in eastern Australia

Early-Middle Palaeozoic basalts of the Hodgkinson Province provide valuable insights into the tectonic evolution of the province and aid towards a better understanding of the tectonic evolution of the (northern part of the) Tasman Fold Belt System in eastern Australia. Basaltic rocks in the Hodgkinson Province have been correlated with basaltic rocks in the Early-Middle Palaeozoic rock sequences of the Broken River Province to the south (e.g. Withnall *et al.* 1997). The Early-Middle Palaeozoic basalts in the Broken River Province show a pattern of decreasing subduction-affinity to more distinct MORB compositions through time and have previously been interpreted to form in an extensional back-arc basin setting (Withnall 1989; Withnall & Lang 1993, Withnall *et al.* 1997). The similarity of basaltic rocks in the Hodgkinson and Broken River Province suggests that changes in the subduction dynamics controlled the development of extensional back-arc basins along the northern portion of the subduction system outboard of

Australia in the Early and Middle Palaeozoic. In addition, in the Lachlan Fold Belt, which forms the southern part of the Tasman Fold Belt System of eastern Australia, a number of terranes have been identified that share geological similarities with the Hodgkinson and Broken River provinces and have been interpreted as back-arc basins (e.g. Dadd 1998; Bierlein *et al.* 2002). Although the evolution of the southern part of the Tasman Fold Belt System in eastern Australia is considered more complex (e.g. Fergusson 2003; Spaggiari *et al.* 2004) than that of the northern part, rollback of the large-scale subduction system outboard of Australia in the Early-Middle Palaeozoic may have controlled the contemporaneous evolution of back-arc basins along the entire margin of Australia at that time.

4.7 CONCLUSIONS

Late Ordovician to Devonian mafic rock assemblages in the Hodgkinson Province consist of basalts and basaltic andesites. The geochemical composition of basalts in the Hodgkinson Province changes through time from volcanic-arc related basalts in the Late Ordovician to basalts resembling MORB in the Devonian. These compositional changes reflect the emplacement of basalts in a widening back-arc basin setting with decreasing influence of an arc-related source, or a subduction-modified

Fig. 4.13 (opposite page): Early Palaeozoic tectonic evolution of the Hodgkinson Province: a) Subduction and associated minor arc magmatism and deposition of the Mountain Creek Conglomerate / Van Dyke Litharenite in the Late Ordovician; b) Incipient back-arc basin opening and extension of continental lithospheric crust associated with ocean-ward stepping of the subduction system at the Ordovician – Silurian boundary. Basaltic rocks are derived from a predominantly sub-continental lithospheric mantle source (remnant slab fragment). Minor mixed shallow-marine sedimentation occurs in basin lows that result from the formation of half-grabens with the development of limestone reefs along the fringes of the fault blocks, BGC / NG = Blackmans Gap Complex / Nundah Granodiorite; c) Early to Middle Devonian accelerated back-arc basin opening, lithospheric extension and basin subsidence in response to steepening and further rollback of the subducting slab. Basaltic rocks are generated from asthenospheric melting and intercalated with deep-marine terrigenous sediments of the Hodgkinson Formation; CYPB = Cape York Peninsula Batholith; d) Late Devonian cessation of back-arc spreading without the development of true ocean crust contemporaneous with basin inversion, potentially in response to closure of a marginal sea and possible collision with the volcanic arc system in conjunction with eastward propagation of the Australian Craton overriding the proto-Pacific Plate.

mantle wedge. Sm-Nd isotope characteristics of the basalts indicate contamination by older continental lithosphere that diminishes over time as the back-arc basin widens. These isotopic characteristics also indicate a change in the location of the basalt source from the sub-continental lithospheric mantle to the asthenosphere at the Siluro-Devonian transition, indicative of accelerated extension. Our work supports the previously reported notion that the nature of the crust underlying the Hodgkinson Province consists of attenuated Proterozoic crust and / or remnants of Early Palaeozoic arc crust. Overall, this suggests that the Hodgkinson Province basalt units formed in an incipient to more evolved back-arc basin setting that developed on top of an attenuated continental substrate in the Late Ordovician to Devonian situated on the landward side of a subduction-volcanic arc system. The development of the back-arc basin and changes in basalt characteristics can be explained by the Early-Middle Palaeozoic dynamics of the subduction system outboard of Australia.

ACKNOWLEDGEMENTS

The study reported herein was conducted as part of the predictive mineral discovery Cooperative Research Centre (pmd*CRG) and this paper is published with the permission of the CEO, pmd*CRG. Analytical work was in part supported by a grant from the Australian Institute of Nuclear Science and Engineering to FPB and IMAV (AINGRA04008). David Garnett (AINSE) is thanked for his support with project set-up and analytical work. P. Donchak and J. Domagala (QLD NRM) are thanked for the provision of relevant samples and thin sections, valuable discussions and review of the manuscript. The manuscript has benefited

from discussions with and input from P. Betts, B. Schaefer, G. Mark (all Monash University) and B. Davis (RSG Global). R. Maas is thanked for assistance with Sm-Nd analyses. Kagara Zinc Pty Ltd (C. Georgees, I. Morrison) is acknowledged for providing sample material. J. Nethery (Nedex Pty Ltd) is thanked for his generous help with logistics in the study area and the provision of maps. We would also like to thank R. Price (University of Waikato) for discussions on the initial dataset. In particular, we were honoured by and thankful for insightful revisions by P. Floyd and J. Winchester.

REFERENCES

- ARNOLD G. O. & FAWCKNER J. F. 1980. The Broken River and Hodgkinson Provinces. *In*: Stephenson H. ed. , pp. 175-189. James Cook University, Department of Geology, Townsville, Australia.
- BAHLBURG H. & BREITKREUZ C. 1991. Paleozoic evolution of active margin basins in the southern Central Andes (northwestern Argentina and northern Chile). *Journal of South American Earth Sciences* 4, 171-188.
- BIERLEIN F. P., GRAY D. R. & FOSTER D. A. 2002. Metallogenic relationships to tectonic evolution; the Lachlan Orogen, Australia. *Earth and Planetary Science Letters* 202, 1-13.
- BLACK L. P. & McCULLOCH M. T. 1990. Isotopic evidence for the dependence of recurrent felsic magmatism on new crust formation; an example from the Georgetown region of northeastern Australia. *Geochimica and Cosmochimica Acta* 54, 183-196.
- BLEWETT R. S. & WELLMAN P. 1994. Asymmetrical lithospheric rifting in Late Silurian; a cause for the Coen Orogeny and development of the Hodgkinson Basin in NE Australia? *Geological Society of Australia Abstracts* 36, 12-13.
- BLEWETT R. S. & BLACK L. P. 1998. Structural and temporal framework of the Coen Region, north Queensland: implications

- for major tectonothermal events in east and north Australia. *Australian Journal of Earth Sciences* 45, 597-609.
- BLEWETT R. S., BLACK L. P., SUN S. S., KNUTSON J., HUTTON L. J. & BAIN J. H. C. 1998. U-Pb zircon and Sm-Nd geochronology of the Mesoproterozoic of North Queensland: implications for a Rodinian connection with the Belt Supergroup of North America. *Precambrian Research* 89, 101-127.
- BULTITUDE R. J., DONCHAK P. J., DOMAGALA J., FORDHAM B. G. & CHAMPION D. C. 1990. Geology and tectonics of the Hodgkinson Province, North Queensland. *Proceedings of the Pacific Rim Congress '90*, 75-81.
- BULTITUDE R. J., DONCHAK P. J., DOMAGALA J. & FORDHAM B. G. 1993. The Pre-Mesozoic stratigraphy and structure of the western Hodgkinson Province and environs. *Queensland Geological Record* 29. Department of Minerals and Energy, Queensland.
- BULTITUDE R. J., REES I. D., GARRAD P. D., CHAMPION D. C. & FANNING C. M. 1996a. Queensland 1:250 000 Geological Series, Explanatory Notes to Mossman Geological Map Sheet SE 55-1. Department of Mines and Energy, Geological Survey of Queensland.
- BULTITUDE R. J., FANNING C. M., CHAMPION D. C. & REES I. D. 1996b. PRE-SILURIAN rocks of the Barnard metamorphics: A basement? block on the SE margin of the Hodgkinson Province, North Queensland. *Geological Society of Australia Abstracts* 41, p.69.
- BULTITUDE R. J., GARRAD P. D., DONCHAK P. J. T., DOMAGALA J., CHAMPION D. C., REES I. D., MACKENZIE D. E., WELLMAN P., KNUTSON J., FANNING C. M., FORDHAM B. G., GRIMES K. G., OVERSBY B. S., RIENKS I. P., STEPHENSON P. J., CHAPPELL B. W., PAIN C. F., WILFORD J. R., RIGBY J. F. & WOODBURY M. J. 1997. Cairns region. In: Bain J. H. C. & Draper J. J. eds. North Queensland Geology, Australian Geological Survey Organisation Bulletin 240, 225-325.
- CHAMPION D. C. & CHAPPELL B. W. 1992. Petrogenesis of felsic I-type granites; an example from northern Queensland. In: Brown P. E. & Chappell B. W. eds. Proceedings on the second Hutton symposium on the origin of granites and related rocks. *Geological Society of America Special Publications* 272, 115-126.
- CHAMPION D. C. & BULTITUDE R. J. 1994. Granites of the eastern Hodgkinson Province II. Their geochemical and Nd-Sr isotopic characteristics and implications for petrogenesis and crustal structure in North Queensland. Department of Minerals and Energy; *Queensland Geological Record* 1994/1.
- CONEY P. J., EDWARDS A., HINE R., MORRISON F. & WINDRIM D. 1990. The regional tectonics of the Tasman orogenic system, eastern Australia. *Journal of Structural Geology* 12, 519-543.
- COOPER J. A., WEBB A. W. & WHITAKER W. G. 1975. Isotopic measurements in the Cape York Peninsula area, North Queensland. *Journal of the Geological Society of Australia* 22, 285-310.
- DADD K. A. 1998. Incipient backarc magmatism in the Silurian Tumut Trough, New South Wales; an ancient analogue of the early Lau Basin. *Australian Journal of Earth Sciences* 45, 109-121.
- DAVIS B. K., BELL C. C., LINDSAY M. & HENDERSON R. A. 2002. A single late orogenic Permian episode of gold mineralization in the Hodgkinson Province, North Queensland, Australia. *Economic Geology* 97, 311-322.
- DAY R. W., MURRAY C. G. & WHITAKER W. G. 1978. The eastern part of the Tasman orogenic zone. *Tectonophysics* 48, 327-364.
- FAWCKNER J. F. 1981. Structural and stratigraphic relations and a tectonic interpretation of the western Hodgkinson Province, Northeastern Australia, James Cook University, Townsville. Unpublished PhD thesis.
- FERGUSON C. L. 2003. Ordovician-Silurian accretion tectonics of the Lachlan Fold

- Belt, southeastern Australia. *Australian Journal of Earth Sciences* 50, 475-490.
- FLOYD P. A. & WINCHESTER J. A. 1975. Magma type and tectonic setting discrimination using immobile elements. *Earth and Planetary Science Letters* 27, 211-218.
- FOSTER D. A. & GRAY D. R. 2000. Evolution and structure of the Lachlan Fold Belt (Orogen) of Eastern Australia. *Annual Reviews in Earth and Planetary Sciences* 28, 47-80.
- HAWKESWORTH C. J., GALLAGHER K., HERGT J. M. & McDERMOTT F. (1993) Mantle and slab contributions in arc magmas. *Annual Reviews in Earth and Planetary Sciences* 21, 175-204.
- HENDERSON R. A. 1980. Structural outline and summary geological history for northeastern Australia. In: Stephenson H. ed. The geology and geophysics of northeastern Queensland, pp 1-26. James Cook University, Department of Geology, Townsville, Australia.
- HENDERSON R. A. 1987. An oblique subduction and transform faulting model for the evolution of the Broken River Province, northern Tasman Orogenic System. *Australian Journal of Earth Sciences* 34, 237-249.
- LE MAITRE R. W., BATEMAN P., DUDEK A., KELLER J., LEMEYRE J., LE BAS M. J., SABINE P. A., SCHMID R., SORENSEN H., STRECKEISEN A., WOOLEY A. R. & ZANETTIN B. 1989. A classification of igneous rocks and glossary of terms. Blackwell Science Publications, Oxford, United Kingdom.
- MESCHEDÉ M. 1986. A method of discriminating between different types of mid-ocean ridge basalts and continental tholeiites with the Nb-Zr-Y diagram. *Chemical Geology* 56, 207-218.
- MORRISON G. W. 1988. Palaeozoic gold deposits of northeastern Queensland. In: Morrison G. W. ed. Epithermal and porphyry style gold deposits in North Queensland. pp. 11-21. Contributions of the Economic Geology Research Unit, James Cook University, Townsville.
- MORRISON I. 2004. Kagara Zinc exploration - looking forward, looking back. AIG North Queensland Exploration and Mining Conference, extended abstracts, p.47.
- PEARCE J. A. & CANN J. R. 1973. Tectonic setting of basic volcanic rocks determined using trace element analyses. *Earth and Planetary Science Letters* 19, 290-300.
- PEARCE T. H., GORMAN B. E. & BIRKETT T. C. 1977. The relationship between major element chemistry and tectonic environment of basic and intermediate volcanic rocks. *Earth and Planetary Science Letters* 36, 121-132.
- PEARCE J. A. 1996. A user's guide to basalt discrimination diagrams. In: Wyman D. A. ed. Trace element geochemistry of volcanic rocks; applications for massive sulphide exploration. *Geological Association of Canada, Short Course Notes* 12, 79-113.
- SAUNDERS A. D. & TARNEY J. 1984. Geochemical characteristics and tectonic significance of back-arc basins. In: Kokelaar B. P. & Howells M. F. eds. Marginal basin geology; volcanic and associated sedimentary and tectonic processes in modern and ancient marginal basins. *Geological Society of London Special Publications* 16, 59-76.
- SPAGGIARI C. V., GRAY D. R. & FOSTER D. A. 2004. Lachlan Orogen subduction-accretion systematics revisited. *Australian Journal of Earth Sciences* 51, 549-553.
- SUN S. S. & McDONOUGH W. F. 1989. Chemical and isotopic systematics of oceanic basalts; implications for mantle composition and processes. In: Saunders A. D. & Norry M. J. eds. Magmatism in the ocean basins, *Geological Society of London Special Publications* 42, 313-345.
- TAYLOR D. H. & CAYLEY R. A. 2000. Character and kinematics of faults within the turbidite-dominated Lachlan Orogen: implications for tectonic evolution of eastern Australia; discussion. *Journal of Structural Geology* 22, 523-528.
- VEEVERS J. J. 1984. Phanerozoic Earth history of Australia. Macquarie University, North Ryde, NSW, Australia. *Oxford*

- Geological Sciences Series* 2.
- WHITE A. H. 1978. The western margin of the Hodgkinson Basin; a reappraisal. *Queensland Government Mining Journal* 79, 26-33.
- WINCHESTER J. A. & FLOYD P. A. 1977. Geochemical discrimination of different magma series and their differentiation products using immobile elements. *Chemical Geology* 20, 325-343.
- WITHNALL I. W., BAIN J. H. C. & RUBENACH M. J. 1980. The Precambrian geology of northeastern Queensland. In: Stephenson H. ed. The geology and geophysics of northeastern Queensland, pp 109-126. James Cook University, Department of Geology, Townsville, Australia.
- WITHNALL I. W., BULTITUDE R. J., LANG S. C., DONCHAK P. J. & HAMMOND R. L. 1987. Geology and tectonic history of the Palaeozoic Hodgkinson and Broken River provinces, North Queensland. *Proceedings of the Pacific Rim Congress '87*, 495-498.
- WITHNALL I. W. 1989. Revision of the stratigraphy of the Broken River area, North Queensland – Ordovician and Silurian rock units. *Queensland Government Mining Journal* 90, 213-218.
- WITHNALL I. W. & LANG S. C. 1990. Tectonic history of the Paleozoic Broken River Province, North Queensland. *Proceedings of the Pacific Rim Congress '90*, 315-323.
- WITHNALL I. W. & LANG S. C. 1993. Geology of the Broken River Province, North Queensland. *Queensland Geology* 4, 34-45.
- WITHNALL I. W., LANG S. C., LAM J. S., DRAPER J. J., KNUTSON J., GRIMES K. G. & WELLMAN P. 1997. Clarke River Region. In: Bain J. H. C. & Draper J. J. eds. North Queensland Geology, *Australian Geological Survey Organisation Bulletin* 240, 327-364.
- WYBORN D. 1992. The tectonic significance of Ordovician magmatism in the eastern Lachlan fold belt. In: Fergusson C. L. & Glen R. A. eds. Tectonics and metallogenesis of the Lachlan fold belt 214, 177-192.
- ZUCCHETTO R. G., HENDERSON R. A., DAVIS B. K. & WYSOCZANSKI R. 1999. Age constraints on deformation of the eastern Hodgkinson Province, North Queensland; new perspectives on the evolution of the northern Tasman orogenic zone. *Australian Journal of Earth Sciences* 46, 105-114.

**THE PALMERVILLE FAULT,
NE QUEENSLAND, AUSTRALIA:
A MULTI-DISCIPLINARY APPROACH TO
UNDERSTANDING MAJOR FAULT SYSTEMS**

I.M.A. Vos, F.P. Bierlein, M.A. Barlow and P. Betts

Journal of Structural Geology, in review.

ABSTRACT

The Palmerville Fault in northeastern Queensland, Australia forms a major terrane-bounding structure that may have controlled the evolution of the adjacent Palaeozoic Hodgkinson Province, the northernmost part of the Tasman Fold Belt System in eastern Australia. The nature and subsurface expression of the Palmerville Fault remain poorly constrained and models for contrasting geometries exist. In addition to structural field and microscopic observations, we combined results from multi-scale wavelet edge analysis ('worming'), forward modelling of regional magnetic and gravity data, and geochemical data sets to develop an improved understanding of the nature and subsurface geometry of the Palmerville Fault. Results from 'worming' suggest a steeply dipping geometry for the Palmerville Fault. Based on constraints from field observations and 'worming', we have generated a number of sections across the Palmerville Fault and forward modelled their magnetic and gravity response to compare with the observed magnetic and gravity response. Our results show that the Palmerville Fault represents a steeply eastward-dipping structure that may become listric at depth (implying the presence of Proterozoic basement underneath the Hodgkinson Province). Our findings imply that the Palmerville Fault was a first-order normal fault that controlled Early-Middle Palaeozoic basin development in the Hodgkinson Province. Subsequently, the fault acted as a (mid-crustal) décollement zone accommodating basin inversion in the Hodgkinson Province during the Late Palaeozoic. These results provide important constraints on the tectonic evolution of the Hodgkinson Province in northeastern Australia and also demonstrate the strength of multi-disciplinary research in areas of low-data density.

5.1 INTRODUCTION

Understanding the nature and subsurface expression of major fault systems is fundamental to understanding the role of fault systems in basin inversion processes (e.g. Hills *et al.* 2003; Betts *et al.* 2004). Combination of structural geology and interpretation of regional geophysical datasets has successfully been applied to determine the geometry of major fault systems (e.g. Grauch *et al.* 2003; Betts *et al.* 2004; Bierlein & Betts 2004). We apply this multi-disciplinary approach to determine the geometry of the Palmerville Fault and its role in the evolution of the Hodgkinson Province in northeastern Queensland, Australia (Fig. 5.1). The Palmerville Fault has previously been described as a steeply dipping normal fault (e.g. de Keyser 1963) as well as a west-dipping thrust fault steepened during later phases of shortening (Shaw *et al.* 1987). To date no seismic reflection data have been collected across the Hodgkinson Province and only regional geophysical datasets are available. The latter include aeromagnetic data (400m line spacing) and gravity data (variably spaced; nominally about 10km between stations) generated by the Geological Survey of Queensland and Geoscience Australia. Based on the limited availability of high-resolution datasets, we classify the Hodgkinson Province and areas to the west of the Palmerville Fault as low-data density.

In this paper we present structural observations from two key areas in the Palmerville Fault region. We integrate our field observations with results from multi-scale wavelet edge analysis ('worming' – Hornby *et al.* 1999), forward modelled magnetic and gravity data and available geochemical data sets. Our findings challenge the validity of a westward-

dipping fault model, and instead favour a model in which the Palmerville Fault forms a steeply eastward-dipping fault structure. In this model, the Palmerville Fault represents a first-order feature controlling Palaeozoic basin development and inversion that played an important role in the evolution of the epicratonic Hodgkinson Province. This paper illustrates the strength of combining structural field mapping with geophysical interpretation to constrain the evolution of low-data density areas. Our approach and findings can greatly contribute to insights into the role and geometry of large-scale faults during basin inversion and can be applied in similar areas elsewhere.

5.2. GEOLOGICAL SETTING

The Palmerville Fault marks the boundary between Proterozoic terranes to the west and the Palaeozoic Hodgkinson Province to the east (Figs. 5.1 and 5.2). The Hodgkinson Province forms the northernmost part of the dominantly Palaeozoic Tasman Fold Belt System in northeastern Australia (inset in Fig. 5.1). The fault strikes to the north and defines the westernmost extent of the Hodgkinson Province. The Palmerville Fault is interpreted to extend northward beneath the Mesozoic Laura Basin (Doutch 1976). In the southern portion of the Hodgkinson Province, the continuation of the fault is obscured by Carboniferous and Permian igneous rocks (de Keyser 1963), but is generally considered to change to a southeastern trend (Fig. 5.2) and most probably continues further south, possibly linking with a major terrane-bounding fault in the adjacent Broken River Province (Fig. 5.1). The Palmerville Fault has been considered to represent a relatively shallow-dipping feature based on the negligible difference in regional gravity across the fault (Fraser *et al.* 1977).

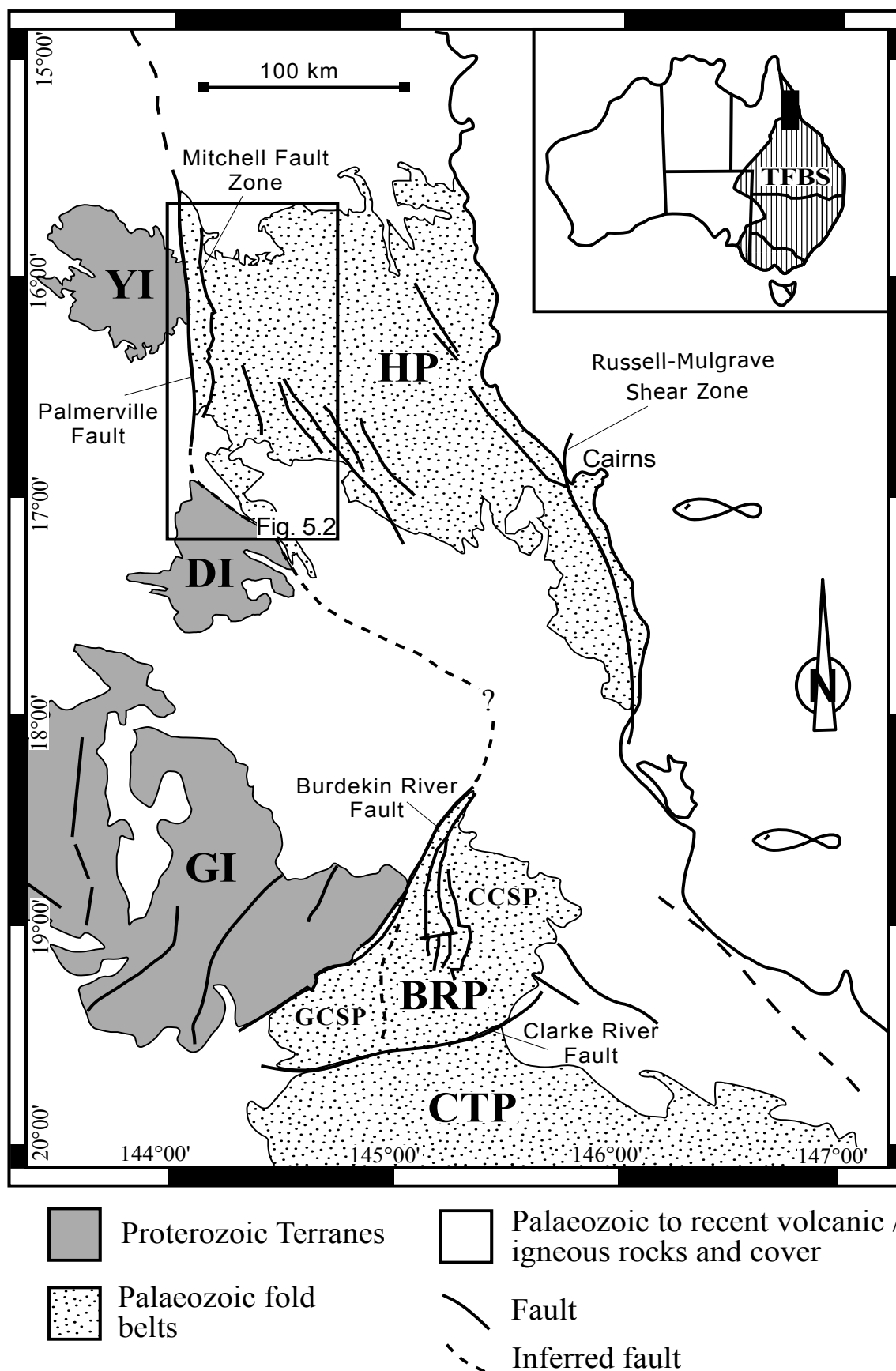


Fig.5.1: General geology and major faults of northeastern Australia; inset indicates the area covered in the Tasman Fold Belt System (TFBS) of eastern Australia. YI = Yambo Inlier, DI = Dargalong Inlier; GI = Georgetown Inlier; HP = Hodgkinson Province; BRP = Broken River Province; CTP = Charters Towers Province; GCSP = Graveyard Creek Subprovince; CCSP = Camel Creek Subprovince.

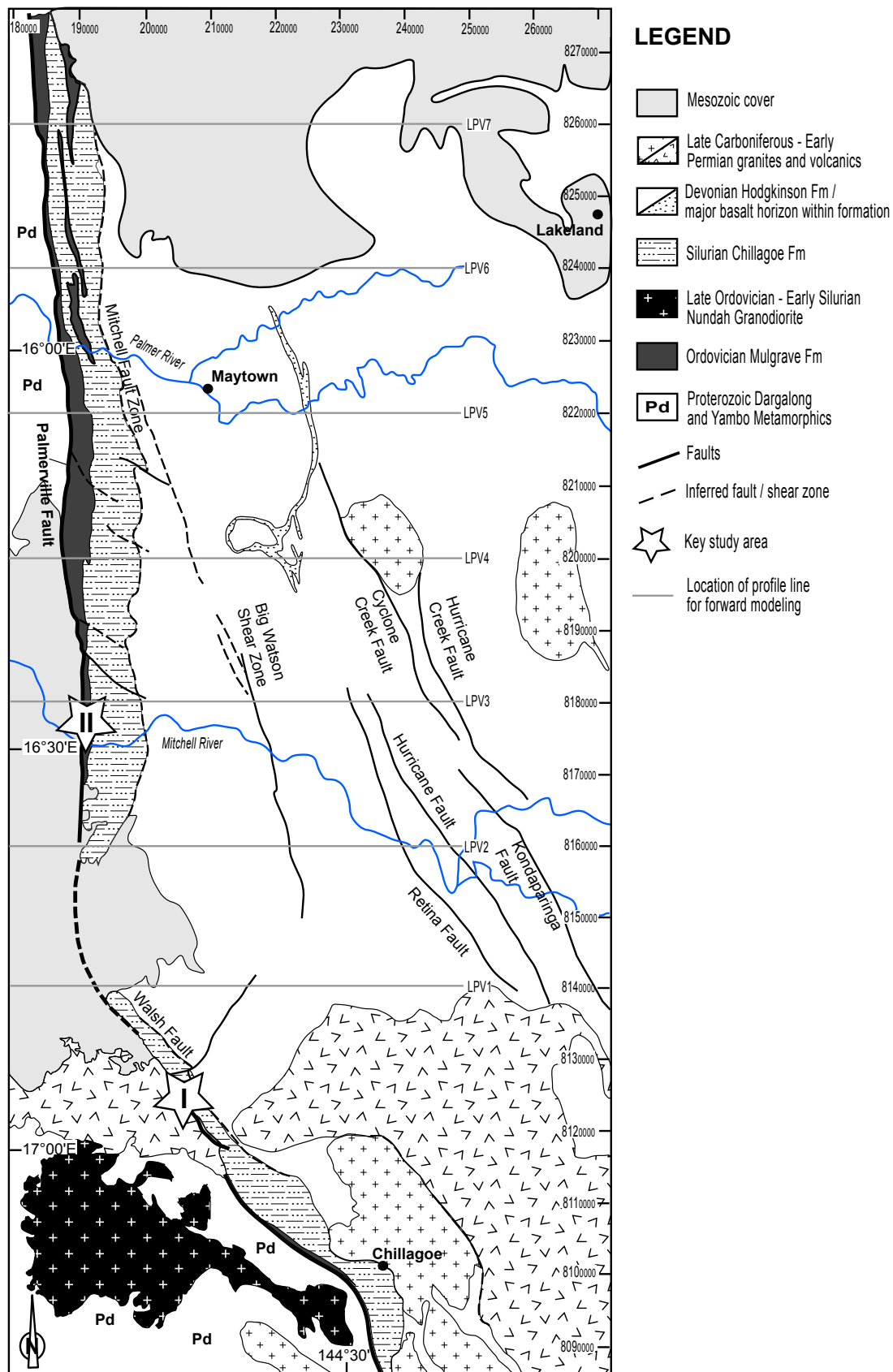


Fig. 5.2: Detailed geology of the western part of the Hodgkinson Province (inset in Fig.5.1) outlining the Palmerville and adjacent faults as well as the locations of profiles across the fault and key study areas.

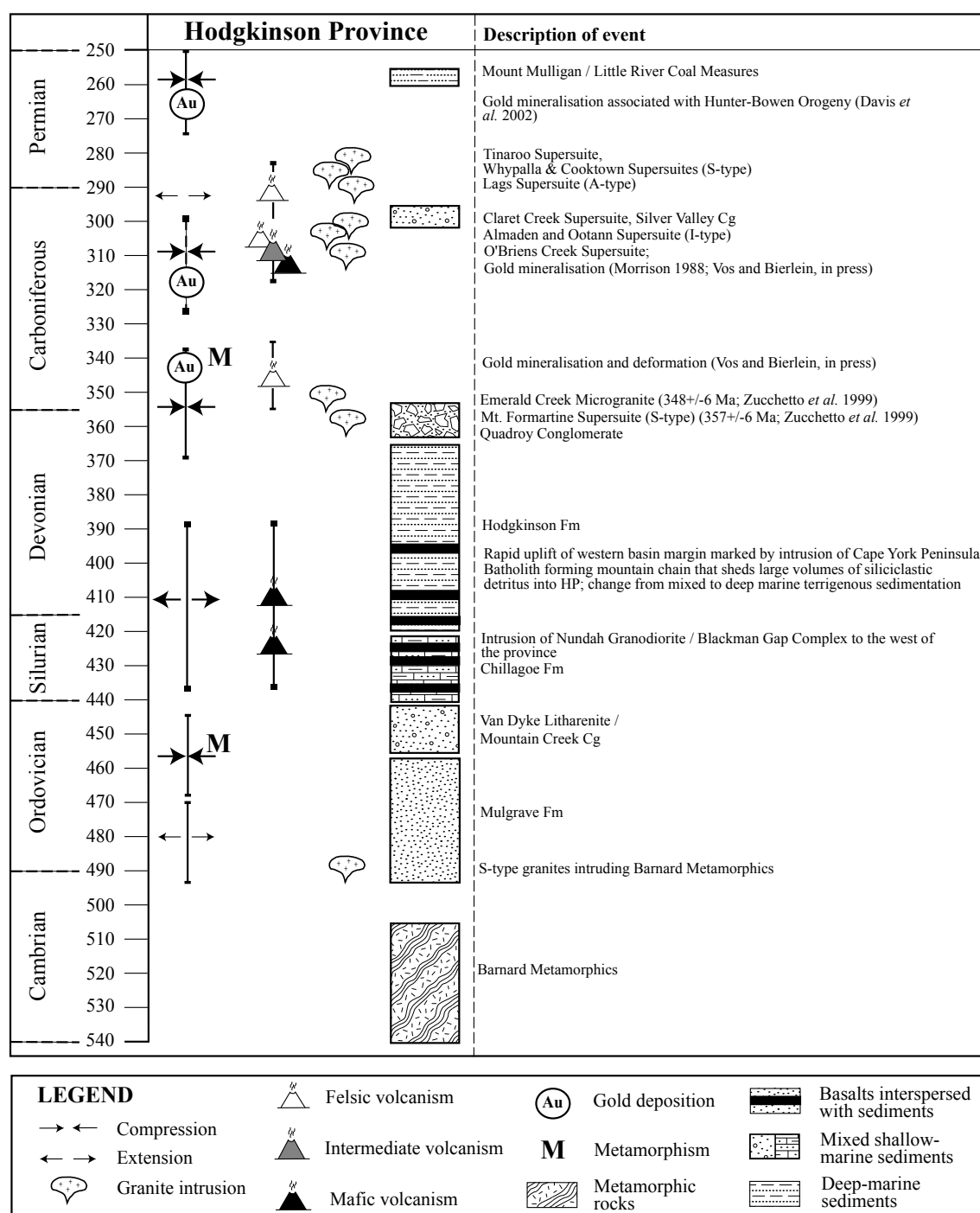


Fig. 5.3: Time-space diagram of Palaeozoic geological events across the Hodgkinson Province (compiled from Morrison 1988; Bultitude *et al.* 1997; Zucchetto *et al.* 1999 and Davis *et al.* 2002).

De Keyser (1963) first recognised the complex movement history of the Palmerville Fault, which has been supported by several more recent studies (e.g. Shaw *et al.* 1987; Bultitude *et al.* 1993, 1997). A detailed summary of the geological history of the Hodgkinson Province is given in Bultitude *et al.* (1997) and Vos *et al.* (in press). The Palaeozoic evolution of

the Hodgkinson Province can be summarised as Late Silurian to Middle Devonian basin development during which the volcanic and sedimentary successions of the Chillagoe and Hodgkinson Formations were emplaced (Fig. 5.3). This was followed by basin inversion during repeated episodes of Late Devonian to Carboniferous deformation that gave rise to

localized high strain zones and steeply-dipping fault parallel cleavage and intense folds (e.g. Bultitude *et al.* 1997).

The Palmerville Fault is considered to represent reactivation of a Precambrian basement structure. This is inferred from basement schistosity attributed to post-1580 Ma deformation and prograde amphibolite / granulite facies metamorphism (Bultitude *et al.* 1993; Bultitude *et al.* 1996). This basement schistosity is represented by high strain mylonite zones in the Proterozoic Yambo and Dargalong inliers directly adjacent to the Palmerville Fault. Bultitude *et al.* (1996) recognized a protracted movement history along the Palmerville Fault between the Neoproterozoic and the Tertiary, with the main movement along the fault occurring pre-Late Carboniferous, since neither the Palmerville Fault or adjacent faults significantly displace Late Carboniferous and Permian granites and volcanics in the area.

5.3. NATURE AND SUBSURFACE EXPRESSION OF THE PALMERVILLE FAULT

5.3.1 Field and microstructural investigations

Structural datasets have been collected from two key areas in the Palmerville Fault region (Fig. 5.2). Key area I is situated on the contact between Early Palaeozoic basin assemblages with Proterozoic basement rocks and Late Palaeozoic granites where the fault strikes

northwest. Key area II is positioned at the contact between Palaeozoic basin assemblages and Proterozoic basement rocks along the north-striking part of the fault. Outcrops of the Palmerville Fault are only sporadically exposed, since the contact is commonly obscured by Mesozoic cover sequences and / or igneous intrusions that presumably utilised the fault as a conduit for magma flux. Where exposed, the extent of deformation in the vicinity of the Palmerville Fault is intense and decreases away from the fault (Fig. 5.4a-d). As previously noted by other authors (e.g. Shaw *et al.* 1987; Bultitude *et al.* 1997), Palaeozoic rock assemblages to the east of the Palmerville Fault generally parallel the strike of the Palmerville Fault (Fig. 5.5a) and have a dominantly steep eastward dip. These rock assemblages are characterised by upright folding, intense cleavage fabrics, and fault-mélange and breccias that surround and incorporate low strain lenses and pods. Shear band boudins, s-c fabrics and rotated porphyroclasts in these assemblages in key area I record a component of sinistral shear (Fig. 5.4a-b). In places, the Palmerville Fault can be identified as a 30-100m wide fault zone that represents the transition from strongly deformed Palaeozoic shales and arenite beds in the east (Fig. 5.4c) to Proterozoic micaceous schist in the west (Fig. 5.4d). Steep as well as shallow lineations were recorded in both key areas (Fig. 5.5b). In key area I, both steep and shallow lineations were observed in the

Fig. 5.4 (opposite page): a) Close-up of shear band boudins in strongly sheared shales in NW-striking section of the Palmerville Fault (key area I) indicating sinistral shear movement (Goscombe and Passchier 2002); b) Close-up of shear bands in quartz vein hosted by sheared shales and arenites in the NW-striking section of the Palmerville Fault (key area I) indicating sinistral sense of shear; c) Chaotic disarray of shale, chert and arenite beds (mélange) as generally observed in the vicinity of the Palmerville Fault (key area II); d) Isoclinal folding of Proterozoic micaceous schists to the west of the Palmerville Fault (key area II); e) Photomicrograph (XPL – thin section cut perpendicular to steep lineation on fault plane) of a section of the Palmerville Fault (key area I -, Fig. 5.2) showing s-c fabrics depicted by mica-rich bands in a matrix of strongly recrystallised quartz indicating a sinistral sense of shear; f) Photomicrograph (XPL – thin section cut perpendicular to steep lineation on fault plane) of a section of the Palmerville Fault (key area I -, Fig. 5.2) showing σ -clasts of garnet as well as s-c fabrics indicating a sinistral sense of shear.



Proterozoic rocks adjacent to the Palmerville Fault. In key area II, only steep lineations were recorded in Proterozoic as well as Palaeozoic rocks.

Microstructural investigations of Proterozoic basement rocks from the Palmerville Fault indicate that in the key areas the Palmerville Fault can be characterised as a proto-mylonite

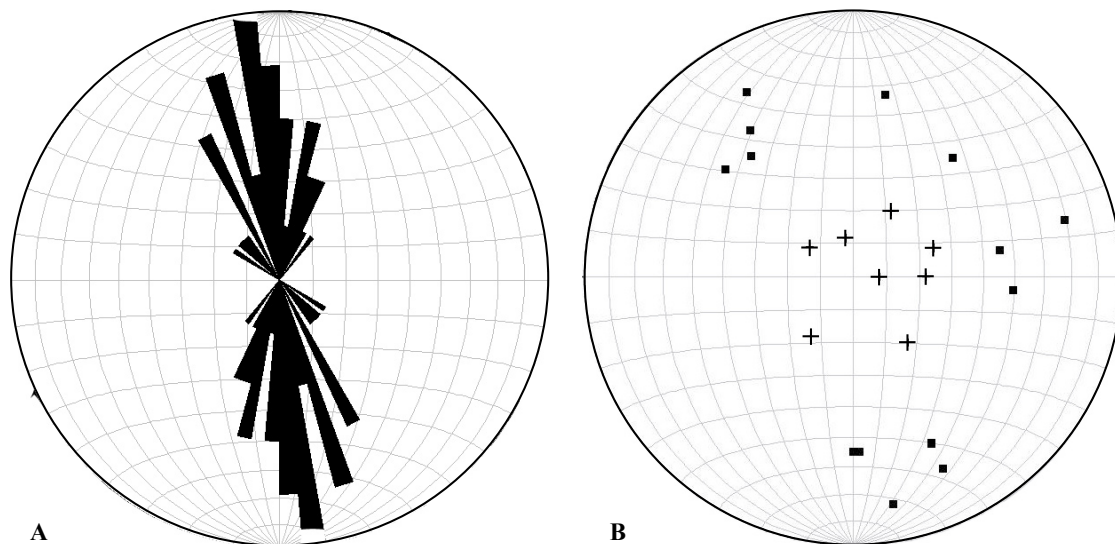


Fig. 5.5: a) Rose diagram (n=35) indicating dominant north to northwest strike of rock assemblages adjacent to the Palmerville Fault (collected from key study areas). b) Lower hemisphere projection of steep (crosses) and shallow (squares) lineations recorded in key study areas.

zone based on the presence of (folded) micaceous shear bands and elongated garnet crystals within strongly recrystallised quartz matrix on sections cut perpendicular to steep lineations on the fault plane (Fig. 5.4e-f). Figure 5.4e and f show that the micaceous shear bands and deformed and rotated quartz crystals indicate a sinistral sense of shear (Fig. 5.4e-f). Micaceous shear bands defining s-c fabrics in sections parallel to the steep lineations on the fault plane indicated normal movement. This indicates that the Proterozoic basement rocks record normal movement with a sinistral sense of shear that may be considered to reflect the earliest movements along the Palmerville Fault in the Early Palaeozoic.

5.3.2 Modelling

To better understand the subsurface geometry and architecture of the Palmerville Fault and to extrapolate the structural relationships observed in the key areas we have undertaken interpretation and forward modelling of magnetic and gravity data (e.g. Betts *et al.* 2003). This includes the interpretation of

multiscale wavelet edges to constrain the nature of lithological and fault contacts and forward modelling to constrain the 3-D subsurface geology of the Palmerville Fault region.

5.3.2.1 WORMING

Multiscale wavelet edges or 'worms' are vectorised points of maximum gradient derived through a process of wavelet transformation and upward continuation of potential field data (Archibald *et al.* 1999; Hornby *et al.* 1999). An array of upward continuation levels provides insight into the behaviour of gradients at different scales and depths (i.e. small upward continuations reflect gradients near surface and large upward continuations map gradients at depth). Depending on the potential field and transformation employed, the strongest gradients relate to contacts of rock-property contrasts (i.e. susceptibility for magnetic fields and density for gravity). Contacts without rock property contrast cannot be imaged, but may be inferred through linear truncations and offsets in overlapping worm sets. Synthetic models indicate that the dip direction of a worm sheet

can mirror its related geological contact (e.g. folds, faults, intrusive bodies; Holden *et al.* 2000). Using the height and length persistence of near-surface worm sheets, inferences can be made about the relative depth of penetration of a geological edge. To investigate the geometry of the Palmerville Fault, worming has been applied to gravity and magnetic datasets for the Hodgkinson Province.

Detailed analysis of worms in the Palmerville Fault area was undertaken to investigate the fault dip (Fig. 5.6). In Figure 5.6, the worm sheet associated with the Palmerville Fault consists of very tightly spaced worms, which suggests a very steeply dipping worm array and hence may be interpreted to mirror the steep dip of the Palmerville Fault. To the east of the Palmerville Fault in this figure, the worm sheet

associated with the Mitchell Fault Zone displays an increasing upward continuation level from west to east. This indicates an easterly dip for this worm array and can be considered to reflect an easterly dip for the Mitchell Fault Zone. Regional results of worming of data covering the area of Figure 5.2 are presented in Figure 5.7a and 5.7b for aeromagnetic and Bouguer gravity data, respectively. Magnetic worms predominantly outline the edges of magnetic rock bodies (i.e. Siluro-Devonian basalts of the Chillagoe Formation) that are considered to parallel fault structures. Gravity data across the Hodgkinson Province is sparse and unevenly distributed. Combined with relatively minor density contrasts, this limits the capacity of (gravity) worming to pick up contacts other than those with the lowest density members (i.e.

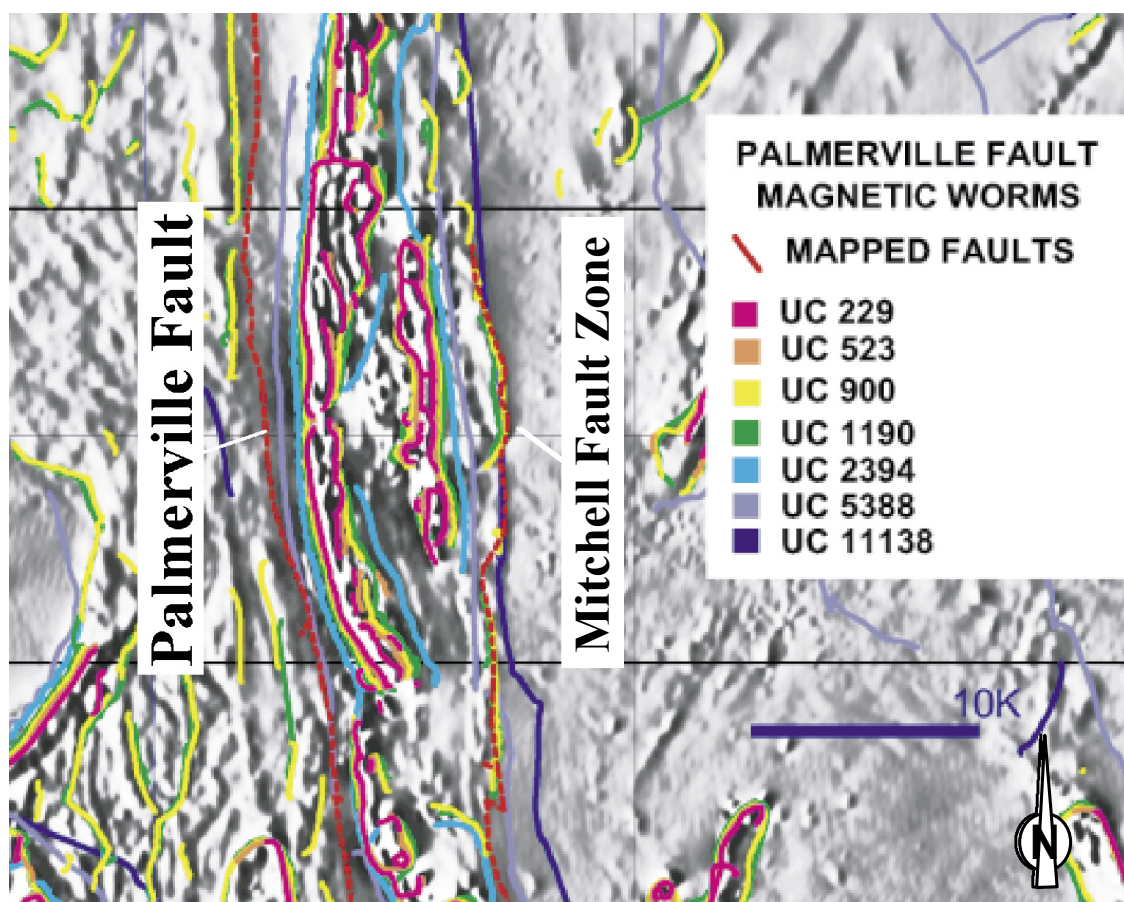


Fig. 5.6: Detailed worming over a section of the Palmerville Fault (location indicated by red dashed line on figure) indicating a steeply dipping fault geometry. Worm sheets associated with the Mitchell Fault Zone suggests a steep eastward-dipping geometry for this structure.

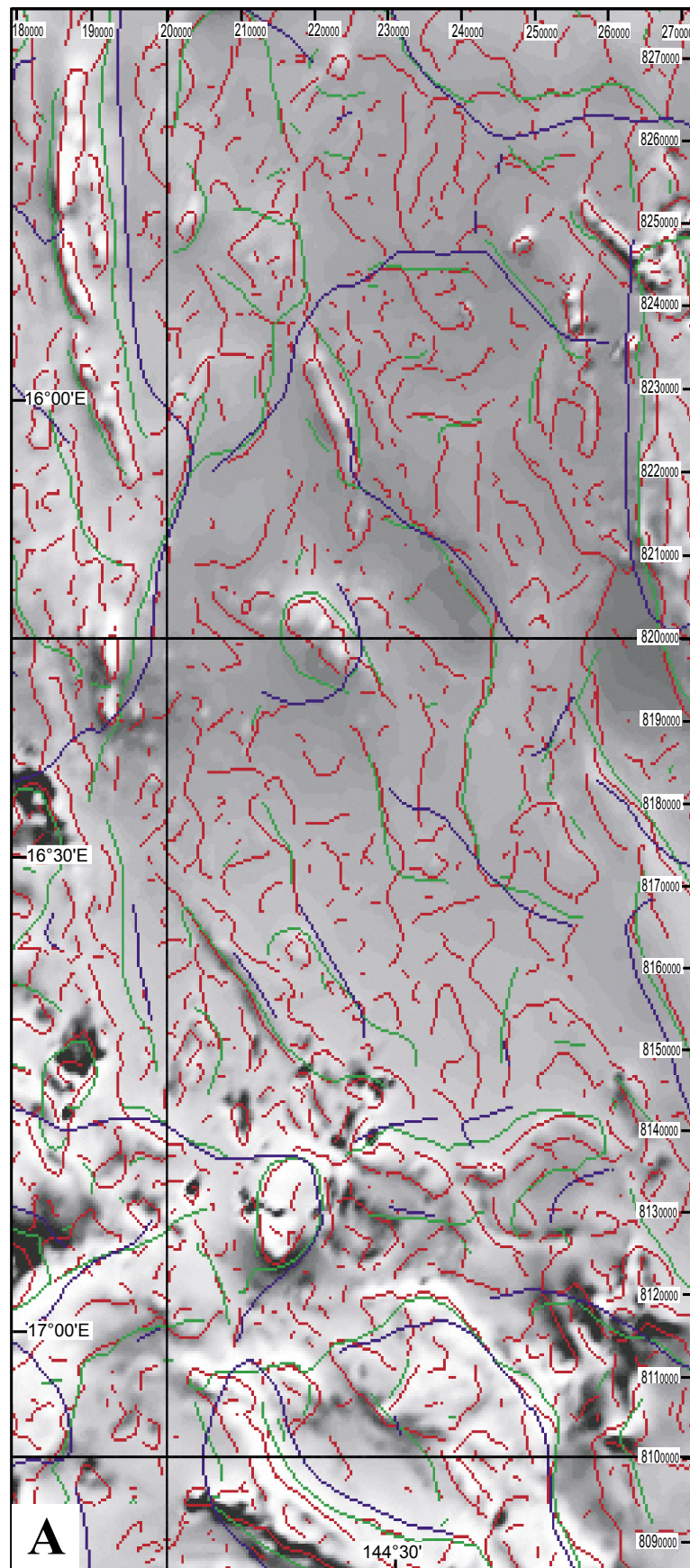


Fig. 5.7a: Magnetic worms over greyscale total magnetic intensity image. Worm colours correspond to upward continued layers: red = 1096m, green = 5269m, blue = 11553m.

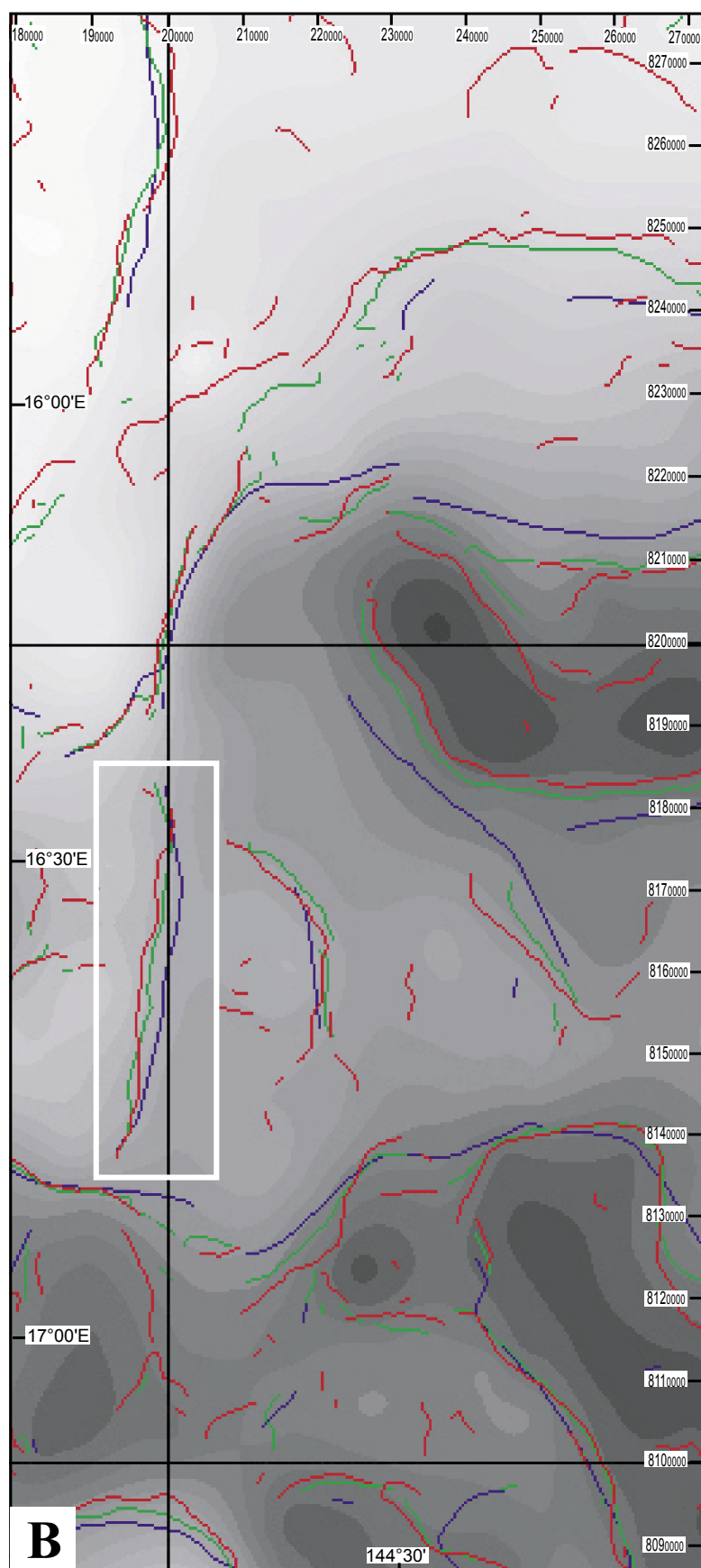


Fig. 5.7b: Gravity worms over greyscale Bouguer gravity image. Worm colours correspond to upward continued layers: red = 1190m, green = 5388m, blue = 11138m. Inset encloses worm sheet that is directly associated with the Palmerville Fault.

Carboniferous to Permian granites). The gravity worms mainly pick up edges of granitic bodies where there is a major density contrast with the country rock. However, despite the minor density contrast between rock assemblages across the Palmerville Fault, gravity worming clearly indicates an eastward dipping worm sheet associated with the Palmerville Fault (inset in Figure 5.7b), suggesting a steep eastward dip for this structure.

5.3.2.2 FORWARD MODELLING

Gravity and magnetic data was forward modelled for seven regional cross-sections across the Palmerville Fault to further constrain the geometry and depth extent of the fault.

Our modelling methodology is based on the following: 1) worming results have been used to constrain block boundaries; 2) representative density and susceptibility values from the region have been used to define the contrasts; 3), the simplest and most conformable model between slices has been developed and; 4) the constructed block model has been tied to surface geology. Modelling was performed with Encom's ModelVision TM software as a series of 2-D slices at 20km intervals along the entire length of the fault (Fig. 5.2). A representative profile is given in Figure 5.8 indicating a) observed (black) and modelled (blue) Bouguer gravity response; b) topography; c) residual magnetics with field response (nT) in black

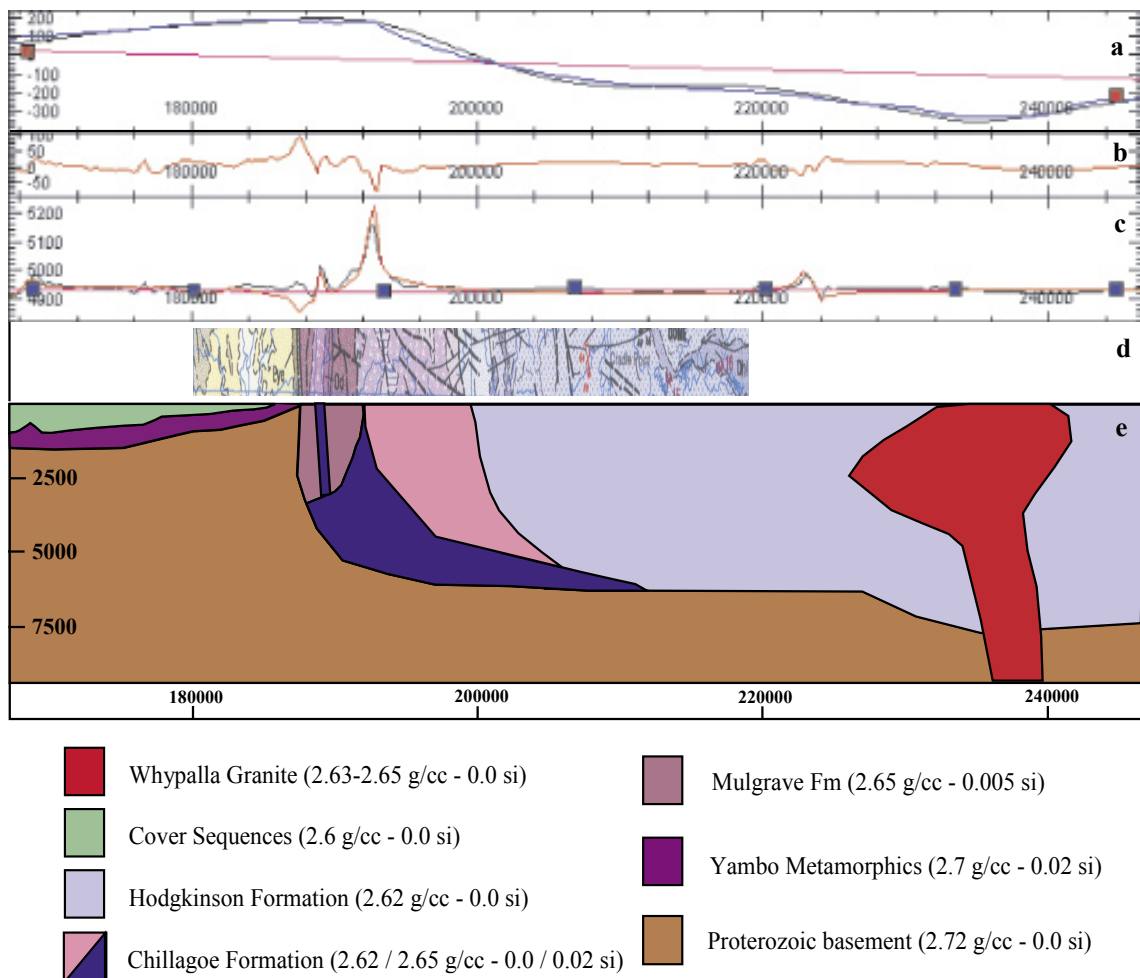


Fig. 5.8: Modelled profile at 8220000N across the Palmerville Fault (LPV5). From top window down: a) Bouguer gravity response (gu) in black and modelled in blue; b) Topography; c) Residual magnetics with field response (nT) in black and modelled response in pink; d) Surface geology slice from 1:250,000 Mossman Map Sheet (Bultitude *et al.* 1996); and e) Proposed block geology model with density and magnetic properties outlined in legend.

and modelled response in pink; d) surface geology; and e) block geology model. The Palmerville Fault is interpreted to represent the boundary between lithologies with contrasting rock properties. Directly east of the fault, the Palaeozoic rocks have been assigned 0.005 - 0.02 SI and 2.62 - 2.65 g/cc for magnetic susceptibility and density respectively. To the west of the fault, Proterozoic rocks have been assigned 0.0 - 0.02 SI and 2.70 - 2.72 g/cc for magnetic susceptibility and density respectively. A decreasing observed gravity gradient is apparent across the fault, indicating less mass to the east of the fault compared to the west of the fault as expected from density differences in the Proterozoic and Palaeozoic rock assemblages. Previously, Champion & Bultitude (1994) and Bultitude *et al.* (1996)

suggested that regional Bouguer anomalies indicate that continental crust with similar characteristics to the metamorphic basement west of the Palmerville Fault extends east of the Palmerville

Fault underneath the Hodgkinson Province. To achieve 'best fit' in our modelling results, the presence of Proterozoic basement underneath the Palaeozoic assemblages is required and thus supports the notion of Champion & Bultitude (1994) and Bultitude *et al.* (1996). A magnetic gradient is observed across the Palmerville Fault from -140nT to the west to +340nT to the east (maximum values). The magnetic response to the east of the Palmerville Fault is controlled by the presence of basaltic units within the Chillagoe Formation. Although variable in distribution along the length of the fault, their

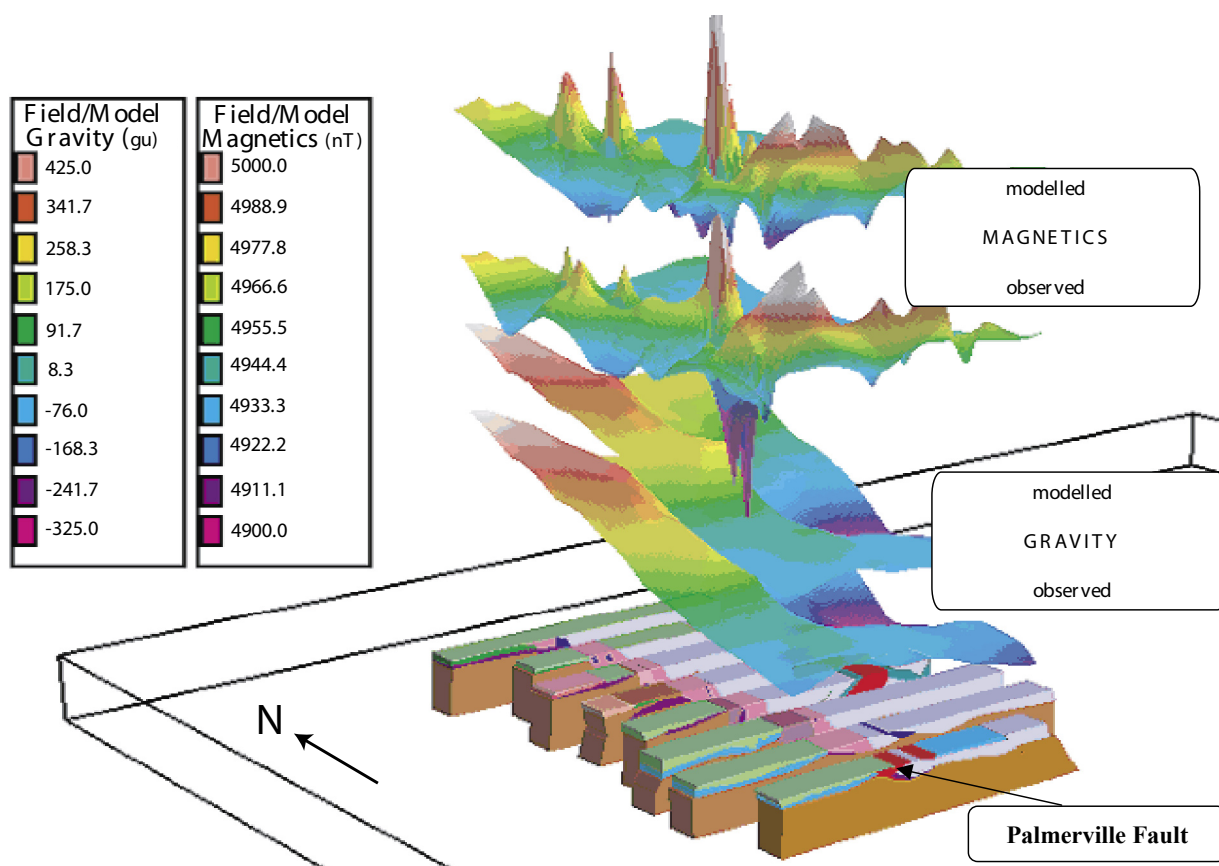


Fig. 5.9: All constructed model sections across the Palmerville Fault created by forward modelling and based on integration of field observations, 'worming' and geochemical datasets illustrating a steeply eastward-dipping Palmerville Fault. Together these sections combine to generate a permissive 3-D block model of the geometry of the western part of the Hodgkinson Province. Modelled and observed magnetic and gravity response are given. Note the close match between observed and modelled magnetics and gravity.

magnetic response suggests the presence of steeply eastward-dipping magnetic bodies to the east of the Palmerville Fault, which can be interpreted to parallel the fault and therefore support a model of a steeply eastward-dipping regional fault structure. All constructed model sections across the Palmerville Fault are given in Figure 5.9. In this figure, the modelled sections are combined to generate a permissive 3-D block model of the western part of the Hodgkinson Province. The close match between the observed and modelled gravity and magnetics over the Hodgkinson Province (Fig. 5.9) illustrate the validity of our modelling work. Overall, a best fit between the observed and calculated geophysical response is achieved when the Palmerville Fault is modelled as a steeply eastward-dipping fault that soles out at a depth of approx. 6km. The fault is modelled as a detachment / décollement, where it ramps to a depth of approx. 7.5km around 40 km east of the Palmerville Fault. Nonetheless, the depth extent of the fault (i.e. the depth to which the fault penetrates into the basement) remains an issue that could not be resolved satisfactorily. Due to the relatively subtle susceptibility and density contrasts within rock assemblages adjacent to the fault, the overall model is relatively insensitive to the total depth of rock displaced by the Palmerville Fault. Although the modelling demonstrates a depth to basement of around 6 - 7.5km, the actual depth extent of the Palmerville Fault and consequently the depth of Proterozoic basement may be several km deeper or shallower than our modelling suggests.

5.4. DISCUSSION

5.4.1 Kinematics of the Palmerville Fault

De Keyser (1963) suggested the occurrence

of at least four phases of movement along the Palmerville Fault. These include: 1) normal movement initiating subsidence in the Hodgkinson Province during the Silurian; 2) reverse displacement causing folding and uplift of the Hodgkinson Province during the Carboniferous; 3) normal movement during the Late Permian; and 4) reverse displacement that may have continued until the Quaternary. Our field and microstructural observations can be associated with the first two phases of movement along the fault. Proterozoic basement rocks to the west of the fault only recorded the initial phase of fault movement. Microstructural investigations from these rocks indicated that normal movement with a component of sinistral shear represents this initial phase of fault movement. The absence of kinematic indicators associated with west-directed thrusting in Proterozoic basement rocks west of the Palmerville Fault indicates that the basement rocks have not been substantially deformed during basin inversion and that the strongly deformed Palaeozoic basin rock assemblages characterised by *mélange* zones and fault-breccias must have accommodated the bulk of west-directed, basin inversion during the Late Palaeozoic. On the basis of 1) the presence of preserved lineations and kinematic indicators that point to normal movement during the initial phase of movement along the Palmerville Fault, 2) the east to west increase of strain in Palaeozoic basin rocks towards the fault and 3) the overall deformation focus on the hanging wall of the fault (i.e. the Palaeozoic rock assemblages) as compared to the footwall of the fault (i.e. the Proterozoic basement rocks), we suggest that the Proterozoic basement rocks and by inference the Palmerville Fault acted like a

buttress during Late Palaeozoic basin inversion. Hanging wall buttressing is considered a common characteristic of inverted normal faults (e.g. Butler 1989; Betts *et al.* 2004). The presence of steep and shallow lineations as well as sinistral shear sense indicators in deformed Palaeozoic rock assemblages along the south-west striking section of the Palmerville Fault in key area I suggests that a component of strike-slip may have been associated with inversion along this portion of the fault.

5.4.2 Implications for the tectonic evolution of the Hodgkinson Province

Our structural observations and modelling results indicate that the Palmerville Fault forms a steeply eastward-dipping structure that becomes listric at depth. This is in contrast with results from Shaw *et al.* (1987), who interpreted the Palmerville Fault as an integral part of a major reverse west-dipping thrust system.

An eastward-dipping model for the Palmerville Fault is complimentary to interpretations of the tectonic evolution of the Hodgkinson Province that comprise inversion of an extensional back-arc basin controlled by episodes of subduction rollback intermittent with microcontinent / ridge subduction outboard of the Palaeozoic Australian Craton (e.g. Bultitude *et al.* 1997; Vos *et al.* in press). Our modelling results imply the presence of Proterozoic basement underneath the Hodgkinson Province. This is in agreement with an eastward-dipping fault model and is in turn supported by geochemical datasets (Champion & Bultitude 1994; Vos *et al.* in press) that indicate that the character of mafic volcanic rocks and granite intrusions in the Hodgkinson Province infers the presence of Proterozoic basement at depth. The presence of Proterozoic basement underneath the Hodgkinson province

and the character and intensity of deformation in Palaeozoic basin rocks in the province implies a mechanism of thin-skinned thrusting during Late Palaeozoic basin inversion. In this scenario, the intensity of the deformation in the Palaeozoic rock assemblages in the hanging-wall of the Palmerville Fault is controlled by their competency contrast with the more competent Proterozoic rocks in the footwall of the fault (e.g. Betts *et al.* 2004). By inference, the Palmerville Fault would have acted not only as a buttress along the western margin of the Hodgkinson Province but also as a low-angle décollement zone between the Palaeozoic basin assemblages and the underlying Proterozoic basement.

The presence of a proto-Palmerville Fault in the Proterozoic (Bultitude *et al.* 1993) most probably controlled the location and development of the Palmerville Fault during Early Palaeozoic extension along the proto-Pacific margin of northeastern Australia. This suggests that during Silurian to Late Devonian extension in the Hodgkinson Province the Palmerville Fault developed as a (mid-crustal) detachment fault along the margin of Proterozoic Australia. During subsequent basin inversion, the Palmerville Fault acted as a mid-crustal décollement zone and Palaeozoic basin assemblages were strongly disrupted in response to thin-skinned thrusting. The kinematics of the Palmerville Fault and the general evolution of the Hodgkinson Province have been illustrated in Figure 5.10.

Although our modelling did not resolve the character of intra-basinal second-order thrust faults in detail, we suggest that these further accommodated shortening in the province and could have been oversteepened in the western part of the province as a result of more intense

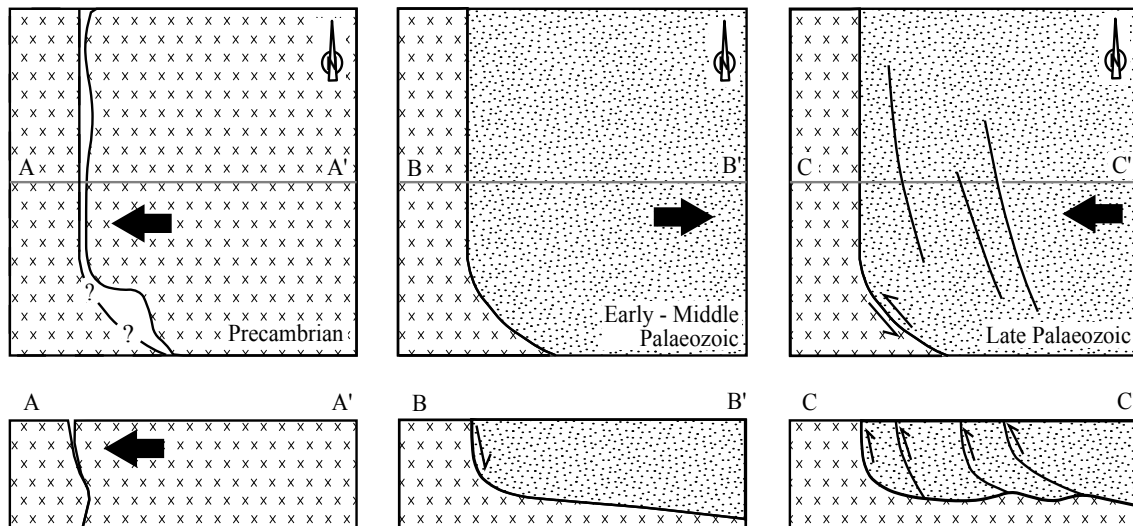


Fig. 5.10: Schematic plan views and cross sections illustrating the role of the Palmerville Fault in the tectonic evolution of the Hodgkinson Province.

deformation. Alternatively, intra-basinal west-dipping structures could be explained by backthrusting adjacent to the Precambrian buttress. Such a scenario is reminiscent of interpretations of the Moyston Fault in the Lachlan Fold Belt in southeastern Australia (Cayley & Taylor 1998). Taylor & Cayley (2000) argued that a doubly-vergent pop-up structure could develop during convergence towards a buttress where a zone of high deformation will be spatially concentrated along the controlling fault. As such, the Palmerville Fault can be regarded as an equivalent structure to the Moyston Fault, where zones of tectonic melange can be found directly adjacent to the major faults.

5.5. CONCLUDING REMARKS

The nature of the subsurface structure of major faults is an important problem (e.g. Lynch & Richards 2001) and commonly integral to understanding the role of large-scale faults in the tectonic evolution of an area (e.g. Betts *et al.* 2004). Especially where faults have undergone multiple reactivations and data density remains low, determinations regarding their subsurface nature and structural evolution are rendered

difficult. The approach of combining geological, geophysical and geochemical datasets has proven particularly useful in determining the nature and character of a major fault system in a low-data density area in northeastern Australia and could be applied successfully in similar regions elsewhere.

Results from integrated working, forward modelling and field studies combined with available geochemical datasets indicate that the Palmerville Fault, which forms the boundary between Proterozoic and Palaeozoic rock assemblages in northeastern Australia, represents a steeply eastward-dipping inverted normal fault. The eastward-dipping nature of the Palmerville Fault above Proterozoic basement implies that the fault probably developed as a basin- and terrane-bounding mid-crustal detachment fault during Early to Middle Palaeozoic extension on the margin of Proterozoic Australia. During subsequent inversion and deformation of the basin in the Late Palaeozoic, the Palmerville Fault acted as a décollement zone that accommodated thin-skinned, west-directed thrusting during a number of episodes of contraction in the Hodgkinson Province.

ACKNOWLEDGEMENTS

Research has been funded by the Cooperative Research Centre for predictive mineral discovery (pmd*CRC) and this paper is published with the permission of the CEO, pmd*CRC. An International Postgraduate Research Scholarship from Monash University is gratefully acknowledged. B. Murphy is thanked for valuable comments on the interpretation of worm data. R. Blewett is thanked for various discussions on the topic of this paper and the provision of additional relevant material. J. Nethery is acknowledged for his logistical support in the field. We further wish to acknowledge A. Hitchmann, B. Goleby and D. Giles for their support during this study.

REFERENCES

- ARCHIBALD N., GOW P. & BOSCHETTI F. 1999. Multiscale edge analysis of potential field data. *Exploration Geophysics* 30, 38-44.
- BETTS P. G., VALENTA R. K. & FINLAY J. 2003. Evolution of the Mount Woods Inlier, northern Gawler Craton, Southern Australia: an integrated structural and aeromagnetic analysis. *Tectonophysics* 366, 83-111.
- BETTS P. G., GILES D. & LISTER G. S. 2004. Aeromagnetic patterns of half-graben and basin inversion: implications for sediment-hosted massive sulfide Pb-Zn-Ag exploration. *Journal of Structural Geology* 26, 1137-1156.
- BIERLEIN F. P. & BETTS P. G. 2004. The Proterozoic Mount Isa Fault Zone, northeastern Australia: is it really a ca. 1.9 Ga terrane-bounding suture? *Earth and Planetary Science Letters* 225, 279-294.
- BULTITUDE R. J., DONCHAK P. J., DOMAGALA J. & FORDHAM B. G. 1993. The Pre-Mesozoic stratigraphy and structure of the western Hodgkinson Province and environs. Department of minerals and energy, Queensland, 259p.
- BULTITUDE R. J., REES I. D., GARRAD P. D., CHAMPION D. C. & FANNING C. M. 1996. Queensland 1:250 000 Geological Series Explanatory Notes to Mossman Geological Map Sheet SE 55-1, Department of Mines and Energy, Geological Survey of Queensland, 128p.
- BULTITUDE R. J., GARRAD P. D., DONCHAK P. J. T., DOMAGALA J., CHAMPION D. C., REES I. D., MACKENZIE D. E., WELLMAN P., KNUTSON J., FANNING C. M., FORDHAM B. G., GRIMES K. G., OVERSBY B. S., RIENKS I. P., STEPHENSON P. J., CHAPPELL B. W., PAIN, C. F., WILFORD J. R., RIGBY J. F. & WOODBURY M. J. 1997. Cairns region. In: Bain, J. H. C. and Draper, J. J. eds. North Queensland geology. *Australian Geological Survey Organisation Bulletin* 240, 225-325.
- BUTLER R. W. H. 1989. The influence of pre-existing basin structure on thrust system evolution in the western Alps. In: Cooper M. A. & Williams G. D. eds. Inversion Tectonics. *Special Publication of the Geological Society of London* 44, 17-39.
- CAYLEY R. A. & TAYLOR D. H. 1998. The Lachlan margin, Victoria; the Moyston Fault, a newly recognized terrane boundary. *Geological Society of Australia Abstracts* 49, 73.
- CHAMPION D. C. & BULTITUDE R. J. 1994. Granites of the eastern Hodgkinson Province. II. Their geochemical and Nd-Sr isotopic characteristics and implications for petrogenesis and crustal structure in North Queensland. Department of Minerals and Energy; *Queensland Geological Record* 1994/1, 113p.
- DAVIS B. K., BELL C. C., LINDSAY M. & HENDERSON R. A. 2002. A single late orogenic Permian episode of gold mineralization in the Hodgkinson Province, North Queensland, Australia. *Economic Geology* 97, 311-322.
- DE KEYSER F. 1963. The Palmerville Fault - a fundamental structure in north

- Queensland. *Journal of the Geological Society of Australia* 10, 273-278.
- DOUTCH H. F. 1976. The Karumba Basin, northeastern Australia and southern New Guinea. *BMR Journal of Australian Geology and Geophysics* 1, 131-140.
- FRASER A. R., DARBY F. & VALE K. R. 1977. The reconnaissance gravity survey of Australia; a qualitative analysis of results. Report - Bureau of Mineral Resources, *Geology and Geophysics* 198, 92p.
- GOSCOMBE B. D. & PASSCHIER C. W., 2003. Asymmetric boudins as shear sense indicators; an assessment from field data. *Journal of Structural Geology* 25, 575-589.
- GRAUCH V. J. S., RODRIGUEZ B. D. & WOODEN J. L. 2003. Geophysical and isotopic constraints on crustal structure related to mineral trends in north-central Nevada and implications for tectonic history. *Economic Geology* 98, 269-286.
- HILLS Q. G., BETTS P. G. & LISTER G. S. 2003. Geophysical interpretation and modelling of the Olary Domain under cover: a hidden inverted rift system. *Australian Journal of Earth Sciences* 50, 633-644.
- HOLDEN D. J., ARCHIBALD N. J., BOSCHETTI F. & JESSELL M. W. 2000. Inferring geological structures using wavelet-based multiscale edge analysis and forward models, *Exploration Geophysics* 31, 617-621.
- HORNBY P., BOSCHETTI F. & HOROWITZ F. G., 1999. Analysis of potential field data in the wavelet domain. *Geophysical Journal International* 137, 175-196.
- LYNCH J. C. & RICHARDS M. A. 2001. Finite element models of stress orientations in well-developed strike-slip fault zones; implications for the distribution of lower crustal strain. *Journal of Geophysical Research, B, Solid Earth and Planets* 106, 26,707-26,729.
- MORRISON G. W. 1988. Palaeozoic gold deposits of northeastern Queensland. *In: Morrison, G. W. ed. Epithermal and porphyry style gold deposits in North Queensland. Contributions of the Economic Geology Research Unit*, 29, 11-21.
- SHAW R. D., FAWCKNER J.F. & BULTITUDE R.J. 1987. The Palmerville Fault System: a major imbricate thrust system in the northern Tasmanides, North Queensland. *Australian Journal of Earth Sciences* 34, 69-93.
- TAYLOR D. H. & CAYLEY R.A. 2000. Character and kinematics of faults within the turbidite-dominated Lachlan Orogen: implications for tectonic evolution of eastern Australia: discussion. *Journal of Structural Geology* 22, 523-528.
- VOS I. M. A. & BIERLEIN, F. P. In press. Characteristics of orogenic gold deposits in the Northcote District, Hodgkinson Province, North Queensland, Australia: Implications for tectonic evolution. *Australian Journal of Earth Sciences*. (Chapter 3 of this dissertation)
- VOS I. M. A., BIERLEIN, F. P. & WEBB J. In press. Geochemistry of Early Palaeozoic basalts in the Hodgkinson Province: a key to tectono-magmatic evolution of the Tasman Fold Belt System in northeastern Queensland, Australia. *International Journal of Earth Sciences*. (Chapter 4 of this dissertation)
- ZUCCHETTO R. G., HENDERSON R. A., DAVIS B. K. & WYSOCZANSKI R. 1999. Age constraints on deformation of the eastern Hodgkinson Province, North Queensland; new perspectives on the evolution of the northern Tasman orogenic zone. *Australian Journal of Earth Sciences* 46, 105-114.

NUMERICAL MODELLING OF A LISTRIC FAULT GEOMETRY: IMPLICATIONS FOR GOLD MINERALISATION IN THE HODGKINSON PROVINCE, NE QLD, AUSTRALIA

I.M.A. Vos, W. Potma and F.P. Bierlein

Australian Journal of Earth Sciences, in review.

ABSTRACT

Coupled mechanical and fluid flow models place constraints on some of the factors that control gold mineralisation and deformation in the Hodgkinson Province in northeastern Queensland, Australia. We attempt to resolve why the N-S striking terrane-bounding Palmerville Fault is barren, while many of the similarly oriented fault zones throughout the Hodgkinson province are spatially associated with gold deposits. A simplified, regional-scale geological model of the Hodgkinson Province was constructed to investigate the primary factors that control deformation and mineralisation in mechanical-fluid flow coupled numerical simulations. The model geometry permitted variation of boundary conditions, material properties and stress regime. This includes variation of lithological properties, the absence of fault zones in some models, and the application of uniaxial compression or transpression. The model outcomes illustrate the importance of a listric fault geometry for the distribution of deformation and fluid flow in zones of relatively high permeability and / or low rock strength throughout the model. Also, the orientation of fault zones with respect to the ruling far-field compressive stress regime can be demonstrated to be a key factor that controls deformation and fluid flow. In addition, inflection points and termination along fault zones are shown to significantly influence the distribution of deformation and fluid flow in our models. Our modelling results provide a critical understanding of first-order factors that control the localisation of deformation in the regional geological architecture of the Hodgkinson Province. Since areas of localised deformation commonly give rise to dilation in our model geometry, our predictions may be of significant value for future exploration in the Hodgkinson Province, and similar mineralised regions elsewhere. The application of our modelling results to the geology of the Hodgkinson Province illustrates the relevance and importance of realistic modelling scenarios in conceptual geoscience.

6.1 INTRODUCTION

Major fault systems that penetrate deep into the crust can provide pathways and foci for both mineralising fluids and magmatism into the upper crust (e.g. Groves *et al.* 1998; Sillitoe 2000; Cox *et al.* 2001). The at least 200 km long, north- to northwest-striking Palmerville Fault is a major structure in northeastern Australia, delineating the boundary between the Palaeozoic Hodgkinson Province and Proterozoic rock assemblages to the west (Fig. 6.1). No mineral occurrences are known along the north-striking section of the Palmerville Fault. Where the strike of the Palmerville Fault changes to northwest, the fault system is intruded by granites and volcanic rocks that formed during Carboniferous to Permian magmatism and host several significant gold-copper and skarn deposits (e.g. Red Dome and Mungana deposits; Nethery & Barr 1998). A number of north- to northwest-striking fault structures that are sub-parallel to the Palmerville Fault traverse the Hodgkinson Province and are associated with orogenic gold-rich regions (e.g.

Peters *et al.* 1990; Garrad & Bultitude 1999).

To overcome limitations imposed by restricted exposure and relatively low data density in the Hodgkinson Province, Vos *et al.* (in review) have integrated structural mapping, potential field analysis, and forward modelling of magnetic and gravity data to gain insight into the nature of the Palmerville Fault and its role in the tectonic evolution of the province. Results from this multi-disciplinary study suggest that the Palmerville Fault represents an eastward-dipping, listric and inverted normal fault that controlled opening of the Hodgkinson Basin in the Ordovician to Devonian. During subsequent Devonian to Carboniferous basin inversion, the Palmerville Fault was reactivated and orogenic gold deposits formed along secondary faults that are sub-parallel to the Palmerville Fault. The newly obtained insights into the geometry and structure of the Hodgkinson Province allow for a improved analysis of processes that controlled gold mineralisation in the region.

Coupled mechanical and fluid-flow numerical simulations were carried out to investigate

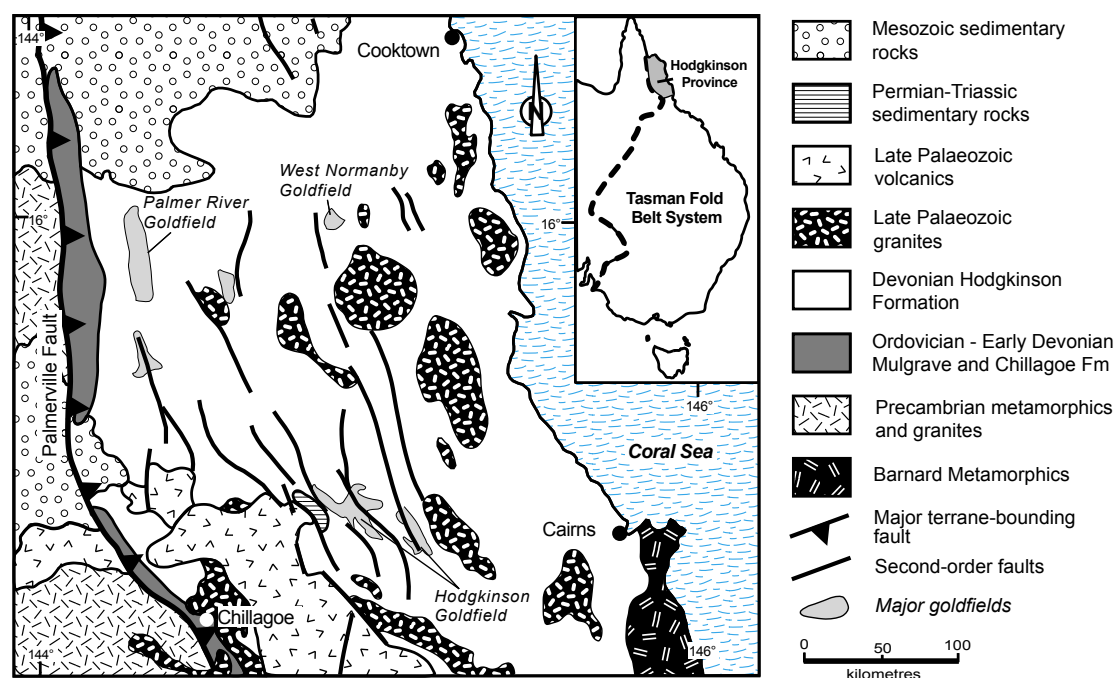


Fig. 6.1: General geology of the Hodgkinson Province with the Palmerville Fault forming the bounding structure at the western margin of the province.

factors that controlled mineralisation processes in the western part of the Hodgkinson Province. In addition, the role of the Palmerville Fault in deformation and fluid flow could be assessed. A number of models have been set up that provide insight into the loci of dilation, anomalous fluid flow and shear strain under varying deformation conditions with different model geometries. Key results from our modelling are compared with the geology of the Hodgkinson Province. The simulated mechanical and fluid flow observations provide insights into the factors that controlled deformation and mineralisation in this province. In particular, we investigate deformation and fluid flow characteristics along the two segments of the Palmerville Fault that have different strikes, and along fault inflections and terminations. Ultimately, we aim to investigate the factors that controlled gold mineralisation along second-order faults in the Hodgkinson Province (e.g. Retina Fault, Kingsborough Fault), and resolve why the main terrane-bounding Palmerville Fault remained largely barren. Although we have used the geology of the Hodgkinson Province as a model for this study, our work provides important implications for the understanding the connection between fluid flow, deformation and gold mineralisation in similar settings elsewhere.

6.2 GEOLOGICAL BACKGROUND

Bultitude *et al.* (1997) and Vos *et al.* (in press) have summarized the Palaeozoic structural history of the Hodgkinson Province. In brief, basin formation during the Late Ordovician to Devonian resulted in the deposition of three lithologies that now make up the majority of the province: 1) arenites of the Late Ordovician Mulgrave Formation along the western edge of

the province; 2) limestones and basalts of the Chillagoe Formation juxtaposed to the east of the Mulgrave Formation; and 3) sandstones and siltstones of the Hodgkinson Formation covering the remainder of the province (Fig. 6.1). The Hodgkinson Province has been affected by at least four deformation phases in the Late Devonian and Carboniferous following Silurian and Devonian basin formation and infill. These deformation phases resulted in the generation of a series of mainly north- to northwest-trending overprinting structures ranging from early isoclinal folds and *mélange* zones to later more open, steeply plunging folds and reverse faults. The Late Carboniferous and Permian mark an episode of magmatism in the Hodgkinson Province (Bultitude *et al.* 1997). The spatial relationship of orogenic gold deposits to secondary faults sub-parallel to the Palmerville Fault is outlined by Peters *et al.* (1990), Vos *et al.* (2004) and Vos & Bierlein (in press), who suggested that these deposits formed from low-salinity homogenous fluids at mid- to upper crustal levels (~10-15km). Furthermore, these authors demonstrated that at least two episodes of orogenic gold mineralisation occurred during the Late Devonian to Carboniferous, and are related to east-west contraction and subsequent transpression. An overview of the main tectonic, metallogenic, magmatic and sedimentary events is provided in Figure 6.2.

6.3 FLAC^{3D} NUMERICAL MODELLING

In the present study, we have used the three-dimensional finite difference code FLAC^{3D} (Cundall & Board 1988; ITASCA 1998) to simulate the coupling of fluid flow and deformation. In FLAC^{3D}, crustal-scale processes can be simulated by modelling

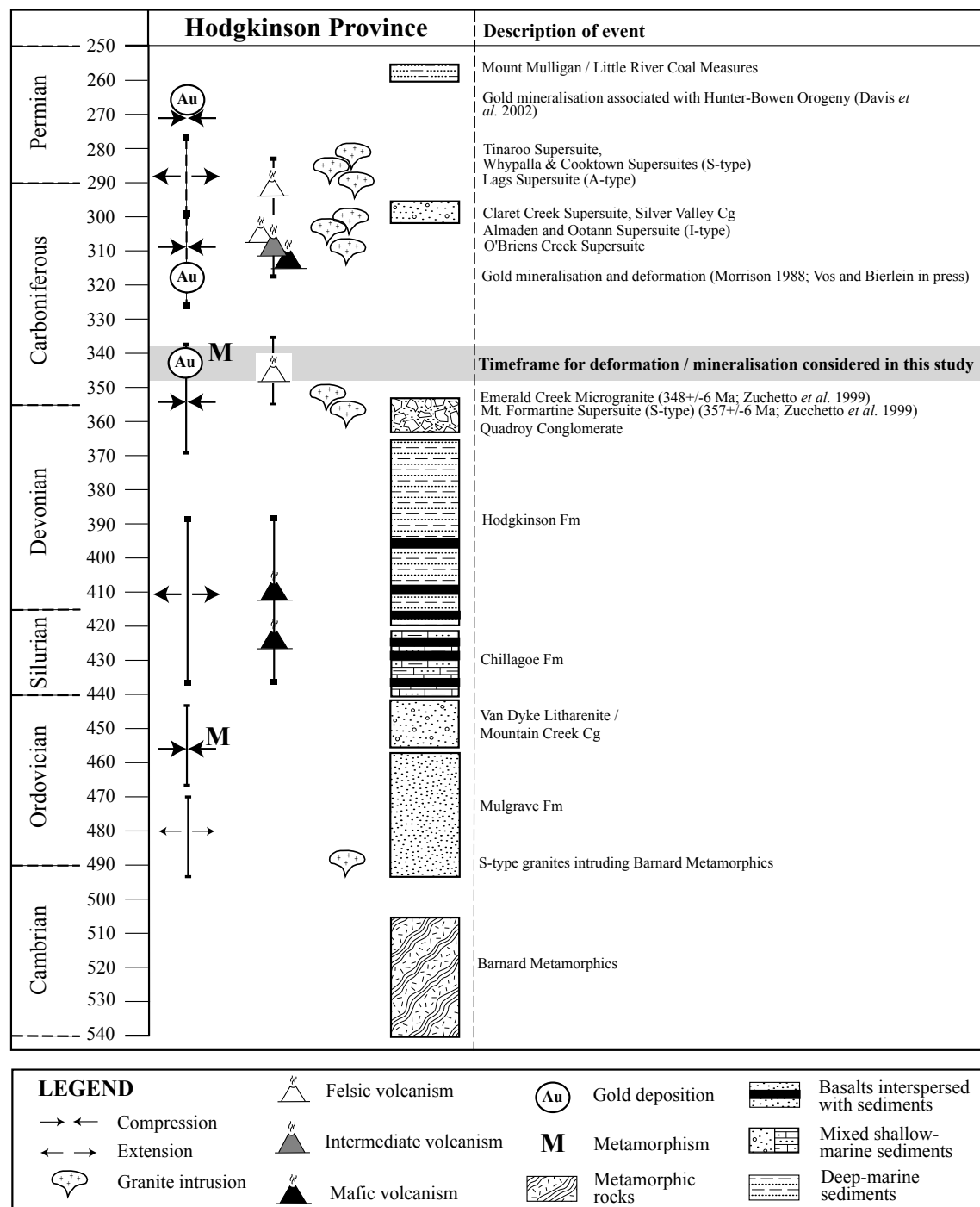


Fig. 6.2: Overview of the Palaeozoic geological evolution of the Hodgkinson Province, including tectonic, metallogenetic, magmatic and sedimentary events. Grey inset indicates the timeframe considered for modelling in this study. Figure modified after Vos & Bierlein (in press).

regionally significant faults and shear zones as zones of different material properties in the finite difference grid (Sorjonen-Ward *et al.* 2002). Numerical simulations are based on: 1) the model architecture, 2) the material properties assigned to the mesh elements, and 3) the boundary conditions considered most

relevant to the purpose of the modelling. Each of these attributes can be systematically varied to test their effects. Results can be compared and used to resolve basic geological questions, such as the relative significance of a listric fault geometry compared to a planar fault geometry (see section 6.5.1).

An extensive overview of characteristics of coupled modelling of deformation and fluid flow with FLAC^{3D} is given by Oliver *et al.* (2001) and Sorjonen-Ward *et al.* (2002) from which we have summarized the main characteristics here:

- Fluid flow in FLAC^{3D} models is governed by Darcy's Law and hence model results are primarily sensitive to variations in hydraulic head and permeability. Dynamic permeability variations are allowed to develop within the constitutive model as a consequence of volume change during deformation since different materials have different degrees of dilation with increasing strain (Ord 1991; Ord & Oliver 1997).
- Feedback between volume change and pore-fluid pressure results in changes in the rate and distribution of fluid flow through the model. On the other hand, changes in pore fluid pressure can result in different rock behaviour through lowering the effective mean stress required for rock failure. As such, the interaction between deformation and fluid flow in FLAC^{3D} can be described as fully coupled.
- Ord & Oliver (1997) have shown that the Mohr-Coulomb or elastic-plastic mode of behaviour is appropriate for modelling coupled deformation and fluid flow in the upper crust. FLAC^{3D} implementation of Mohr-Coulomb mechanical deformation is not dependent on strain rate, thus the number of model steps simulated is not directly related to the duration of a deformation event (the mechanics-only timestep is a non-dimensional number). However, the fluid flow timestep is

an absolute time-value, and because fluid flow is intrinsically coupled with mechanical deformation, we can derive the mechanical timestep as an absolute value and thus calculate the strain rate in the models.

6.4 MECHANICAL AND FLUID FLOW MODELLING OF A LISTRIC FAULT GEOMETRY

6.4.1 Structure of the listric fault models

We have constructed a FLAC^{3D} model that represents a block of crust 50 km wide, 50 km long and 5 km deep (Fig. 6.3). The length axis (i.e. y direction) of the model is orientated north-south, parallel to the simulated northern segment of the listric Palmerville Fault. The upper model surface of the model is placed under pressures equivalent to 12.5 km to account for erosion as based on lower-greenschist facies metamorphic conditions throughout the Hodgkinson Province (Peters *et al.* 1990; Garrad & Bultitude 1999; Vos *et al.* 2004). The dimensions and orientation of the model, as well as the internal structural geometry have been constrained by integrated geological, geophysical and geochemical datasets (Vos *et al.* in review). Vos *et al.* (in review) indicated that the terrane-bounding Palmerville Fault represents a steeply eastward dipping structure that becomes listric at depth, where it acted as a décollement zone that accommodated basin inversion in the Hodgkinson Province during the Late Palaeozoic.

The model geometries comprise two or three lithologies with variable rock properties that simulate the dominant lithologies in the Hodgkinson Province, which may be transected and / or separated by fault zones. In the models a listric geometry always characterises the

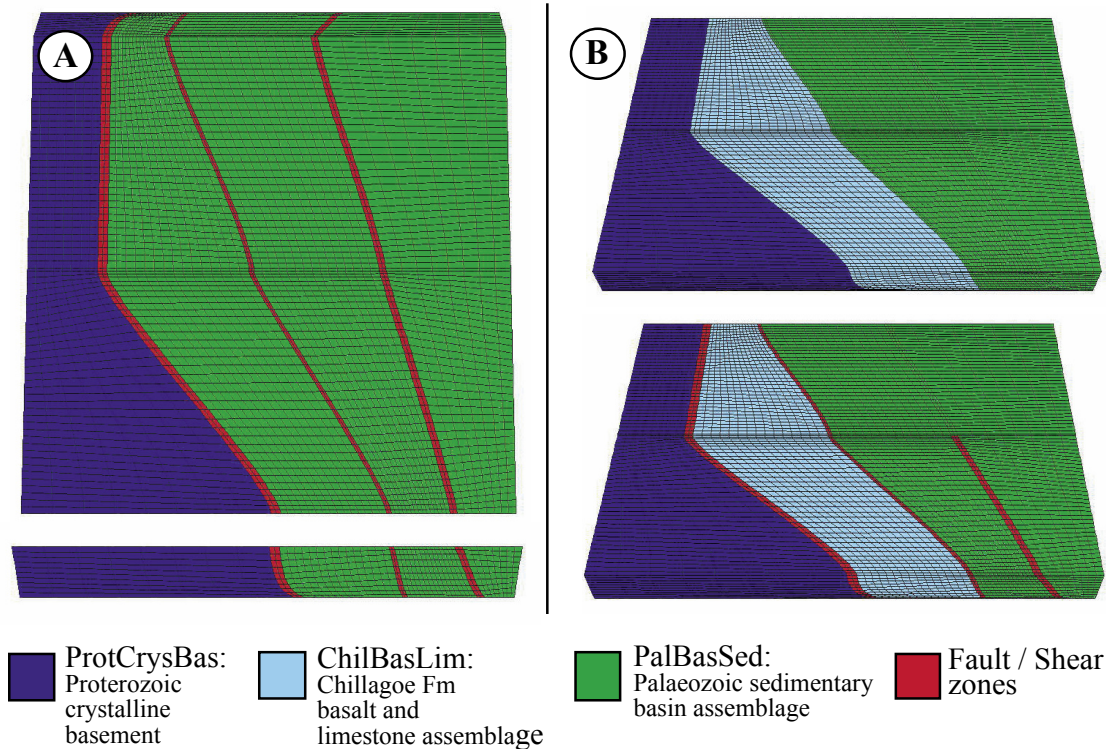


Fig. 6.3: Overall model architecture representing a block of crust 50 km wide, 50 km long and 5 km deep – a) Base architecture with two lithologies and three through going faults showing the model setup in plan view (top) and cross-section (bottom); b) Variations on the base architecture with three lithologies and no faults (top) and three lithologies, two through going faults and a fault segment covering half the blocks length (bottom).

westernmost fault zone that is representative of the Palmerville Fault in the Hodgkinson Province geology. An overview of constructed model architectures, where number of faults, lithologies and pore pressure were varied, is given in Table 6.1 and two examples of model geometries are given in Figure 6.3.

6.4.2 Material properties and boundary conditions

We have used a Mohr-Coulomb elastic-plastic constitutive model for our FLAC^{3D} simulations, which means that materials deform in an elastic manner up to a critical yield point, after which plastic deformation occurs (Fig. 6.4). The material properties used in our models are

Table 6.1: overview of various model setups, with varying number of faults, lithologies and pore pressure.

Model setup	Faults	Lithologies	Pore pressure	Comments
1	3	2	0.5 x lithostatic	also used with planar fault geometry
2	1	2	0.5 x lithostatic	also used with planar fault geometry
3	2.5	2	0.8 x lithostatic	
4	2.5	3	0.5 x lithostatic	
5	-	3	0.5 x lithostatic	
6	2.5	3	0.5 x lithostatic	revised properties for ChilBasLim
7	-	3	0.5 x lithostatic	revised properties for ChilBasLim
8	2.5	3	0.5 x lithostatic	listric fault treated as separate entity
9	-	3	0.5 x lithostatic	basalt layers added in place of faults
10	-	3	0.5 x lithostatic	fat cell mesh for fault zones
11	2.5	3	0.5 x lithostatic	fat cell mesh for fault zones

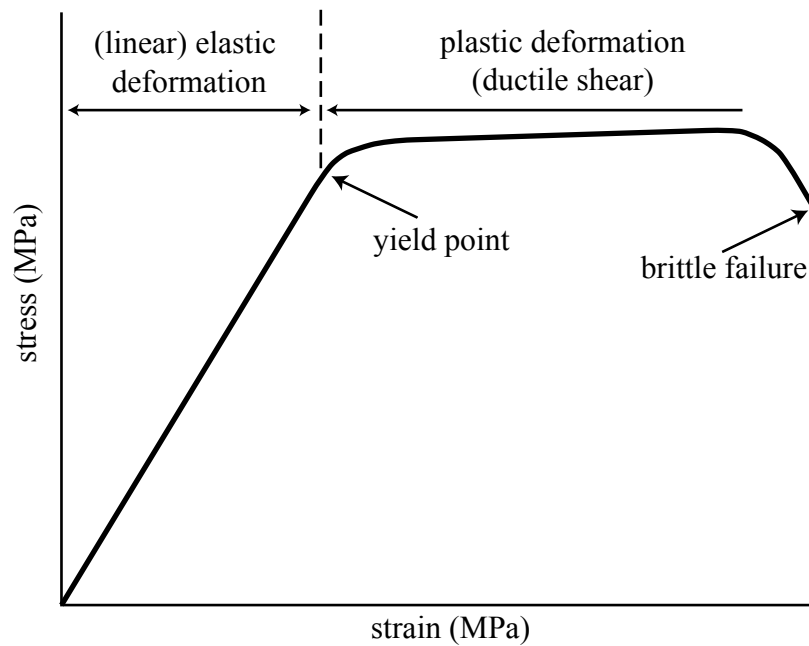


Fig. 6.4: Generalised stress-strain curve illustrating the behaviour of material in a Mohr-Coulomb elastic-plastic constitutive model used for this study.

Table 6.2: rock properties for lithologies used in model setups

Rock type	Density	Bulk modulus	Shear modulus	Cohesion	Tensile strength	Friction angle	Dilation angle	Permeability	Porosity
	(kg / m-3)	(Pa)	(Pa)	(Pa)	(Pa)			(m2)	
ProtCrysBas	3.03E+03	1.07E+11	3.2E+10	9.0E+07	5.0E+06	35	2	1.0E-16	0.2
ChilBasLim	2.82E+03	1.07E+11	2.0E+10	5.0E+07	6.0E+06	35.5	2	1.0E-14	0.2
ChilBasLim2	2.82E+03	8.0E+10	2.0E+10	5.0E+07	6.0E+06	32.5	2	1.0E-14	0.2
PalBasSed	2.72E+03	3.0E+10	1.0E+10	3.0E+07	7.5E+06	30	2	1.0E-14	0.2
Faults	2.72E+03	1.0E+10	3.2E+09	1.0E+07	1.0E+06	15	2	1.0E-13	0.2

Table 6.3: modes of deformation used in model runs

Deformation mode	Description
1	Contraction along azimuth 090
2	Contraction along azimuth 090 with component of strike slip (=0.5 x contraction)
3	like 1 but with allowing permeability to change with failure
4	like 2 but with allowing permeability to change with failure
5	like 1 but with forced fluid flux of 1.0 e-10 through sediments
6	like 2 but with forced fluid flux of 1.0 e-10 through sediments
7	like 1 but with forced fluid flux of 2.0 e-09 through sediments
8	like 2 but with forced fluid flux of 2.0 e-09 through sediments
9	contraction along azimuth 070
10	contraction along azimuth 070 with component of strike-slip (=0.5 x contraction)
11	like 1 but with forced fluid flux of 2.0e-09 through secondary faults
12	like 2 but with forced fluid flux of 2.0e-09 through secondary faults
13	like 5 but in addition allowing permeability to change with failure
14	like 6 but in addition allowing permeability to change with failure
15	like 11 but in addition allowing permeability to change with failure
16	like 12 but in addition allowing permeability to change with failure

presented in Table 6.2. These data simulate rock properties in the Hodgkinson Province and are based on established data for typical rocks (e.g. Turcotte & Schubert 1982). The material properties are kept constant during deformation and fluid-flow simulations with the exception of permeability, which is variable in some models so that fluid flow would be focussed on zones of failure. In these scenarios, the permeability of a mesh cell varies with failure state (e.g. deformation modes 3 and 4; Table 6.3), which means that when a model cell fails in response to tension or shear, permeability of that cell is increased by a factor of 50 and 10, respectively. In all our models, fault zones have been assigned inherently higher permeabilities than adjacent rocks. Additional models were run to determine whether fault zones would develop along lithological contacts when no weak faults had been predefined (e.g. model setup 5, Table 6.1). A set of models were also run where a fluid flux was set at a specific value and restricted to a predefined mesh cell set (e.g. representing a particular lithology or fault zone; see Table 6.3) along the base of the model to simulate fluid focus in particular units and the effects on our model geometry. This includes forced restricted fluid flux into faults or the sedimentary assemblage as illustrated in Figure 6.12.

Modelling limitations commonly give rise to boundary effects that may occur as stress, strain and fluid flow anomalies in mechanical deformation models. Such anomalies may for instance develop where mesh orientation is poorly aligned with model mesh boundaries or at impermeable surfaces in the model geometry. A bounding box was created around the actual model architecture that acts as a buffer zone and absorbs anomalies that may potentially

arise. The properties of a sedimentary assemblage (i.e. relatively permeable and structurally weak, see Table 6.2 - PalBasSed) were assigned to the bounding box. However, where faults exist in the model architecture, these were continued into the bounding box and the properties of a fault (Table 6.2) were assigned to the relevant cells. The dimensions of the bounding box and its relationships to the actual model architecture (internal model box) are illustrated in Figure 6.5A and its effects on the pore pressure distribution in the model are illustrated in Figure 6.5B.

Stress and velocity values were applied to the boundaries of the model to simulate both tectonic deformation and appropriate boundary conditions. These include: 1) free movement of the model top boundary surface in all directions with an implementation of overburden stress equal to the product of density, the gravitational constant and depth taken as 12.5 km ($\rho \cdot g \cdot z$), 2) model top surface remains impermeable, 3) the bottom surface of the model is free to slide in the horizontal plane, but no vertical movement is allowed, and 4) model bottom surface remains impermeable, except where fluid flux is applied locally. As a result, the topographic elevation and lateral variations in density are not inherently compensated for isostasy. All models commence with an initial phase of stress balancing to obtain model equilibrium prior to the application of deformation. Also, the models can be regarded as fluid-saturated, in a way that where deformation at the upper surface is associated with volume increase, fluid supply is maintained. In order to simulate tectonic deformation, all vertical sides are subjected to velocity fields that generate geologically reasonable strain rates in the order of 10^{-13} s^{-1} .

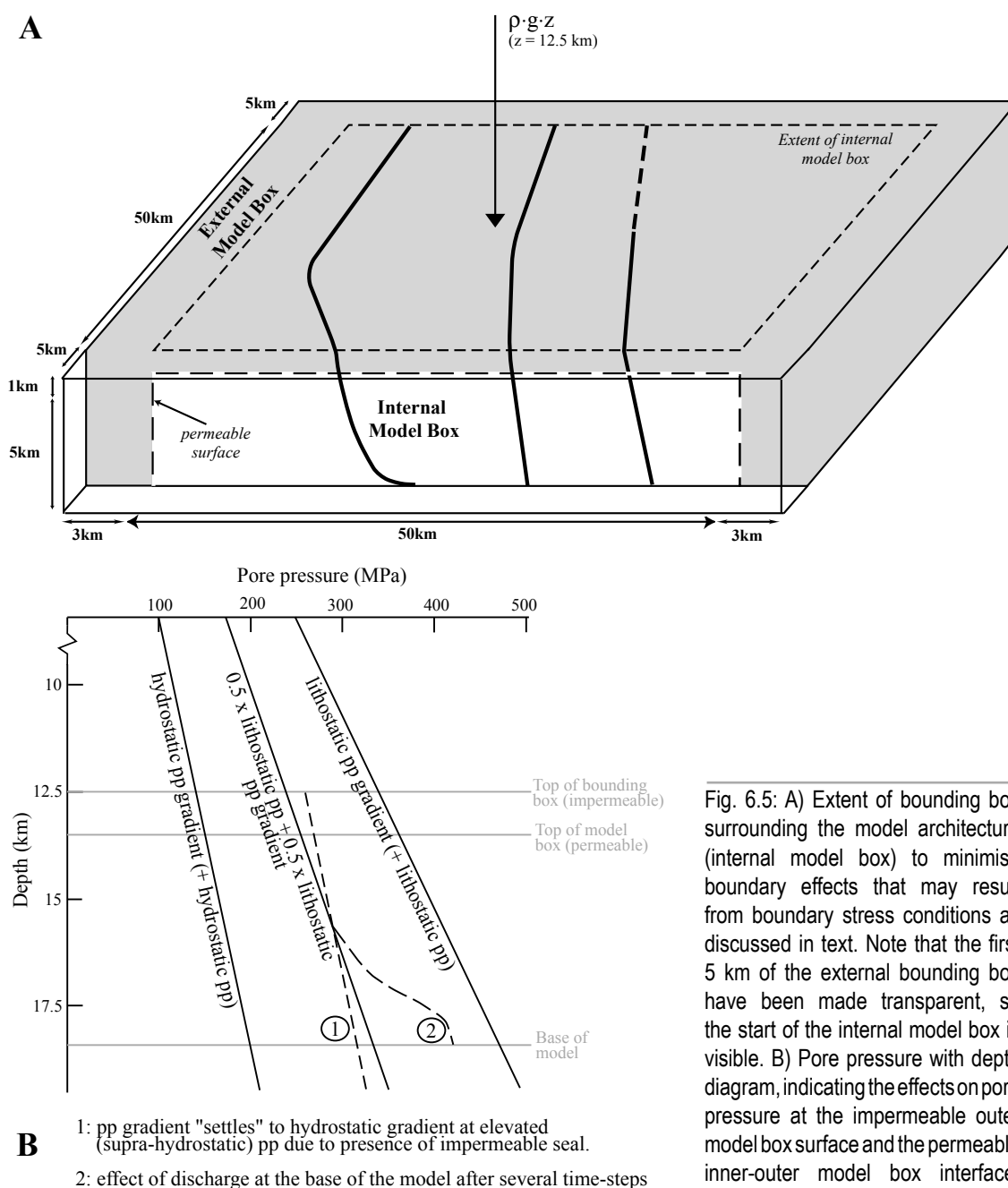


Fig. 6.5: A) Extent of bounding box surrounding the model architecture (internal model box) to minimise boundary effects that may result from boundary stress conditions as discussed in text. Note that the first 5 km of the external bounding box have been made transparent, so the start of the internal model box is visible. B) Pore pressure with depth diagram, indicating the effects on pore pressure at the impermeable outer model box surface and the permeable inner-outer model box interface.

6.4.3 Deformation and stress regime

Based on the summary of the structural evolution, and the timing of gold mineralisation outlined above (i.e. the presumed relationship of gold mineralisation to deformation), all models have been deformed by shortening. Shortening is achieved by applying a constant displacement rate in an east-west direction (uniaxial compression) for one set of models and an east-west direction with a sinistral component of strike-slip (i.e. transpression) for another

set of models (Fig. 6.6). These two scenarios reflect the most likely principal shortening directions associated with mineralisation in the Hodgkinson Province (Peters *et al.* 1990; Vos *et al.* 2004). Models have been shortened by up to 10%, which was approximately the maximum shortening values our model geometries could sustain before becoming numerically unstable due to geometric grid deficiencies. Such deficiencies commonly limit the outcome of FLAC models when dealing with large strain

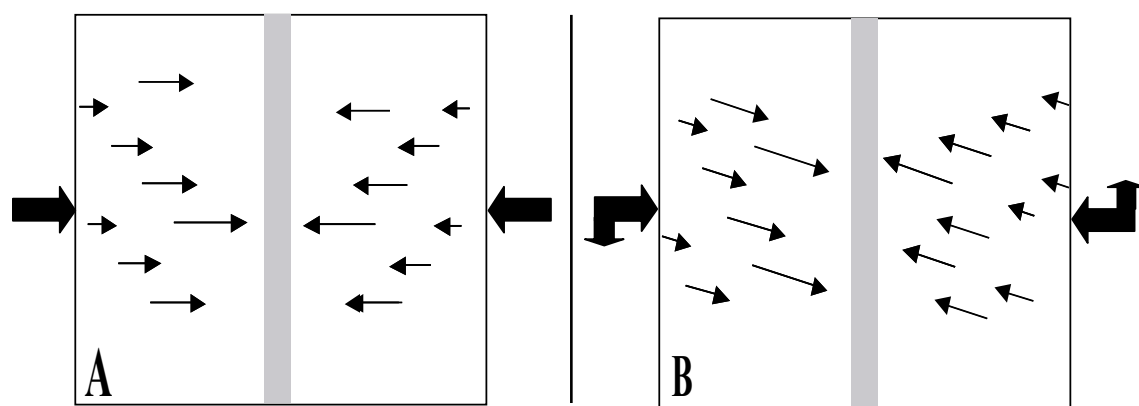


Fig. 6.6: Model deformation conditions. Each model geometry is subjected to 10% uniaxial shortening along its long axis (A) as well as 10% shortening along its long axis with 5% sinistral strike-slip deformation along its short axis (B). Arrows indicate the magnitude and direction of forces working on the cell mesh.

Table 6.4: overview of completed model runs indicating model architecture (see Table 4.1) and deformation mode (see Table 4.3) used.

Model Run	Model Setup	Deformation Mode	Completed (out of 10%)
1	1	1	9%
2	1	2	10%
3	3	1	9%
4	3	2	10%
5	4	1	10%
6	4	2	10%
7	4	3	10%
8	4	4	10%
9	4	5	9%
10	4	6	10%
11	5	1	10%
12	5	2	10%
13	7	7	7%
14	7	8	7%
15	6	9	10%
16	7	10	10%
17	8	11	10%
18	8	12	10%
19	6	13	10%
20	6	14	10%
21	8	15	10%
22	8	16	10%
23	9	7	10%
24	9	8	10%
25	10	1	10%
26	10	2	10%
27	11	3	10%
28	11	4	10%

deformation. We recognise that the deformation in the Hodgkinson Province and the associated development of numerous orogenic gold deposits may have been substantially greater. However, we argue that first-order fluid and deformation effects, which can be considered to be enhanced with increased deformation, can be recognized in our models. A summary of the deformation modes and boundary conditions applied to our models is presented in Table 6.3.

6.5 MODEL RESULTS AND INTERPRETATIONS

Results and interpretation of key outcomes of our modelling work are presented as a series of illustrations generated with FracSIS software for selected model scenarios that are outlined in Tables 6.1 and 6.3. Since not all model runs were completed to 10%, we show model results after 9% of shortening, which represents the maximum amount of deformation obtained for all selected models (see comments in previous section). An overview of all model runs is given in Table 6.4.

6.5.1 Listric vs. planar fault

To better understand the primary effects on deformation and fluid flow in a listric fault scenario, a comparison with a planar fault geometry was made initially. Here we present results of model run 1 and 2 (Table 6.4) for both a listric and planar fault geometry. Figures 6.7 and 6.8 illustrate the distribution of cumulative shear strain and dilation, respectively, after 9% shortening.

6.5.1.1 SHEAR STRAIN DISTRIBUTION

The shear strain distribution for the listric and planar fault scenarios are presented in Figure

6.7. In the listric fault scenario (Fig. 6.7A-B), shear strain is partitioned along all faults, although less so in the northern segment of the listric fault. Figure 6.7A-B shows that high shear strain is particularly associated with the base (i.e. the listric portion) of the southern, NW-SE striking segment of the listric fault and with inflections along the other fault. In the planar fault scenario (Fig. 6.7C-D), shear strain is mostly distributed along the easternmost fault. In the case of transpressional deformation, some shear strain is also distributed along the central and western faults (Fig. 6.7D), particularly along those fault segments that are at an angle with the principal shortening direction.

6.5.1.2 DILATION

Figure 6.8 illustrates the distribution of dilation, which in combination with the distribution of shear strain (Fig. 6.7) controls fluid flow. Since Darcy's Law controls fluid flow in the models, dilation will generally be accompanied by reduction in hydraulic head and possibly pore pressure, which, in turn, will induce local flow perturbation. Shear failure of a group of cells (e.g. in a fault / shear zone) will result in increased permeability (see section on material properties and boundary conditions), which will intensify flow rates along the failure surface. In the listric fault scenario (Fig. 6.8A-B), dilation, like the distribution of shear strain (Fig. 6.7A-B), is also partitioned along the faults with the important exception of the northern segment of the listric fault. The largest dilation occurs along the southern, NW-SE striking segment of the listric fault. In the planar fault scenario (Fig. 6.8C-D), dilation mostly occurs along the easternmost fault, where only in the case of transpression, minor dilation occurs along the central and western faults (Fig. 6.8D).

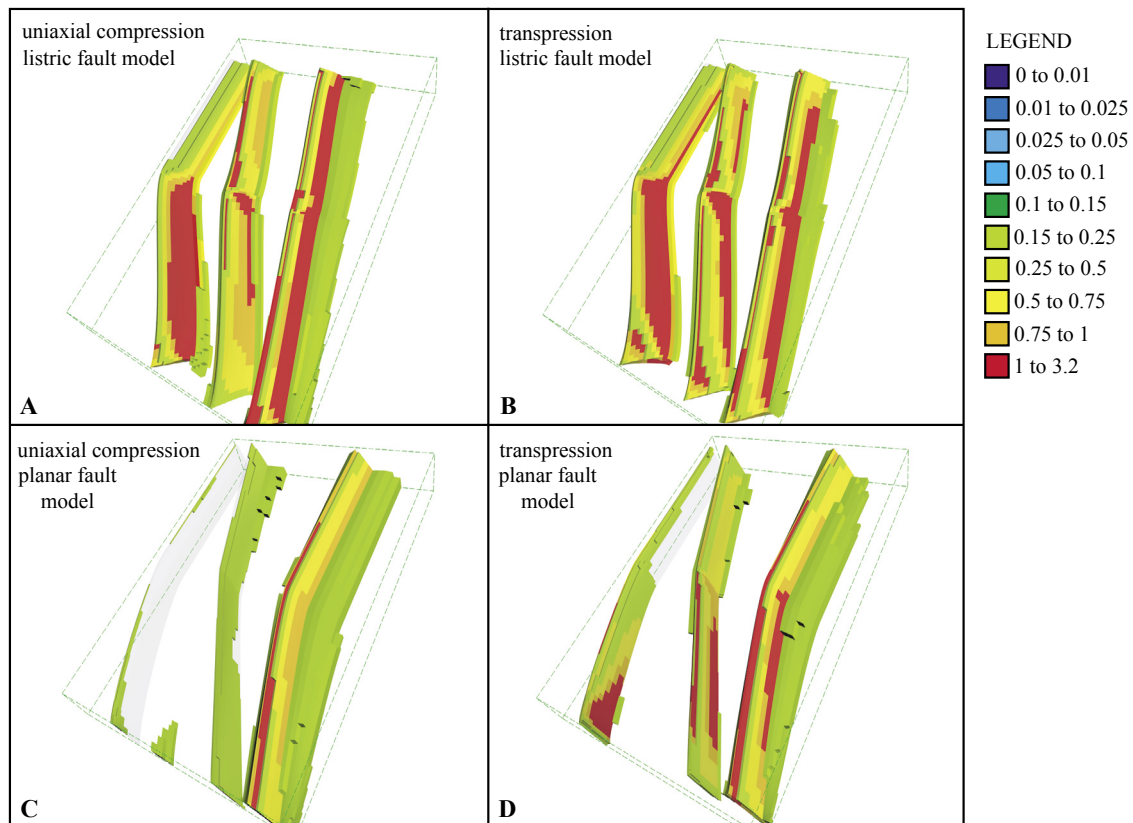


Fig. 6.7: 3-D representation of cumulative shear strain (in % length loss) distribution: A) after 9% uniaxial shortening in a listric fault scenario; B) after 9% transpression in a listric fault scenario; C) after 9% uniaxial shortening in planar fault scenario; D) after 9% transpression in a planar fault scenario.

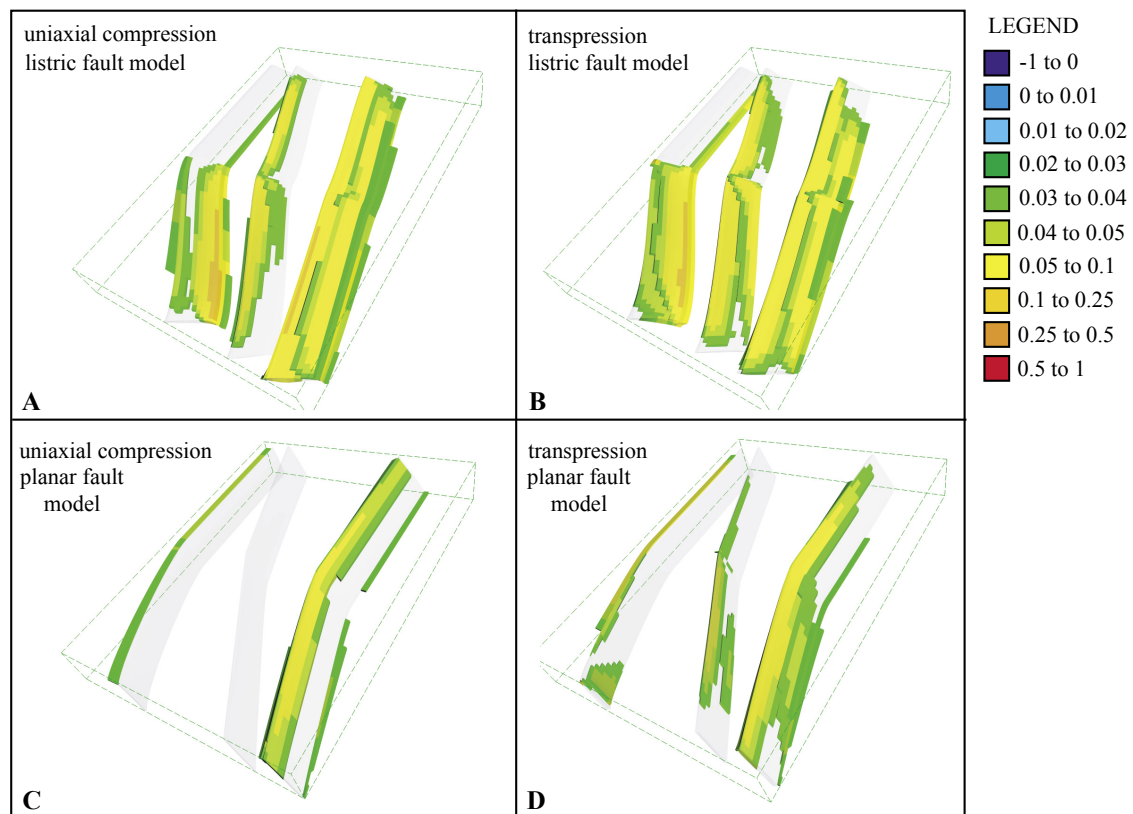


Fig. 6.8: 3-D representation of cumulative distribution of dilation (% volume gain): A) after 9% uniaxial shortening in a listric fault scenario; B) after 9% transpression in a listric fault scenario; C) after 9% uniaxial shortening in planar fault scenario; D) after 9% transpression in a planar fault scenario.

6.5.1.3 INTERPRETATION

Based on our modelling results, the presence of a listric fault on the western side of our model is interpreted to control the partitioning of shear strain and dilation along fault structures in the remainder of the model. This suggests that the listric nature of the fault allows perturbation of stresses throughout the model, whereas in the case of the planar fault model, shear strain was distributed only along the easternmost planar structure and no partitioning was observed. Furthermore, fault geometry can be considered to influence the distribution of shear strain, which is slightly higher at or around fault inflections. In the planar fault model, the distribution of shear strain and dilation is controlled by other factors like the orientation of strike and dip of fault structures with respect to the principal stress orientation.

6.5.2 Variations in pore fluid pressure, lithological properties and permeability

Here we present results from model runs 3 to 8 (Table 6.4) to obtain insight into the effects on deformation and fluid flow with: 1) increase of pore fluid pressure (0.8 x lithostatic pp compared to 0.5 x lithostatic pp in other models); 2) change of lithological properties between the western and central fault; and 3) increase in permeability every time a cell deforms during the model run. Note that in these and other models, except those discussed in the section on listric vs. planar faults below, the easternmost fault only partly transects the model. This was done to compare the effects of stress propagation in parts of the model that were both faulted and unfaulted. Also, the effects on shear strain distribution and fluid flow along the fault termination could be monitored.

6.5.2.1 SHEAR STRAIN DISTRIBUTION

Figure 6.9 shows that the distribution and magnitude (except Fig. 6.9E-F, see below) of shear strain does not seem to vary significantly from Figure 6.7A-B, and under the various model conditions remains partitioned along the predefined fault structures. In the case of uniaxial compression, with increased pore fluid pressure (Fig. 6.9A), some shear strain is distributed along the northern segment of the listric fault. Figure 6.9C and E show that minor to no shear strain is distributed along the northern segment of the listric fault after uniaxial deformation. Figure 6.9B and D further show that minor shear strain is distributed along the northern segment of the listric fault with transpression. When permeability is set to increase after cell failure, model cells are less likely to fail again due to a decrease in pore fluid pressure. Figure 6.10 represents a Mohr diagram that conceptually illustrates the change between a cell at failure and after failure when permeability of that cell has increased. This figure further indicates that for cell failure to occur again, pore fluid pressure (or differential stress) is first required to increase to critical values, which leads to a situation, where model regions that are not controlled by inherently high permeabilities and low intrinsic strength (such as fault zones) become more likely to fail. This provides an explanation for the low values of accumulated shear strain in Figure 6.9E-F.

6.5.2.2 DARCY FLUID FLOW

Figure 6.11 shows the distribution and magnitude of Darcy fluid flow for the various model conditions discussed in this section. Generally, fluid flow is concentrated along the fault zones, although the northern segment of

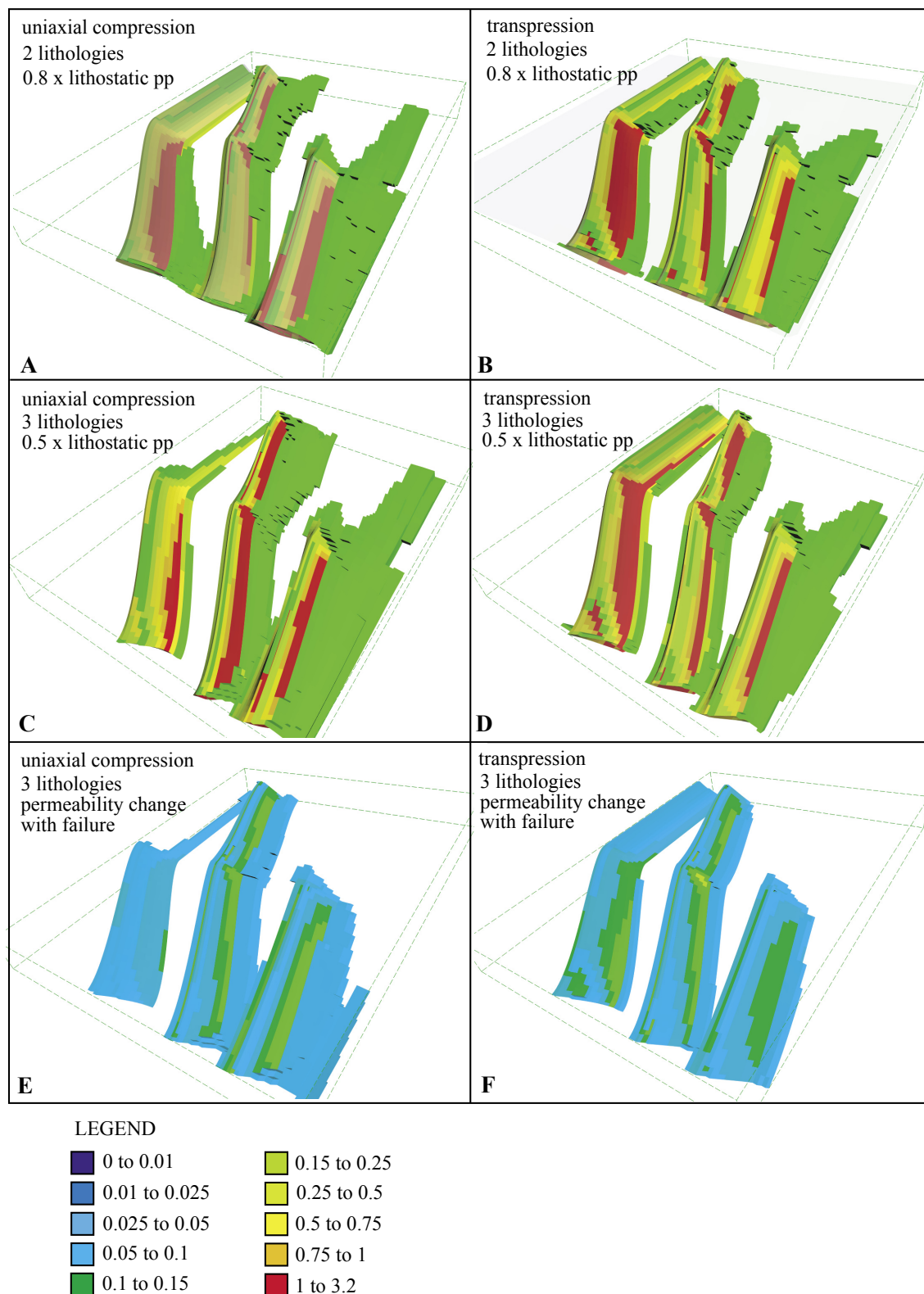


Fig. 6.9: 3-D representation of cumulative shear strain distribution (in % length loss) in a listric fault scenario: A) two lithologies after 9% uniaxial shortening with increased initial pore fluid pressure (0.8 x lithostatic); B) two lithologies after 9% transpression with increased initial pore fluid pressure (0.8 x lithostatic); C) three lithologies after 9% uniaxial shortening; D) three lithologies after 9% transpression; E) three lithologies after 9% uniaxial shortening with cell permeability increasing when a cell is deformed; F) three lithologies after 9% transpression with cell permeability increasing when a cell is deformed.

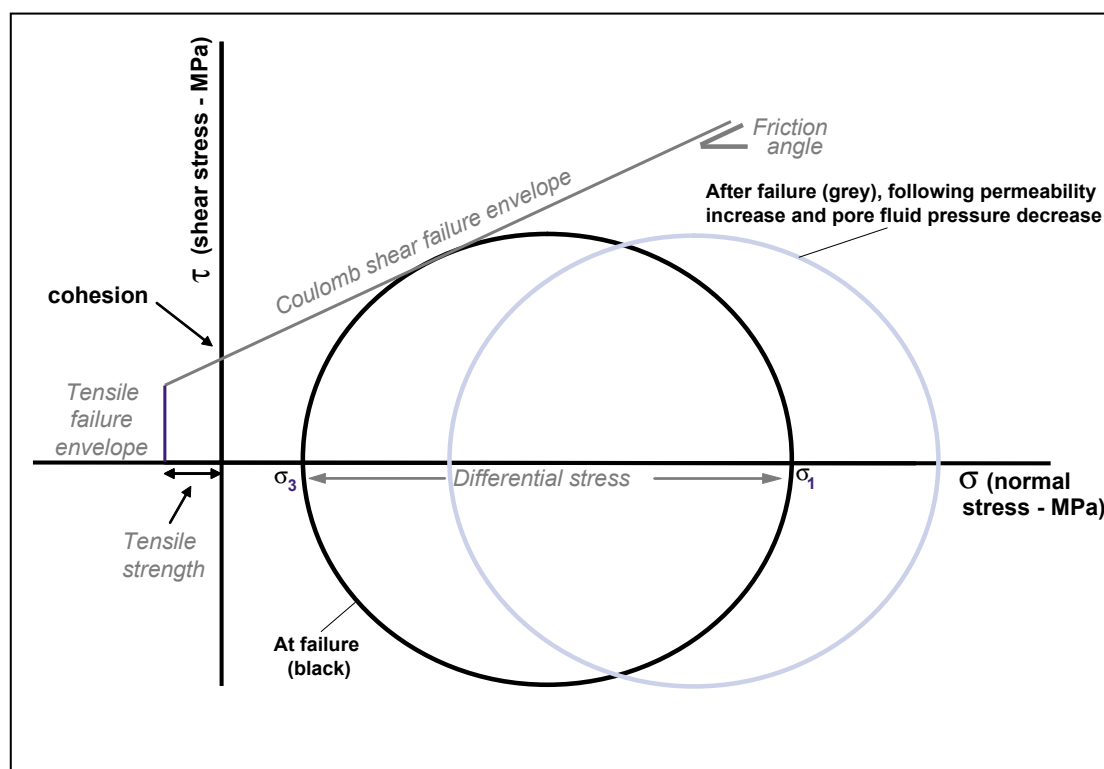


Fig. 6.10: Mohr-Coulomb diagram indicating the effects on shear strain behaviour when permeability increases after cell failure during a model run.

the listric fault does not act as a significant fluid conduit. If fluid flow occurs along the northern segment of the listric fault, flow is mainly along the strike of the fault and directed towards the southern segment of the fault. With increased pore fluid pressure, we note that the magnitude of Darcy fluid flow along the faults increases, in particular along the tops of the fault structures (Fig. 6.11A-B). Figure 6.11C-D shows a pattern of outward flow that includes upward, lateral and downward flow along the faults. In addition, in Figure 6.11C fluids migrate into the hanging wall along the base of the southern segment of the listric fault. In Figure 6.11E-F, the fluid flow describes a similar pattern of upward, lateral and downward flow along the faults as that observed in Figure 6.11C-D, although here fluid flow is of significantly greater magnitude. In this case the highest upward fluid flow rates are centred on the central fault. Also, in Figure 6.11E-F, high values of disseminated fluid flow

can be observed in the northeastern section of the model that represents non-faulted sedimentary rocks. Where permeability increases after failure of a model cell (Fig. 6.11E-F), overall higher fluid flow is a natural consequence of the model conditions, even though overall cumulative shear strain distribution remains low (Fig. 6.9E-F).

6.5.2.3 INTERPRETATION

Based on the modelling results presented in this section, we interpret that: 1) an increase in pore fluid pressure does not significantly affect the distribution and magnitude of shear strain (except for the moderate values of shear strain distributed along the northern segment of the listric fault) and fluid flow, which remains focussed along fault structures in our models (Fig. 6.11A-B) and is comparable in magnitude to Figure 6.7A-B. Since this is at odds with natural situations, where increased pore fluid pressure generally leads to increased fracturing

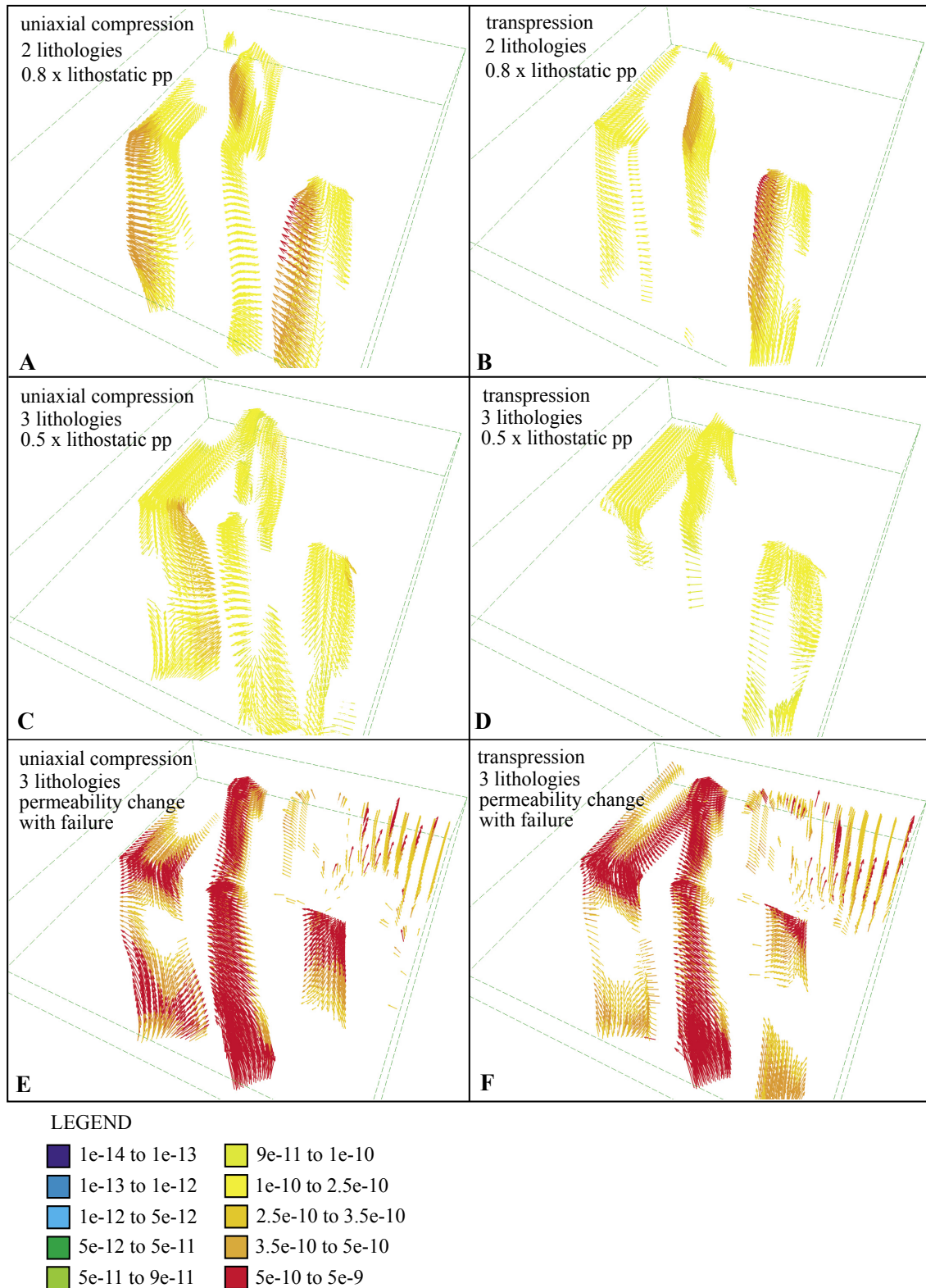


Fig. 6.11: 3-D representation of instantaneous fluid flow vectors indicating magnitude of Darcy fluid flow (m/s) for model scenarios as described in the caption of Figure 6.9.

and shear, we infer that the inherently high permeabilities and structural weakness of the fault zones are the main factors that control the distribution and magnitude of shear strain

and fluid flow, rather than pore fluid pressure; 2) changes of lithological parameters do not significantly influence the magnitude of fluid flow and deformation along the faults, but do

influence the direction of fluid flow along the listric fault (compare Fig. 6.11A-B with Fig. 6.11C-D); and 3) increase in permeability with cell failure, can distribute fluid flow away from the obvious areas that focus fluid flow (i.e. faults / shear zones) as illustrated in Figure 6.11E-F, where fluid flow occurs in the northeastern, non-faulted section of the model, where the magnitude of cumulative shear strain remains low.

A strong correlation exists between the areas of maximum shear strain and the areas of maximum Darcy fluid flow in our models. Even when permeability increases with cell failure and model regions with low-medium permeabilities and high intrinsic strength are more likely to

accommodate shear strain and fluid flow, shear strain still remains preferentially distributed along fault zones (e.g. Fig. 6.9E). We suggest that the presence of a listric fault allows propagation of stress throughout the base of the model and therefore provides a mechanism through which shear strain can be distributed into favourably oriented and intrinsically weak zones.

6.5.3 Restricted fluid flux

In this section, we present modelling results from model runs 9, 10, 13, 14, 17 and 18 (Table 6.4) in which we manipulated the fluid flux in the models as follows: 1) restricted fluid flux ($1.0\text{e-}10$ m/s) through the sedimentary

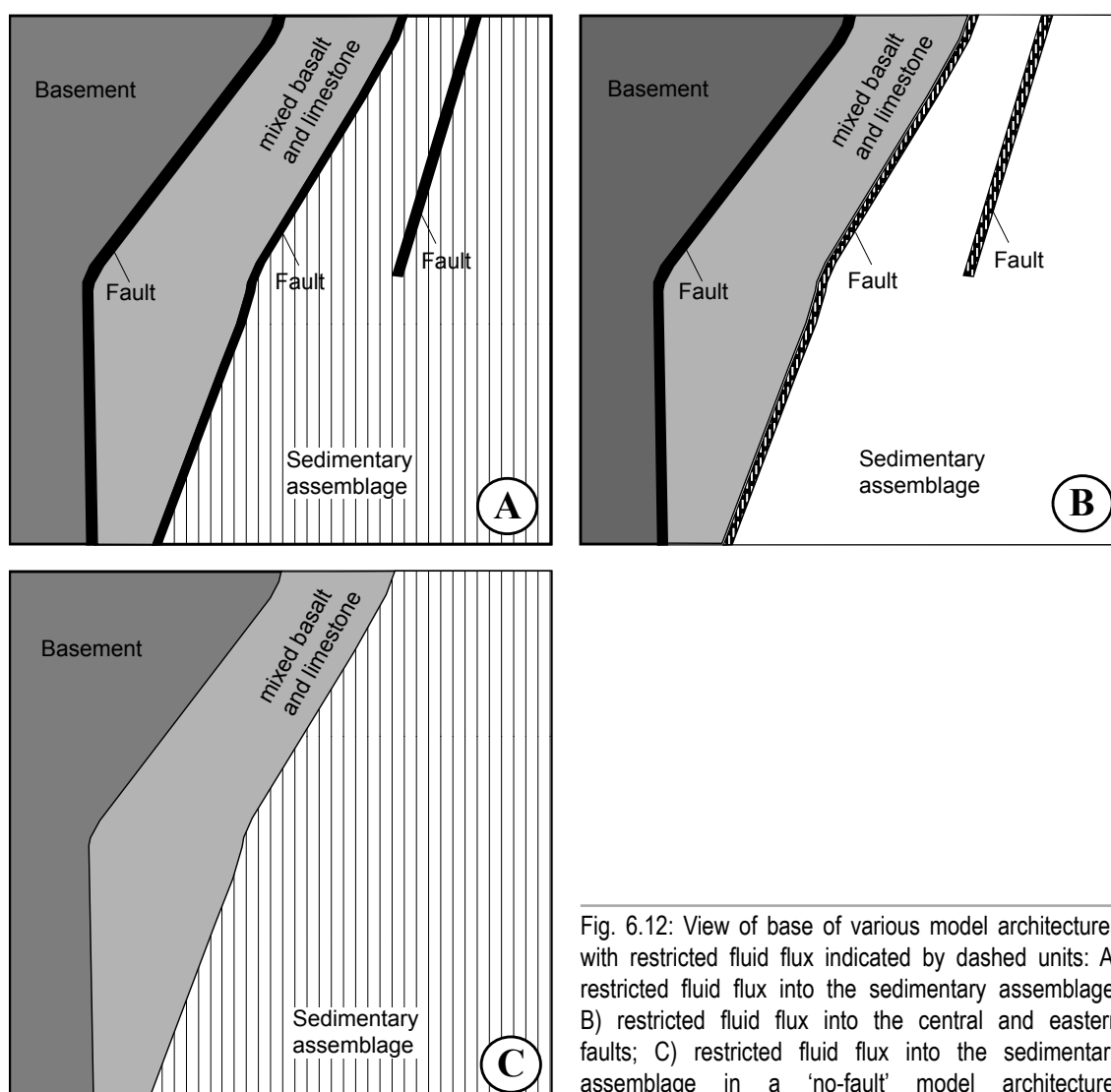
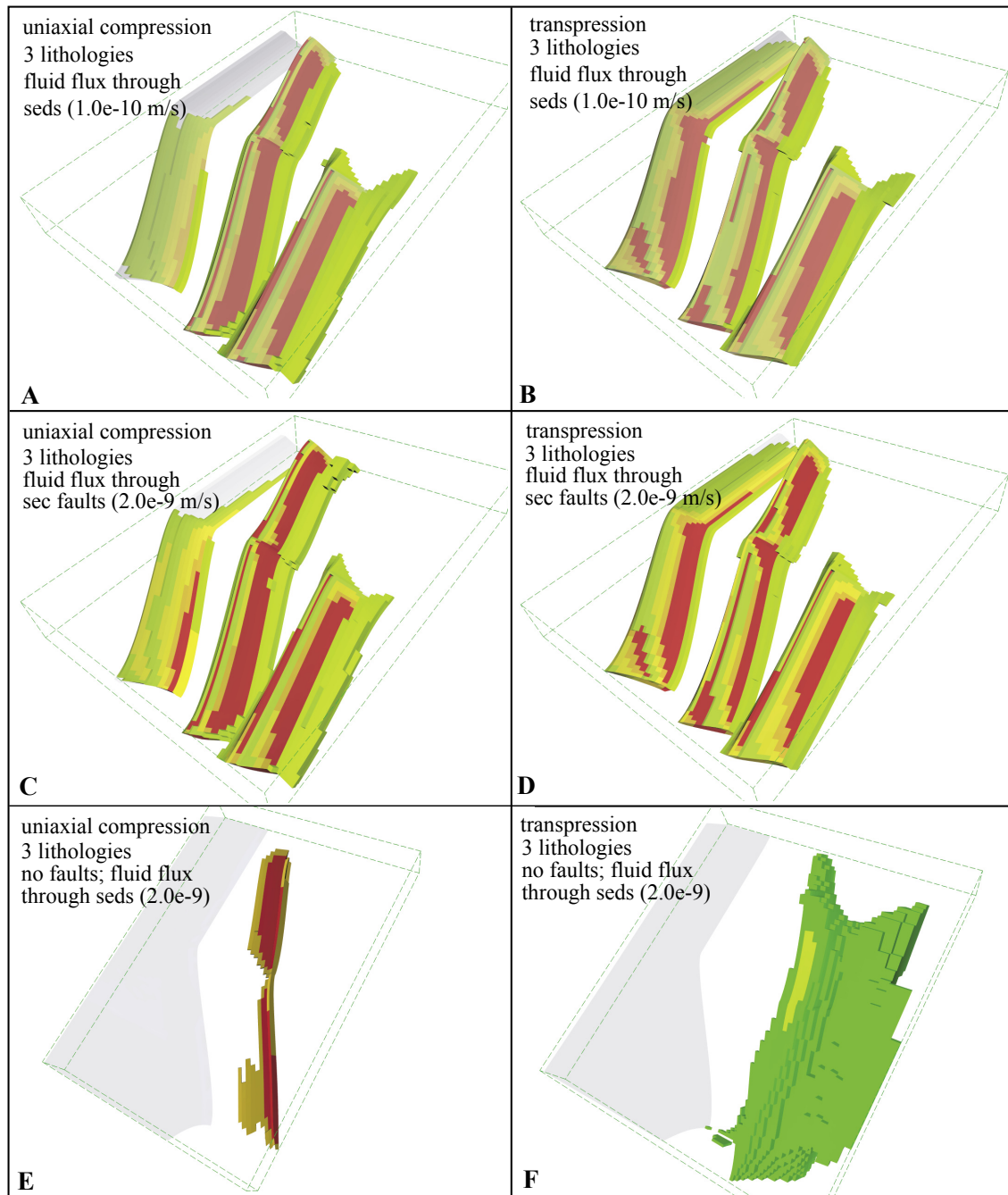


Fig. 6.12: View of base of various model architectures with restricted fluid flux indicated by dashed units: A) restricted fluid flux into the sedimentary assemblage; B) restricted fluid flux into the central and eastern faults; C) restricted fluid flux into the sedimentary assemblage in a 'no-fault' model architecture.



LEGEND

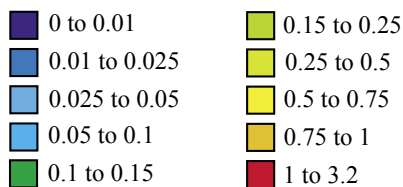


Fig. 6.13: 3-D representation of cumulative shear strain distribution (in % length loss) in a listric fault scenario: A) 9% uniaxial shortening with restricted fluid flux through sedimentary assemblage; B) 9% transpression with restricted fluid flux through sedimentary assemblage; C) 9% uniaxial shortening with restricted fluid flux through central and eastern faults; D) 9% transpression with restricted fluid flux through central and eastern faults; E) 9% uniaxial shortening with restricted fluid flux through sedimentary assemblage and faults absent; F) 9% transpression with restricted fluid flux through sedimentary assemblage and faults absent.

assemblage to simulate a proximal fluid source (i.e. fluid flow still dispersed through the sediments; Fig. 6.12A); 2) restricted fluid flux (2.0×10^{-9} m/s) through the central and eastern faults to simulate a distal fluid source (i.e. fluid already focussed along fault pathways; Fig. 6.12B); and 3) a model geometry without faults and restricted fluid flux (2.0×10^{-9} m/s) through the sedimentary assemblage to investigate if preferential fluid flow pathways would be generated (Fig. 6.12C). Fluid flux rates are based on Thompson (1997) and amplified by one order of magnitude to obtain illustrative modelling results.

6.5.3.1 SHEAR STRAIN DISTRIBUTION

No significant variations of shear strain distribution can be observed with respect to Figures 6.7A-B or 6.9C-D in the case of restricted fluid flux through the sedimentary assemblage or the central and eastern fault (Fig. 6.13A-D; see (1) and (2) above). Shear strain remains focussed along the fault structures, with minor augmentation along fault inflections and some shear strain distributed along the base of the hanging wall of the central and eastern faults. Figure 6.13E-F shows that without the presence of faults (see (3) above), deformation of our model remains very small and shear strain is distributed in the weaker sedimentary assemblage controlled by lithological contrasts. Figure 6.13E shows a narrow zone of moderate shear strain along the contact between the mixed basalt-limestone unit and the sedimentary unit, while Figure 6.13F shows a dispersed distribution of shear strain along the eastern portion of the model that represents the sedimentary assemblage.

6.5.3.2 DARCY FLUID FLOW

With restricted fluid flux into the sedimentary assemblage (Fig. 6.14A-B), resulting fluid flow occurs throughout the sedimentary assemblage, but remains of greater magnitude along the faults that still act as a preferential fluid conduit. Dispersed fluid flow of moderate magnitude can be observed in the northeastern section of the model. Despite the absence of initial fluid flux into the listric fault, minor fluid flow occurs along its base and top, suggesting that deformation along its length instigated additional fluid flow. Figure 6.14C-D indicates how fluid flow is augmented and remains restricted along the faults only, when no fluids are fluxed into the surrounding lithological units. Again, minor fluid flux occurs along sections of the listric fault, although no fluids were fluxed into this fault. Figure 6.14E-F shows an even distribution of fluid flow throughout the sedimentary assemblage, with a slight increase of distribution towards the western end.

6.5.3.3 INTERPRETATION

The similarity of modelling results with restricted fluid flux compared to normal fluid flux, suggests that restricted fluid flux in these models can be considered comparable to normal fluid flux resulting from model deformation with specified fault permeability (i.e. $1.0 \times 10^{-13} \text{ m}^2$). The distribution of shear strain in Figure 6.13E-F can be interpreted to represent the development of a fault structure as a result of the lithological contrast between the sedimentary assemblage in the east and the mixed basalt-limestone assemblage in the centre. The fluid flow distribution throughout the sedimentary assemblage, as observed in Figure 6.14A-B, can be interpreted to represent the potential for disseminated alteration and

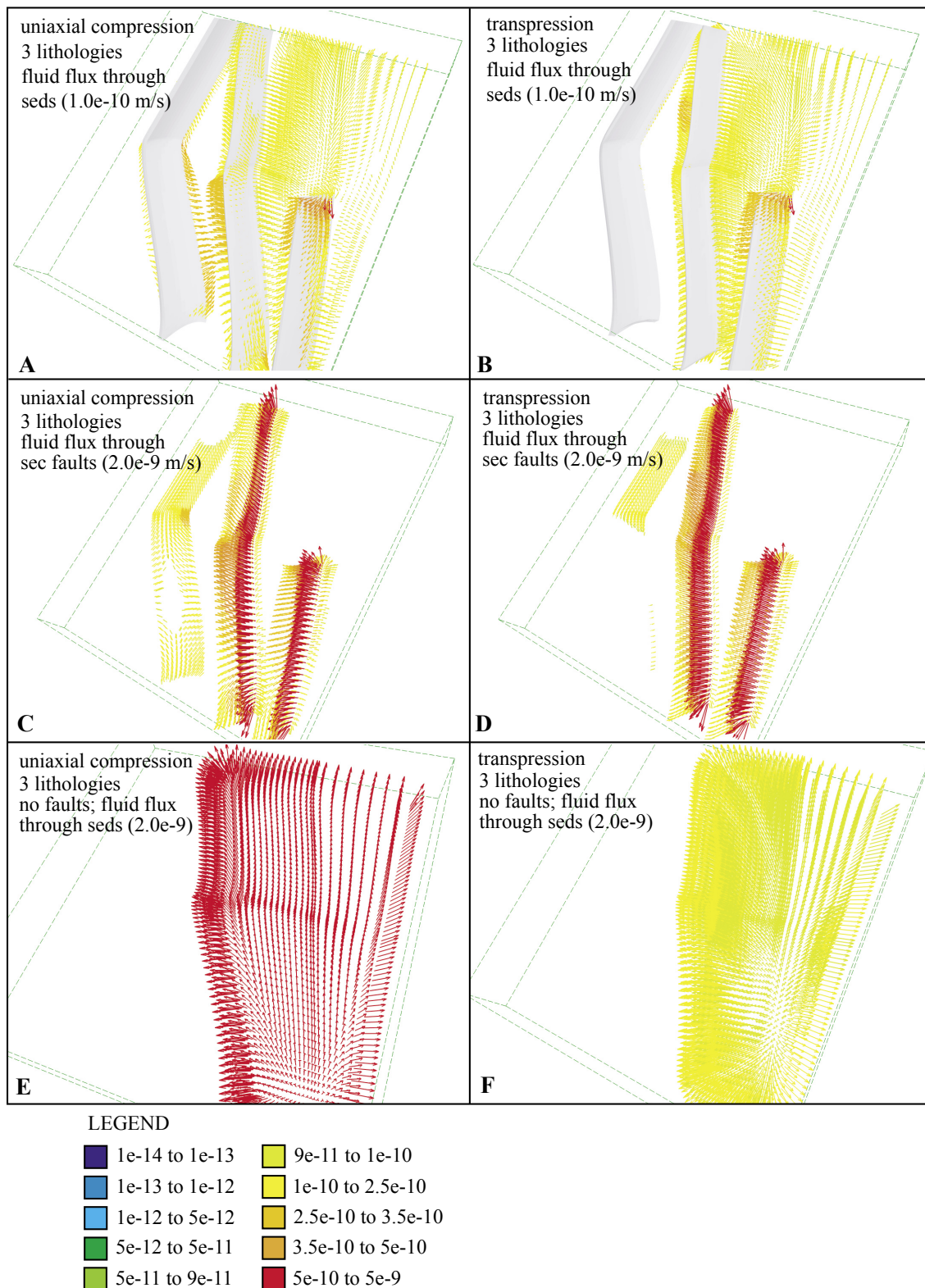


Fig. 6.14: 3-D representation of instantaneous fluid flow vectors indicating magnitude of Darcy fluid flow (m/s) for model scenarios as described in the caption of Figure 10.

mineralisation. Based on our observations in Figure 6.14C-D, we interpret that even without initial forced fluid flux, deformation along the listric fault will instigate minor to moderate

fluid flow along parts of this fault. The even distribution of fluid flow throughout the sedimentary assemblage in Figure 6.14E-F is considered to reflect excessively high values

for restricted fluid flux that gave improbable model results and may thus be disregarded. In this regard, our model outcomes fail to illustrate whether lithological contrast only would be able to focus fluid flow in the zone of high shear strain that develops along the lithological contact.

6.5.4 Fault inflection and termination

A common characteristic in our models is the presence of enhanced shear strain rate and fluid flow along fault inflections and terminations. Figures 6.7A-B, 6.9A-F and 6.13A-D show that the highest values of shear strain in our models are invariably associated with the points of inflection along the fault structures. It seems that these regions at least partly correspond with regions of high fluid flow (although this is not always upward fluid flow) in our models (Figs. 6.9A, C, E and F), or connect to zones of high fluid flow (e.g. Fig. 6.8A-B). In addition, an increase in shear strain and fluid flow can generally be observed at the termination of the eastern fault. In Figures 6.9A-D and 6.13A-D, localized zones of distributed shear extend along strike of the terminated fault into the host rocks. At the same time, high rates of fluid flow (into or out of the fault) are associated with the termination of the eastern fault (Figures 6.11E-F and 6.14A-D), which suggest the occurrence of fluid pumping into the host rocks or fluid scavenging from the host rocks at the fault termination depending on the model conditions.

6.6 IMPLICATIONS FOR MINERALISATION IN THE HODGKINSON PROVINCE

The experiments carried out in this study are relatively simplistic and are primarily intended to describe first-order controls on deformation

and fluid flow that may be used to explain deformation, mineralisation, alteration and magmatism (particularly along the southwest-striking segment of the Palmerville Fault) in the Hodgkinson Province. For this purpose, the effects of strike variations and the listric nature of a fault as well as fault inflections and terminations on the distribution of shear strain and fluid flow are considered.

6.6.1 Regional-scale strike changes

Field observations in the Hodgkinson Province have indicated that the Palmerville Fault forms a zone of high strain of which the northern, north-striking segment is not associated with significant fluid flow (Vos *et al.* in review a) as indicated by the absence of significant alteration, mineralisation or magmatism. In contrast, the presence of granites and volcanics that host several porphyry and skarn deposits (e.g. Nethery & Barr 1998) along the southern, northwest-striking segment of the Palmerville Fault (Fig. 6.1) may reflect the occurrence of significant dilation and fluid flow along this fault segment.

Although the magnitude of shear strain and fluid flow varies in our model results, generally, values of maximum shear strain and fluid flow are spatially associated with the southern segment of the listric fault. In most models, minor to no shear strain and fluid flow is associated with the northern segment of the listric fault (which strikes orthogonal to the far-field compressive stress regime), although some shear strain and fluid flow is evident when transpression is applied. These results indicate that the change in strike of the Palmerville Fault under the ruling stress regime was the dominant factor that controlled the occurrence of dilation and fluid flow along the

fault. If the strike direction of a fault segment is not orthogonal to, but at an angle less than 90° to the ruling far-field compressive stress regime, dilation and fluid flow are likely to be induced. In part this effect may be controlled by the listric nature of the fault (see next section), but in itself our results demonstrate that the variation in strike of particular fault segments could have controlled the spatial distribution of intrusions in the Hodgkinson Province that in turn controlled the formation of porphyry and skarn mineralisation.

The distribution of high shear strain rates (accompanied by high fluid flow rates) along the southern segment of the Palmerville Fault in our modelling results is at odds with the occurrence of numerous relatively undeformed (i.e. post-tectonic) granites along this part of the fault, which is considered to have acted as a dilational jog during Carboniferous-Permian magmatism (e.g. Bultitude *et al.* 1997). However, even if deformation had occurred after the emplacement of these granites in the Hodgkinson Province, a change in the far-field compressional stress regime (for instance to NW-SE) could remove the component of high shear strain while high fluid flow remains along the southern segment of the fault as observed in our models.

6.6.2 Listric nature of a terrane-bounding fault

The Palmerville Fault is a major structure that separates the Hodgkinson Province from the Precambrian regions to the west and southwest. Although the fault seems to be of regional importance, we note that the fault remains unmineralised along most of its strike with respect to orogenic gold mineralisation, while several gold deposits formed along sub-

parallel shear and fault zones during Early Palaeozoic episodes of contraction throughout the province.

Our results illustrate the importance of the presence of a listric fault (orthogonal to the far-field compressive stress regime) for the partitioning of shear strain and fluid flow along (sub-)parallel, second-order faults. A terrane-bounding listric fault seems to allow distribution of shear strain and fluid flow along zones of relative weakness and relatively high permeability throughout the model (Fig. 6.8A-B). This is not the case with a planar terrane-bounding fault, where shear strain and fluid flow are instead distributed only along the fault that is preferentially oriented with respect to prevailing stress regime (in this case the fault with the shallowest dip; Fig. 6.8C-D). From these results, we infer that the listric nature of a terrane-bounding fault controls the distribution of fluid flow (and by inference, mineral deposits) along sub-parallel faults, while at the same time, the listric fault itself may not act as a significant conduit for focused fluid flow. In applying these results to the geology of the Hodgkinson Province, we reason that the listric nature of the Palmerville Fault controlled dilation and (gold) mineralisation along preferentially-oriented structures in at least the western part of the province during Early Palaeozoic deformation. In the Hodgkinson Province, an increase in deformation intensity can be observed towards the Palmerville Fault. We note that such an increase is only observed in our modelling results that consider listric fault geometries (Fig. 6.7A-B), while planar fault geometries display the opposite (Fig. 6.7C-D). These results are not necessarily applicable to listric faults in general, since it has been shown that listric faults may act as a significant fluid

conduit (Bierlein *et al.* 1998). Importantly, however, many first-order faults do not show evidence for strong fluid flux gradients, at least at upper crustal levels. This may explain why mineral deposits generally do not form within these faults, and instead are preferentially associated with second-order structures (e.g. Cox *et al.* 2001).

6.6.3 Fault inflections and terminations

Orogenic gold deposits form the most widespread ore deposit type that is not related to Carboniferous-Permian magmatism in the Hodgkinson Province (e.g. Garrad & Bultitude 1999). Peters *et al.* (1990) suggested that fault splays, intersections and inflections exert a strong control on the location of ore shoots within orogenic gold deposits in the Hodgkinson Province. Our model results similarly indicate that fault inflections and terminations in many cases provide a focus for fluid flow. Fault inflections are generally associated with regions of higher fluid flow within the fault units in our models. In the case of fault termination, scavenging of fluids from the host rocks at the fault tip can be observed in models with very high fault permeability (Fig. 6.11E-F) and restricted fluid flux through the sediments (Fig. 6.14A-B). Fluid flux into the host rocks occurs at the fault tip in models where fluid flux is restricted to the faults only (Fig. 6.14C-D).

Our findings are in accord with findings by Cox *et al.* (2001) who demonstrated that high fluid flux in faults or shear zones is localized in sites with high fracture aperture and / or fracture density like jogs, bends and splays. In our models, fault inflections and terminations are equally important regions for focused fluid

flow, and therefore may be interpreted to be favourable regions for mineral deposition. We speculate that a penetrative cleavage may develop at a fault tip or inflection, and thus may form more permeable regions at these locations in the surrounding host rocks.

6.6.4 Application to mineral exploration

Quantification of the contrasting relationship between first-order barren fault systems and second-order fault structures associated with gold-rich regions, such as observed in the Hodgkinson Province has not previously been illustrated in mineral exploration scenarios. Our modelling outcomes confirm firstly that first-order fault systems, even when barren, are likely to control mineralisation in the surrounding regions. Secondly, where mineralisation in regions adjacent to barren, first-order fault systems does occur, the geometry of the first-order fault system partly determines the overall endowment of the surrounding regions. This notion, together with insights on more local controls on mineralisation obtained through this modelling exercise, can greatly aid future exploration in the Hodgkinson Province and may also be applicable to similar regions elsewhere.

6.7 CONCLUSIONS

Coupled mechanical and fluid flow numerical modelling has been carried out on model geometries that resemble the geology of the western Hodgkinson Province to obtain insights into the factors that control deformation and fluid flow (and by inference mineralisation) in that province. From our modelling exercise several key factors could be identified that controlled the distribution of shear strain and fluid flow. These include regional-scale strike changes,

the listric nature of the terrane-bounding fault and fault inflections and terminations. The variation in strike between the northern and southern segment of the Palmerville Fault, and in particular the orientation of the southern segment of this fault with respect to the ruling far-field stress regime, is inferred to be a key factor in the occurrence of dilation and magmatism along this fault segment in the Carboniferous and Permian. A listric fault geometry has been shown to control the distribution and partitioning of shear strain and fluid flow in zones of relatively high permeability and / or low rock strength throughout the model geometry. In the case of a planar fault geometry, no partitioning of shear strain and fluid flow will occur, but all shear strain and fluid flow will be focussed on a single structure, which is likely to be the structure with the shallowest dip. These results suggest that the listric nature of the Palmerville Fault may have been crucial for the occurrence of mineralisation associated with second-order fault structures (e.g. Retina Fault, Kingsborough Fault) throughout the western part of the province, while the first-order Palmerville Fault itself remained barren. Furthermore, it has been shown that fault inflections and fault terminations are characterised by maximum values of shear strain and fluid flow along the structures. As such, these locations may be considered prospective for gold mineralisation in the Hodgkinson Province as was earlier suggested by Peters *et al.* (1990). The identification of these factors and the understanding of their importance to mineralisation may aid in future exploration in the Hodgkinson Province and similar settings elsewhere.

ACKNOWLEDGEMENTS

Research has been funded by the Cooperative Research Centre for predictive mineral discovery (pmd*CRIC) and this paper is published with the permission of the CEO, pmd*CRIC. An International Postgraduate Research Scholarship from Monash University is gratefully acknowledged. The numerical modelling could not have been conducted successfully without the valuable aid of Peter Schaub, Heather Sheldon, Klaus Gessner and Thomas Poulet at CSIRO. Roberto Weinberg and Klaus Gessner are thanked for comments on the manuscript and J. McLellan and ?? for review of the manuscript.

REFERENCES

- BIERLEIN F. P., FULLER T., STÜWE K., ARNE D. C. & KEAYS R.R. 1998. Wallrock alteration associated with turbidite-hosted gold deposits; examples from the Palaeozoic Lachlan fold belt in central Victoria, Australia. *Ore Geology Reviews* 13, 345-380.
- BULTITUDE R. J., GARRAD P.D., DONCHAK P. J., T. DOMAGALA J., CHAMPION D. C., REES I. D., MACKENZIE D. E., WELLMAN P., KNUTSON J., FANNING C. M., FORDHAM B. G., GRIMES K. G., OVERSBY B. S., RIENKS I. P., STEPHENSON P. J., CHAPPELL B. W., PAIN C. F., WILFORD J. R., RIGBY J. F. & WOODBURY M. J. 1997. Cairns region. In: Bain J. H. C. & Draper J. J. eds. North Queensland geology. *Australian Geological Survey Organisation Bulletin* 240, 225-325.
- COX S. F., KNACKSTEDT M. A. & BRAUN J. 2001. Principles of structural control on permeability and fluid flow in hydrothermal systems. *Reviews in Economic Geology* 14, 1-24.
- CUNDALL P. J. & BOARD M. 1988. A microcomputer program for modelling large-strain in plasticity problems. In: Swoboda C. ed. Numerical methods in geomechanics, *Proceedings of the 6th*

- international conference on numerical methods in geodynamics*, 2101-2108.
- GARRAD P.D. & BULTITUDE R.J. 1999. Geology, mining history and mineralisation of the Hodgkinson and Kennedy Provinces, Cairns region, North Queensland. *Queensland Minerals and Energy review series*, Department of Mines and Energy, Brisbane, 305p.
- GROVES D. I., GOLDFARB R. J., GEBRE-MARIAM M., HAGEMANN S. G. & ROBERT F. 1998. Orogenic gold deposits: A proposed classification in the context of their crustal distribution and relationship to other gold deposit types. *Ore Geology Reviews* 13, 7-27.
- ITASCA. 1998. FLAC: Fast Lagrangian Analysis of Continua, *User's guide*. Itasca Consulting Group Inc., Minneapolis.
- NETHERY J. E. & BARR M. J. 1998. Red Dome and Mungana gold-silver-copper-lead-zinc deposits. In: Berkman D. A. & Mackenzie D. H. eds. *Geology of Australian and Papua New Guinean mineral deposits. Australasian Institute of Mining and Metallurgy Monograph Series* 22, 723-728.
- OLIVER N. H. S., ORD A., VALENTA R. K. & UPTON P. 2001. Deformation, fluid flow, and ore genesis in heterogeneous rocks, with examples and numerical models from the Mount Isa district, Australia. *Reviews in Economic Geology* 14, 51-73.
- ORD A. 1991. Deformation of rock; a pressure-sensitive, dilatant material. *Pure and Applied Geophysics* 137, 337-366.
- ORD A. & OLIVER N. H. S. 1997. Mechanical controls on fluid flow during regional metamorphism; some numerical models. *Journal of Metamorphic Geology* 15, 345-359.
- PETERS S. G., GOLDING S. D. & DOWLING K. 1990. Melange- and sediment-hosted gold-bearing quartz veins, Hodgkinson Gold Field, Queensland, Australia. *Economic Geology* 85, 312-327.
- SILLITOE R. H. 2000. Gold-rich porphyry deposits: Descriptive and genetic models and their role in exploration and discovery. *Reviews in Economic Geology* 13, 315-345.
- SORJONEN-WARD P., ZHANG Y. & ZHAO C. 2002. Numerical modelling of orogenic processes and gold mineralisation in the southeastern part of the Yilgarn Craton, West Australia. *Australian Journal of Earth Sciences* 49, 935-964.
- THOMPSON A. B. 1997. Flow and focusing of metamorphic fluids. In: Jamtveit B. & Yardley B.W.D. eds. *Fluid flow and transport in rocks*, pp. 297-314. Chapman and Hall, London.
- TURCOTTE D. L. & SCHUBERT G. 1982. *Geodynamics: Applications of Continuum Physics to Geological Problems*. John Wiley and Sons, New York, 450p.
- VOS I. M. A., BIERLEIN F. P., MURPHY B. & BARLOW M. 2004. The mineral potential of major fault systems: case studies from northeastern Queensland, Australia. In: BARNICOAT A. C. & KORSCH R. J. eds. *Geoscience Australia Record* 2004/09, 209-212.
- VOS I. M. A. & BIERLEIN F. P. In press. Characteristics of orogenic gold deposits in the Northcote district, Hodgkinson Province, North Queensland, Australia: Implications for tectonic evolution. *Australian Journal of Earth Sciences*. (Chapter 3 of this dissertation)
- VOS I. M. A., BIERLEIN F. P. & WEBB J. In press. Geochemistry of Early Palaeozoic basalts in the Hodgkinson Province: a key to tectono-magmatic evolution of the Tasman Fold Belt System in northeastern Queensland, Australia. *International Journal of Earth Sciences*. (Chapter 4 of this dissertation)
- VOS I. M. A., BIERLEIN F. P., BARLOW M. A. & BETTS P. G. In review. The Palmerville Fault, NE Queensland, Australia: A multi-disciplinary approach to understanding major fault systems. *Journal of Structural Geology*. (Chapter 5 of this dissertation)

THE PALAEOZOIC TECTONO-METALLOGENIC EVOLUTION OF THE NORTHERN TASMAN FOLD BELT SYSTEM, AUSTRALIA: INTERPLAY OF SUBDUCTION ROLLBACK AND ACCRETION

I.M.A. Vos, F.P. Bierlein and D. Phillips
Ore Geology Reviews, in preparation

ABSTRACT

The Tasman Fold Belt System in eastern Australia provides a record of the Palaeozoic geological history and growth of the Australian continent along the proto-Pacific margin of Gondwana inboard of an extensive and long-lived subduction system. The Hodgkinson and Broken River provinces represent prominent geological elements of this system and together form the northern Tasman Fold Belt System. Geochronological age dating of the timing of gold formation in the Amanda Bel Goldfield in the Broken River Province and the Hodgkinson Goldfield in the Hodgkinson Province provides constraints on the occurrence of deformation and mineralisation episodes in the Early Devonian and Late Devonian – Early Carboniferous, respectively. In addition, petrogenetic characteristics of Late Carboniferous – Permian volcano-intrusive rocks from the Broken River Province indicate that these rocks formed in an extensional setting along the proto-Pacific margin of Gondwana. Integration of these newly-obtained data with a time-space evaluation of the geological evolution of the Hodgkinson and Broken River provinces, as well as other terranes in the northern Tasman Fold Belt System, allows for the development of a geodynamic model for the Palaeozoic evolution of the northern Tasman Fold Belt System. Our model indicates that three cycles of extension – contraction occurred during the Palaeozoic evolution of the northern Tasman Fold Belt System. Episodes of extension were controlled by roll-back of the subduction system along the Australian margin, whereas episodes of contraction resulted from accretion following the arrival of positively buoyant segments (i.e., micro-continental blocks / oceanic plateaux) at the subducting trench. Our composite interpretative model on the geodynamic evolution of the northern Tasman Fold Belt System integrates the timing of the development of mineral deposits throughout this part of the system and provides a significant advancement in the understanding of Palaeozoic geodynamics along the margin of Gondwana in northeast Australia and allows comparison with the southern part of the Tasman Fold Belt System.

7.1. INTRODUCTION

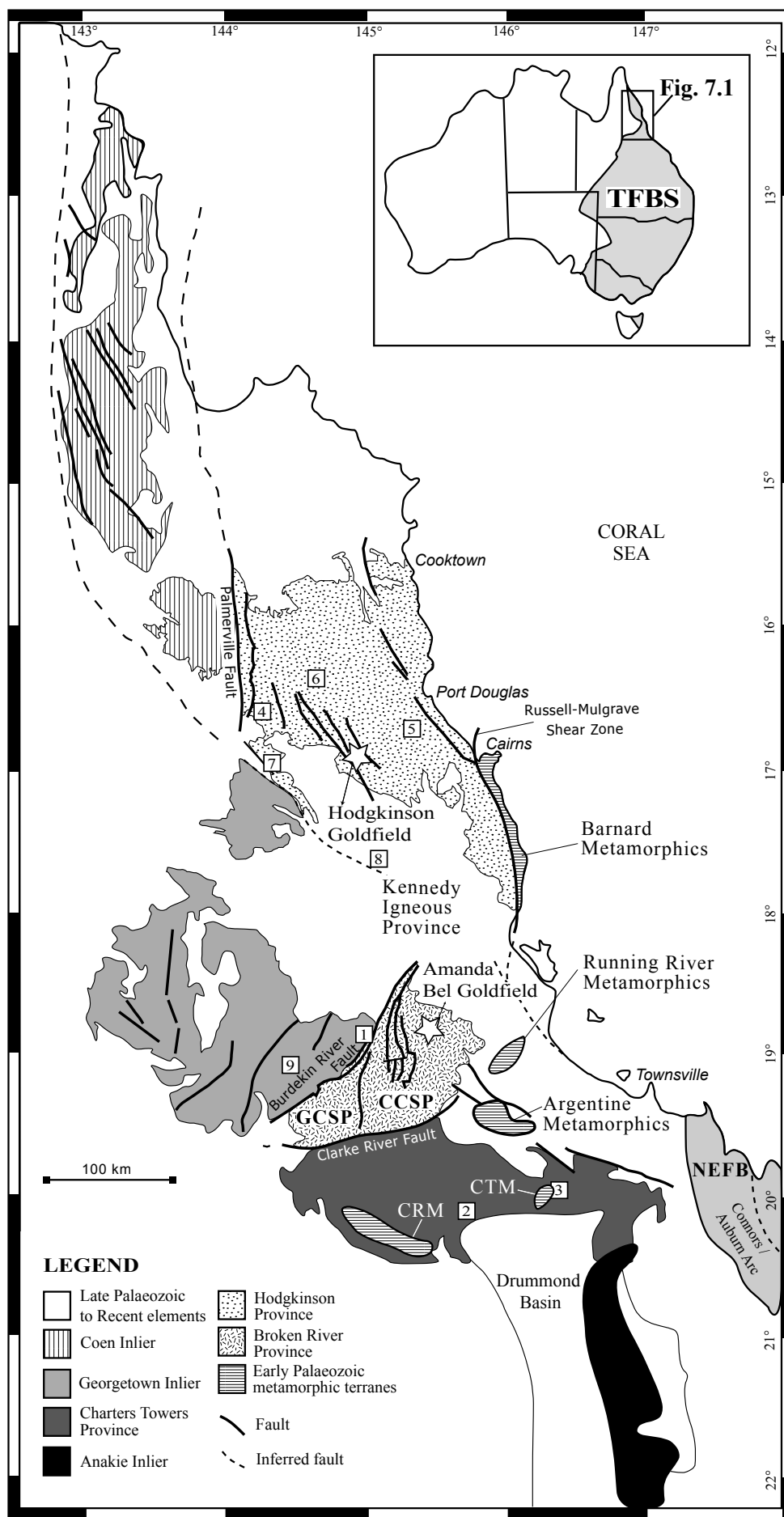
The Tasman Fold Belt System in eastern Australia (inset in Fig. 7.1) represents an assemblage of fold belts that were active orogenic regions in the Palaeozoic (e.g. Coney *et al.* 1990), and which formed from accretionary processes inboard of an extensive, long-lived subduction system (e.g. Cawood 2005 and references therein; Glen 2005; Fig. 7.2). This system stretches over 4,000 km from north to south and is up to 1,500 km wide, with at least one-third of the original orogen extended and submerged beneath the Tasman and Coral seas as a result of late Mesozoic and Cenozoic rifting and sea-floor spreading (e.g. Coney *et al.* 1990). An intimate understanding of the geological history of the various fold belts within the system can provide important insights into the geodynamic evolution of the Australian portion of Gondwana (e.g. Murray 1990; Coney 1992; Walshe *et al.* 1995; Foster *et al.* 1999). Specifically, the characteristics, distribution and timing of emplacement of mineral deposits throughout these fold belts can be directly related to tectonic setting and geodynamic framework (Bierlein *et al.* 2002). The Hodgkinson and Broken River provinces in the northern part of the Tasman Fold Belt System are important geological elements (Fig. 7.1; e.g. Henderson 1987) that have received relatively little scientific attention, compared with other parts of the system, such as the metallogenically well-endowed and well-studied Lachlan Fold Belt in southeastern Australia (e.g. Bierlein *et al.* 2002). For this

reason, several recent studies have focused on metallogenic and tectonic aspects in the Hodgkinson and Broken River provinces. These studies focus on the development of constraints on the timing of mineralisation and deformation (e.g. Davis *et al.* 2002; Vos *et al.* in press a; Vos & Bierlein in press), the emplacement of oceanic-character basalts during back-arc extension in the Hodgkinson Province (Vos *et al.* in press b), and the nature and role of the Palmerville Fault, which separates the Hodgkinson Province from the Precambrian terranes to the west, in the evolution of the province (e.g. Vos *et al.* in review).

Two main tectonic models have been suggested previously for the geodynamic evolution of the Hodgkinson and Broken River provinces. Arnold & Fawcner (1980) and Henderson (1980, 1987) proposed a model that involves subduction associated with an Andean-type continental margin volcanic arc on the Precambrian craton to the west. An alternative model in which the Hodgkinson and Broken River provinces developed as marginal rift basins behind a continental margin magmatic arc, was preferred in Fawcner (1981) and remains favourable at present based on the petrogenetic characteristics of volcano-intrusive rocks and the presence of continental basement in the Hodgkinson Province (for discussion see Bultitude *et al.* 1997).

This paper is concerned with the relative timing of orogenic gold deposits in the Hodgkinson and Broken River provinces and reports new $^{40}\text{Ar}/^{39}\text{Ar}$ age dating results from selected gold

Fig. 7.1 (opposite page): Geological element map of northeastern Queensland incorporating the Hodgkinson and Broken River provinces and indicating major faults and location of goldfields and ore deposits mentioned in text. Inset indicates the extent of the Tasman Fold Belt System (TFBS) in eastern Australia, with the area covered by Figure 1 specified. GCSP = Graveyard Creek Subprovince; CCSP = Camel Creek Subprovince; NEFB = New England Fold Belt; CRM = Cape River Metamorphics; CTM = Charters Towers Metamorphics. Volcanogenic massive sulphide deposits: Balcooma, Dry River, Surveyor (1), Thalanga (2), OK (4), Mt. Molloy (5), Dianne (6). Gold deposits: Charters Towers (3), Kidston (9). Skarn deposits: Red Dome (7), Mt. Garnet (8); for description of deposits see Table 7.4.



deposits. In addition, new petrogenetic data from volcano-intrusive rocks from the Broken River Province are presented. These, together with petrogenetic characteristics of volcano-intrusive rocks in the Hodgkinson are used to review the Palaeozoic tectono-magmatic evolution of the Hodgkinson and Broken River provinces.

The newly-obtained ages from gold deposits and new insights into the tectono-magmatic evolution of the Hodgkinson and Broken River provinces are integrated with available geological constraints from these as well as the remaining regional geological elements of the northern Tasman Fold Belt System. This permits the development of a revised geodynamic model for the Palaeozoic evolution of the northern Tasman Fold Belt System. Results indicate that three cycles of extension and contraction occurred during the Palaeozoic evolution of the continental margin of Gondwana in Australia, and that each of these cycles is closely related to characteristic styles of metallogenesis.

7.2. BACKGROUND AND GEOLOGICAL SETTING OF THE NORTHERN TASMAN FOLD BELT SYSTEM

The Neoproterozoic to Late Palaeozoic Terra Australis Orogen extends across the former margins of Gondwana in Australasia, Antarctica, South Africa and South America (Fig. 7.2; Cawood 2005). The dominantly Palaeozoic Tasman Fold Belt System (TFBS) forms the Australian section of the Terra Australis Orogen and makes up the eastern third of the Australian continent. The TFBS includes the Kanmantoo, Lachlan, Thompson, New England and Hodgkinson-Broken River fold belts (e.g. Coney *et al.* 1990; Scheibner & Veevers 2000; Glen 2005). The TFBS forms a composite of strato-tectonic assemblages and micro-continental fragments that accreted onto the Australian margin of Gondwana as a result of increased coupling along the continental margin during ongoing Palaeozoic subduction (e.g. Cawood 2005).

The northern part of the TFBS in eastern Australia is dominated by the Hodgkinson and Broken River provinces (also termed the Hodgkinson-Broken River Fold Belt; e.g. Murray 1990; see Fig. 7.1). These provinces are separated by extensive Permo-Carboniferous granites of the Kennedy Igneous Province. To the west, the boundary with the Precambrian Coen and Georgetown Provinces is manifested by the Palmerville and Burdekin River faults (Fig. 7.1). The Clarke River Fault marks the boundary between the Broken River Province and the Charters Towers Province, which together with the northern New England Fold Belt, is situated to the southeast (Fig. 7.1). The Broken River Province is further divided

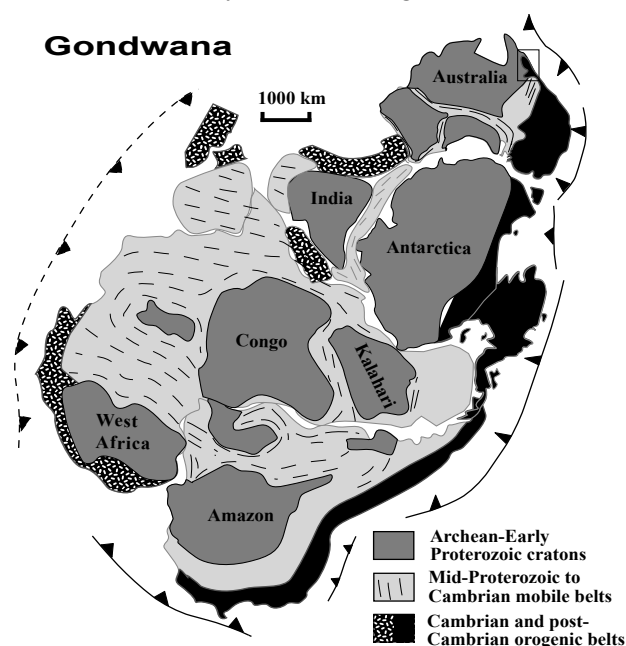


Fig. 7.2: Distribution of Palaeozoic orogenic belts along the margin of Gondwana and extent of the Palaeozoic subduction system along the margin of Gondwana. Inset in Australia indicates area covered in Figure 7.1. Figure modified after Gray & Foster (2002) and Cawood (2005).

into the Graveyard Subprovince and the Camel Creek Subprovince (Fig. 7.1). The Graveyard Creek and Camel Creek subprovinces are joined along the Gray Creek Fault. The Graveyard Creek Subprovince comprises mainly multiply-deformed, greenschist-facies metamorphosed, Ordovician to Early Carboniferous meta-sedimentary and volcanic rocks. The Camel Creek Subprovince contains similarly deformed and metamorphosed Ordovician to Devonian sedimentary assemblages that are considered to have once been continuous with similar assemblages in the Hodgkinson Province (e.g. Arnold & Fawcner 1980; Bultitude *et al.* 1997; Withnall *et al.* 1997b). The Palaeozoic geology and deformation episodes in the Hodgkinson and Broken River provinces are discussed in detail in Bultitude *et al.* (1997) and Withnall *et al.* (1997b), respectively. The tectono-metallogenic relationships within the provinces are further elucidated in Vos & Bierlein (2005), Vos & Bierlein (in press) and Vos *et al.* (in press a). An overview of the main Palaeozoic tectonic, magmatic, metallogenic and depositional events in the Hodgkinson and Broken River provinces is given in Figure 7.3.

7.3. CONSTRAINTS ON THE TIMING OF GOLD MINERALISATION IN THE HODGKINSON AND BROKEN RIVER PROVINCES

7.3.1 Orogenic gold deposits in the Hodgkinson and Amanda Bel goldfields

Vos *et al.* (in press a) have shown, on the basis of structural, paragenetic and fluid inclusion studies, that gold and antimony deposits in the Amanda Bel Goldfield in the Camel Creek Subprovince of the Broken River Province formed during three mineralising episodes in the Early Devonian, Late Devonian

– Early Carboniferous and middle to Late Carboniferous. In addition, Vos & Bierlein (in press) have shown, on the basis of structural, paragenetic and ore fluid characteristics of gold and antimony deposits in the Northcote District of the Hodgkinson Goldfield, that these deposits formed during two mineralising episodes in the Late Devonian – Early Carboniferous and middle to Late Carboniferous. Structural and metallogenic characteristics associated with the Late Devonian – Early Carboniferous and middle to Late Carboniferous episodes of mineralisation in both goldfields are remarkably similar. Similarities include: 1) the presence of invisible gold in acicular arsenopyrite and a strong relationship between mineralised quartz veins and regional fault structures associated with Late Devonian – Early Carboniferous mineralisation, 2) antimony mineralisation overprinting and disrupting earlier gold-quartz veins during the middle to Late Carboniferous mineralisation, and 3) ore deposition from low to moderate temperature (~120-320°C), low to moderate salinity (generally up to 9 wt% NaCl equivalent), CO₂-poor ore-forming fluids. On the other hand, a marked difference between gold deposits in the studied goldfields is the dominant trend of mineralised quartz veins, which strikes northwest in the Hodgkinson Goldfield, compared to northeast in the Amanda Bel Goldfield. The similarities between the deposits in the goldfields and their structural relationships within the overall framework for the Hodgkinson and Broken River provinces suggest that the orogenic gold deposits formed simultaneously during at least two episodes of deformation inboard of the subduction system along the northeast Australian margin of Gondwana (Vos & Bierlein 2005). The difference in dominant strike-direction in both

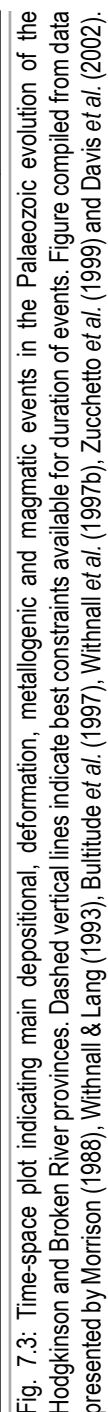


Fig. 7.3: Time-space plot indicating main depositional, deformation, metallogenic and magmatic events in the Palaeozoic evolution of the Hodgkinson and Broken River provinces. Dashed vertical lines indicate best constraints available for duration of events. Figure compiled from data presented by Morrison (1988), Withnall & Lang (1993), Bultitude *et al.* (1997), Withnall *et al.* (1997b), Zucchetto *et al.* (1999) and Davis *et al.* (2002).

goldfields (and provinces) may be explained by the wrapping of fabrics during deformation of sedimentary assemblages around the Georgetown Inlier promontory (Fig. 7.1).

7.3.2 $^{40}\text{Ar}/^{39}\text{Ar}$ age dating

The presence of sericite around and within gold-bearing quartz veins in the goldfields in the Hodgkinson and Broken River provinces enables the application of $^{40}\text{Ar}/^{39}\text{Ar}$ geochronology to constrain the age of hydrothermal alteration and, by inference, mineralisation (e.g. Goldfarb *et al.* 1991; Perkins *et al.* 1995). We utilised a novel technique that integrates dating results from matrix sericite separates and mica inclusion-bearing pyrite separates. This technique is based on the assumption that mica inclusions in most pyrite grains are shielded against complete resetting during later hydrothermal events, and therefore may allow the delineation of hydrothermal / metamorphic events related to sericite and pyrite precipitation (e.g. Smith *et al.* 2001; Miller *et al.* 2004; Miller & Phillips 2005). This technique can provide important constraints on the timing of gold mineralisation, where gold deposition can be demonstrated to occur simultaneous with sericite / pyrite precipitation (as is the case in the studies samples).

Pyrite-bearing samples, as well as sericite-bearing host rock samples were collected from the Airport deposit (AP-Pit6) and

the Minnie Moxham gold deposit (MM03-C2). The Airport gold deposit is situated in the Amanda Bel Goldfield in the Camel Creek Subprovince of the Broken River Province (Vos *et al.* in press a; Fig. 7.1). This deposit consists of several gold-bearing quartz and stibnite veins within strongly deformed arsenic (\pm gold)-rich shales of Silurian to Early Devonian age. Figure 7.4 shows an inclusion-bearing pyrite crystal from the Airport deposit used for dating. The Minnie Moxham gold deposit is located in the Hodgkinson Goldfield in the Hodgkinson Province (e.g. Vos & Bierlein in press; Fig. 7.1). This deposit consists of several gold-bearing quartz veins along anastomosing fault gouge zones that transect mica-rich sandstones of Devonian age.

7.3.2.1 DATING METHODS

An overview of the $^{40}\text{Ar}/^{39}\text{Ar}$ dating technique is given by McDougall & Harrison (1999). Sericite and pyrite separates were prepared using standard crushing, sieving, electro-

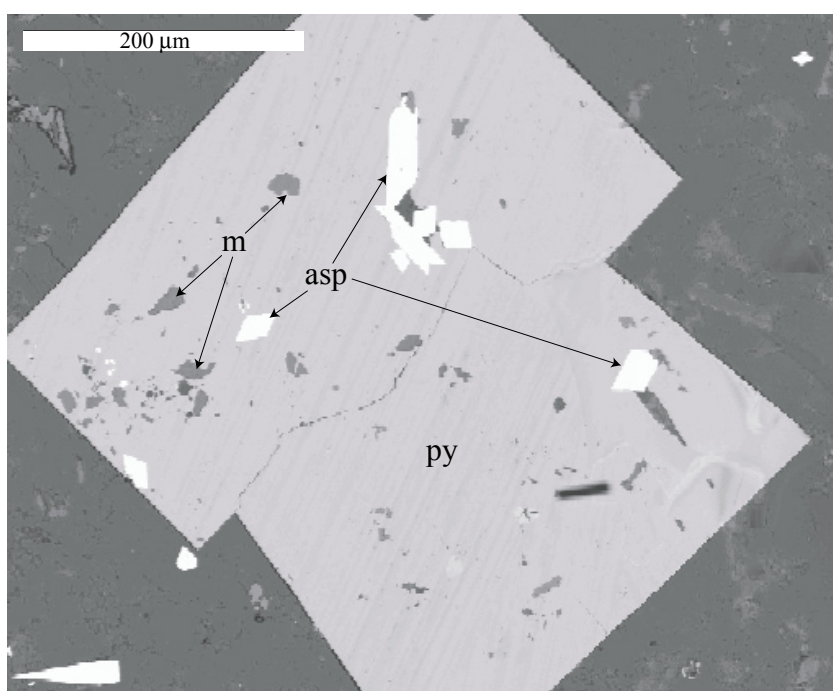


Fig. 7.4: Inclusion-bearing pyrite from the Airport deposit in the Amanda Bel Goldfield. Py = pyrite; Asp = Arsenopyrite; m = mica \pm quartz assemblage.

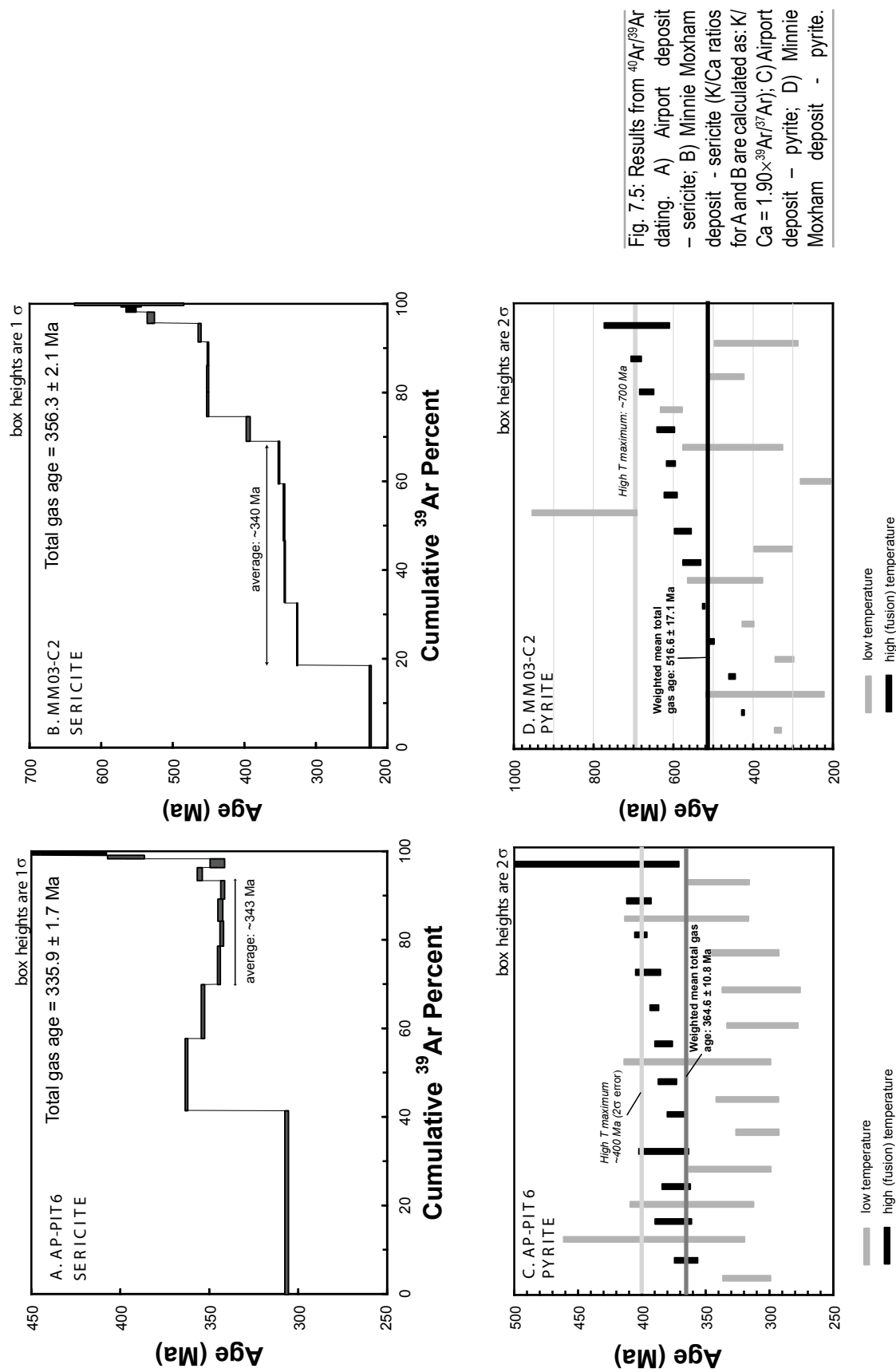


Fig. 7.5: Results from ⁴⁰Ar/³⁹Ar dating. A) Airport deposit - sericite; B) Minnie Moxham deposit - sericite (K/Ca ratios for A and B are calculated as: K/Ca = 1.90 × ³⁹Ar/³⁷Ar); C) Airport deposit - pyrite; D) Minnie Moxham deposit - pyrite.

magnetic, and heavy liquid mineral separation techniques. The sericite-bearing host rocks contained hydrothermal as well as detrital mica grains. Each sericite separate was hand-picked to greater than 90% purity. Pyrite separates could confidently be estimated at greater than 99% purity, where minor contamination with arsenopyrite and quartz / mica could have occurred. Samples were packaged in aluminium foil within a quartz tube and irradiated in the McMaster University Reactor, Canada, along with the flux monitor GA1550 biotite (Renne *et al.* 1998; age = 98.8 ± 0.5 Ma). K_2SO_4 salts were also included in the package to determine correction factors for K-produced ^{40}Ar . Correction factors for interfering reactions are: $(^{36}Ar/^{37}Ar)_{Ca} = 2.70 \times 10^{-4}$; $(^{39}Ar/^{37}Ar)_{Ca} = 6.79 \times 10^{-4}$; $(^{40}Ar/^{39}Ar)_K = 2.89 \times 10^{-2}$. Samples were analysed at the $^{40}Ar/^{39}Ar$ Laboratory, School of Earth Sciences, The University of Melbourne.

Weighed sericite samples were packed in tin foil and step-heated in a double vacuum tantalum furnace, with the liberated gas then being purified by SAES Zr–Al getters. Argon isotopic analyses for sericite separates were conducted on a VG3600 micromass mass spectrometer, which utilizes a Daly detector. Mass discrimination was monitored by analyses of purified air aliquots from a Dorflinger pipette.

Step heating analyses were carried out on 12 aliquots of pyrite from the Minnie Moxham as well as the Airport deposits (2–5 pyrite grains per aliquot; two steps: low fusion temperature and high fusion temperature) using a Spectron Nd-YAG 1064nm laser. Argon isotopic analyses for pyrite separates were then conducted on a MM5400 mass spectrometer, which also utilizes a Daly detector.

7.3.2.2 RESULTS

The complete step-heating results for sericite and pyrite separates (1σ errors) are presented in Appendix 1 and 2, respectively. The isotopic data have been corrected for mass spectrometer backgrounds, mass discrimination and radioactive decay. Decay constants are those reported by Steiger & Jäger (1977). Corrected data from the sericite step-heating analyses are presented in Figure 7.5A–B and summarized in Table 7.1. Results from the pyrite step-heating analyses are presented in Figure 7.5C–D and summarized in Table 7.2. The weighted mean ages indicated on Figure 7.5C and D represent the average of all analyses from individual weighted ages calculated from the high-temperature and low-temperature analyses.

7.3.2.2.1 Airport Deposit (AP-Pit6)

Sericite ages from the Airport deposit (AP-Pit6) exhibit a discordant, somewhat sigmoidal-shaped apparent age spectrum, with apparent ages ranging from ~307 to 680 Ma for a total gas age of 335.9 ± 3.4 Ma (Fig. 7.5a). An age range between 342 and 363 Ma for 40 to 97% of the total gas released from may provide the best constraint on the timing of mica growth associated with metamorphism at this deposit. This age range correlates with the final stages of Late Devonian – Early Carboniferous deformation identified in the Amanda Bel Goldfield by Vos *et al.* (in press a). On the basis of structural and paragenetic relationships, Vos *et al.* (in press a) argued that gold mineralisation in the Amanda Bel Goldfield was related to regional deformation and metamorphism and therefore this age provides a permissive maximum constraint on the timing of gold mineralisation. Considering the Siluro-Devonian age of the rocks hosting the deposit,

Table 7.1: Summary of $^{40}\text{Ar}/^{39}\text{Ar}$ analytical results from sericite separates (2σ error).

Sample	Minimum age (Ma)	Maximum age (Ma)	Total-gas age (Ma)
Ap-Pit6	306.7 ± 1.8	679.9 ± 160.6	335.9 ± 3.4
MM03-C2	223.6 ± 2.4	560.5 ± 152.6	356.3 ± 4.2

Table 7.2: Summary of $^{40}\text{Ar}/^{39}\text{Ar}$ analytical results from pyrite separates from the Airport and Minnie Moxham Deposits (2σ error).

Sample	Ap-Pit6	MM03-C2
minimum total gas age (Ma)	347.3 ± 12.8	397.1 ± 5.2
maximum total gas age (Ma)	386.5 ± 26.2	652.7 ± 39.4
mean total gas age (Ma)	364.6 ± 21.6	516.6 ± 34.2
minimum low T age (Ma)	305.6 ± 27.8	238.6 ± 45.2
maximum low T age (Ma)	389.1 ± 70.8	823.5 ± 130.2
mean low T age (Ma)	335.3 ± 35.4	438.4 ± 67.6
minimum high T age (Ma)	365.7 ± 9.0	427.5 ± 3.2
maximum high T age (Ma)	449.7 ± 76.4	694.7 ± 12.6
mean high T age (Ma)	389.5 ± 14.8	578.4 ± 18.6

older apparent ages from higher temperature steps ($>1050^\circ\text{C}$) are considered to represent outgassing of detrital muscovite.

Age results from pyrite grains from the Airport deposit are shown in Figure 7.5c and the main results are summarised in Table 7.2. Total gas ages range from ~ 347 to 387 Ma. For most pyrite grains low temperature steps yielded younger apparent ages than high temperature steps, suggesting argon loss, despite the fact that the sericite grains were included in pyrite. High-temperature fusion ages range from ~ 366 to 450 Ma. The majority of the high-temperature however display increasing apparent ages over a narrow age interval before reaching a maximum of around 400 Ma. If the high temperature ages also reflect at least some argon loss, then the oldest ca. 400 Ma ages may provide the best approximation for the timing of mica growth associated with metamorphism. Whether or not this age reflects the timing of mineralisation remains equivocal, although it does correspond with an Early Devonian timing of initial orogenic gold mineralisation in the

Airport deposit as suggested by Vos *et al.* (in press a).

7.3.2.2.2 Minnie Moxham deposit (MM03-C2)
Sericite ages from the Minnie Moxham deposit (MM03-C2) exhibit a discordant apparent age spectrum, with apparent ages increasing with increasing temperature and ranging from ~ 224 to 560 Ma for a total gas age of 356.3 ± 4.2 Ma (Fig. 7.5b). The complex age spectrum most probably reflects argon loss and ages from mixed reservoirs (i.e. detrital and hydrothermal). A mean age of ~ 340 Ma (for 19 to 69% of the total gas released) may provide the best constraint on the timing of metamorphism associated with mica growth at this deposit. This age correlates well with the best age estimate for metamorphism obtained from AP-Pit6 and with the final stages of Late Carboniferous – Early Devonian deformation in the Hodgkinson Province. In addition, intermediate temperature steps obtained from the Airport deposit fall in the same age range of ~ 330 – 350 Ma to those obtained from the

Minnie Moxham deposit. Vos & Bierlein (in press) indicated that gold mineralisation in the Northcote District of the Hodgkinson Goldfield is strongly related to regional deformation and metamorphism and therefore this age provides a permissive constraint on the timing of the earliest phase of gold mineralisation in this goldfield. Considering the age of the host rocks, older apparent ages from high temperature steps ($>750^{\circ}\text{C}$) likely represent outgassing of detrital muscovite grains. Ages obtained from these higher temperature steps correlate with the timing of basement metamorphism and granite magmatism between 500 and 400 Ma in the Coen and Georgetown inliers (see Fig. 7.3; Blewett *et al.* 1997; Withnall *et al.* 1997a) and elsewhere in the TFBS (e.g. Cawood 2005).

Age results from pyrite grains from the Minnie Moxham deposit are shown in Figure 7.5d and the main results are summarised in Table 7.2. Total gas ages range from ~397 to 653 Ma. In most cases, lower temperature steps produced younger apparent ages than high temperature (fusion) steps. For most pyrite grains low temperature steps yielded younger apparent ages than high temperature steps, suggesting argon loss, despite the fact that the sericite grains were included in pyrite. High-temperature fusion ages display a broad range in apparent ages from ~420 to 680 Ma. Considering that Late Silurian to Devonian rocks host the Minnie Moxham deposit, the older apparent ages could be due to the presence of excess argon, or inclusion of detrital micas in the pyrite. As the matrix sericite sample exhibits older ages from high temperature steps, the latter interpretation is favoured. Similarity of the high temperature ages with the ~500-400 Ma interval for basement metamorphism and magmatism in the Georgetown and Coen inliers

further supports the notion of the inclusion of detrital micas in pyrite at the Minnie Moxham deposit.

7.3.3 Implications for the tectono-metallogenic evolution of the HBRP

The formation of orogenic gold deposits is generally related to episodes of crustal thickening and accretion at active continental margins involving subduction and / or underthrusting (Groves *et al.* 1998). Although a Late Devonian - Early Carboniferous episode of deformation has been recognised previously in the northern Tasman Fold Belt System (e.g. Bultitude *et al.* 1997; Withnall *et al.* 1997b), our findings from geochronological investigations are the first to place age constraints on the timing of metamorphism / orogenic gold mineralisation in the Hodgkinson and Broken River provinces and support a ca. 340 Ma age for the formation of these gold deposits in an active subduction-accretion setting, potentially preceded by an earlier episode of metamorphism and gold mineralisation at the Airport deposit.

7.4. CONSTRAINTS FROM PETROGENESIS OF VOLCANO-INTRUSIVE ASSEMBLAGES

The petrogenesis of volcano-intrusive rocks is commonly used to investigate the tectonic setting in which these rocks have originated (e.g. Pearce & Cann 1973; Winchester & Floyd 1977). Consequently, petrogenesis of the various volcano-intrusive assemblages in the Hodgkinson and Broken River provinces can be used in the reconstruction of the Palaeozoic tectonic evolution of these provinces. In this section, we present new results on the petrogenesis of Late Carboniferous - Permian intrusions in the Camel Creek Subprovince and review previous studies on volcano-

intrusive assemblages in the Hodgkinson and Broken River provinces to develop a better understanding of the tectonic setting in which these assemblages formed.

7.4.1 Petrogenesis of volcano-intrusive rocks in the Broken River Province

Mafic volcanic rocks are dispersed within various formations in the Broken River Province. Withnall & Lang (1993) discussed the geochemistry of basalts in the Early Ordovician Wairuna, Pelican Range and Judea formations (Fig. 7.3) and suggested that these formed in a rifting environment on a passive margin, or in a back-arc basin setting. This episode of rifting was followed by bimodal volcanism represented by rhyolitic, andesitic and basaltic lavas of the Everetts Creek Volcanics and Carriers Well Formation in the Late Ordovician. Withnall *et al.* (1997b) showed that these basaltic rocks have distinct subduction-related characteristics. The occurrence of subduction during this episode is further corroborated by the presence of arc-related intrusions (Netherwood and Saddington tonalites) in the Graveyard Creek Subprovince.

Another episode of rifting can be inferred from the presence of MORB-related basaltic units in the Silurian to Early Devonian Perry Creek Formation (Withnall & Lang 1993), which very strongly resemble the Silurian and Devonian basaltic units in the Hodgkinson Province. This period was followed by the emplacement of granite intrusions that display an eastward younging progression from the Broken River Province into the Charters Towers Province (Fig. 7.1). These granites were emplaced during two distinct episodes during the latest Devonian and Late Carboniferous to Permian and belong to the Kennedy Igneous Province, for which

the interpreted tectonic setting is described in Section 7.4.2.

To further constrain the tectonic setting in which these rocks formed, the petrogenetic characteristics of seven Late Carboniferous to Permian intermediate to mafic volcanic rocks that intrude the Devonian Kangaroo Hills Formation in the Amanda Bel Goldfield (Fig. 7.1) have been investigated. Results from major, trace and rare earth element (REE) geochemical analysis are presented in Table 7.3. A total alkali-silica (TAS) diagram after Le Maitre (1989) indicates that the studied samples can be classified as basalts, basaltic andesites and andesites (Fig. 7.6). On a Ti-Zr-Y tectonic discrimination diagram (Fig. 7.7; from Pearce & Cann 1973), the intermediate to mafic intrusive rocks plot in the calc-alkaline basalt field and may be considered to be volcanic-arc related (e.g. Pearce 1996). In addition, samples analysed for Th, Ta and Yb have been plotted on a Th/Yb vs. Ta/Yb diagram (Fig. 7.8) and fall in the field representative of active continental margin settings. Our investigations suggest that Late Carboniferous to Permian volcano-intrusive activity occurred in a supra-subduction zone setting as suggested previously by other authors (e.g. Withnall & Lang 1993).

7.4.2 Petrogenesis of volcano-intrusive rocks in the Hodgkinson Province

Previous studies have investigated the petrogenesis of Silurian to Devonian tholeiitic and calc-alkaline basalts in the Chillagoe and Hodgkinson formations in the Hodgkinson Province and suggested that these were emplaced in an extensional back-arc basin setting (e.g. Bultitude *et al.* 1997; Vos *et al.* in press c). Geochemical analysis of these basalts revealed a gradually decreasing input from magmatic arc-like sources in the Late Ordovician and

Table 7.3: Results from major, trace and rare earth element analysis of intermediate to mafic intrusives from the Amanda Bel Goldfield in the Camel Creek Subprovince.

		D.L.	GClod1-5	GC03-01c	MtD-52	Spa-01	Spa-02	Lod-1-01	CC1
Major elements									
SiO ₂	%	0.01	53.8	52	50.3	57.6	59.8	69.2	58.4
TiO ₂	%	0.01	0.67	0.65	2.91	0.625	0.59	0.455	0.62
Al ₂ O ₃	%	0.01	15.1	13.8	13.9	15.4	15.3	11.8	15.5
Fe ₂ O ₃	%	0.01	6.07	7.84	12.6	6.45	6.3	3.7	6.24
FeO	%	0.01	5.46	7.05	11.34	5.8	5.67	3.33	5.61
MnO	%	0.01	0.09	0.1	0.19	0.11	0.13	0.06	0.12
MgO	%	0.01	6.42	8.39	4.33	4.92	4.89	1.53	5.22
CaO	%	0.01	4.91	4.42	6.88	6.44	5.79	2.14	3.52
Na ₂ O	%	0.01	4.62	3.23	3.12	2.98	2.64	3.92	4.38
K ₂ O	%	0.01	0.21	0.29	1.93	1.96	1.41	1.2	0.67
P ₂ O ₅	%	0.01	0.13	0.1	0.63	0.1	0.12	0.13	0.13
LOI	%		7.94	8.91	2.4	3.07	3.38	5.58	4.96
Total	%		99.96	99.73	99.19	99.66	100.35	99.72	99.76
Trace elements									
Ba	ppm	100	162	189	451	185	358	242	546
Cr	ppm	2	487	639	41.3	276	276	43.7	279
Cu	ppm	2	45	15	7	5	33	14	24
Nb	ppm	10	bdl	bdl	bdl	bdl	bdl	bdl	bdl
Ni	ppm	2	220	145	20	44	42	16	32
Pb	ppm	5	60	bdl	8	bdl	38	8	14
Rb	ppm	20	bdl	bdl	69.4	97.9	63.8	80.7	32.6
Sr	ppm	5	410	330	360	210	230	340	700
Th	ppm	0.2	8.26	5.31	5.2	6.71	7.33	11.7	6.66
V	ppm	20	110	140	300	110	110	50	120
Y	ppm	1	17	17	43	18	20	18	18
Zr	ppm	5	100	72	290	84	94	62	86
Sc	ppm	0.1	19.8	26.7	33.1	23.6	22.2	9.72	23.3
Hf	ppm	0.2	3.21	2.32	7.8	2.52	2.82	4.24	2.61
Co	ppm	0.5	33.7	34.6	37.4	26.1	25	8.96	25.4
Zn	ppm	50	134	67.8	112	56.9	69.9	50.1	63
Ga	ppm	1	15	15	22	14	17	14	20
As	ppm	1	18.1	12.2	19.4	1.56	2.25	107	1.7
Sn	ppm	5	14	8	8	14	16	8	14
Sb	ppm	0.2	2.64	0.72	1.21	2.24	1.08	21.2	1.3
Cs	ppm	0.5	1.35	1.21	2.48	4.09	7	7.26	1.89
U	ppm	1	bdl	bdl	bdl	bdl	2.71	bdl	1.85
Ta	ppm	0.5	bdl	0.52	1.12	0.79	1.5	1.03	0.79
Au	ppb	5	bdl	bdl	bdl	bdl	bdl	31.6	bdl
Rare-earth elements									
La	ppm	0.05	22.3	13.7	30.9	14.1	15.3	30.2	15
Ce	ppm	0.5	41.5	27.4	68.3	29.2	31.4	57.2	30.5
Nd	ppm	1	19	13.2	40.1	14.5	16.2	23.2	14.7
Sm	ppm	0.01	3.87	2.91	9.25	3.09	3.27	4.37	3.26
Eu	ppm	0.02	1.07	0.65	2.61	0.87	0.83	0.97	0.87
Tb	ppm	0.1	0.59	0.51	1.69	0.57	0.58	0.62	0.59
Ho	ppm	0.1	0.71	0.7	2.09	0.78	0.82	0.84	0.81
Yb	ppm	0.03	1.68	1.72	4.49	1.95	2.12	2.01	1.97
Lu	ppm	0.01	0.24	0.26	0.64	0.28	0.31	0.28	0.29
Abbreviations: D.L. = detection limit; bdl = below detection level									

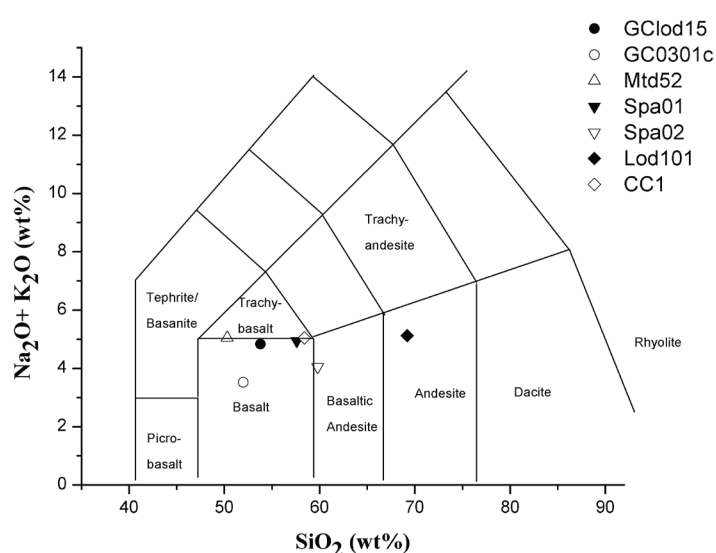


Fig. 7.6: TAS classification diagram (after Le Maitre 1989) for Late Carboniferous – Permian intrusive rocks in the Amanda Bel Goldfield.

Silurian towards input from mainly depleted mantle sources in the Devonian (Vos *et al.* in press c). Vos *et al.* (in press c) suggested that the petrogenetic evolution of the basalts in the Hodgkinson Province could be explained by roll-back and eastward stepping of the long-lived subduction system along the proto-Pacific margin of Gondwana in northeastern Queensland.

Subsequent volcano-intrusive activity entails two distinct episodes in the latest Devonian

and Late Carboniferous to Permian. These are represented by extensive granites and volcanics of the Kennedy Igneous Province (Fig. 7.1). The Late Carboniferous to Permian granites and volcanics show characteristics of emplacement in a supra-subduction zone extensional environment, where the locus of granite emplacement shows an eastward progression with time (e.g. Champion & Bultitude 1994; Bultitude *et al.* 1997). These characteristics

suggests that these rocks formed during Late Carboniferous – Permian rollback or steepening of the subduction system along the proto-Pacific margin of Gondwana in northeastern Queensland.

7.4.3 Implications for the tectono-magmatic evolution of the HBRP

The recognition of the tectonic setting in which Palaeozoic volcano-intrusives rocks of the Hodgkinson and Broken River provinces

formed adds to the understanding of the Palaeozoic geodynamic framework of the northern Tasman Fold Belt System for which five distinct tectonic periods can be recognised. These include: 1) Cambrian – Early Ordovician development of mafic

volcanic rocks in an extensional back-arc setting in the Broken River Province only; 2) Middle to Late Ordovician arc-related volcanism in the Broken River Province, that may have extended

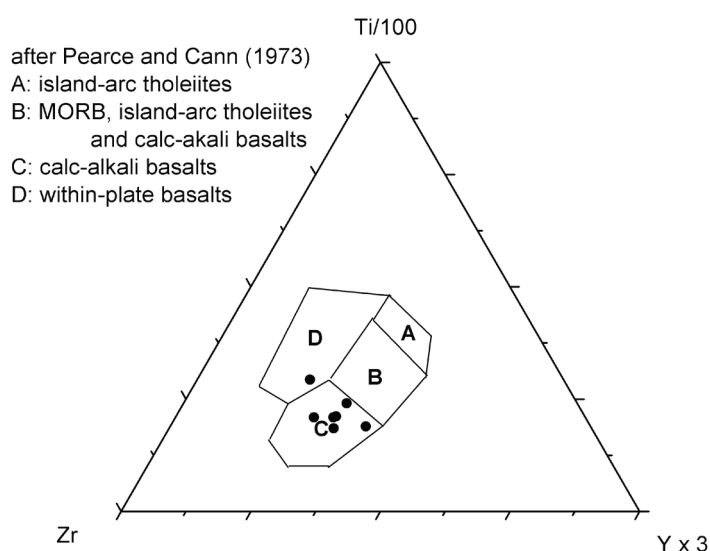


Fig. 7.7: Ti-Zr-Y tectonic discrimination diagram (after Pearce & Cann, 1973) indicating calc-alkaline affinities for the Late Carboniferous - Permian intrusive rocks in the Amanda Bel Goldfield.

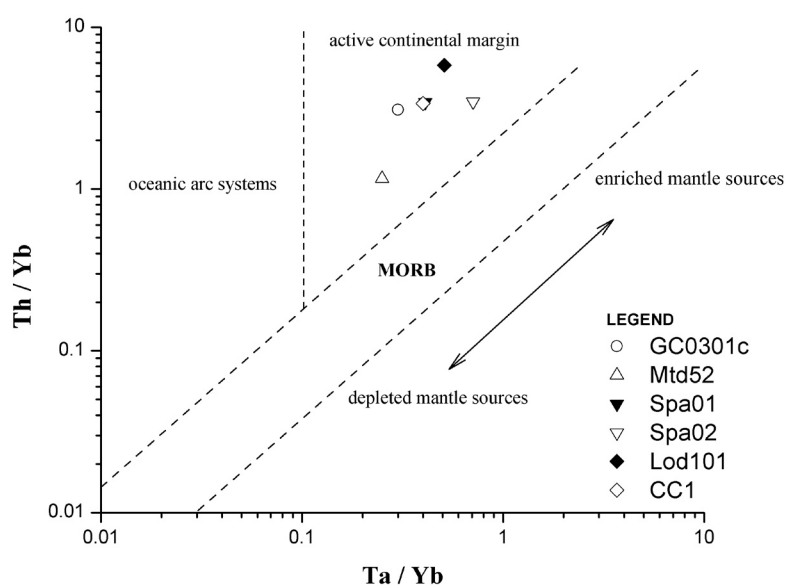


Fig. 7.8: Th/Yb vs. Ta/Yb tectonic discrimination diagram indicating that the intrusive rocks from the Amanda Bel Goldfield were emplaced in an active continental margin setting.

into the Hodgkinson Province (e.g. Vos *et al.* in review); 3) Silurian to Devonian emplacement of mafic volcanic rocks in an extensional back-arc setting; 4) latest Devonian emplacement of minor granites during deformation (Zucchetto *et al.* 2001); and 5) Late Carboniferous to Permian development of arc-related volcano-intrusive rocks in an extensional supra-subduction zone setting.

7.5. TIME-SPACE EVOLUTION OF REGIONAL GEOLOGICAL ELEMENTS IN THE NORTHERN TASMAN FOLD BELT SYSTEM

We have integrated our findings on the timing of gold mineralisation / deformation episodes and the development of volcano-intrusive rocks in the Hodgkinson and Broken River provinces with available geological data from the various terranes in the northern Tasman Fold Belt System. These include the Georgetown, Coen and Charters Towers provinces, as well as the northern part of the New England Fold Belt (Fig. 7.1). A time-space summary of the geological history of these terranes is presented

in Figures 7.3 and 7.9. The New England Fold Belt has not been included in Figures 7.3 and 7.9, and its evolution is discussed elsewhere (e.g. Murray *et al.* 1987; Korsch *et al.* 1990; Holcombe *et al.* 1997a; Holcombe *et al.* 1997b; Fergusson *et al.* 2001; Jenkins *et al.* 2002).

A composite interpretative time-space evolution for the Gondwanan continental margin in the Palaeozoic is shown in Figure 7.10.

This figure illustrates the geodynamic evolution of the northern Tasman Fold Belt System as schematic cross-sections that highlight the main geological events occurring in the northern Tasman Fold Belt System in the area now situated between 15° and 22° S. The main geological events for each time slice are discussed in the following sections.

7.5.1 Cambrian rifting and microcontinent development

The ~560 Ma Marlborough Ophiolite in the northern New England Fold Belt represents fragments of oceanic lithosphere that formed during sea-floor spreading outboard of the Late Neoproterozoic margin of Gondwana (Bruce *et al.* 2000). Fergusson *et al.* (2001) suggested that the Palaeozoic development of the northern Tasman Fold Belt System commenced with an episode of Late Neoproterozoic to Early Cambrian ocean-ward stepping of a subduction system. This is supported by the presence ~540 Ma stretching lineations and metamorphism recorded in the Anakie Inlier and the presence of the Marlborough Ophiolite and younger, ~530

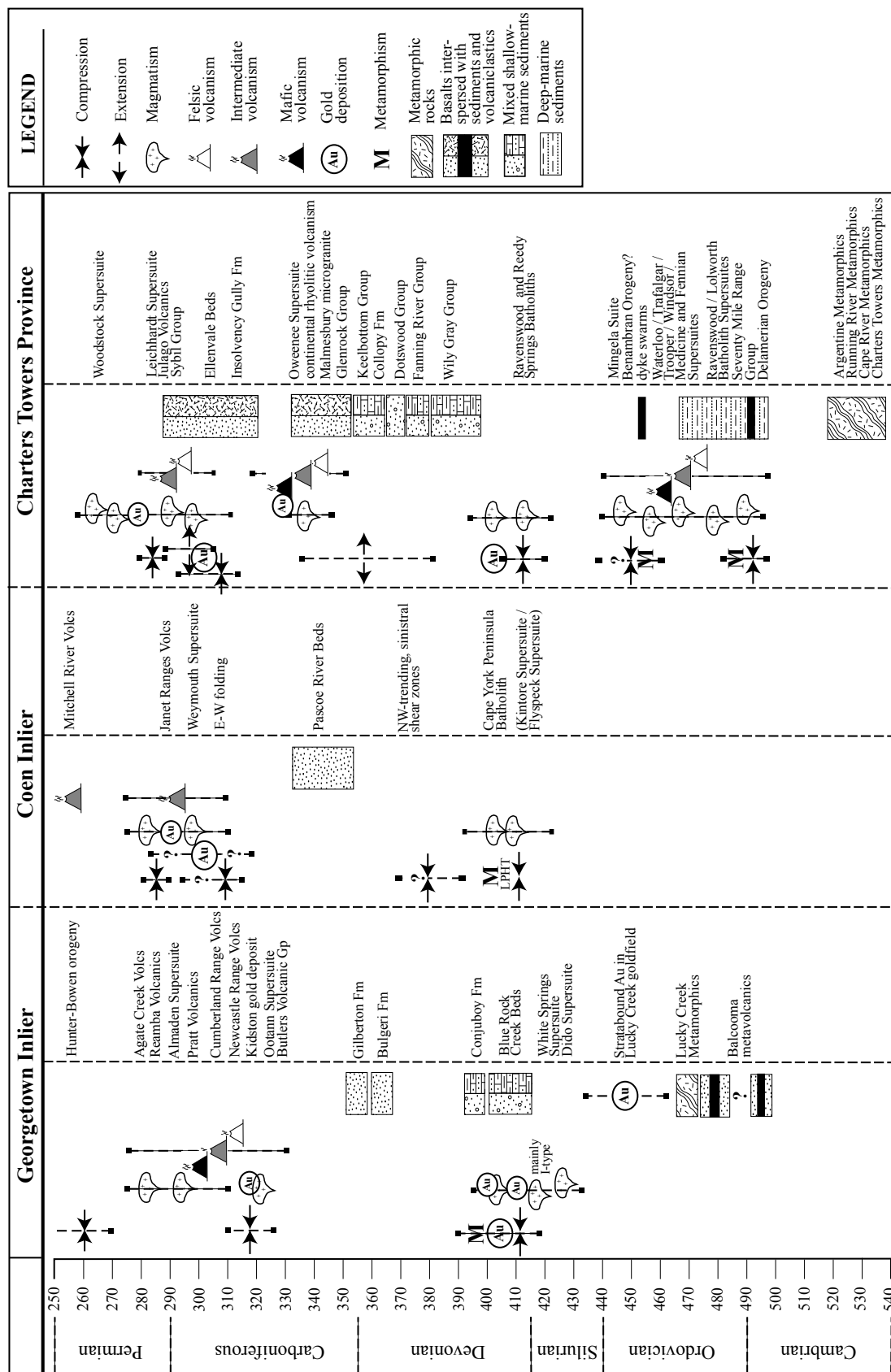


Fig. 7.9: Time-space plot indicating main depositional, deformation, metallogenic and magmatic events in the Palaeozoic evolution of the Georgetown, Coen and Charters Towers regions. Dashed vertical lines indicate best constraints available for duration of events. Figure compiled from data presented by Blewett *et al.* (1997), Huston *et al.* (1997) and Withnall *et al.* (1997a).

Ma ophiolitic rocks along the Peel Fault System that are interpreted to have formed in a back-arc basin (Aitchison *et al.* 1992; Yang & Seccombe 1997). Outstepping of the subducting slab may also have controlled extension and rifting along the Proto-Pacific margin of northeastern Queensland that resulted in attenuation of the continental margin crust, and calving of microcontinental fragments from the margin. The Barnard, Argentine, Cape River and Anakie Metamorphics terranes (Fig. 7.1) are potential candidates in northeastern Queensland that may represent such microcontinents that have been accreted back onto the Gondwanan margin during the Palaeozoic (e.g. Fergusson *et al.* 2001). Scheibner & Veevers (2000) indicated that 560-530 Ma attenuation of the Australian continental margin coincided with a major change in plate dynamics during crustal relaxation after collision between East and West Gondwana, which may have culminated in the inception of subduction along the margin of Gondwana.

7.5.2 Late Cambrian-Middle Ordovician subduction, attenuation of the continental margin and basin infill

By Late Cambrian – Early Ordovician times, westward subduction was established along the entire margin of Palaeozoic Australia (e.g. Coney *et al.* 1990; Scheibner & Veevers 2000) and controlled the generation of arc-related volcanic rocks in the Charters Towers Province, as well as back-arc related calc-alkaline assemblages in the Georgetown and Broken River provinces in the northern Tasman Fold Belt System (e.g. Withnall & Lang 1993). An episode of deformation recorded in the Cape River Metamorphics of the Charters Towers Province and the Anakie Inlier at around 500 Ma (e.g. Withnall *et al.* 1996; Hutton *et al.*

1997) supports the occurrence of subduction at this time and may be correlated with the Delamerian Orogeny in southeastern Australia (Scheibner & Veevers 2000).

Attenuation of the marginal continental crust and the development of marginal back-arc basins associated with roll-back of the subducting slab outboard of the northern Tasman Fold Belt System is represented by the deposition of the Seventy Mile Range Group, the Balcooma Metavolcanics, the Wairuna Formation and the Mulgrave Formation (Fig. 7.3 and 7.9; e.g. Bultitude *et al.* 1997; Withnall *et al.* 1997a, b; see also sections 7.4.1 and 4.2). The occurrence of extension in the Early to Middle Ordovician is supported by the recognition of extensional growth faulting during deposition of the Seventy Mile Range Group in the Charters Towers Province (Berry *et al.* 1992) and extensional fabrics in the Cape River Metamorphics (Fergusson *et al.* 2005). Kuroko-style VHMS deposits such as the Thalanga deposit (Fig. 7.1) were generated in rocks of the Seventy Mile Range Group during this episode (Murray 1990). Fukui *et al.* (1995) interpreted that high-PT, allochthonous, glaucophane- and actinolite-bearing rocks in melange zones along the Peel Fault in the southern New England Fold Belt formed during ca. 470 Ma metamorphism related to subduction in the Early-Middle Ordovician. These authors also suggested that subduction occurred continuously over the ~530-470 Ma episode.

7.5.3 Late Ordovician microcontinent accretion and closure of marginal basins

A Late Ordovician (~460-440 Ma) phase of deformation is recorded in the marginal basin sedimentary rocks of the Hodgkinson, Broken River and Charters Towers provinces

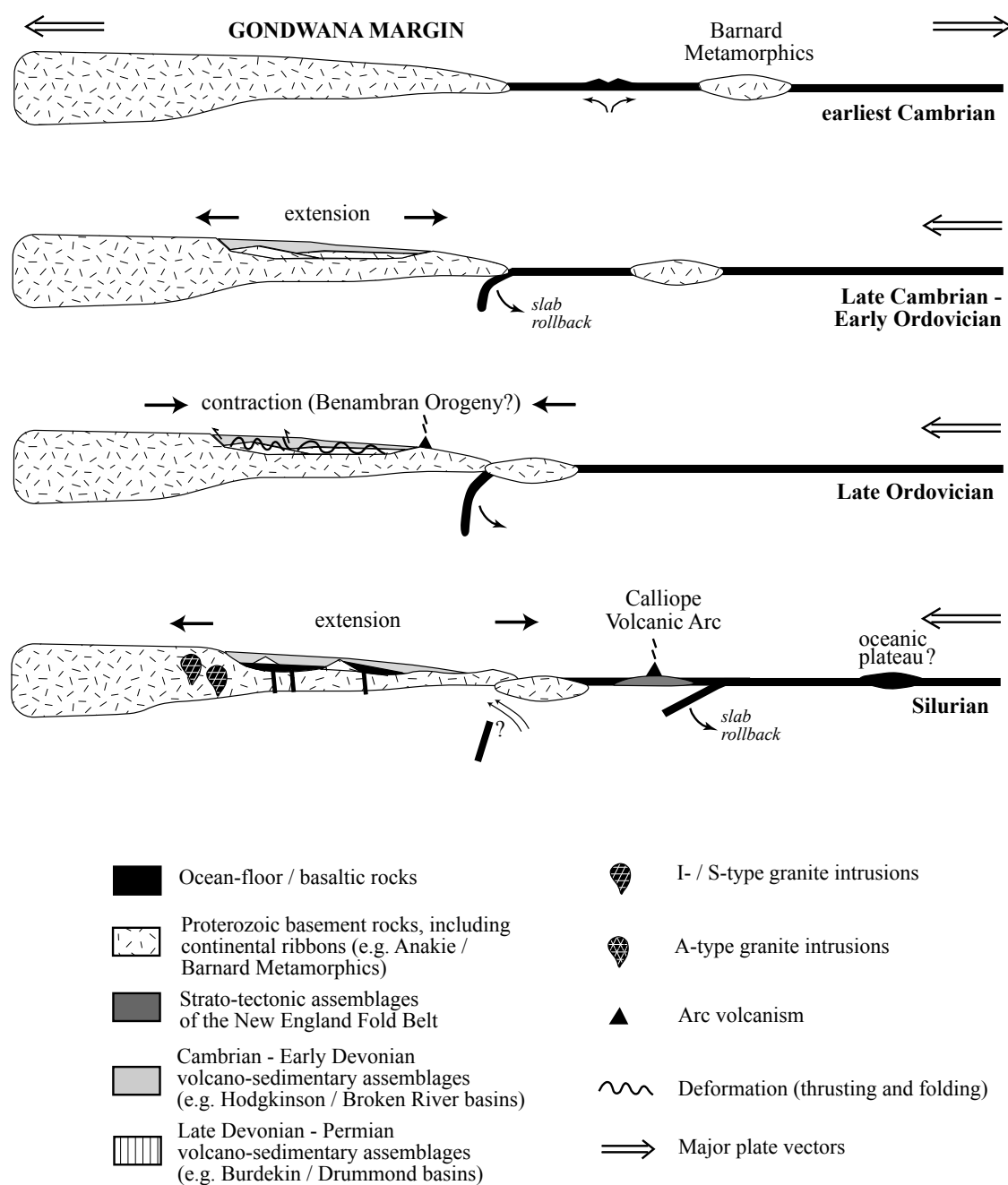
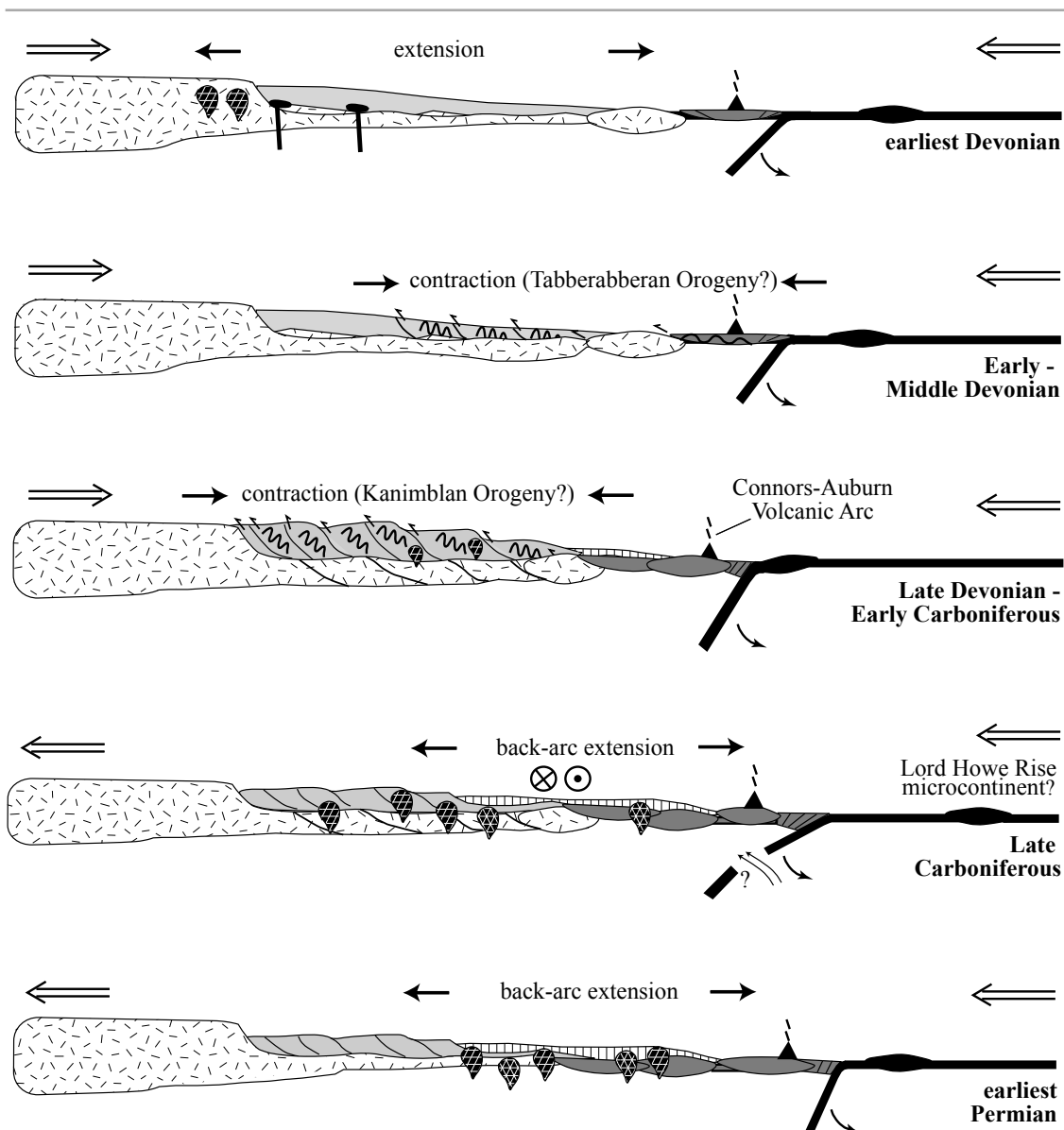


Fig. 7.10 (continues next page): Composite interpretative diagram for the Palaeozoic time-space evolution of the northern Tasman Fold Belt System for the area between 15° and 22° S (Fig. 7.1). Main events for each individual time-slice are discussed in the text.

(e.g. Bultitude *et al.* 1997; Hutton *et al.* 1997; Withnall *et al.* 1997b). This episode of deformation is contemporaneous with calc-alkaline arc-style volcanism in the Hodgkinson and Broken River provinces (as represented by ca. 455 Ma dacite clasts in the Mountain Creek Conglomerate and the Everett Creek Volcanics; Bultitude *et al.* 1997; Withnall *et al.* 1997b) and

resulted in (partial) closure of marginal basins. This episode of deformation has also been recognised in the Barnard Metamorphics (e.g. Bultitude *et al.* 1997), possibly suggesting that the Barnard Terrane arrived at the subduction trench around this time and accreted onto the continental margin. This accretion resulted in lock-up of the subduction system in the northern



Tasman Fold Belt System and coincided with similar subduction lock-up in the Lachlan Fold Belt in the southern Tasman Fold Belt System (e.g. Glen *et al.* 1998). There, subduction lock-up is considered to have culminated in slab break-off at the end of the Ordovician (Vos *et al.* in press b). Only minor evidence for deformation has been recorded in the cratonised Georgetown and Coen inliers around this time (e.g. Blewett *et al.* 1997; Withnall *et al.* 1997a), which suggests that deformation may have focussed mainly on the previously attenuated, and therefore weaker, continental back-arc regions.

7.5.4 Silurian subduction relocation and initiation of back-arc basin extension

The deposition of shallow-marine limestone and sedimentary assemblages and contemporaneous emplacement of mafic volcanic rocks in the Hodgkinson Province and Camel Creek Subprovince indicate that crustal attenuation occurred after initial deposition of terrigenous conglomerates (i.e. Mountain Creek Conglomerate / van Dyke Litharenite) in a deepening extensional back-arc basin setting (Vos *et al.* in press c). This episode of back-arc extension occurred synchronous with the

development of the Silurian to Middle Devonian intra-oceanic Calliope Volcanic Arc of the New England Fold Belt (e.g. Murray 1990). The development of this Silurian to Middle Devonian arc system suggests that renewed subduction was initiated after ocean-ward stepping following lock-up in the Late Ordovician. The absence of voluminous volcanic detritus within the Silurian and Devonian sedimentary sequences suggests spatial separation between volcanic arc and back-arc basins (e.g. Withnall & Lang 1993). The initiation of back-arc extension during this episode could be related to changing stress conditions along the continental margin related to ocean-ward stepping of the subduction system. The back-arc basin assemblages in the Hodgkinson Province and Camel Creek Subprovince of the Broken River Province are considered to have formed a continuous tract along the Silurian-Devonian proto-Pacific margin of Gondwana (e.g. Arnold & Fawcner 1980). Terrigenous sedimentation occurred during this episode at ~430 Ma in the Graveyard Creek Subprovince (i.e. Graveyard Creek Group) synchronous with the emplacement of the White Springs and Dido supersuites (Fig. 7.9) that mark the initial development of the Pama Province, which is defined as all Siluro-Devonian granitic rocks in northeastern Australia (e.g. Blewett *et al.* 1997). These events indicate that crustal attenuation occurred over a region more extensive than just the Hodgkinson and Broken River provinces, and we suggest that regionally extensive uplift and attenuation of the crust may have been associated with mantle upwelling.

7.5.5 Earliest Devonian (418-400 Ma)

back-arc basin widening

The earliest Devonian part of the evolution of the Hodgkinson and Broken River provinces was marked by the initiation of deposition of a thick succession of turbidites represented by the Hodgkinson and Kangaroo Hills formations. A distinct change in sedimentation characteristics is marked by the dominantly marine sedimentary rocks in these formations compared to the previously deposited, dominantly shallow-marine formations in the Silurian (e.g. Bultitude *et al.* 1997). This change in sedimentary conditions can be attributed to increased rates of crustal attenuation resulting in back-arc basin deepening during the Early Devonian, as supported by isotopic evidence from basaltic units in the Hodgkinson Formation (Vos *et al.* in review). The continuation of crustal attenuation into the Devonian resulted in emplacement of the Cape York Peninsula, Ravenswood and Reedy Springs batholiths of the Pama Province in the Georgetown, Coen and Charters Towers terranes from around 410 to 380 Ma (e.g. Blewett *et al.* 1997; Hutton *et al.* 1997; Withnall *et al.* 1997a). Mesothermal granite-hosted gold mineralisation in the world-class Charters Towers Province (e.g. Hutton *et al.* 1997) was generated during this episode of magmatism.

7.5.6 Early - Middle (400-370 Ma) Devonian initial arc collision and localised deformation

In the Middle Devonian, mafic MORB-related volcanism, granite magmatism and basin infill diminished in the Hodgkinson and Broken River provinces, marking a reversal to an overall compressional regime. This change is supported by the formation of melange possibly related to initial accretion and deformation of the Calliope Volcanic Arc assemblages (which include the

Yarrol Trough) in the New England Fold Belt (e.g. Scheibner & Veevers 2000). It coincides with a major change in plate vectors as indicated by Scheibner & Veevers (2000) who suggested that the Silurian to earliest Devonian episode was characterised by a dominantly northwest-directed plate vector, whereas the Early and Middle Devonian episode was marked by a dominantly southwest-directed plate vector for the Proto-Pacific Plate (plate vectors in present-day configuration of Australia). This episode of deformation is considered to be responsible for the formation of orogenic gold mineralisation in the Amanda Bel Goldfield (e.g. Vos *et al.* in press a) and can also be correlated with the Tabberabberan Orogeny in the southern Tasman Fold Belt System. Pyrite age dating results from the Airport deposit suggest that metamorphism associated with mineralisation in this deposit may have occurred as early as 400 Ma.

7.5.7 Late Devonian to Early Carboniferous (~370-330 Ma) basin closure, arc accretion and gold mineralisation

Coney *et al.* (1990) suggested that continuation of the previous episode of convergence resulted in progressive accretion along the margin of Gondwana between ~370 to 330 Ma. This would lead to consolidation of the Hodgkinson and Broken River provinces from deep-marine margin conditions into cratonic Australia. An episode of minor magmatism occurred at around ~360 Ma (e.g. Withnall & Lang 1993; Zucchetto *et al.* 2001) in the Hodgkinson and Broken River provinces, which may have resulted from crustal thickening of the previously attenuated regions that were exposed to high geothermal gradients. A major episode of deformation of the Siluro-Devonian volcano-sedimentary assemblages occurred in the Late Devonian to Early Carboniferous (e.g. Bultitude *et*

al. 1997; Withnall *et al.* 1997a). Previous studies on gold deposits in the Hodgkinson and Broken River provinces (Vos & Bierlein in press; Vos *et al.* in press a) together with our results from $^{40}\text{Ar}/^{39}\text{Ar}$ dating suggest that regional deformation and gold mineralisation potentially related to an episode of regional peak metamorphism occurred between ~345 and 335 Ma. From latest Devonian to Early Carboniferous times, deposition of back-arc basin volcano-sedimentary assemblages continued in the Burdekin, Clarke River and Bundock Creek basins (e.g. Withnall & Lang 1993; Figs. 7.3 and 7.9) and the Drummond Basin (e.g. Henderson *et al.* 1998; for location see Fig. 7.1). Henderson *et al.* (1998) suggested that the widespread extent of subduction-related volcanism and magmatism in the Late Devonian – Early Carboniferous indicates that shallow-angle subduction occurred during this episode. In agreement with Coney *et al.* (1990), we suggest that this episode of deformation controlled further closure of the marginal back-arc basins, following progressive accretion of the strato-tectonic terranes of the New England Fold Belt. The latter is marked by the transition from intra-oceanic arc volcanism of the Calliope Volcanic Arc to continental arc volcanism of the Connors-Auburn Arc (e.g. Offler & Gamble 2002) and the development of the Yarrol-Campwyn fore-arc basin system (Day *et al.* 1978; Henderson *et al.* 1993). We propose that deformation ended with lock-up of the subduction system following the arrival of an oceanic plateau at the subduction trench, although no geological evidence for the existence of such a plateau has been documented to date. The lock-up possibly caused slab break-off around middle Carboniferous times.

7.5.8 Late Carboniferous (330-300 Ma)

granite magmatism and associated mineralisation

The Late Carboniferous evolution of the northern Tasman Fold Belt System is dominated by the emplacement of voluminous granites and largely felsic volcanic rocks of the Coastal Ranges Igneous Province / Kennedy Province (Fig. 7.1) during widespread crustal melting in an overall extensional setting (e.g. Bultitude *et al.* 1997; Withnall *et al.* 1997b). This episode of magmatism was associated with the generation of numerous mineral deposits characterised by variable metal assemblages, such as the Red Dome and Kidston deposits (e.g. Perkins & Kennedy 1998; for location see Fig. 7.1). Veevers *et al.* (1994) proposed that magmatism along the entire Australian margin around this time was related to dextral transtension during anticlockwise rotation of Gondwana. In the northern New England Fold Belt, simultaneous widespread crustal extension and magmatism has been related to back-arc extension related to slab roll-back (e.g. Holcombe *et al.* 1997a; Jenkins *et al.* 2002). On the basis of our overall evaluation, we prefer an equally valid mechanism of stress reorganisation on the continental margin following eastward-stepping and renewal of the subduction system after subduction lock-up around middle Carboniferous times.

7.5.9 Permian magmatism and the Hunter-Bowen Orogeny

In the Early Permian, the development of the Mount Mulligan and Little River Coal Measures together with emplacement of the Nychum and Featherbed Volcanics mark the continuation of dextral transtension. Bultitude *et al.* (1997) related granite alteration characteristics and the eastward progression of granitic activity with time to roll-back and steepening of the

subducting slab during this episode. In the northern New England Fold Belt, Jenkins *et al.* (2002) similarly suggested retreat of the subducting slab to explain the occurrence of back-arc related volcanism.

This was followed by compressional tectonism along the entire margin of Gondwana later in the Early Permian, associated with the ca. 270 to 230 Ma Hunter-Bowen Orogeny (e.g. Fergusson, 1991; Holcombe *et al.* 1997b). Scheibner & Veevers (2000) suggested that this episode of deformation may be related to accretion of the Lord Howe Rise microcontinent onto the Permian continental margin of Australia.

7.6. THE PALAEOZOIC TECTONO-METALLOGENIC EVOLUTION OF THE NORTHERN TASMAN FOLD BELT SYSTEM

7.6.1. Model characteristics and deficiencies

Our proposed model for the tectono-metallogenic evolution of the northern Tasman Fold Belt System illustrates that the Palaeozoic geodynamic evolution of the northern Tasman Fold Belt System is characterised by successive episodes of extension and contraction along the continental margin of Gondwana. The main features of the proposed model are: 1) integration of the tectono-stratigraphic terranes of the northern New England Fold Belt with the geodynamic framework for the northern Tasman Fold Belt System; 2) the accretion of microcontinental fragments / arc segments / oceanic plateaux which focused deformation in the previously attenuated back-arc regions; and 3) the development of extensive back-arc regions and the emplacement of bimodal volcano-intrusive rocks controlled by slab-rollback. Point 1 (above) can be explained by

the occurrence of dextral transtension along the continental margin of Gondwana in the Late Carboniferous and Permian, during which the New England Fold Belt is considered to have moved southward ~500km (e.g. Murray *et al.* 1987). Reconstruction of the northern New England Fold Belt to its position prior to the Late Carboniferous would roughly place it outboard of the Hodgkinson and Broken River provinces. Point 2 (above) is based on the assumption that episodes of deformation along the Gondwana margin were controlled by either one or a combination of two mechanisms: 1) the transfer of horizontal compressive stress because of greater coupling between the converging plates in relation to the arrival of oceanic plateaux at the subducting margin and associated change to a flat subduction angle (e.g. Gutscher *et al.* 2000), or 2) the arrival and accretion of microcontinental fragments / blocks at the continental margin (e.g. Cloos 1993; Cawood 2005). Our findings on the timing of deformation related to orogenic gold mineralisation (this study; Vos & Bierlein in press; Vos *et al.* in press a) confirm the occurrence of at least two such episodes in the Early Devonian and Late Devonian – Early Carboniferous, with two additional episodes of deformation occurring in the Late Ordovician and Permian. Point 3 (above) is based on the notion that slab roll-back along the craton-verging subduction system provided a mechanism that controlled attenuation of the margin lithosphere and emplacement of bimodal volcano-intrusive rocks (e.g. Molnar & Atwater 1978). Our findings on the tectonic setting in which volcano-intrusive rocks developed in the Broken River Province during the Late Carboniferous – Permian infer the occurrence of an episode of extension most

probably controlled by slab roll-back. Based on geochemical analyses from basaltic rock units in the Hodgkinson Province, Vos *et al.* (in press c) previously suggested that a major episode of extension linked to slab break-off also occurred there in the Silurian and Early Devonian.

Due to limited geological data in some areas, and the orogen-wide scale of our study, a number of specific issues regarding the tectonic evolution of the northern Tasman Fold Belt System remain unresolved. These include: 1) Deformation in the Early - Middle Devonian has only been recorded in the Camel Creek Subprovince and the New England Fold Belt terranes (e.g. Scheibner & Veevers 2000), whereas no evidence of deformation has been recorded in the Hodgkinson Province. We speculate that localised deformation in the Camel Creek Subprovince may have occurred due to the initial collision of the Gondwanan margin with segments of the Calliope Volcanic Arc in response to a major change in plate dynamics around that time (e.g. Scheibner & Veevers 2000). Back-arc basin spreading continued in the Hodgkinson Province owing to the absence of a collisional arc segment in this region and continued rollback of the subduction system; 2) We propose that the Late Devonian – Early Carboniferous (Kanimblan?) deformation was controlled by the subduction of an oceanic plateau and associated increased coupling between the oceanic and continental plates. There is however no explicit geological evidence that confirms the existence of this oceanic plateau, although the presence of ophiolites in the New England Fold Belt (see section 7.5.1) indicates that ocean-floor obduction did occur at some stage during the evolution of the northern Tasman Fold Belt System; 3) The position

of continental basement crust of the Charters Towers Province along-strike and outboard of the younger, marginal Hodgkinson and Broken River provinces remains somewhat problematic in tectonic reconstruction scenarios, but could potentially be accounted for by segmentation and subsequent accretion of a continental fragment that rifted from the continental margin in the earliest Palaeozoic (as represented by the metamorphic terranes in the Charters Towers Province). These continental segments were then overprinted and further dismembered by Palaeozoic granite emplacement. An alternative explanation for the position of the Charters Towers Province may be the occurrence of sinistral transform faulting along the Clarke River Fault Zone in the Early Palaeozoic. This transform would have moved the portion of the TFBS to the north of that fault (including the Hodgkinson and Broken River province) farther inboard in relation to the portion to the south. Hutton *et al.* (1997) suggested that sinistral movement did indeed occur along the Clarke River Fault Zone and may correlate with deformation and metamorphism of the Cape River Metamorphics in the Middle Ordovician or Silurian.

7.6.2 Extension – contraction cycles and implications for metallogenesis

Three cycles of extension – contraction that each lasted approximately 100 million years can be identified in our geodynamic model. These include a Cambrian – Late Ordovician cycle (1), a Silurian – Early Carboniferous cycle (2), and a Late Carboniferous – Permian cycle (3). Each of the successive episodes of extension and contraction can be matched to characteristic styles of metallogenesis. These are briefly reviewed in the following and characteristics of

mineral deposits mentioned here are indicated in Table 7.4 (for locations see Fig. 7.1): During the initial cycle, Kuroko-style VHMS deposits such as the Thalanga, Balcooma, Surveyor, Dry River deposits (e.g. Huston *et al.* 1992) were formed during extension of the continental margin. No mineral deposits are known throughout northeastern Queensland that could be related to the Late Ordovician contractional episode that concluded the first cycle. During the second cycle, Silurian to Early Devonian Besshi-Kieslager-type VMS deposits such as the Dianne, OK, Mount Molloy (e.g. Garrad & Bultitude 1999) and the mesothermal granite-hosted gold deposits of the world-class Charters Towers Goldfield (e.g. Hartley *et al.* 1994) formed mainly in back-arc basin extensional settings. The subsequent phase of contraction was characterised by two major deformational episodes that can be correlated with the formation of orogenic gold mineralisation in the Amanda Bel Goldfield in the Broken River Province (Vos *et al.* in press a) and the Hodgkinson and Palmer River goldfields in the Hodgkinson Province (e.g. Vos & Bierlein in press). Results from $^{40}\text{Ar}/^{39}\text{Ar}$ dating of matrix sericite from orogenic gold deposits in both provinces (Section 7.3) further corroborate this notion, and indicate that this phase of gold mineralisation predated major magmatic activity in the Carboniferous and Permian. During the final cycle, extensive magmatism, back-arc extension and strike-slip movement along the Gondwanan continental margin was associated with the development of numerous epithermal, porphyry, skarn and greisen poly-metallic deposits. Most production from deposits associated with Late Carboniferous – Permian magmatic rocks has been from the Chillagoe – Herberton -

Table 7.4: Characteristics and total commodities for deposits mentioned in text. Total commodities from Ewers *et al.*, 1997 (for Minnie Moxham based on indicated resource as reported in Bultitude *et al.*, 1997).

Deposit (no. in Fig. 1)	Deposit age	Commodity	Deposit type	Total commodities (tonnes)	Host rocks	Reference
Thalanga (2)	?Cambrian - Ordovician	base metals	Kuroko-style VHMS	103,219t Pb, 65,762t Cu, 277,872t Zn, 78.5t Ag; 5t Au	Late Cambrian - Ordovician Seventy Mile Range Group	Huston <i>et al.</i> (1992)
Balcooma (1)	Ordovician	base metals	Kuroko-style VHMS	154,250t Pb, 121,549t Cu, 353,541t Zn, 354.8t Ag; 3.9t Au	(Late Cambrian? -) Ordovician Balcooma Metavolcanics	Huston <i>et al.</i> (1992)
Surveyor (1)	Ordovician	base metals	Kuroko-style VHMS	42,106t Pb, 18,026t Cu, 134,022t Zn, 121.9t Ag; 1.1t Au	(Late Cambrian? -) Ordovician Balcooma Metavolcanics	Huston <i>et al.</i> (1992)
Dry River South (1)	Ordovician	base metals	Kuroko-style VHMS	55,180t Pb, 8,378t Cu, 121,820t Zn, 118.5t Ag; 0.9t Au	(Late Cambrian? -) Ordovician Balcooma Metavolcanics	Huston <i>et al.</i> (1992)
Dianne (6)	Silurian - Early Devonian	base metals	Besshi-Kiesslager-style VHMS	2,000t Cu; 1t Ag	Devonian Hodgkinson Formation	Garrad & Bultitude (1999)
OK (4)	Silurian - Early Devonian	base metals	Besshi-Kiesslager-style VHMS	3.6t Au	Devonian Hodgkinson Formation	Garrad & Bultitude (1999)
Mount Molloy (5)	Silurian - Early Devonian	base metals	Besshi-Kiesslager-style VHMS	3,885t Cu	Devonian Hodgkinson Formation	Garrad & Bultitude (1999)
Charters Towers (3)	Early Devonian	gold	granite-hosted mesozonal gold deposit	154.3t Au; 96.1t Ag	Siluro-Devonian Lolworth and Ravenswood Batholiths	Hartley <i>et al.</i> (1994)
Airport (this paper)	Late Devonian - Early Carboniferous	gold / antimony	epizonal gold-stibnite-quartz veins	0.2 t Au	Siluro-Devonian Kangaroo Hills Formation	Vos <i>et al.</i> (in press a)
Minnie Moxham (this paper)	Late Devonian - Early Carboniferous	gold / antimony	epizonal gold-stibnite-quartz veins	5.6t Au	Devonian Hodgkinson Formation	Vos & Bierlein (in press)
Mount Garnet (8)	Late Carboniferous	base metals	skarn deposit	16,250t Cu, 209,700t Zn; 87.8t Ag	Silurian Chillagoe Formation	Murray (1990)
Red Dome (7)	Late Carboniferous-Permian	gold / base metals	skarn deposit	13,576t Cu, 36,892t Pb, 36,892t Zn, 37.6t Ag; 21.5t Au	Late Carboniferous Almaden and Ootann Supersuites	Perkins & Kennedy (1998)
Kidston (9)	Early to Late Carboniferous	gold	breccia-hosted / epithermal gold deposit	146.6t Au; 8.9t Ag	Late Carboniferous Ootann Supersuite	Perkins & Kennedy (1998)

Mt. Garnet region along the southwestern edge of the Hodgkinson Province (e.g. Murray 1990). The magnitude of mineralisation associated with this event suggests the occurrence of a major heat pulse that may be driven by slab break-off that controlled initial mineralisation and magmatism following mantle upwelling in a fashion similar to that proposed by Vos *et al.* (in press b). Subsequent contraction during the Hunter-Bowen Orogeny gave rise to the development of numerous orogenic gold, base metal and other poly-metallic deposits in the New England Fold Belt (e.g. Murray 1990; Holcombe *et al.* 1997b).

7.6.3 Orogenic gold endowment in the northern Tasman Fold Belt System

Episodes of deformation in the northern Tasman Fold Belt System are associated with relatively minor amounts of orogenic gold mineralisation, when compared with, for example, the far greater-endowed accretion-subduction complex of the western Lachlan Orogen (e.g. Bierlein *et al.* 2002). Comparison between the tectonic evolution of the southern and the northern portions of the TFBS provides constraints on the factors that may have controlled this difference in orogenic gold endowment. In the Lachlan Fold Belt of the southern Tasman Fold Belt System, the occurrence of primitive ocean-floor in the subsurface has been regarded as one of the crucial factors that controls the development of orogenic gold deposits (e.g. Haeussler *et al.* 1995; Bierlein *et al.* 2001). In stark contrast, very minor, if any, oceanic-character crust developed during the Palaeozoic evolution of the northern part of the TFBS. In particular, the absence of primitive mafic rocks and previously non-dehydrated oceanic-character crust, and the occurrence of deformation on a relatively

thick, evolved continental-type margin in the Late Ordovician, could explain the lack of more extensive orogenic gold formation. Another important factor that may have influenced the limited gold endowment could be the low metamorphic grades associated with limited and shallow-level deformation in the majority of the northern Tasman Fold Belt System (e.g. Bultitude *et al.* 1997; Withnall *et al.* 1997b), and the availability of only minor to moderate amounts of metamorphic fluid to form orogenic gold deposits.

7.7. CONCLUSIONS

Geological, structural, geochemical and geochronological similarities between orogenic gold deposits in the Hodgkinson and Amanda Bel goldfields in the northern part of the Tasman Fold Belt System strongly suggest that these deposits formed contemporaneously during regional deformation. Absolute age dating of sericite and pyrite from the Airport and Minnie Moxham deposits in these goldfields point to the occurrence of at least two episodes of metamorphism, and by inference gold mineralisation and deformation in the Early Devonian and Late Devonian – Early Carboniferous, respectively.

Petrogenetic characteristics of volcano-intrusive rocks in the Hodgkinson and Broken River provinces indicate that at least five tectonic periods can be distinguished in their evolution. Petrogenetic evidence from volcano-intrusive rocks in the Broken River Province further support the occurrence of extension in that region in Late Carboniferous- Permian times.

Integration of our findings with available geological data enabled the construction of an interpretative geodynamic model for the

evolution of the entire northern portion of the TFBS. Our model invokes three cycles of extension-contraction, and each of these are closely related to the development of mineral deposits throughout the system. Slab roll-back and arrival of microcontinental fragments / oceanic plateaux are identified as the primary mechanisms that controlled the evolution of the northern Tasman Fold Belt System. In addition, the development of a model for the Palaeozoic geodynamic evolution of the northern Tasman Fold Belt System highlights shortcomings in our understanding of its evolution and provides opportunities for comparison with the far better-studied southern Tasman Fold Belt System, and analogous orogenic systems elsewhere.

ACKNOWLEDGEMENTS

The manuscript has benefited from discussion with and reviews by G. Begg and P. Betts.

REFERENCES

- AITCHISON J.C., IRELAND T.R., BLAKE M.C. & FLOOD P.G. 1992. 530 Ma zircon age for ophiolite from the New England Orogen; oldest rocks known from eastern Australia. *Geology* 20, 125-128.
- ARNOLD G.O. & FAWCKNER J.F. 1980. The Broken River and Hodgkinson Provinces. In: Stephenson H. ed. The geology and geophysics of northeastern Queensland, pp. 175-189. James Cook University, Department of Geology, Townsville, Australia.
- BERRY R.F., HUSTON D.L., STOLZ A.J., HILL A.P., BEAMS S.D., KURONEN U. & TAUBE A. 1992. Stratigraphy, structure, and volcanic-hosted mineralization of the Mount Windsor Subprovince, North Queensland, Australia. *Economic Geology* 87, 739-763.
- BIERLEIN F.P., ARNE D.C., FOSTER D.A. & REYNOLDS P. 2001. A geochronological framework for orogenic gold mineralisation in central Victoria, Australia. *Mineralium Deposita* 36, 741-767.
- BIERLEIN F.P., GRAY D.R. & FOSTER D.A. 2002. Metallogenic relationships to tectonic evolution; the Lachlan Orogen, Australia. *Earth and Planetary Science Letters* 202, 1-13.
- BLEWETT R.S., DENARO T.J., KNUTSON J., WELLMAN P., MACKENZIE D.E., CRUICKSHANK B.I., WILFORD J.R., VON GNIELINSKI F.E., PAIN C.F., SUN S.S. & BULTITUDE R.J. 1997. Coen Region. In: Bain J.H.C. & Draper J. J. eds. North Queensland Geology. *Australian Geological Survey Organisation Bulletin* 240, 117-158.
- BRUCE M.C., NIU Y., HARBORT T.A. & HOLCOMBE R.J. 2000. Petrological, geochemical and geochronological evidence for a Neoproterozoic ocean basin recorded in the Marlborough Terrane of the northern New England fold belt. *Australian Journal of Earth Sciences* 47, 1053-1064.
- BULTITUDE R.J., GARRAD P.D., DONCHAK P.J.T., DOMAGALA J., CHAMPION D.C., REES I.D., MACKENZIE D.E., WELLMAN P., KNUTSON J., FANNING C.M., FORDHAM B.G., GRIMES K.G., OVERSBY B.S., RIENKS I.P., STEPHENSON P.J., CHAPPELL B.W., PAIN C.F., WILFORD J.R., RIGBY J.F. & WOODBURY M.J. 1997. Cairns region. In: Bain J.H.C. & Draper J.J. eds. North Queensland Geology. *Australian Geological Survey Organisation Bulletin* 240, 225-325.
- CAWOOD P.A. 2005. Terra Australis Orogen: Rodinia breakup and development of the Pacific and Iapetus margins of Gondwana during the Neoproterozoic and Paleozoic. *Earth-Science Reviews* 69, 249-279.
- CHAMPION D.C. & BULTITUDE R.J. 1994. Granites of the eastern Hodgkinson Province. II. Their geochemical and Nd-Sr isotopic characteristics and implications for petrogenesis and crustal structure in North Queensland. Department of Minerals and Energy; *Queensland Geological Record* 1994/1, 113p.
- CLOOS M. 1993. Lithospheric buoyancy and collisional orogenesis; subduction

- of oceanic plateaus, continental margins, island arcs, spreading ridges, and seamounts. *Geological Society of America Bulletin* 105, 715-737.
- CONEY P.J. 1992. The Lachlan Fold Belt of eastern Australia and Circum-Pacific tectonic evolution. *Tectonophysics* 214, 1-25.
- CONEY P.J., EDWARDS A., HINE R., MORRISON F. & WINDRIM D. 1990. The regional tectonics of the Tasman orogenic system, eastern Australia. *Journal of Structural Geology* 12, 519-543.
- DAVIS B.K., BELL C.C., LINDSAY M. & HENDERSON R.A. 2002. A single late orogenic episode of gold mineralization in the Hodgkinson Province, North Queensland, Australia. *Economic Geology* 97, 311-323.
- DAY R.W., MURRAY C.G. & WHITAKER W.G. 1978. The eastern part of the Tasman orogenic zone. *Tectonophysics* 48, 327-364.
- EWERS G., EVANS N., & HAZELL M. 2002. OZMIN Mineral Deposits Database. (compiled by Kilgour B.), Geoscience Australia, Canberra.
- FAWCKNER J.F. 1981. Structural and stratigraphic relations and a tectonic interpretation of the western Hodgkinson Province, northeast Australia. Ph.D. thesis. James Cook University of North Queensland.
- FERGUSON C.L., CARR P.F., FANNING C.M. & GREEN T.J. 2001. Proterozoic-Cambrian detrital zircon and monazite ages from the Anakie Inlier, central Queensland: Grenville and Pacific-Gondwana signatures. *Australian Journal of Earth Sciences* 48, 857-866.
- FERGUSON C.L., HENDERSON R.A., LEWTHWAITE D., PHILLIPS D. & WITHNALL I.W. 2005. Structure of the Early Palaeozoic Cape River Metamorphics, Tasmanides of north Queensland: evaluation of the roles of convergent and extensional tectonics. *Australian Journal of Earth Sciences* 52, 261-278.
- FOSTER D.A., GRAY D.R. & BUCHER M. 1999. Chronology of deformation within the turbidite-dominated Lachlan Orogen: implications for the tectonic evolution of eastern Australia and Gondwana. *Tectonics* 18, 452-485.
- FUKUI S., WATANABE T., ITAYA T. & LEITCH E.C. 1995. Middle Ordovician high PT metamorphic rocks in eastern Australia; evidence from K-Ar ages. *Tectonics* 14, 1014-1020.
- GARRAD P. D. & BULTITUDE R. J. 1999. Geology, mining history and mineralisation assessment of the Hodgkinson and Kennedy Provinces, Cairns Region, North Queensland. *Queensland Minerals and Energy Review Series*. Department of Mines and Energy, Queensland, 305p.
- GLEN R.A. 2005. The Tasmanides of eastern Australia. In: Vaughan A.P.M., Leat P.T. & Pankhurst R.J. eds. Terrane processes at the margins of Gondwana. *Special Publications of the Geological Society of London* 246, 23-96.
- GLEN R.A., WALSH J.L., BARRON L.M. & WATKINS J.J. 1998. Ordovician convergent-margin volcanism and tectonism in the Lachlan sector of east Gondwana. *Geology* 26, 751-754.
- GOLDFARB R.J., SNEE L.W., MILLER L.D. & NEWBERRY R.J. 1991. Rapid dewatering of the crust deduced from ages of mesothermal gold deposits. *Nature* 354, 296-298.
- GROVES D.I., GOLDFARB R.J., GEBRE-MARIAM M., HAGEMANN S.G. & ROBERT F. 1998. Orogenic gold deposits; a proposed classification in the context of their crustal distribution and relationship to other gold deposit types. *Ore Geology Reviews* 13, 7-27.
- GUTSCHER M.A., SPAKMAN W., BIJWAARD H. & ENGDAHL E.R. 2000. Geodynamics of flat subduction; seismicity and tomographic constraints from the Andean margin. *Tectonics* 19, 814-833.
- HAEUSSLER P.J., BRADLEY D.C., GOLDFARB R.J., SNEE L.W. & TAYLOR C.D. 1995. Link between ridge subduction and gold mineralization in Southern Alaska. *Geology* 23, 995-998.
- HARTLEY J.S., HUTTON L.J. & RIENKS I.P. 1994. Metallogenesis in the Charters Towers Province. In: Henderson R.A. &

- Davis B.K. eds. New developments in geology and metallogeny; northern Tasman orogenic zone. *Contributions of the Economic Geology Research Unit* 50, James Cook University, Townsville. pp. 7-11.
- HENDERSON R.A. 1980. Structural outline and summary geological history for northeastern Australia. In: Stephenson H. ed. The geology and geophysics of northeastern Queensland, pp. 1-26. James Cook University, Department of Geology, Townsville.
- HENDERSON R.A. 1987. An oblique subduction and transform faulting model for the evolution of the Broken River Province, northern Tasman Orogenic System. *Australian Journal of Earth Sciences* 34, 237-249.
- HENDERSON R.A., FERGUSON C.L., LEITCH E.C., MORAND V.J., REINHARDT J.J. & CARR P.F. 1993. Tectonics of the northern New England Fold Belt. In: Flood P.G. & Aitchison J.C. eds. New England Orogen, eastern Australia, pp. 505-515. Department of Geology and Geophysics, University of New England, Armidale.
- HENDERSON R.A., DAVIS B.K. & FANNING C.M. 1998. Stratigraphy, age relationships and tectonic setting of rift-phase infill in the Drummond Basin, central Queensland. *Australian Journal of Earth Sciences* 45, 579-595.
- HOLCOMBE R.J., STEPHENS C. J., FIELDING C. R., GUST D., LITTLE T.A., SLIWA R., MCPHIE J. & EWART A. 1997a. Tectonic evolution of the northern New England Fold Belt: Carboniferous to Early Permian transition from active accretion to extension. In: Ashley P.M. & Flood P.G. eds. Tectonics and metallogenesis of the New England Orogen. *Geological Society of Australia, Special Publication* 19, 66-79.
- HOLCOMBE R.J., STEPHENS C. J., FIELDING C. R., GUST D., LITTLE T.A., SLIWA R., KASSAN J., MCPHIE J. & EWART A. 1997b. Tectonic evolution of the northern New England Fold Belt: The Permian-Triassic Hunter-Bowen event. In: Ashley P.M. & Flood P.G. eds. Tectonics and metallogenesis of the New England Orogen. *Geological Society of Australia, Special Publication* 19, 52-65.
- HUSTON D.L., TAYLOR T., FABRAY J. & PATTERSON D.J. 1992. A comparison of the geology and mineralization of the Balcooma and Dry River South volcanogenic massive sulfide deposits, northern Queensland. *Economic Geology* 87, 785-811.
- HUTTON L.J., DRAPER J.J., RIENKS I.P., WITHNALL I.W. & KNUTSON J. 1997. Charters Towers Region. In: Bain J.H.C. & Draper J.J. eds. North Queensland Geology. *Australian Geological Survey Organisation Bulletin* 240, 165-224.
- JENKINS R.B., LANDENBERGER B. & COLLINS W.J. 2002. Late Palaeozoic retreating and advancing subduction boundary in the New England fold belt, New South Wales. *Australian Journal of Earth Sciences* 49, 467-489.
- KORSCH R.J., HARRINGTON H.J., MURRAY C.G., FERGUSON C.L. & FLOOD P.G. 1990. Tectonics of the New England Orogen. *Australian Bureau of Mineral Resources Bulletin* 232, 35-52.
- LE MAITRE R.W. ed. 1989. A classification of igneous rocks and glossary of terms: Recommendations of the International Union of Geological Sciences Subcommittee on the Systematics of igneous rocks. Blackwell Scientific Publishing, Oxford.
- MCDUGALL I. & HARRISON T.M. 1999. Geochronology and thermochronology by the $^{40}\text{Ar}/^{39}\text{Ar}$ method, Oxford University Press, Oxford.
- MILLER J. McL., KENDRICK M. & PHILLIPS D. 2004. Testing the 'Fool's clock' and tales from fluid inclusions. In: Barnicoat A.C. & Korsch R.J. eds. Predictive Mineral Discovery Cooperative Research Centre - Extended Abstracts from the June 2004 Conference. *Geoscience Australia Record* 2004/09, 133-139.
- MILLER J. McL. & PHILLIPS D. 2005. Testing the fool's clock: $^{40}\text{Ar}/^{39}\text{Ar}$ dating of pyrite. In: Hancock H. *et al.* Structure, Tectonics and Ore Mineralisation

- p>Processes, Abstract Volume.
-
- Contributions of the Economic
 Geology Research Unit*
- 64, James
-
- Cook University, Townsville, p. 91.
- MOLNAR P. & ATWATER T. 1978. Interarc
 spreading and Cordilleran tectonics as
 alternates related to the age of subducted
 oceanic lithosphere. *Earth and
 Planetary Science Letters* 41, 330-340.
- MORRISON G.W. 1988. Palaeozoic gold deposits of
 northeastern Queensland. In: Morrison
 G.W. ed. Epithermal and porphyry style
 gold deposits in North Queensland.
*Contributions of the Economic
 Geology Research Unit* 29, 11-21.
 James Cook University, Townsville.
- MURRAY C.G. 1990. Tasman Fold Belt in
 Queensland. In: F.E. Hughes ed.
 Geology of the mineral deposits of
 Australia and Papua New Guinea.
 Australasian Institute of Mining and
 Metallurgy, Melbourne, pp. 1431-1450.
- MURRAY C.G., FERGUSSON C.L., FLOOD P.G.,
 WHITAKER W.G. & KORSCH, R.J.
 1987. Plate tectonic model for the
 Carboniferous evolution of the New
 England Fold Belt. *Australian Journal
 of Earth Sciences* 34, 213-236.
- OFFLER R. & GAMBLE J. 2002. Evolution of
 an intra-oceanic island arc during
 the Late Silurian to Late Devonian,
 New England fold belt. *Australian
 Journal of Earth Sciences* 49, 349-366.
- PEARCE J.A. & CANN J.R. 1973. Tectonic setting
 of basic volcanic rocks determined
 using trace element analyses. *Earth and
 Planetary Science Letters* 19, 290-300.
- PEARCE J.A. 1996. A user's guide to basalt
 discrimination diagrams. In: Wyman
 D.A. ed. Trace element geochemistry
 of volcanic rocks; applications
 for massive sulphide exploration.
*Geological Association of Canada
 Short Course Notes* 12, 79-113.
- PERKINS C. & KENNEDY A.K. 1998. Permo-
 Carboniferous gold epoch of Northeast
 Queensland. *Australian Journal
 of Earth Sciences* 45, 185-200.
- PERKINS C., WALSH J.L. & MORRISON G. 1995.
 Metallogenic episodes of the Tasman
 fold belt system, eastern Australia.
Economic Geology 90, 1443-1466.
- RENNE P.R., SWISHER C.C., DEINO A.L., KARBER
 D.B., OWENS T.L. & DEPAOLO D.J. 1998.
 Intercalibration of standards, absolute
 ages and uncertainties in $^{40}\text{Ar}/^{39}\text{Ar}$
 dating. *Chemical Geology* 145, 117-152.
- SCHEIBNER E. & VEEVERS J.J. 2000. Tasman
 Fold Belt System. In: Veevers, J.J. ed.
 Billion-year earth history of Australia
 and neighbours in Gondwanaland,
 pp. 154-234. GEMOC press, Sydney.
- SMITH P.E., EVENSEN N.M., YORK D., SZATMARI
 P. & DE OLIVEIRA D.C. 2001. Single-
 crystal ^{40}Ar - ^{39}Ar dating of pyrite; no
 fool's clock. *Geology* 29, 403-406.
- STEIGER R.H. & JÄGER E. 1977. Subcommittee
 on geochronology; convention on
 the use of decay constants in geo-
 and cosmochronology. *Earth and
 Planetary Science Letters* 36, 359-362.
- VEEVERS J.J., CONAGHAN P.J. & POWELL C. McA.
 1994. Eastern Australia. In: Veevers
 J.J. & Powell C. McA. eds. Permian-
 Triassic Pangean basins and foldbelts
 along the Panthalassic margin of
 Gondwanaland. *Geological Society
 of America Memoirs* 184, 11-171.
- VOS I.M.A. & BIERLEIN F.P. 2005 Gold systems
 in northeastern Queensland: a key to
 tectonic evolution of the northern
 Tasman Fold Belt System, Australia.
 In: Mao J. & Bierlein F.P. eds.
 Mineral Deposit Research: Meeting
 the Global Challenge, Springer
 Verlag, Heidelberg, p. 593-596.
- VOS I.M.A. & BIERLEIN F.P. in press.
 Characteristics of orogenic gold deposits
 in the Northcote district, Hodgkinson
 Province, North Queensland, Australia:
 Implications for tectonic evolution.
Australian Journal of Earth Sciences.
 (Chapter 3 of this dissertation)
- VOS I.M.A., BIERLEIN F.P. & TEALE G.S. in
 press a. Genesis of orogenic gold
 deposits in the Broken River Province,
 northeastern Queensland, Australia.
Australian Journal of Earth Sciences.
 (Chapter 2 of this dissertation)
- VOS I.M.A., BIERLEIN F.P. & HEITHERSAY P.S.

- in press b. A crucial role for slab break-off in the generation of world-class mineral deposits: insights from central and eastern Australia. *Mineralium Deposita*. (Chapter 8 of this dissertation)
- VOS I.M.A., BIERLEIN F.P. & WEBB J. in press c. Geochemistry of Early Palaeozoic basalts in the Hodgkinson Province: a key to tectono-magmatic evolution of the Tasman Fold Belt System in northeastern Queensland, Australia. *International Journal of Earth Sciences*. (Chapter 4 of this dissertation)
- VOS I.M.A., BIERLEIN F.P. BARLOW, M.A. & BETTS P.G. in review. The Palmerville Fault, NE Queensland, Australia: A multi-disciplinary approach to understanding major fault systems. *Journal of Structural Geology*. (Chapter 5 of this dissertation)
- WALSHE J.L., HEITHERSAY P.S. & MORRISON G.W. 1995. Toward an understanding of the metallogeny of the Tasman Fold Belt System. *Economic Geology* 90, 1382-1401.
- WINCHESTER J.A. & FLOYD P.A. 1977. Geochemical discrimination of different magma series and their differentiation products using immobile elements. *Chemical Geology* 20, 325-343.
- WITHNALL I.W. & LANG S.C. 1993. Geology of the Broken River province, north Queensland. *Queensland Geology* 4, Department of Resource Industries, Queensland.
- WITHNALL I.W., MacKENZIE D.E. DENARO T.J. BAIN J.H.C., OVERSBY B.S., KNUTSON J., DONCHAK P.J.T., CHAMPION D.C., WELLMAN P., CRUIKSHANK B.I., SUN S.S. & PAIN C.F. 1997a. Georgetown Region. In: Bain J.H.C. & Draper J.J. eds. North Queensland Geology. *Australian Geological Survey Organisation Bulletin* 240, 19-116.
- WITHNALL I.W., LANG S.C., LAM J.S., DRAPER J.J., KNUTSON J., GRIMES K.G. & WELLMAN, P. 1997b. Clarke River Region. In: Bain J.H.C. & Draper J.J. eds. North Queensland Geology. *Australian Geological Survey Organisation Bulletin* 240, 327-363.
- YANG K. & SECCOMBE P.K. 1997. Geochemistry of the mafic and ultramafic complexes of the northern Great Serpentine Belt, New South Wales: implications for first-stage melting. In: Ashley P.M. & Flood P.G. eds. Tectonics and metallogenesis of the New England Orogen. *Geological Society of Australia Special Publication* 19, 197-211.
- ZUCCHETTO R.G., HENDERSON R.A., DAVIS B.K. & WYSOCZANSKI R. 1999. Age constraints on deformation of the eastern Hodgkinson Province, north Queensland: new perspectives on the evolution of the northern Tasman Orogenic Zone. *Australian Journal of Earth Sciences* 46, 105-114.

APPENDIX 7.1:

⁴⁰Ar/³⁹Ar analytical results from sericite separates from AP-Pit6, Airport deposit.

Temp (°C)	Cum ³⁹ Ar (%)	³⁶ Ar (moles)	³⁷ Ar (moles)	³⁹ Ar (moles)	⁴⁰ Ar (moles)	⁴⁰ Ar* %	Ca/K	⁴⁰ Ar*/ ³⁹ Ar	Age (Ma)	Error ±1s.d.
600	41.55	375.16E-	172.15E-	266.14E-	466.13E-	76.1	0.116	13.347	306.66	0.91
650	57.81	239.17E-	341.16E-	104.14E-	174.13E-	95.8	0.059	16.055	363	0.72
700	70.05	240.17E-	206.16E-	783.15E-	130.13E-	94.4	0.047	15.611	353.88	1.05
750	78.71	201.17E-	137.16E-	555.15E-	902.14E-	93.2	0.044	15.163	344.64	0.83
800	84.38	148.17E-	908.17E-	362.15E-	591.14E-	92.4	0.045	15.089	343.1	0.92
850	89.39	546.17E-	750.17E-	320.15E-	647.14E-	74.9	0.042	15.126	343.88	1.37
900	93.54	188.17E-	339.17E-	266.15E-	457.14E-	87.7	0.022	15.067	342.64	1.09
950	96.47	150.17E-	811.17E-	187.15E-	338.14E-	86.8	0.078	15.698	355.67	1.44
1000	98.47	226.17E-	838.17E-	128.15E-	262.14E-	74.4	0.118	15.213	345.66	4.04
1050	99.23	339.17E-	773.17E-	484.16E-	186.14E-	46.2	0.287	17.745	397.27	10.36
1100	99.41	528.17E-	173.16E-	114.16E-	180.14E-	13.1	2.74	20.692	455.54	81.19
1150	99.51	360.17E-	417.16E-	654.17E-	120.14E-	11.9	11.5	21.903	478.95	114.57
1450	100	279.16E-	669.15E-	318.16E-	926.14E-	11.5	38.5	34.026	697.93	80.25
Total		971.16E-	101.14E-	640.14E-	123.12E-			14.743	335.93	1.72

i) Errors are one sigma uncertainties and exclude uncertainties in the J-value.

ii) Data are corrected for mass spectrometer backgrounds, discrimination and radioactive decay.

iii) Interference corrections: (³⁶Ar/³⁷Ar)Ca = 2.70E-4; (³⁹Ar/³⁷Ar)Ca = 6.79E-4; (⁴⁰Ar/³⁹Ar)K = 2.89E-2

iv) J-value = 0.013882 ± 0.000028 based on an age of 98.8 Ma for GA-1550 biotite; mass = 0.00120 g

⁴⁰Ar/³⁹Ar analytical results from sericite separates from MM03-C2, Minnie Moxham deposit.

Temp (°C)	Cum (%)	³⁹ Ar (moles)	³⁷ Ar (moles)	³⁹ Ar (moles)	⁴⁰ Ar (moles)	⁴⁰ Ar* %	Ca/K	⁴⁰ Ar*/ ³⁹ Ar	Age (Ma)	Error ±1s.d.
550	18.44	954.17E-	337.16E-	796.15E-	104.13E-	72.7	0.08	9.503	223.56	1.22
600	32.45	216.17E-	164.16E-	605.15E-	926.14E-	92.9	0.051	14.235	325.34	0.73
650	46.51	155.17E-	799.17E-	606.15E-	962.14E-	95.1	0.024	15.086	343.04	0.73
700	59.27	149.17E-	525.17E-	551.15E-	879.14E-	94.8	0.018	15.128	343.91	0.76
750	68.83	104.17E-	314.17E-	412.15E-	670.14E-	95.2	0.014	15.461	350.78	0.94
800	74.43	149.17E-	118.16E-	242.15E-	469.14E-	90.5	0.092	17.57	393.76	2.93
850	79.91	109.17E-	147.17E-	237.15E-	516.14E-	93.6	0.011	20.421	450.27	1.47
900	85.92	121.17E-	281.17E-	259.15E-	566.14E-	93.6	0.020	20.432	450.48	1.2
950	91.26	110.17E-	526.17E-	230.15E-	504.14E-	93.4	0.043	20.416	450.17	1.09
1000	95.46	113.17E-	603.17E-	181.15E-	414.14E-	91.8	0.063	21.018	461.88	2.12
1050	97.95	118.17E-	200.17E-	108.15E-	300.14E-	88.3	0.035	24.582	529.68	5.12
1100	99.14	171.17E-	476.17E-	514.16E-	185.14E-	72.6	0.175	26.084	557.51	6.66
1150	99.42	262.17E-	983.17E-	121.16E-	109.14E-	28.9	1.54	26.071	557.27	13.95
1450	100	238.16E-	806.16E-	251.16E-	767.14E-	8.6	6.08	26.248	560.52	76.34
Total		511.16E-	191.15E-	432.14E-	831.13E-			15.728	356.28	1.77

i) Errors are one sigma uncertainties and exclude uncertainties in the J-value.

ii) Data are corrected for mass spectrometer backgrounds, discrimination and radioactive decay.

iii) Interference corrections: (³⁶Ar/³⁷Ar)Ca = 2.70E-4; (³⁹Ar/³⁷Ar)Ca = 6.79E-4; (⁴⁰Ar/³⁹Ar)K = 2.89E-2

iv) J-value = 0.013882 ± 0.000028 based on an age of 98.8 Ma for GA-1550 biotite; mass = 0.00150 g.

APPENDIX 7.2:

⁴⁰ Ar/ ³⁹ Ar Laser Probe analytical results for pyrite separates from AP-Pit6, Airport deposit											
Grain No.	Step No.	Cum ³⁹ Ar (%)	³⁶ Ar (moles)	³⁷ Ar (moles)	³⁹ Ar (moles)	⁴⁰ Ar (moles)	⁴⁰ Ar*	Ca/K	⁴⁰ Ar*/ ³⁹ Ar	Age (Ma)	Error ±1s.d.
1	1	77.2	2.815E-18	4.373E-17	9.135E-17	2.216E-15	62.5	0.862	15.17	342.8	12.3
	2	100.0	1.115E-18	1.349E-17	2.692E-17	8.813E-16	62.7	0.902	20.52	449.7	38.2
2	1	43.0	3.751E-17	2.145E-16	2.096E-16	1.448E-14	23.5	1.840	16.26	365.2	24.1
	2	100.0	3.426E-18	1.847E-16	2.777E-16	6.036E-15	83.3	1.200	18.13	402.7	4.7
3	1	29.4	8.479E-17	1.217E-16	1.911E-16	2.808E-14	10.8	1.150	15.85	356.8	28.6
	2	100.0	1.817E-18	1.032E-16	4.597E-16	8.427E-15	93.6	0.404	17.16	383.3	3.4
4	1	40.5	4.375E-17	1.014E-16	2.954E-16	1.707E-14	24.3	0.618	14.03	319.2	13.1
	2	100.0	4.166E-18	1.423E-16	4.349E-16	9.081E-15	86.4	0.589	18.05	401.2	2.4
5	1	27.1	6.332E-17	9.489E-17	3.637E-16	2.358E-14	20.6	0.470	13.38	305.6	13.9
	2	100.0	2.424E-18	1.478E-16	9.792E-16	1.789E-14	95.9	0.272	17.52	390.6	1.7
6	1	41.6	2.717E-17	7.912E-17	2.830E-16	1.187E-14	32.4	0.503	13.58	309.9	8.3
	2	100.0	1.217E-18	6.842E-17	3.970E-16	6.992E-15	94.8	0.310	16.69	373.9	3.4
7	1	38.5	4.458E-17	7.231E-18	4.195E-16	1.905E-14	30.8	0.031	13.97	318.1	9.3
	2	100.0	2.159E-18	2.786E-17	6.699E-16	1.157E-14	94.3	0.075	16.29	365.7	4.5
8	1	47.4	5.122E-18	1.448E-17	8.077E-17	2.693E-15	43.8	0.323	14.59	331.0	16.0
	2	100.0	1.253E-18	1.679E-17	8.979E-17	1.912E-15	80.6	0.337	17.16	383.3	9.7
9	1	47.8	1.444E-17	9.422E-17	1.703E-16	6.550E-15	34.9	0.996	13.43	306.7	15.3
	2	100.0	3.080E-18	1.688E-16	1.863E-16	4.211E-15	78.6	1.630	17.77	395.7	5.0
10	1	39.6	4.070E-17	1.807E-16	2.888E-16	1.605E-14	25.1	1.130	13.97	317.9	12.2
	2	100.0	2.295E-18	1.481E-16	4.413E-16	8.186E-15	91.7	0.604	17.02	380.4	3.6
11	1	48.2	8.578E-17	1.382E-16	3.199E-16	3.049E-14	16.9	0.778	16.08	361.4	24.1
	2	100.0	1.531E-18	5.009E-17	3.442E-16	6.197E-15	92.6	0.262	16.67	373.6	5.5
12	1	44.0	3.879E-17	6.068E-17	1.228E-16	1.360E-14	15.7	0.890	17.45	389.1	35.4
	2	100.0	1.315E-18	5.058E-17	1.562E-16	2.996E-15	87.0	0.583	16.69	373.9	7.1
I) Errors are one sigma uncertainties and exclude uncertainties in the J-value.											
ii) Data are corrected for mass spectrometer backgrounds, discrimination and radioactive decay.											
iii) Interference corrections: (³⁶ Ar/ ³⁷ Ar)Ca = 2.70E-4; (³⁹ Ar/ ³⁷ Ar)Ca = 6.79E-4; (⁴⁰ Ar/ ³⁹ Ar)K = 2.89E-2											
iv) J-value = 0.013797 ± 0.000034 based on an age of 98.8 Ma for GA-1550 biotite.											

⁴⁰ Ar/ ³⁹ Ar Laser Probe analytical results for pyrite separates from MM03-C2, Minnie Moxham deposit												
Grain No.	Step No.	Cum ³⁹ Ar (%)	³⁶ Ar (moles)	³⁷ Ar (moles)	³⁹ Ar (moles)	⁴⁰ Ar (moles)	⁴⁰ Ar*	Ca/K	⁴⁰ Ar*/ ³⁹ Ar	Age (Ma)	Error ±1s.d.	
1	1	39.3	1.490E-17	7.931E-18	5.756E-17	5.654E-15	22.1	0.248	21.69	472.2	46.8	
	2	100.0	8.206E-19	3.016E-18	8.886E-17	2.568E-15	90.5	0.061	26.14	555.7	11.1	
2	1	34.2	1.591E-17	6.074E-17	1.107E-16	7.079E-15	33.6	0.988	21.51	468.9	21.9	
	2	100.0	1.241E-18	2.071E-17	2.129E-16	7.618E-15	95.1	0.175	34.05	694.7	6.3	
3	1	25.7	1.393E-17	1.113E-16	2.914E-16	9.575E-15	57.0	0.687	18.74	414.9	7.4	
	2	100.0	1.734E-18	4.549E-17	8.412E-16	2.114E-14	97.5	0.097	24.50	525.3	1.5	
4	1	70.0	4.211E-17	6.825E-17	2.960E-16	2.102E-14	40.8	0.415	28.97	606.7	13.5	
	2	100.0	1.408E-18	6.910E-17	1.270E-16	4.539E-15	90.9	0.980	32.49	668.1	8.8	
5	1	34.8	1.657E-17	8.914E-17	4.304E-16	1.137E-14	56.9	0.373	15.04	340.1	4.3	
	2	100.0	5.879E-18	1.314E-16	8.054E-16	1.736E-14	89.9	0.294	19.38	427.5	1.6	
6	1	58.3	8.769E-18	6.040E-19	4.682E-17	3.422E-15	24.2	0.023	17.71	394.4	52.3	
	2	100.0	9.414E-19	1.908E-17	3.354E-17	1.416E-15	80.4	1.020	33.95	693.1	40.7	
7	1	57.0	2.053E-17	2.706E-17	4.115E-16	1.194E-14	49.1	0.118	14.24	323.7	11.5	
	2	100.0	2.250E-18	7.548E-18	3.106E-16	7.973E-15	91.6	0.044	23.50	506.7	3.5	
8	1	43.7	2.410E-17	3.631E-17	1.741E-16	9.843E-15	27.6	0.375	15.63	352.2	23.7	
	2	100.0	1.161E-18	1.259E-18	2.242E-16	6.484E-15	94.6	0.010	27.36	577.8	10.2	
9	1	33.7	1.083E-17	1.141E-17	1.073E-16	4.301E-15	25.6	0.191	10.25	238.6	22.6	
	2	100.0	1.771E-18	4.288E-18	2.110E-16	6.654E-15	92.1	0.037	29.03	607.7	5.3	
10	1	31.0	1.857E-17	9.556E-18	4.867E-17	6.496E-15	15.5	0.353	20.70	453.3	62.4	
	2	100.0	1.021E-18	4.694E-18	1.084E-16	3.533E-15	91.4	0.078	29.77	620.8	10.9	
11	1	20.7	5.029E-17	3.223E-17	5.697E-17	1.725E-14	13.8	1.020	41.93	823.5	65.1	
	2	100.0	3.265E-18	1.405E-17	2.188E-16	7.327E-15	86.8	0.116	29.06	608.3	7.9	
12	1	25.1	6.044E-17	4.558E-17	9.359E-17	1.941E-14	8.0	0.877	16.61	372.3	74.0	
	2	100.0	1.777E-18	1.091E-16	2.789E-16	6.320E-15	91.7	0.704	20.78	454.8	3.9	
I) Errors are one sigma uncertainties and exclude uncertainties in the J-value.												
ii) Data are corrected for mass spectrometer backgrounds, discrimination and radioactive decay.												
iii) Interference corrections: (³⁶ Ar/ ³⁷ Ar)Ca = 2.70E-4; (³⁹ Ar/ ³⁷ Ar)Ca = 6.79E-4; (⁴⁰ Ar/ ³⁹ Ar)K = 2.89E-2												
iv) J-value = 0.013797 ± 0.000034 based on an age of 98.8 Ma for GA-1550 biotite.												

A CRUCIAL ROLE FOR SLAB BREAK-OFF IN THE GENERATION OF MAJOR MINERAL DEPOSITS: INSIGHTS FROM CENTRAL AND EASTERN AUSTRALIA

I.M.A. Vos, F.P. Bierlein and P.S. Heithersay

Mineralium Deposita, in press

ABSTRACT

In the Lachlan Fold Belt of southeastern Australia, major orogenic gold and porphyry gold-copper deposits formed simultaneously within distinct tectonic settings during a very short time interval at ca. 440 Ma. The driving mechanism that controlled the temporal coincidence of these deposits remains largely unexplained. A review of contemporaneous metallogenic, tectonic, magmatic and sedimentological events in central and eastern Australia reveals that a change in subduction dynamics along the Australian sector of the Early Palaeozoic circum-Gondwana mega-subduction system could have influenced lithospheric stress conditions far inboard of the subduction margin. The magnitude of ore formation and the spatial extent of related events are proposed here to have been controlled by the interplay of mantle processes and lithospheric changes that followed slab break-off along a portion of the mega-subduction system surrounding Gondwana at that time. Slab break-off following subduction lock-up caused mantle upwelling that, in turn, provided an instantaneous heat supply for magmatic and hydrothermal events. Coincident reorganisation of lithospheric stress conditions far inboard of the proto-Pacific margin of Australia controlled reactivation of deep-lithospheric fault structures. These fault systems provided a pathway for fluids and heat fuelled by mantle upwelling into the upper lithosphere and caused the deposition of ~440 Ma gold deposits in the Lachlan Fold Belt, as well as a range of metallogenic, tectonic and sedimentary changes elsewhere in central and eastern Australia.

8.1 INTRODUCTION

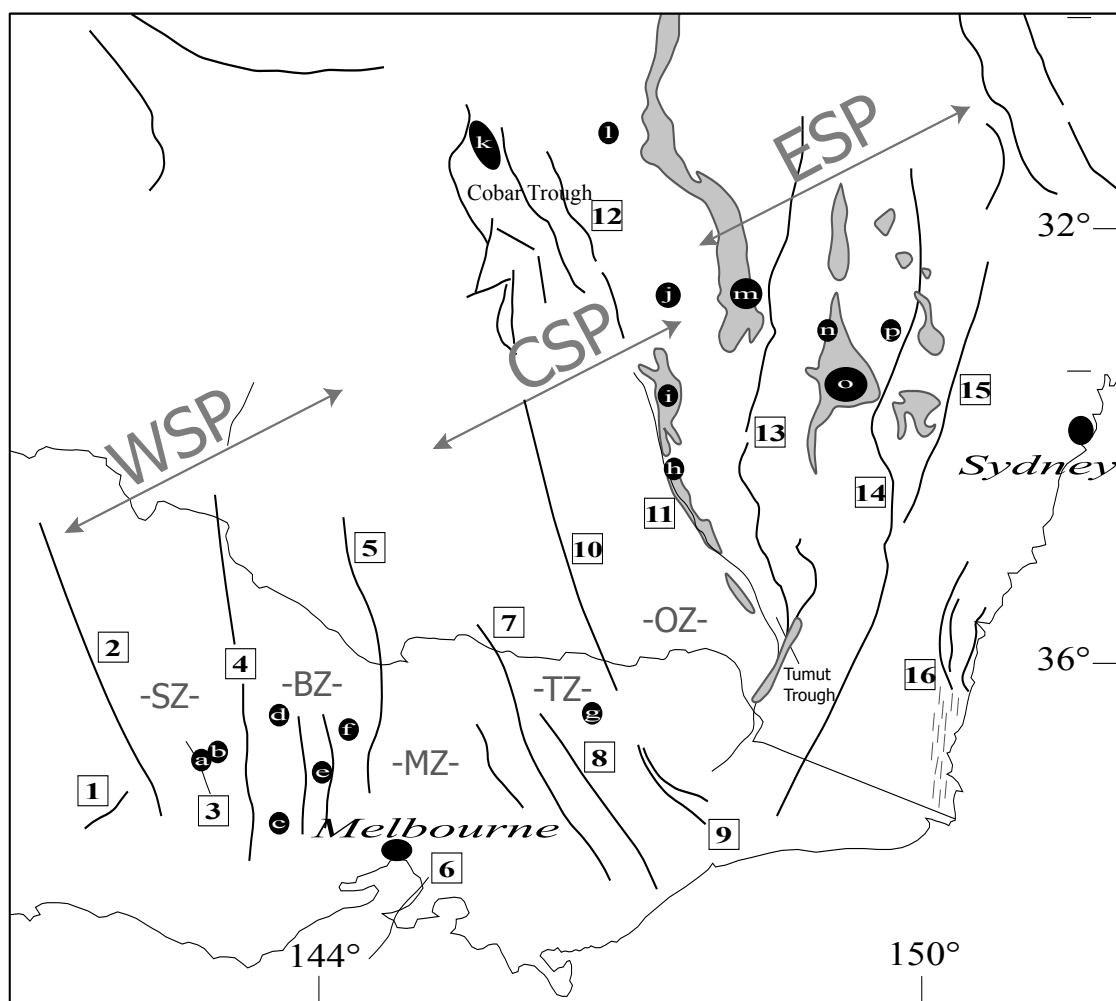
An extraordinary large number of mineralisation ages for gold deposits in the Lachlan Fold Belt in southeastern Australia (Fig. 8.1) concentrate around 440 Ma (Perkins *et al.* 1995; Foster *et al.* 1998; Bierlein *et al.* 2002). These deposits reflect distinct mineralisation styles that include orogenic gold deposits formed in fore-arc to back-arc-like settings in the western subprovince of the fold belt, and porphyry gold-copper deposits that formed in an intra-arc setting in the eastern subprovince (Bierlein *et al.* 2002; Gray *et al.* 2002). Contemporaneous with the generation of these gold deposits, metallogenic, tectonic and magmatic events occurred in central and eastern Australia (e.g. Mawby *et al.* 1999; Vandenberg *et al.* 2000; Elburg *et al.* 2003; Groves *et al.* 2003). This contemporaneity of events provides an interesting enigma for which the driving force remains unresolved.

Various authors have attempted to offer a mechanism to explain some of these ~440 Ma events. Wang and White (1993) suggested that extensional orogenic collapse controlled the development of structures and mineral deposits in the western subprovince of the Lachlan Fold Belt. Elburg *et al.* (2003) suggested that simultaneous hydrothermal-magmatic activity in central Australia and mineralisation in central and eastern Australia at ~440 Ma were controlled by the global redistribution of tectonic plates following the Taconian orogeny. Furthermore, Squire & Miller (2003) proposed that the generation of major gold deposits at ~440 Ma across the Lachlan Fold Belt could be attributed to slab rollback and mantle upwelling along the margin of Gondwana. In this paper, we offer an alternative driving mechanism that rationalizes diverse ore genesis models in

spatially separated, distinct tectonic settings. We first review the metallogenic, magmatic and tectonic events at ~440 Ma in central and eastern Australia and then link these to a lithospheric-scale phenomenon that may have affected an area in excess of 1 million square kilometres, far greater than the accretion-subduction system of the Lachlan Fold Belt. We postulate that slab break-off along a portion of a 'mega-subduction' system outboard of Palaeozoic Australia drove the genesis of giant gold as well as base metal deposits around 440 Ma in the Lachlan and Adelaide fold belts, and also controlled related tectono-magmatic events elsewhere in Australia. A commonality between geological models for the genesis of major gold deposits seems to be the interplay of heat anomalies along long-lived, convergent margin subduction systems (e.g. Barley *et al.* 1989; Kerrich & Wyman 1990; Haeussler *et al.* 1995; Condie 2000). Our findings substantiate that the recognised interplay of slab break-off and mantle upwelling is also an important driving force for the generation of major mineral deposits. Moreover, the occurrence of slab break-off and mantle upwelling in a supercontinent – mega-subduction zone setting can be considered to significantly increase the size of at least some of the resulting mineral deposits.

8.2 The ~440 MA EVENT IN EASTERN AUSTRALIA

As previously noted by Elburg *et al.* (2003), several metallogenic, tectonic, magmatic and sedimentological events occurred simultaneously at ~440 Ma across wide regions in central and eastern Australia (Figs. 8.2 and 8.3):



Fault zones

1. Marathon Fault
2. Moyston Fault
3. Landsborough Fault
4. Avoca Fault
5. Heathcote Fault
6. Waratah Fault
7. Mt Wellington Fault
8. Governor Fault
9. Cassilis Fault Zone
10. Kiewa Fault
11. Gilmore-Indi Fault Zone
12. Rookery Fault
13. Coolac-Narromine Fault
14. Yalmy-Copperhania Fault
15. Yarralaw Fault
16. Narooma Fault Zone

Gold deposits

- a. Stawell
- b. Cambrian
- c. Ballarat
- d. Bendigo
- e. Wattle Gully
- f. Fosterville
- g. Tarnagulla
- h. Gidgingbung
- i. Lake Cowal
- j. Fifield
- k. Cobar
- l. Girilambone
- m. Goonumbla
- n. Copper Hill
- o. Cadia
- p. Hill End

Structural Zones

- SZ = Stawell Zone
 BZ = Bendigo Zone
 MZ = Melbourne Zone
 TZ = Tabberabbera Zone
 OZ = Omea Zone

Subprovinces

- WSP = Western Subprovince
 CSP = Central Subprovince
 ESP = Eastern Subprovince

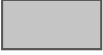

-  Ordovician volcanics
-  Accretionary complex

Figure 8.1: Geological element map of the Lachlan Fold Belt (modified after Gray *et al.* 2002) indicating fault structures and major ~440 Ma gold deposits in the western, central and eastern subprovinces.

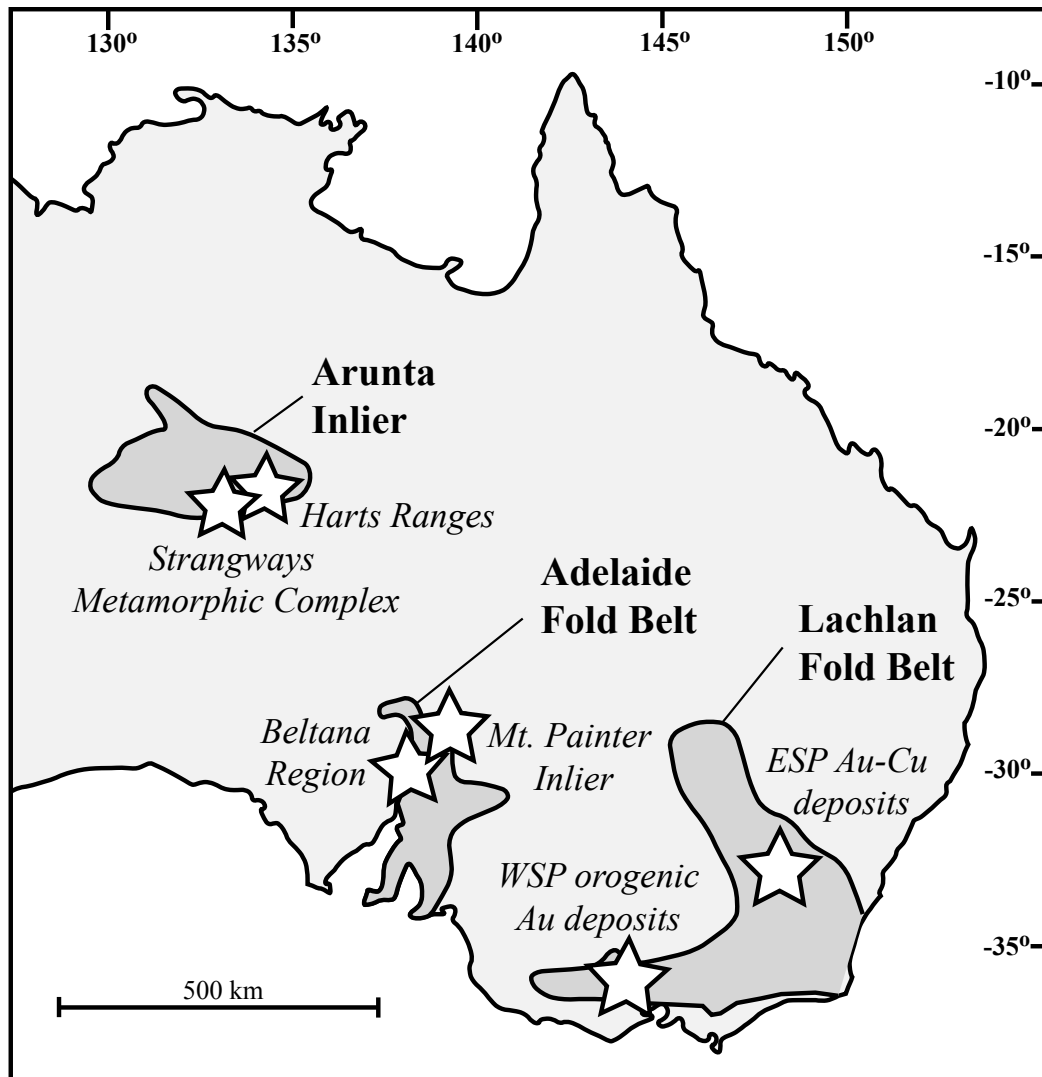


Figure 8.2: Location and distribution of ~440 Ma events in central and eastern Australia. WSP / ESP = Western / Eastern Subprovince of the Lachlan Fold Belt.

8.2.1 Orogenic gold mineralisation, western Lachlan Fold Belt

Gold mineralisation in the Western Subprovince of the Lachlan Fold Belt (Fig. 8.1) includes the genesis of world-class (i.e. > 100 tonnes of Au) orogenic gold deposits at Bendigo, Stawell and Ballarat during and shortly after peak deformation and metamorphism in an episodically eastward stepping subduction-accretion system (Foster *et al.* 1998; Bierlein *et al.* 2001).

8.2.2 Porphyry-style copper-gold mineralisation, eastern Lachlan Fold Belt

Several major porphyry-style gold-copper

deposits (>50 t Au) are hosted in the Macquarie Volcanic Arc in the Eastern Subprovince of the Lachlan Fold Belt (Fig. 8.1). The arc formed above part of the circum-Gondwana subduction zone from the early Ordovician to earliest Silurian (Glen *et al.* 1998). Ca. 440 Ma gold-copper deposits such as those at Northparkes and Cadia, formed during the final stages of distinct K-rich (shoshonitic) arc magmatism (Heithersay & Walshe 1995; Perkins *et al.* 1995; Glen *et al.* 1998).

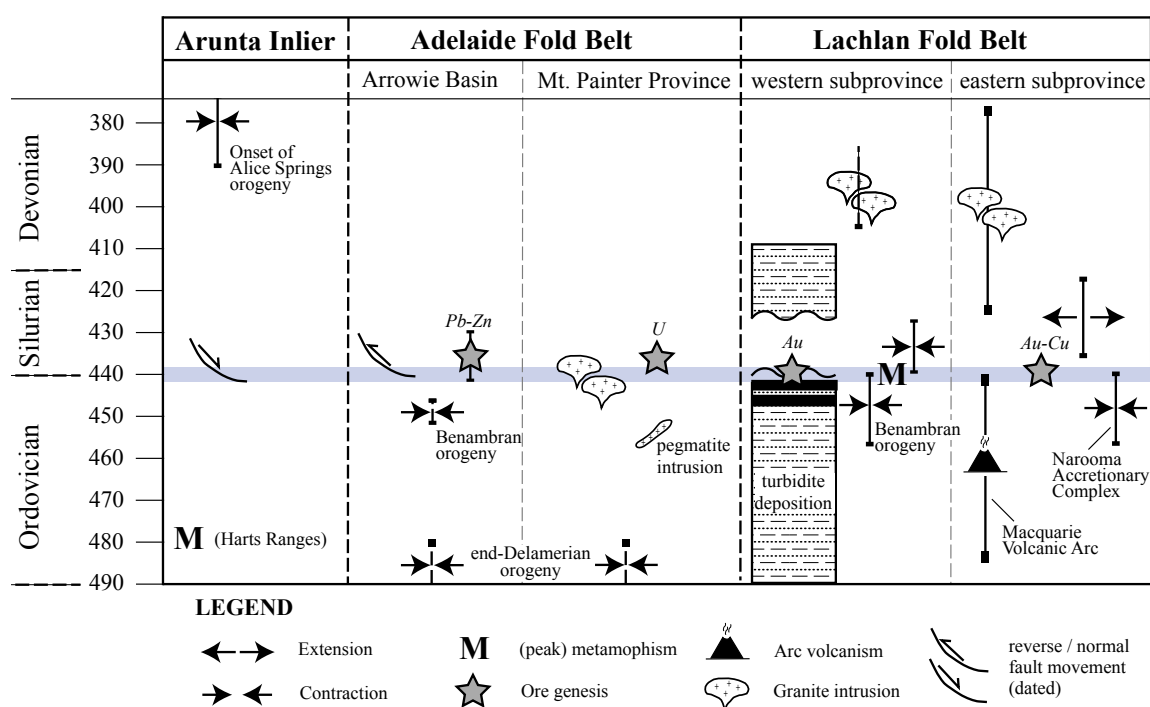


Figure 8.3: Time-space diagram indicating the culmination of ~440 Ma metallogenic, tectonic, magmatic and sedimentological events in central and eastern Australia. See text for references.

8.2.3 Change in sedimentary and tectonic character in the Lachlan Fold Belt

A rapid change from shale- to more sand-dominated turbidite sedimentation occurred simultaneously with a change from overall contraction to partial contraction and basin formation throughout the Lachlan Fold Belt (Vandenberg *et al.* 2000; Vos *et al.* 2003; Fig. 8.3).

8.2.4 Magmatic-hydrothermal mineralisation, Mt. Painter Inlier

Elburg *et al.* (2003) recorded a magmatic-hydrothermal event in the Mt. Painter Inlier in the Flinders Ranges in the Adelaide Fold Belt, South Australia (Figs. 8.2 and 8.3). Their findings were based on extensive geochronological and isotopic (Rb-Sr, Sm-Nd and U-Pb) studies. Ages of ~440 Ma were obtained by these authors from the I/S-type British Empire Granite situated in the north of the inlier and numerous diopside-titanite veins

throughout the inlier. Furthermore, Elburg *et al.* (2003) postulated ages of ~440 Ma for quartz-hematite and uranium mineralisation in the Mt. Gee area in the center of the inlier, based on monazite age dating and a spatial connection with diopside-titanite veins as indicated by the occurrence of Nb-Y oxide.

8.2.5 Zinc-lead mineralisation, Adelaide Fold Belt

The Beltana region in the northwestern part of the Adelaide Fold Belt (Fig. 8.2) is host to Australia's largest willemite (Zn_2SiO_4) deposit, as well as a number of lead deposits. Groves *et al.* (2003) reported a ca. 435 Ma K-Ar age for lead-zinc mineralisation from coronadite ($\text{MnPbMn}_6\text{O}_{14}$) temporally related to willemite ore (Fig. 8.3). According to Groves *et al.* (2003) these deposits derived from a low- to moderate temperature hydrothermal system (50°-170°C) and are spatially associated with major thrust faults, which are considered to be reactivated growth faults.

8.2.6 Large-scale geodynamic changes, Arunta Inlier

In the Palaeoproterozoic to Palaeozoic Arunta Inlier in Central Australia (Fig. 8.2), evidence exists for large-scale geodynamic changes around 440 Ma (Fig. 8.3) following Early Ordovician regional extensional deformation (e.g. Hand *et al.* 1999). The occurrence of a Late Ordovician compressional event has been postulated based on U-Pb and Sm-Nd age dating that indicates movement along major mid-crustal upper amphibolite facies (>650°C, 6kbar) mylonite zones in the Harts Ranges (Mawby *et al.* 1999; Scrimgeour & Raith 2001a). Furthermore, zircon growth associated with shear zone movement in the Strangways Metamorphic Complex has been dated at 443 ± 6 Ma (Möller *et al.* 1999). The ~440 Ma geodynamic change is also documented in the sedimentary record of the basins surrounding the Arunta Inlier and represented by major depocentre shifts, a marked increase in sediment influx and a change from mostly marine to non-marine sedimentation conditions associated with disruption of the Larapintine Seaway from ca. 450 Ma onwards (Haines *et al.* 2001; Scrimgeour & Raith 2001b). These authors recorded a significant break in the sedimentation record at the Ordovician-Silurian boundary (ca. 440 Ma), which extended into the Silurian and suggested that this break indicated exhumation of the region. Exhumation is supported by 445-435 Ma ages obtained from amphibolite grade shears along the Delny-Mt. Sainthill Fault Zone and Entire Point Faults together with Silurian cooling ages from the northern Harts Range (Scrimgeour & Raith 2001a).

8.3 SLAB BREAK-OFF: A POSSIBLE DRIVING MECHANISM?

Slab break-off is not a new concept in

lithosphere dynamics and is well recognized in the Mediterranean region (e.g. Wortel & Spakman 2000), where a close relationship to mineralisation has been proposed (De Boorder *et al.* 1998). Wong *et al.* (1997) suggested that the arrival of buoyant fragments, such as continental lithospheric material, at the trench of a subduction zone could initiate the process of slab break-off. Wortel & Spakman (2000) further suggested that the arrival of any weakness zone (e.g. transform fault, spreading ridge segment) might initiate slab break-off. Slab break-off is generally considered to occur at such shallow depths that asthenospheric material can rise to fill the newly formed gap as shallow as 50 km providing an advective-type heat source or thermal anomaly of a transient nature (Davies & Von Blanckenburg 1995; Wortel & Spakman 2000). Besides the termination of subduction with slab break-off, other implications of slab break-off and final break-off include magmatism, metamorphism, major tectonic activity including fault movement and variations in the stress field, mineralisation and rapid uplift of the overlying lithosphere associated with major unconformities in the sedimentary record (Wortel & Spakman 2000). Throughout most of the Neoproterozoic to Mesozoic, Australia was situated on the margin of Gondwana inboard of a mega-subduction system that virtually surrounded the entire supercontinent (e.g. Foster & Gray 2000; Cawood 2005; Fig. 8.4). Previous studies have proposed a model that focussed on subduction lock-up at ca. 455 Ma following the arrival of a buoyant seamount or ridge along the southeast Australian portion of this subduction system (Glen *et al.* 1998; Squire & Miller 2003). Arrival of such positively buoyant fragments in a subduction system is likely to trigger

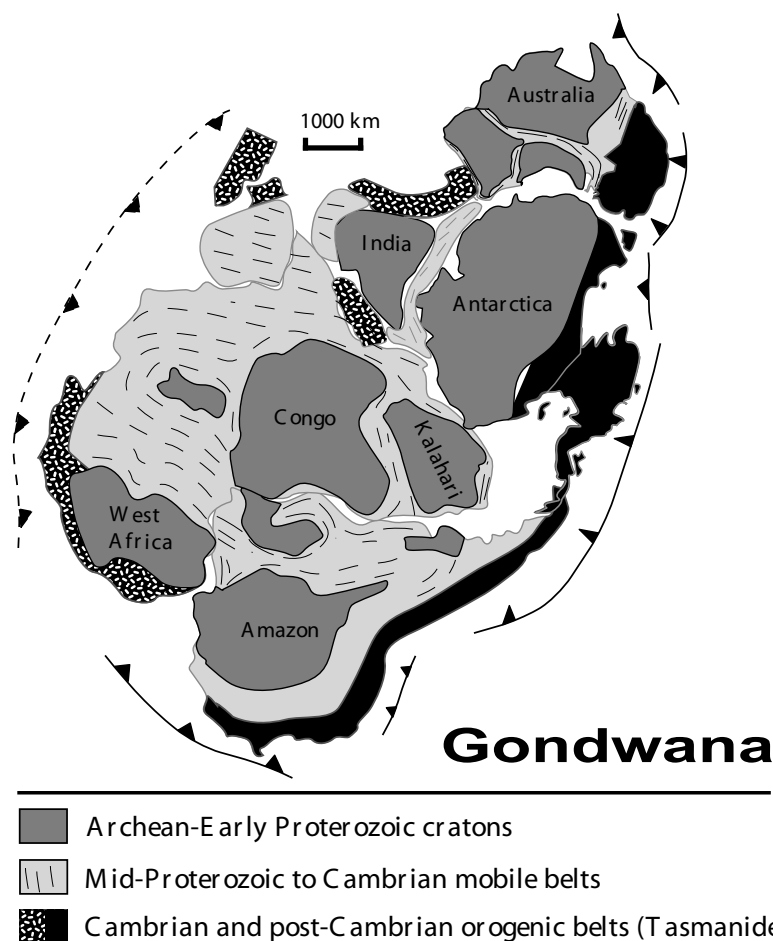


Figure 8.4: Schematic reconstruction of Early Palaeozoic Gondwana and the circum-Gondwana subduction system controlling the evolution of the Tasmanides (in black). Figure modified from Foster & Gray (2000).

changes in subduction dynamics that could, in turn, lead to slab break-off (Davies & Von Blanckenburg 1995; Haeussler *et al.* 1995; Wortel & Spakman 2000). Thus, resistance to subduction following the arrival of a buoyant seamount at the mega-subduction zone outboard of southeastern Australia could have initiated slab break-off that eventually led to break-off of a portion of the subducted circum-Gondwana oceanic slab at ~440 Ma. The process of lateral migration of a slab tear that is generally considered to precede slab break-off (e.g. Wortel & Spakman 2000) thus could have occurred between 455 and 440 Ma.

Slab break-off together with transitory termination of subduction along the southeast Australian portion of the circum-

Gondwana mega-subduction zone could account for the change of lithospheric stress conditions around 440 Ma in central and eastern Australia. We postulate that this large-scale rearrangement controlled: 1) the culmination of deformation and peak metamorphic conditions in the western Lachlan Fold Belt (Foster *et al.* 1998; Bierlein *et al.* 2001); 2) the cessation of accretion along the proto-Pacific margin in the Narooma Fault Zone (Miller & Gray 1996; Glen *et al.* 2004; Fig. 8.2); and 3) the reactivation of major (pre-existing) fault structures in the Lachlan Fold Belt (Foster *et al.* 1998) and central Australia (Mawby *et al.* 1999; Scrimgeour & Raith 2001a).

Furthermore, the occurrence of slab break-off along the southeast Australian subduction

margin would have initiated mantle upwelling and anomalous thermal conditions (e.g. Wortel & Spakman 2000) and it is these interrelated processes that may account for the range of tectono-magmatic and metallogenic events that were recorded in central and eastern Australia at this time. These include: 1) mantle isotopic signatures associated with the magmatic-hydrothermal event in the Mt. Painter Inlier (Elburg *et al.* 2003), and distinct K-rich (shoshonitic) volcanism (Heithersay & Walshe 1995) as well as Au-Cu mineralisation in the eastern subprovince of the Lachlan Fold Belt (Carr *et al.* 1995); 2) the cessation of arc magmatism in the intra-oceanic Macquarie Arc (Perkins *et al.* 1995); 3) synchronous gold-copper, orogenic gold and zinc-lead deposition along a decreasing temperature gradient away from the Early Palaeozoic proto-Pacific subduction margin; 4) rapid uplift reflecting isostatic rebound of the overlying lithosphere after slab break-off and associated mantle heat release (Davies & Von Blanckenburg 1995; Buiter *et al.* 2002) as indicated by erosional unconformities in central and eastern Australia (Vandenberg *et al.* 2000; Haines *et al.* 2001); and potentially 5) the melting of the Early Palaeozoic turbidite pile at mid-crustal levels providing the onset of granite magmatism in the Wagga-Omeo Zone of the Lachlan Fold Belt (e.g. Foster *et al.* 2000; Fig. 8.1).

Previously, lithospheric delamination has been implicated as an important driving mechanism in the evolution of the Lachlan Fold Belt (e.g. Wang & White 1993; Collins 1994). We concur that a model of delamination of lithospheric mantle may equally well be applicable to explain the ~440 Ma events, because responses in lithospheric stress conditions and anomalous temperature conditions due to mantle upwelling

are difficult to distinguish from slab break-off and these processes may commonly compliment one another (e.g. Wortel & Spakman 2000; Lips 2002). We rationalize, however, that it is pertinent to propose and discuss the mechanism of slab break-off to explain ~440 Ma events in central and eastern Australia considering strong supporting evidence from elsewhere that suggests a close link between slab break-off and punctuated metal deposition across wide regions (e.g. De Boorder *et al.* 1998; Lips 2002). In this regard, we would argue that slab break-off could not only have triggered tectonic mode switches, but also supplied the heat source required for magmatism and metallogenesis at different lithospheric levels, which in turn led to the concomitant formation of distinct deposit types in central and eastern Australia. Although we recognise that as a result of data resolution slab break-off remains in the realm of *suggested* explanations for a range of observed phenomena at ~440 Ma, we argue that this concept is in agreement with all available data and thus should be considered in subsequent research. In particular, we note that the mechanism of slab rollback as proposed by Squire & Miller (2003) is inadequate to account for the observed temporal coincidence of magmatic, metallogenic and tectonic events in central and eastern Australia. Although slab rollback would generate thermo-mechanical responses of the lithosphere comparable to slab break-off, the two processes differ considerably in their temporal and spatial characteristics (e.g. Lips 2002). This includes a unilateral spread of mineralisation ages in the case of slab rollback (e.g. Sillitoe 1991). This is at odds with the punctuated ~440 Ma mineralisation and magmatic and tectonic events documented in central and eastern Australia. Although we

recognize that slab rollback was an important contributing mechanism in the evolution of the Lachlan Fold Belt, we do not agree that it supplied the sole driving mechanism for ~440 Ma events.

8.4 THE ROLE OF SLAB BREAK-OFF IN THE GENESIS OF MAJOR MINERAL DEPOSITS

Repeated episodes of subduction along a long-lived subduction system allow long-term enrichment of the convergent margin lithosphere (e.g. Barley *et al.* 1998; Goldfarb *et al.* 1998). Metal deposition occurred throughout the Palaeozoic during several episodes along the proto-Pacific margin in eastern Australia, however, the vast amounts of metal that were deposited along this margin in southeastern Australia around 440 Ma remain exceptional. In this regard, slab break-off may be considered an important mechanism in controlling the formation of major mineral deposits in addition to long-lived subduction, and may explain the punctuated genesis of major ore deposits in similar settings worldwide as previously suggested by De Boorder *et al.* (1998) and Qiu & Groves (1998). We take this notion one step further and speculate that the occurrence of slab break-off in a long-lived supercontinent – mega-subduction zone can give rise to particularly large ore deposits.

The effects of slab break-off and associated mantle upwelling in a supercontinent – mega-subduction zone setting resembling the Palaeozoic circum-Gondwana subduction system (Fig. 8.3) are poorly studied and understood. It has been argued previously that the insulating effects of large continental masses can develop hot regions at shallow levels in the mantle during periods of subduction (e.g. Busse 1978; Anderson 1981; Ballard & Pollack

1987; Anderson *et al.* 1992). Lithospheric characteristics, such as the presence of trans-lithospheric fault systems, may localize the effects of mantle upwelling (e.g. Sawkins 1976; Sykes 1978), which suggests that a feedback mechanism between plate tectonics, lithospheric stress conditions and mantle upwelling exists (Anderson *et al.* 1992). This implies that the presence of hot regions in the shallow mantle underneath supercontinents can amplify the effects of mantle upwelling associated with slab break-off.

In view of this geodynamic relationship, we speculate that the combination of amplified heat build-up as a consequence of long-lived subduction and slab break-off along the southeast Australian sector of the circum-Gondwana mega-subduction system may have triggered an extra-ordinary mantle upwelling event. In turn, this may have governed the formation of exceptionally large ca. 440 Ma gold deposits in southeastern Australia compared to other gold deposits generated at any other time during the Palaeozoic evolution of eastern Australia (e.g. Goldfarb *et al.* 2001). The decreasing temperature gradient in metal deposits from east to central Australia away from the proposed locus of slab break-off supports the notion of an extra-ordinary mantle upwelling event, since its effects were recorded over 1000 km inboard of the proto-Pacific subduction margin. We emphasize that although short-lived, multiple subduction zones may have existed inboard of the proto-Pacific mega-subduction zone during the evolution of the Lachlan Fold Belt, these are considered secondary to the long-lived circum-Gondwana subduction system (Cawood 2005). We do note, however, that these short-lived subduction systems, as well as additional factors that operate at the terrane-

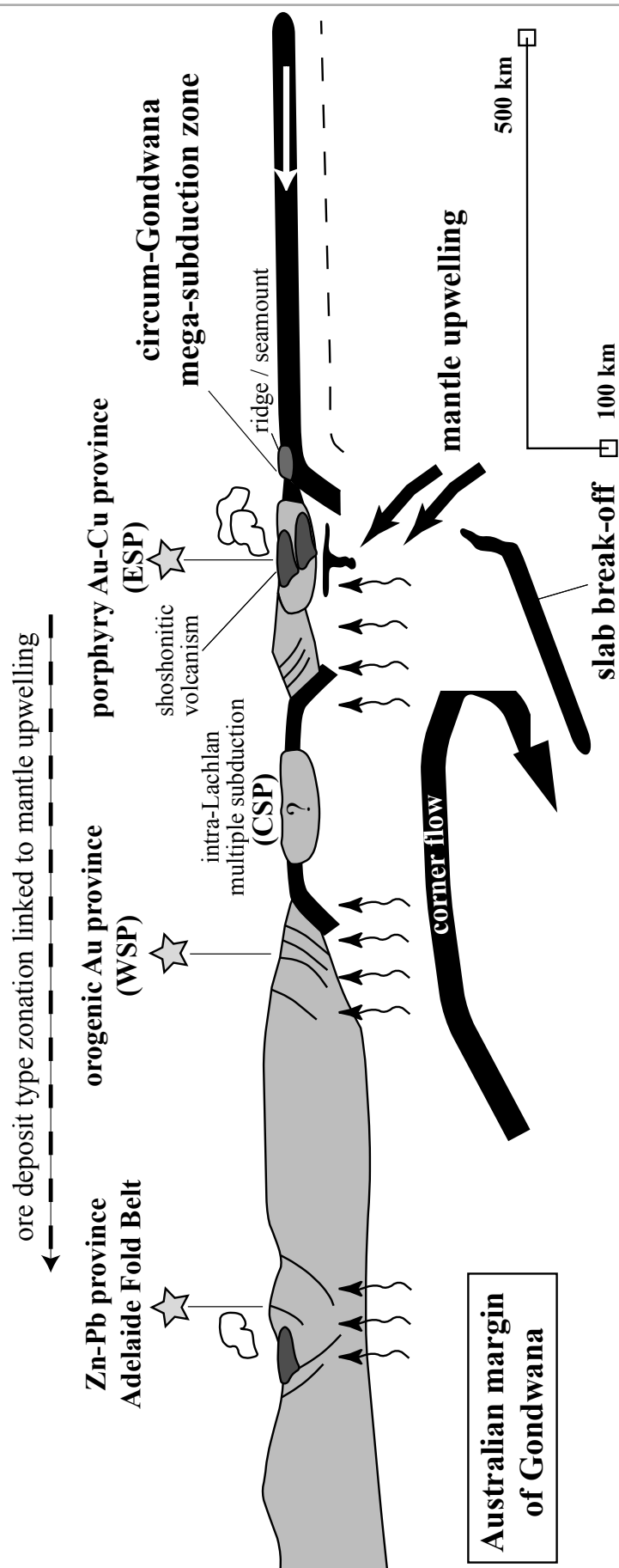


Figure 8.5: Schematic cross-section of southeastern Australia around 440 Ma illustrating break-off of a portion of the mega-subduction zone on the margin of Gondwana. Slab break-off triggers tectonic activity and mantle upwelling, which provides heat (\pm metals) to the lithosphere (as indicated by small arrows) for the simultaneous generation of world-class gold provinces in the eastern and western Lachlan Fold Belt (ESP and WSP, resp.) and zinc-lead deposits far inboard of the subduction margin. Data from Veevers (2000) and references in text. Intra-Lachlan Fold Belt geodynamics (CSP = central subprovince), which include the presence of multiple subduction zones, are only schematically represented in this figure and the reader is referred to Fergusson (2003) and Spaggiari *et al.* (2004) for a comprehensive overview.

scale, may have augmented the fertility of particular regions in the Lachlan Fold Belt. Even so, as this is not the topic of this paper, we do not discuss the geodynamics of the multiple subduction systems in detail and refer the reader to Fergusson (2003) and Spaggiari *et al.* (2004) for a comprehensive overview.

8.5 CONCLUSIONS

The simultaneous occurrence of metallogenic, tectonic, magmatic and sedimentological events in central and eastern Australia, in particular the genesis of major copper-gold and orogenic gold deposits in the Lachlan Fold Belt, can be explained by slab break-off along a portion of the circum-Gondwana mega-subduction zone system at ~440 Ma. Slab break-off was initiated by the arrival of a buoyant seamount or ridge along the subduction system outboard southeast Australia at ~455 Ma and culminated in slab break-off and termination of subduction at ~440 Ma. The interplay of slab break-off and mantle upwelling caused rapid uplift as well as changes in lithospheric stress conditions far inboard of the proto-Pacific subduction margin. These led to the reactivation of large-scale fault systems and disturbance of sedimentation patterns throughout central and eastern Australia. Activated fault systems focused and transported substantial quantities of heat and metal-bearing fluids to the upper lithosphere, which enabled the genesis of ore deposits in distinct tectonic settings along a decreasing temperature gradient away from the locus of slab break-off. The supercontinent - mega-subduction zone setting potentially played a crucial role in the magnitude of ore deposition as a result of amplified mantle upwelling. This paper highlights the importance of long-lived and extensive convergent margins in the

generation of fertile areas for mineralisation. Importantly, the recognition of the role of slab break-off and mantle upwelling along parts of long-lived subduction systems as a driving mechanism for major ore deposit genesis is of relevance for conceptual exploration models targeting giant ore deposits.

ACKNOWLEDGEMENTS

I.M.A.V. would like to acknowledge financial support from the pmd*CRC and Monash University for the duration of his PhD candidature. I.M.A.V. is especially grateful to G. Lister for providing the incentive for this study and initial intellectual input. We express our gratitude to B. Collins, P. Betts, K. Gessner, D. Giles, C. Willman, R. Cayley, D. Taylor and F. Vandenberg, who contributed to the ideas presented in this paper. The paper has benefited from thorough reviews by R. Goldfarb, H. de Boorder and P. Cawood.

REFERENCES

- ANDERSON D. L. 1981. Hotspots, basalts, and the evolution of the mantle. *Science* 213, 82-89.
- ANDERSON D. L., TANIMOTO T. & ZHANG Y. 1992. Plate tectonics and hotspots; the third dimension. *Science* 256, 1645-1651.
- BALLARD S. & POLLACK H. N. 1987. Diversion of heat by Archean cratons; a model for Southern Africa. *Earth and Planetary Science Letters* 85, 253-264.
- BARLEY M. E., EISENLOHR B. N., GROVES D. I., PERRING C. S. & VEARNCOMBE J. R. 1989. Late Archean convergent margin tectonics and gold mineralization; a new look at the Norseman-Wiluna Belt, Western Australia. *Geology* 17, 826-829.
- BARLEY M. E., KRAPEZ B., GROVES D. I. & KERRICH R. 1998. The late Archean bonanza; metallogenic and environmental consequences of the interaction between mantle plumes, lithospheric tectonics

- and global cyclicity. In: Percival J. A. & Ludden J. N. eds. Precambrian '95 symposium; Earth's evolution through the Precambrian; a debate. Volume 91, pp. 65-90. Montreal, PQ, Canada.
- BIERLEIN F. P., ARNE D. C., FOSTER D. A. & REYNOLDS P. 2001. A geochronological framework for orogenic gold mineralisation in central Victoria, Australia. *Mineralium Deposita* 36, 741-767.
- BIERLEIN F. P., GRAY D. R. & FOSTER D. A. 2002. Metallogenic relationships to tectonic evolution; the Lachlan Orogen, Australia. *Earth and Planetary Science Letters* 202, 1-13.
- BUIJTER S. J. H., GOVERS R. & WORTEL M. J. R. 2002. Two-dimensional simulations of surface deformation caused by slab detachment. *Tectonophysics* 354, 195-210.
- BUSSE F. H. 1978. A model of time-periodic mantle flow. *Geophysical Journal of the Royal Astronomical Society* 52, 1-12.
- CARR G. R., DEAN J. A., SUPPEL D. W. & HEITHERSAY P. S. 1995. Precise lead isotope fingerprinting of hydrothermal activity associated with Ordovician to Carboniferous metallogenic events in the Lachlan Fold Belt. *Economic Geology* 90, 1467-1505.
- CAWOOD P. A. 2005. Terra Australis Orogen: Rodinia breakup and development of the Pacific and Iapetus margins of Gondwana during the Neoproterozoic and Paleozoic. *Earth-Science Reviews* 69, 249-279.
- COLLINS W. J. 1994. Upper- and middle-crustal response to delamination; an example from the Lachlan fold belt, eastern Australia. *Geology* 22, 143-146.
- CONDIE K. C. 2000. Episodic continental growth models: afterthoughts and extensions. *Tectonophysics* 322, 153-162.
- DAVIES J. H. & VON BLANCKENBURG F. 1995. Slab breakoff; a model of lithosphere detachment and its test in the magmatism and deformation of collisional orogens. *Earth and Planetary Science Letters* 129, 85-102.
- DE BOORDER H., SPAKMAN W., WHITE S. H. & WORTEL M. J. R. 1998. Late Cenozoic mineralization, orogenic collapse and slab detachment in the European Alpine Belt. *Earth and Planetary Science Letters* 164, 569-575.
- ELBURG M. A., BONIS P. D., FODEN J. & BRUGGER J. 2003. A newly defined Late Ordovician magmatic-thermal event in the Mt. Painter Province, northern Flinders Ranges, South Australia. *Australian Journal of Earth Sciences* 50, 611-631.
- FERGUSON C. L. 2003. Ordovician-Silurian accretion tectonics of the Lachlan Fold Belt, southeastern Australia. *Australian Journal of Earth Sciences* 50, 475-490.
- FOSTER D. A., GRAY D. R., KWAK T. A. P. & BUCHER M. 1998. Chronology and tectonic framework of turbidite-hosted gold deposits in the Western Lachlan fold Belt, Victoria. ⁴⁰Ar-³⁹Ar results. *Ore Geology Reviews* 13, 229-250.
- FOSTER D. A. & GRAY D. R. 2000. Evolution and structure of the Lachlan fold belt (orogen) of eastern Australia. *Annual Reviews in Earth and Planetary Sciences* 28, 47-80.
- GLEN R. A., WALSH J. L., BARRON L. M. & WATKINS J. J. 1998. Ordovician convergent-margin volcanism and tectonism in the Lachlan sector of east Gondwana. *Geology* 26, 751-754.
- GLEN R. A., STEWART I. T. & PERCIVAL I. G. 2004. Narooma Terrane: implications for the construction of the outboard part of the Lachlan Orogen. *Australian Journal of Earth Sciences* 51, 859-884.
- GOLDFARB R. J., PHILLIPS G. N. & NOKLEBERG W. J. 1998. Tectonic setting of synorogenic gold deposits of the Pacific Rim. *Ore Geology Reviews* 13, 185-218.
- GOLDFARB R. J., GROVES D. I. & GARDOLL S. 2001. Orogenic gold and geologic time; a global synthesis. *Ore Geology Reviews* 18, 1-75.
- GRAY D. R., FOSTER D. A. & BIERLEIN F. P. 2002. Geodynamics and metallogeny of the Lachlan Orogen. *Australian Journal*

- of *Earth Sciences* 49, 1041-1056.
- GROVES I. M., CARMAN C. E. & DUNLAP W. J. 2003. Geology of the Beltanawille mite deposit; Flinders Ranges, South Australia. *Economic Geology* 98, 797-818.
- HAEUSSLER P. J., BRADLEY D., GOLDFARB R., SNEE L. & TAYLOR C. 1995. Link between ridge subduction and gold mineralisation in southern Alaska. *Geology* 23, 995-998.
- HAINES P. W., HAND M. & SANDIFORD M. 2001. Palaeozoic synorogenic sedimentation in central and northern Australia; a review of distribution and timing with implications for the evolution of intracontinental orogens. *Australian Journal of Earth Sciences* 48, 911-928.
- HAND M., MAWBY J., KINNY P. D. & FODEN J. 1999. U-Pb ages from the Harts Range, central Australia; evidence for early Ordovician extension and constraints on Carboniferous metamorphism. *Journal of the Geological Society of London* 156, 715-730.
- HEITHERSAY P. S. & WALSHE J. L. 1995. Endeavour 26 North; a porphyry copper-gold deposit in the Late Ordovician, shoshonitic Goonumbla volcanic complex, New South Wales, Australia. *Economic Geology* 90, 1506-1532.
- KERRICH R. & WYMAN D. 1990. Geodynamic setting of mesothermal gold deposits; an association with accretionary tectonic regimes. *Geology* 18, 882-885.
- LIPS A. L. W. 2002. Correlating magmatic-hydrothermal ore deposit formation over time with geodynamic processes in SE Europe. In: Blundell D. J., Neubauer F. & Von Quadt A. eds. The timing and location of major ore deposits in an evolving orogen. *Geological Society of London Special Publication* 204, 69-79.
- MAWBY J., HAND M. & FODEN J. 1999. Sm-Nd evidence for high-grade Ordovician metamorphism in the Arunta Block, central Australia. *Journal of Metamorphic Geology* 17, 653-668.
- MILLER J. M. & GRAY D. R. 1996. Fossil subduction in the eastern Lachlan Fold belt; significance and tectonic implications. *Geological Society of Australia Special Publication* 41, 298.
- MÖLLER A., ARMSTRONG R. A., HENSEN B. J. & WILLIAMS I. S. 1999. Dating metamorphic events & deformation; SHRIMP U-Pb zircon examples from the Strangways metamorphic complex, Arunta Inlier, Australia. *European Union of Geosciences conference Abstracts* 4, 711.
- PERKINS C., WALSHE J. L. & MORRISON G. 1995. Metallogenic episodes of the Tasman fold belt system, eastern Australia. *Economic Geology* 90, 1443-1466.
- QIU Y. & GROVES D. I. 1999. Late Archean collision and delamination in the Southwest Yilgarn Craton; the driving force for Archean orogenic lode gold mineralization? *Economic Geology* 94, 115-122.
- SAWKINS F. J. 1976. Widespread continental rifting; some considerations of timing and mechanism. *Geology* 4, 427-430.
- SCRIMGEOUR I. & RAITH J. G. 2001a. High-grade reworking of Proterozoic granulites during Ordovician intraplate transpression, eastern Arunta Inlier, central Australia. In: Miller J. A., Holdsworth R. E., Buick I. S. & Hand M. eds. *Orogenesis in the Outback*, 261-287.
- SCRIMGEOUR I. & RAITH J. G. 2001b. Tectonic and thermal events in the northeastern Arunta Province, *Report - Northern Territory Geological Survey*, Department of Mines and Energy, 45p.
- SILLITOE R. H. 1991. Gold metallogeny of Chile - an introduction. *Economic Geology* 86, 1187-1205.
- SPAGGIARI C. V., GRAY D. R. & FOSTER D. A. 2004. Lachlan Orogen subduction-accretion systematics revisited. *Australian Journal of Earth Sciences* 51, 549-553.
- SQUIRE R. J. & MILLER J. M. L. 2003. Synchronous compression and extension in East Gondwana; tectonic controls on world-class gold deposits at 440 Ma. *Geology* 31, 1073-1076.
- SYKES L. R. 1978. Intraplate seismicity, reactivation of preexisting zones of weakness, alkaline magmatism, and other tectonism postdating continental

- fragmentation. *Reviews in Geophysics and Space Physics* 16, 621-688.
- VANDENBERG A. H. M., WILLMAN C. E., MAHER S., SIMONS B. A., CAYLEY R. A., MORAND V. J., MOORE D. H. & RADOJKOVIC A. 2000. The Tasman Fold Belt System in Victoria. Geological Survey of Victoria Special Publication.
- VEEVERS J. J., SCHEIBNER E. & WALTER M. R. 2000. Billion-year earth history of Australia and neighbours in Gondwanaland. Gemoc Press, North Ryde, NSW.
- VOS I. M. A., LISTER G. S. & BIERLEIN F. P. 2003. The 440 Ma mineralising event in the Lachlan Fold Belt: result of a tectonic mode switch. *Geological Society of Australia Abstracts* 70, 58.
- WANG G. M. & WHITE S. H. 1993. Gold mineralization in shear zones within a turbidite terrane, examples from central Victoria, S.E. Australia. *Ore Geology Reviews* 8, 163-188.
- WONG S. Y. M., TON A., WORTEL M. J. R. 1997. Slab detachment in continental collision zones; an analysis of controlling parameters. *Geophysical Research Letters* 24, 2095-2098.
- WORTEL M. J. R. & SPAKMAN W. 2000. Subduction and slab detachment in the Mediterranean-Carpathian region. *Science* 290, 1910-1917.